

POLITECNICO DI TORINO

Corso di Laurea Magistrale in Ingegneria Elettronica

Tesi di Laurea Magistrale

**Modelling Molecular Technologies
for Nuclear Magnetic Resonance
Quantum Computing**



Relatori:

Prof. Maurizio ZAMBONI

Prof. Mariagrazia GRAZIANO

Prof. Gianluca PICCININI

Candidato:

Mario SIMONI

April 2020

*To my beloved mother, Livia, and the
memory of my precious grandparents,
Paola and Marcello.*

Summary

Standard CMOS circuits are expected to be no longer able to satisfy nowadays demand for higher performances and lower power consumption. The research has traditionally taken two paths: More-Moore and More-Than-Moore. Both paths brought radical innovations. However, quantum computing, whose fundamental quantity of information is the **qubit**, is not just an innovation, it is expected to be an actual change of paradigm. Not only it demands the exploitation of new technologies, but it also requires a completely new way of approaching computer science and logic.

An intuitive tool to visualise one-qubit states is the **Bloch sphere** (Figure 1): North pole is state $|0\rangle$, while South pole is state $|1\rangle$. They represent the classical bits 0 and 1. The qubit, represented by a blue arrow in the Bloch sphere, is a linear superposition of both eigenstates and when measured, it collapses to a classical bit. The latitude on the sphere represents the probability of which pole the state will collapse to. There are at least two main reasons for which quantum computing is expected to broaden computation horizons. First, specific algorithms can be engineered, manipulating the probability amplitudes of different states, to exploit the quantum superposition principle and achieve high parallelism. Second, quantum computing speaks the same language Nature does: quantum mechanics. Physical systems may be extremely complex, preventing a classical computer to perform reliable simulations. The hardware of quantum computers is represented by quantum systems, thus quantum computing is expected to be spontaneously suitable to handle the complexity of physical systems.

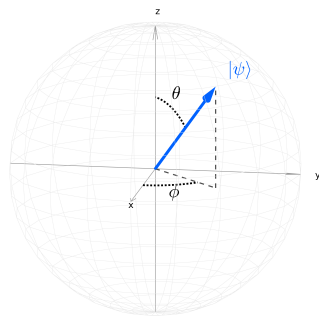
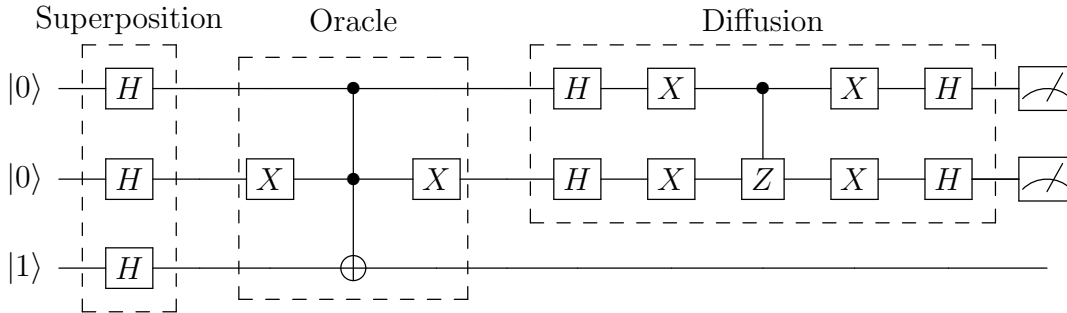


Figure 1: Bloch sphere.

Quantum computing requires the cooperation of several scientific fields: theoretical and experimental physics, chemistry, mathematics, electronic engineering, computer science. Consequently, it is hard to find in the nowadays available literature a comprehensive source which presents the theory and the physical feasibility of quantum computing, with an engineering perspective. In order to fill this gap, the leading idea while writing has been to highlight the operations and algorithms a quantum computer must be able to perform and, then, to propose a hardware solution, providing the rigorous physical treatment mandatory for a deep understanding and for an appropriate modelling.

Thus, after an introduction devoted to the essential mathematical and physical preliminaries which lay the foundation for the understanding of the thesis, the first chapters address the design of quantum algorithms (Figure 3), highlighting the main differences with respect to the classical counterpart and focusing on

Grover’s search algorithm, whose corresponding circuit is derived from fundamentals:



The latter is then described in **Quantum Assembly (QASM)**, which can be seen as the quantum equivalent of VHDL, and simulated on IBM Q Experience [1].

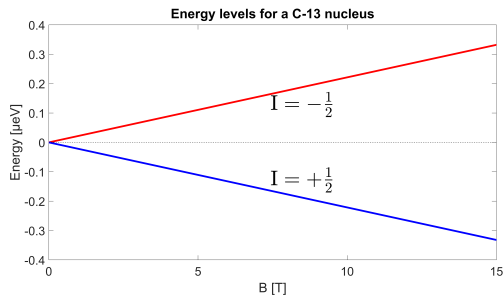


Figure 2: The Zeeman effect for a ^{13}C nucleus.

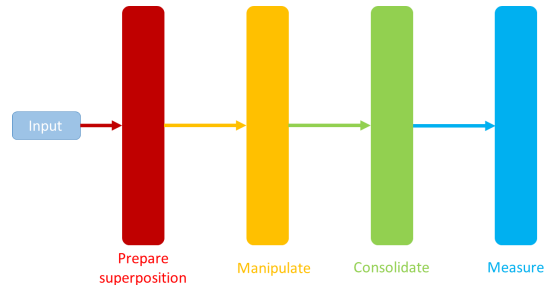


Figure 3: Steps for the execution of a quantum algorithm.

The following chapters deal with a possible physical implementation of quantum processors: the encoding of qubits on **nuclear spins** in diamagnetic molecules. When a static magnetic field ($\sim 10\text{ T}$) is applied to a spin- $\frac{1}{2}$ nucleus, two well-defined energy eigenstates arise, as a result of the **Zeeman effect** (Figure 2). Each of them can be associated with a qubit eigenstate. Thanks to **nuclear magnetic resonance** principles, the probability with which one of the two eigenstates is measured can be handled by the superposition of a radio frequency field at the resonance frequency of the nucleus. This can be interpreted as a rotation of the spin (Figure 4), and so of the qubit, about the RF field and enables the execution of **single qubit quantum gates**, since they are simple rotations of the state vector. The two-qubit **CNOT** gate is obtained through the interaction of spins via **J-coupling**. Considering that these gates constitute a *universal set*, every quantum algorithm can theoretically be run on an NMR processor.

Different nuclei have different resonant frequencies, but the addressing of a specific spin can be achieved also in homonuclear molecules (as the ^{13}C in crotonic acid) since the resonant frequency depends also on the nuclear environment. This phenomenon is known as **nuclear shielding**.

While unwanted J-couplings can be removed thanks to the application of the **refocusing** technique, spin decoherence and relaxation phenomena (Figure 5) force an upper limit to the allowed timescale. A main advantage



of NMR is that this timescale is very long (1 s), even at room temperature. Conversely, scalability is still an issue.

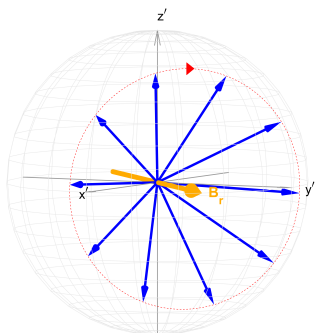


Figure 4: Spin precession on resonance in a rotating coordinate reference system.

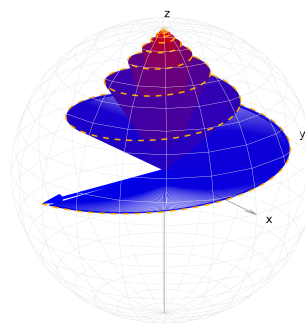


Figure 5: Relaxation and decoherence: eventually, the magnetization will be found along the \hat{z} axis.

A NMR quantum computer **MATLAB** model, **Quantum_MOLE**, based on the relations derived from first principles in the thesis, is proposed to prove the feasibility of NMR quantum processors. The input technological parameters, as chemical shielding and J-coupling, can be computed resorting on **ORCA** [2, 3], or obtained from experimental data. The model, able to run a universal set of quantum gates and tested on a benchmark of simple algorithms, can be useful to find an optimal operating point as a compromise between molecule physical properties and the quantities which can be controlled by nowadays NMR instrumentation. It can be run at different levels of approximation, trading off CPU time and accuracy. **Quantum_MOLE** and takes into consideration several non-idealities, as decoherence, relaxation, unwanted coupled evolution due to J-coupling during one-qubit operations and the effect of off-resonance pulses on not-addressed qubits in homonuclear molecules. Finally, **Quantum_MOLE** is also provided with an embedded support for Virtual-Z method and refocusing techniques.

Table of contents

Summary	ii
I Theoretical quantum computation	1
1 Linear algebra and quantum mechanics	2
1.1 Linear algebra for quantum mechanics	3
1.1.1 Vector spaces	3
1.1.2 Linear operators	5
1.1.3 Eigenvalues and eigenvectors	6
1.1.4 Pauli matrices	8
1.1.5 Spectral decomposition	9
1.1.6 Kronecker tensor product	11
1.2 Quantum mechanics for quantum computation	14
1.2.1 Fundamental postulates	14
1.2.1.1 Wave function and superposition	14
1.2.1.2 Observables	16
1.2.1.3 Measurements	17
1.2.1.4 Schrödinger equation	23
1.2.2 The wavefunction and the state vector	25
1.2.3 Assembled systems, entanglement and superposition	26
1.2.4 Mixed states and density matrix formalism	29
1.2.4.1 Properties of the density operator	30
1.2.4.2 Time evolution	33
1.2.4.3 Density operator of a subsystem	34
1.2.4.4 Measurements	38
1.2.4.5 Separable and inseparable states	39
1.2.4.6 Fidelity	39
2 Theory of quantum computing	41
2.1 Introduction to quantum computing	44
2.1.1 Bits and qubits	44
2.1.2 Multi-qubit systems	46
2.1.3 Matrix formalism for classical logic gates	48
2.1.3.1 NOT gate	48
2.1.3.2 AND gate	48
2.1.3.3 NAND gate	49
2.1.4 Parallel and sequential operations	50
2.1.4.1 Sequential operations	50
2.1.4.2 Parallel operations	50
2.1.4.3 Mixed operations	50

2.1.5	Bloch sphere	52
2.1.5.1	Pure states	52
2.1.5.2	Mixed states	54
2.1.6	Quantum gates	56
2.1.6.1	One-qubit quantum gates	57
2.1.6.2	Multi-qubit and controlled quantum gates	64
2.1.6.3	Some useful equivalences	69
2.1.6.4	Universal set of quantum gates	70
2.1.7	No-cloning theorem	70
2.2	Quantum algorithms	72
2.2.1	Quantum parallelism and interference	72
2.2.2	Grover's search algorithm	75
2.2.2.1	The oracle	75
2.2.2.2	Geometrical interpretation	76
2.2.2.3	Quantum circuit	80
2.3	Quantum assembly	89
2.3.1	Syntax	90
2.3.2	Grover's search algorithm QASM	92
2.3.3	Simulation of Grover's search algorithm	93

II Nuclear magnetic resonance physical theory 95

3 Introduction to magnetism 96

3.1	Classical magnetism	96
3.1.1	The fundamental concepts	96
3.1.2	The magnetic moment	99
3.1.2.1	The magnetic moment of a rotating electron	100
3.1.2.2	The energy and the force of a magnetic dipole in a magnetic field	101
3.1.2.3	Torque and classical precession	103
3.2	Quantum mechanical interpretation of magnetism	107
3.2.1	The angular momentum in the quantum mechanics picture	107
3.2.1.1	The eigenvalues and eigenstates of the angular mo- ment	108
3.2.1.2	The spin	109
3.2.1.3	Angular momenta of composite system	112
3.2.2	Microscopic magnetism	114
3.2.2.1	Electron magnetism	115
3.2.2.2	Nuclear magnetism	121
3.2.2.3	Some remarks on microscopic magnetism	125

4 Nuclear magnetic resonance 127

4.1	Single spin	128
4.1.1	The radio-frequency field	132
4.1.1.1	The classical picture	134

4.1.1.2	The quantum picture	137
4.1.2	The off-resonance field: the Bloch-Siegert effect	146
4.2	Spin ensemble	149
4.2.1	Thermal equilibrium	151
4.2.2	The magnetization vector	154
4.2.3	Free precession	156
4.2.4	The radio-frequency field	158
4.2.4.1	Excitation of coherences	160
4.2.4.2	Inversion of populations	160
4.3	Phenomenology of relaxation and decoherence	162
4.3.1	Transverse relaxation	163
4.3.2	Longitudinal relaxation	165
4.3.3	Relaxation phenomena	166
5	Nuclear spin interactions	169
5.1	Direct spin-spin coupling	171
5.2	Chemical shielding	177
5.2.1	The Hamiltonian of the chemical shielding	181
5.2.2	The origin of the chemical shielding	182
5.2.2.1	Time independent perturbation theory: some hints	182
5.2.2.2	Perturbation Hamiltonian	186
5.2.2.3	Computation of the current density	192
5.2.2.4	Computation of the chemical shielding	196
5.2.3	A practical approach to chemical shielding	203
5.3	Indirect spin-spin coupling	205
5.3.1	The origin of the J-coupling	209
5.3.1.1	The spin-dipole mechanism	211
5.3.1.2	The Fermi contact mechanism	212
5.3.1.3	The computation of the J constant	215
5.3.1.4	Hints on the molecular orbital interpretation of FC J-coupling	219
5.3.1.5	The transmission of coupling	223

III Physical implementation of an NMR quantum computer **224**

6	The NMR quantum computer	225
6.1	The Hamiltonian for weakly coupled spins	226
6.1.1	Heteronuclear molecules	227
6.1.2	Homonuclear molecules	230
6.2	NMR quantum gates	232
6.2.1	One-qubit gates in many-qubit molecules	232
6.2.2	Two-qubit gates in two-qubit molecules	236
6.2.2.1	The CNOT gate	236
6.2.2.2	The controlled Z gate	242

6.2.3	Two-qubit gates in many-qubit molecules: the refocusing . . .	243
6.3	Hints on experimental issues	248
6.3.1	Pseudopure states	248
6.3.2	Quantum state tomography	249
7	Quantum_MOLE: an NMR quantum computer model	250
7.1	The structure of the model	251
7.1.1	The input parameters	251
7.1.1.1	The input physical parameters	253
7.1.1.2	The QASM description of the algorithm	253
7.1.2	The approximate computation	254
7.1.2.1	The qubit representation and the initial state . . .	254
7.1.2.2	Rotation about x or y	255
7.1.2.3	Rotation about z	256
7.1.2.4	The Hadamard gate	257
7.1.2.5	Free J-evolution with refocusing	258
7.1.2.6	The CNOT gate	258
7.1.2.7	The controlled-Z gate	259
7.1.2.8	The time evolution of the density operator	260
7.1.2.9	The handling of output data	261
7.1.3	The exact computation	262
7.1.3.1	Rotation about x or y	262
7.1.3.2	Free J-evolution with refocusing	264
7.1.4	The exact computation with automatic refocusing	265
7.1.4.1	Rotation about x and y	266
7.2	User manual	267
7.3	Hints on the use of ORCA	269
8	Simulations and characterizations	271
8.1	Chloroform	272
8.1.1	Fidelity optimization	272
8.1.2	The Grover's search benchmark	273
8.1.3	Exact computation	276
8.2	Cytosine	277
8.2.1	Fidelity optimization	277
8.2.2	The Grover's search benchmark	279
8.2.2.1	Automatic refocusing	280
8.3	Crotonic acid	282
8.3.1	Fidelity optimization	283
8.3.2	The Grover's search benchmark	284
8.4	Future improvements	287
	Conclusions	288
	Bibliography	291

Part I

Theoretical quantum computation

Chapter 1

Linear algebra and quantum mechanics

A deep understanding of the very core of quantum mechanics and quantum computation cannot be achieved without getting familiar with some elegant mathematics. Quantum mechanics is *inherently* mathematical. After all, quantum mechanics is a description of Nature and Nature is written in a mathematical language. Nevertheless, the mathematical formalism is definitely the first hurdle a non-insider has to deal with. The leading idea while writing has been to make things as simple as possible, assuming the reader has no familiarity with fine mathematical and physical jargon and leading them in the world of quantum computation, trying to provide a real feel for the subject in an almost self-contained work. This is the reason for which the first chapter is completely devoted to the mathematical and physical preliminaries essential to a basic understanding of quantum computation. The reader who feels familiar with linear algebra and the matrix formalism for quantum mechanics can move to chapter 2.

1.1 Linear algebra for quantum mechanics

1.1.1 Vector spaces

Quantum states are defined using complex vectors belonging to complex vector spaces. It is useful to review some basic definitions.

Definition 1.1.1. A **complex vector space** \mathbb{V} is a non empty set of objects, called **vectors**, with two operations:

- (i) Addition: $\forall \mathbf{u}, \mathbf{v} \in \mathbb{V} \implies \mathbf{u} + \mathbf{v} \in \mathbb{V}$.
- (ii) Scalar multiplication: $\forall \mathbf{v} \in \mathbb{V}, a \in \mathbb{C} \implies a\mathbf{v} \in \mathbb{V}$.

and an element called the **zero vector** $\mathbf{0} \in \mathbb{V}$. For all $\mathbf{u}, \mathbf{v}, \mathbf{w} \in \mathbb{V}$ and for all $a, b, c \in \mathbb{C}$ the following properties must hold true:

- (i) Associativity of addition: $\mathbf{u} + (\mathbf{v} + \mathbf{w}) = (\mathbf{u} + \mathbf{v}) + \mathbf{w}$.
- (ii) Commutativity of addition: $\mathbf{u} + \mathbf{v} = \mathbf{v} + \mathbf{u}$.
- (iii) Identity element of addition: $\mathbf{u} + \mathbf{0} = \mathbf{u}$.
- (iv) Every element has an inverse: $\mathbf{u} + (-\mathbf{u}) = \mathbf{0}$.
- (v) Identity element of scalar multiplication: $1 \cdot \mathbf{u} = \mathbf{u}$.
- (vi) Compatibility of scalar multiplication with complex multiplication: $a(b\mathbf{u}) = (ab)\mathbf{u}$
- (vii) Scalar multiplication distributes over addition: $a(\mathbf{u} + \mathbf{v}) = a\mathbf{u} + a\mathbf{v}$
- (viii) Scalar multiplication distributes over complex addition: $(a + b)\mathbf{u} = a\mathbf{u} + b\mathbf{u}$

Definition 1.1.2. The vectors $\{\mathbf{u}_1, \mathbf{u}_2, \dots, \mathbf{u}_n\} \in \mathbb{V}$ are said to be **linearly independent** if no vector in the set can be written as the linear combination of the remaining vectors in the set.

Definition 1.1.3. Every set of n linearly independent vectors $\{\mathbf{u}_1, \mathbf{u}_2, \dots, \mathbf{u}_n\} \in \mathbb{V}^n$ realizes a **basis** of \mathbb{V}^n and every $\mathbf{v} \in \mathbb{V}^n$ can be written as a linear combination of the basis vectors

$$\mathbf{v} = \sum_{i=1}^n c_i \mathbf{u}_i \quad \forall i, c_i \in \mathbb{C} \quad (1.1.1)$$

where n is the dimension of the vector space.

In particular, if

$$\mathbf{u}_i \cdot \mathbf{u}_j = \delta_{ij} \quad (1.1.2)$$

then the set is an **orthonormal basis** of \mathbb{V}^n

The following definition is required to introduce the Dirac formalism.

Definition 1.1.4. Given a matrix \mathbf{A} , its Hermitian conjugate is

$$\mathbf{A}^\dagger : (A^\dagger)_{jk} = A_{kj}^* \quad \forall j,k \quad (1.1.3)$$

In the framework of quantum mechanics, it is customary to adopt the **Dirac notation** to ease the most common calculations.

Definition 1.1.5. An element of \mathbb{C}^n is denoted as a **ket**

$$|\psi\rangle = \begin{pmatrix} \psi_1 \\ \vdots \\ \psi_n \end{pmatrix} = (\psi_1 \ \dots \ \psi_n)^t, \psi_i \in \mathbb{C} \quad (1.1.4)$$

where t denotes the transpose operation. The Hermitian conjugate of a ket is known as **bra**

$$\langle\psi| = (\psi_1^* \ \dots \ \psi_n^*) \quad (1.1.5)$$

The following properties and definitions are presented using the bra-ket notation, in order to get familiar with this new way of writing vectors (further examples in [4]). First of all, the definition of inner product.

Definition 1.1.6. Let $|\psi\rangle, |\phi\rangle \in \mathbb{V}^n$ the **inner product** is defined as

$$\langle\psi|\phi\rangle = \sum_{i=1}^n \psi_i^* \phi_i \quad (1.1.6)$$

Theorem 1.1.1. Let $\{|e_i\rangle\}$ be an orthonormal basis of \mathbb{V}^n , then the **completeness relation** holds true

$$\sum_i^n |e_i\rangle\langle e_i| = \mathbb{I} \quad (1.1.7)$$

where \mathbb{I} is the identity matrix.

Proof. Let $|\psi\rangle \in \mathbb{V}^n$, then $|\psi\rangle = \sum_{i=1}^n c_i |e_i\rangle$. The c_j component can be rewritten as

$$\langle e_j|\psi\rangle = \sum_{i=1}^n \langle e_j|c_i|e_i\rangle = \sum_{i=1}^n c_i \langle e_j|e_i\rangle = \sum_{i=1}^n c_i \delta_{ji} = c_j$$

Replacing in the expansion of $|\psi\rangle$

$$|\psi\rangle = \sum_{i=1}^n c_i |e_i\rangle = \sum_{i=1}^n \langle e_i|\psi\rangle |e_i\rangle = \sum_{i=1}^n |e_i\rangle \langle e_i|\psi\rangle = \left(\sum_{i=1}^n |e_i\rangle\langle e_i| \right) |\psi\rangle = \mathbb{I} |\psi\rangle$$

since $\langle e_i|\psi\rangle$ is a number. □

In the framework of quantum mechanics, quantities are customarily defined in a specific complex vector space, known as Hilbert space.

Definition 1.1.7. A **Hilbert space** \mathbb{H}^n is a complex vector space with an inner product.

1.1.2 Linear operators

A linear operator acting on a vector space is represented by a matrix. The latter depends on the the chosen (orthonormal) basis for the vector space. For the sake of clearness, suppose $\{|e_i\rangle\}$ is an orthonormal basis of \mathbb{H}^n ¹. A generic $|\psi\rangle \in \mathbb{H}^n$ can be expanded as $|\psi\rangle = \sum_{i=1}^n c_i |e_i\rangle$. Because of *linearity*, the action of the operator $\mathbf{A} : \mathbb{H}^n \rightarrow \mathbb{H}^n$ on an arbitrary vector belonging to \mathbb{H}^n is defined when its action in the basis vectors is specified. As a matter of fact

$$\mathbf{A} |\psi\rangle = \sum_{i=1}^n c_i \mathbf{A} |e_i\rangle \tag{1.1.8}$$

Since, by definition, $\mathbf{A} |e_i\rangle$ is a vector, it can be expanded as

$$\mathbf{A} |e_i\rangle = \sum_{k=1}^n A_{ki} |e_k\rangle$$

Taking the inner product with $\langle e_j|$, one gets

$$A_{ji} = \langle e_j| \mathbf{A} |e_i\rangle \tag{1.1.9}$$

which are the elements of the matrix representation of the linear operator \mathbf{A} , chosen a specific orthonormal basis $\{|e_i\rangle\}$.

¹Note that it is actually enough to consider a generic complex finite dimensional vector space.

Theorem 1.1.2. Given the orthonormal basis $\{|e_i\rangle\}$ of \mathbb{H}^n , the matrix representation of a linear application $\mathbf{A} : \mathbb{H}^n \rightarrow \mathbb{H}^n$ is

$$\mathbf{A} = \sum_{i,j} A_{ij} |e_j\rangle\langle e_i| \quad (1.1.10)$$

Proof. Exploiting theorem 1.1.1 and the equality 1.1.9:

$$\begin{aligned} \mathbf{A} &= \mathbb{I}\mathbf{A}\mathbb{I} = \sum_i |e_i\rangle\langle e_i| \cdot \mathbf{A} \cdot \sum_j |e_j\rangle\langle e_j| \\ &= \sum_{i,j} |e_i\rangle \underbrace{\langle e_i| \mathbf{A} |e_j\rangle}_{A_{ij}} \langle e_j| = \sum_{i,j} A_{ij} |e_j\rangle\langle e_i| \end{aligned}$$

□

In the following, some fundamentals linear operators are defined.

Definition 1.1.8. The **projection operator**

$$\mathbf{P}_k = |e_k\rangle\langle e_k| \quad (1.1.11)$$

projects a vector $|\psi\rangle$ to a vector parallel to $|e_k\rangle$

$$\mathbf{P}_k |\psi\rangle = |e_k\rangle \langle e_k|\psi\rangle = \alpha |e_k\rangle \quad (1.1.12)$$

where α is a number.

Definition 1.1.9. A matrix $\mathbf{A} : \mathbb{H}^n \rightarrow \mathbb{H}^n$ is said to be a **Hermitian matrix** if and only if $\mathbf{A}^\dagger = \mathbf{A}$.

Definition 1.1.10. A matrix $\mathbf{U} : \mathbb{H}^n \rightarrow \mathbb{H}^n$ is said to be a **unitary matrix** if and only if $\mathbf{U}^\dagger = \mathbf{U}^{-1}$.

A unitary matrix with $\det(U) = 1$ is said to be a **special unitary matrix** ($\text{SU}(n)$).

1.1.3 Eigenvalues and eigenvectors

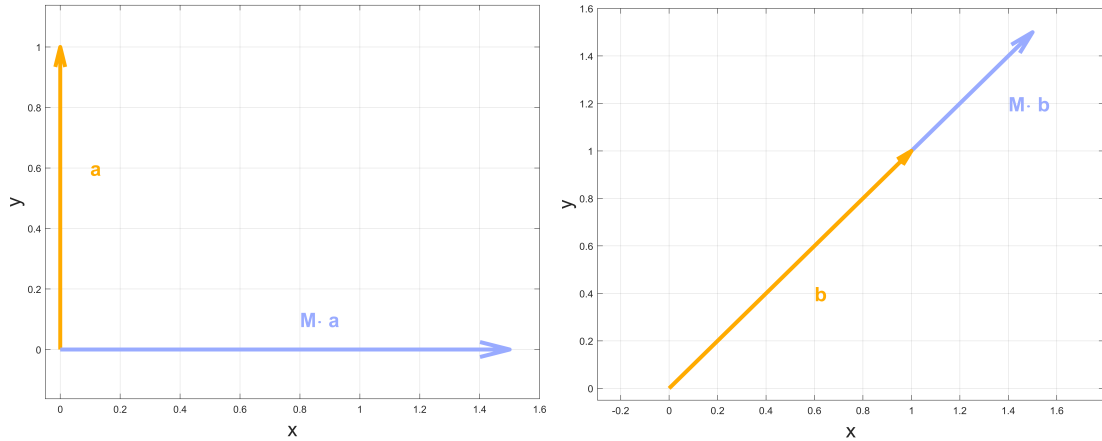
Consider the matrix \mathbf{M} defined as

$$\mathbf{M} = \begin{pmatrix} 0 & \frac{1}{2} \\ \frac{1}{2} & 0 \end{pmatrix} \quad (1.1.13)$$

and suppose that it is applied to a vector $\mathbf{a} = \begin{pmatrix} 0 & 1 \end{pmatrix}^t$:

$$\mathbf{M}\mathbf{a} = \begin{pmatrix} 0 & \frac{1}{2} \\ \frac{1}{2} & 0 \end{pmatrix} \cdot \begin{pmatrix} 0 \\ 1 \end{pmatrix} = \begin{pmatrix} \frac{3}{2} \\ 0 \end{pmatrix} = \frac{3}{2} \begin{pmatrix} 1 \\ 0 \end{pmatrix} \quad (1.1.14)$$

It is evident that \mathbf{M} causes a variation of both the length and the direction of the vector \mathbf{a} , to which it is applied: this is the general case when a matrix is applied to an arbitrary vector (Figure 1.1a).



(a) \mathbf{a} is not an eigenvector of \mathbf{M} .

(b) \mathbf{b} is an eigenvector of \mathbf{M} .

Figure 1.1: Graphical representation of the action of a matrix on a vector.

Now, consider another vector $\mathbf{b} = \begin{pmatrix} 1 & 1 \end{pmatrix}^t$:

$$\mathbf{M}\mathbf{b} = \begin{pmatrix} 0 & \frac{1}{2} \\ \frac{1}{2} & 0 \end{pmatrix} \cdot \begin{pmatrix} 1 \\ 1 \end{pmatrix} = \begin{pmatrix} \frac{3}{2} \\ \frac{3}{2} \end{pmatrix} = \frac{3}{2} \begin{pmatrix} 1 \\ 1 \end{pmatrix} \quad (1.1.15)$$

There is an obvious difference with respect to the previous case: matrix \mathbf{M} prompts just a variation of the length of \mathbf{b} , leaving its direction unaffected. It is as if \mathbf{b} were multiplied by a scalar (Figure 1.1b).

This example leads to the definition of eigenvectors and eigenvalues.

Definition 1.1.11. Let $\mathbf{A} \in \mathbb{C}^{n \times n}$, if there is a number $\lambda \in \mathbb{C}$ and a vector $|\psi\rangle \neq \mathbf{0} \in \mathbb{C}^n$ such that

$$\mathbf{A}|\psi\rangle = \lambda|\psi\rangle \quad (1.1.16)$$

then λ is an **eigenvalue** of \mathbf{A} and $|\psi\rangle$ is an **eigenvector** of \mathbf{A} associated with λ .

Theorem 1.1.3. All the eigenvalues of a **Hermitian** matrix are **real** and two eigenvectors associated with different eigenvalues are orthogonal.

Proof. Let $\mathbf{A}|\psi\rangle = \lambda|\psi\rangle$. The Hermitian conjugate is $\langle\psi|\mathbf{A} = \lambda^*\langle\psi|$. So

$$\langle\psi|\mathbf{A}|\psi\rangle = \lambda\langle\psi|\psi\rangle = \lambda^*\langle\psi|\psi\rangle \implies \lambda = \lambda^*$$

Let $\mathbf{A}|\phi\rangle = \zeta|\phi\rangle$ with $\zeta \neq \lambda$. Since $\zeta \in \mathbb{R}$, then $\langle\phi|\mathbf{A} = \zeta\langle\phi|$. Now, consider

$$\begin{aligned}\langle\phi|\mathbf{A}|\psi\rangle &= \zeta\langle\phi|\psi\rangle \\ \langle\phi|\mathbf{A}|\psi\rangle &= \lambda\langle\phi|\psi\rangle\end{aligned}$$

The element by element subtraction reads

$$0 = (\lambda - \zeta)\langle\phi|\psi\rangle \implies \langle\phi|\psi\rangle = 0$$

since $\zeta \neq \lambda$. □

The eigenvectors of a Hermitian matrix are chosen to be orthonormal, which means that

$$\sum_{i=1}^n |\psi_i\rangle\langle\psi_i| = \mathbb{I} \tag{1.1.17}$$

1.1.4 Pauli matrices

Definition 1.1.12. Pauli matrices represent a fundamental set of Hermitian unitary traceless matrices:

$$\boldsymbol{\sigma}_x = \begin{pmatrix} 0 & 1 \\ 1 & 0 \end{pmatrix} \quad \boldsymbol{\sigma}_y = \begin{pmatrix} 0 & -i \\ i & 0 \end{pmatrix} \quad \boldsymbol{\sigma}_z = \begin{pmatrix} 1 & 0 \\ 0 & -1 \end{pmatrix} \tag{1.1.18}$$

It is straightforward to show that

$$\det(\boldsymbol{\sigma}_i) = -1 \implies \boldsymbol{\sigma}_i \notin \text{SU}(2) \tag{1.1.19}$$

and that the eigenvalues are ± 1 and eigenvectors

$$|\psi_x\rangle^+ = \frac{1}{\sqrt{2}} \begin{pmatrix} 1 \\ 1 \end{pmatrix} \quad |\psi_x\rangle^- = \frac{1}{\sqrt{2}} \begin{pmatrix} 1 \\ -1 \end{pmatrix} \quad (1.1.20)$$

$$|\psi_y\rangle^+ = \frac{1}{\sqrt{2}} \begin{pmatrix} 1 \\ i \end{pmatrix} \quad |\psi_y\rangle^- = \frac{1}{\sqrt{2}} \begin{pmatrix} 1 \\ -i \end{pmatrix} \quad (1.1.21)$$

$$|\psi_z\rangle^+ = \begin{pmatrix} 1 \\ 0 \end{pmatrix} \quad |\psi_z\rangle^- = \begin{pmatrix} 0 \\ 1 \end{pmatrix} \quad (1.1.22)$$

Definition 1.1.13. Let \mathbf{A} and \mathbf{B} be two arbitrary matrices. The **commutator** is defined as

$$[\mathbf{A}, \mathbf{B}] \triangleq \mathbf{AB} - \mathbf{BA} \quad (1.1.23)$$

Property 1.1.1. The Pauli matrices satisfy the following relation

$$[\boldsymbol{\sigma}_i, \boldsymbol{\sigma}_j] = 2i \sum_k \varepsilon_{ijk} \boldsymbol{\sigma}_k \quad (1.1.24)$$

which is different from zero is $i \neq j$. The Levi-Civita symbol ε is defined as

$$\varepsilon_{ijk} = \begin{cases} +1 & \text{if } (i, j, k) = (1, 2, 3), (2, 3, 1), (3, 1, 2) \\ -1 & \text{if } (i, j, k) = (2, 1, 3), (1, 3, 2), (3, 2, 1) \\ 0 & \text{otherwise} \end{cases}$$

Consequently, Pauli matrices **do not commute**.

1.1.5 Spectral decomposition

Theorem 1.1.4. Let \mathbf{A} be a Hermitian matrix², then its **spectral decomposition** is

$$\mathbf{A} = \sum_i \lambda_i |\psi_i\rangle\langle\psi_i| \quad (1.1.25)$$

where $|\psi_i\rangle$ are the eigenvectors of \mathbf{A} and λ_i the associated eigenvalues.

Proof. From the completeness relation and Equation 1.1.17:

$$\mathbf{A} = \mathbf{A}\mathbb{I} = \sum_{i=1}^n \mathbf{A} |\psi_i\rangle\langle\psi_i| = \sum_{i=1}^n \lambda_i |\psi_i\rangle\langle\psi_i|$$

²It is actually sufficient \mathbf{A} is normal.

□

In order to derive a simple relation to evaluate the exponential of a Pauli matrix, it is useful to introduce a generic projection operator.

Definition 1.1.14. Let λ_a be a generic eigenvalue of a Hermitian matrix \mathbf{A} and let $\{|\psi_{a,k}\rangle, (1 \leq k \leq g_a)\}$ be the distinct eigenvectors associated with λ_a (which has a *degeneracy* g_a). The **projection operator** to the g_a -subspace corresponding to λ_a is

$$\mathbf{P}_a = \frac{\prod_{m \neq a} (\mathbf{A} - \lambda_m \mathbb{I})}{\prod_{n \neq a} (\lambda_a - \lambda_n)} \quad (1.1.26)$$

The following theorem can be easily shown [5, p.21].

Theorem 1.1.5. Let f be an **analytic function** and \mathbf{A} a Hermitian matrix. Then

$$f(\mathbf{A}) = \sum_a f(\lambda_a) \mathbf{P}_a \quad (1.1.27)$$

Corollary 1.1.5.1. Let $\hat{\mathbf{n}} \in \mathbb{R}^3$ be a unit vector and $\alpha \in \mathbb{R}$. Then

$$e^{i\alpha \hat{\mathbf{n}} \boldsymbol{\sigma}} = \cos \alpha \cdot \mathbb{I} + i(\hat{\mathbf{n}} \boldsymbol{\sigma}) \sin \alpha \quad (1.1.28)$$

where $\boldsymbol{\sigma} = (\sigma_x \quad \sigma_y \quad \sigma_z)^t$

Proof. Let

$$\mathbf{A} = \hat{\mathbf{n}} \boldsymbol{\sigma} = n_x \sigma_x + n_y \sigma_y + n_z \sigma_z = \begin{pmatrix} n_z & n_x - in_y \\ n_x + in_y & -n_z \end{pmatrix}$$

The eigenvalues of \mathbf{A} are $\lambda_1 = +1$ and $\lambda_2 = -1$. According to definition 1.1.14, the projection operators are:

$$\begin{aligned} \mathbf{P}_1 &= \frac{\prod_{m \neq 1} (\mathbf{A} - \lambda_m \mathbb{I})}{\prod_{n \neq 1} (\lambda_1 - \lambda_n)} = \frac{\mathbf{A} - (-1)\mathbb{I}}{1 - (-1)} = \frac{\mathbf{A} + \mathbb{I}}{2} = \frac{1}{2} \begin{pmatrix} 1 + n_z & n_x - in_y \\ n_x + in_y & 1 - n_z \end{pmatrix} \\ \mathbf{P}_2 &= \frac{\prod_{m \neq 2} (\mathbf{A} - \lambda_m \mathbb{I})}{\prod_{n \neq 2} (\lambda_2 - \lambda_n)} = \frac{\mathbf{A} - (+1)\mathbb{I}}{-1 - (+1)} = \frac{\mathbf{A} - \mathbb{I}}{-2} = \frac{1}{2} \begin{pmatrix} 1 - n_z & -n_x + in_y \\ -n_x - in_y & 1 + n_z \end{pmatrix} \end{aligned}$$

Theorem 1.1.5 reads

$$\begin{aligned}
 e^{i\alpha\mathbf{A}} &= e^{i\alpha\lambda_1}\mathbf{P}_1 + e^{i\alpha\lambda_2}\mathbf{P}_2 \\
 &= \frac{e^{i\alpha}}{2} \begin{pmatrix} 1 + n_z & n_x - in_y \\ n_x + in_y & 1 - n_z \end{pmatrix} + \frac{e^{-i\alpha}}{2} \begin{pmatrix} 1 - n_z & -n_x + in_y \\ -n_x - in_y & 1 + n_z \end{pmatrix} \\
 &= \cos \alpha \cdot \mathbb{I} + i(\hat{\mathbf{n}}\boldsymbol{\sigma}) \sin \alpha
 \end{aligned}$$

□

1.1.6 Kronecker tensor product

The tensor product is a fundamental building operation of quantum systems.

Definition 1.1.15. Let \mathbf{A} be an $m \times n$ matrix and \mathbf{B} be a $p \times q$ matrix, then

$$\mathbf{A} \otimes \mathbf{B} = \begin{pmatrix} a_{11}\mathbf{B} & a_{12}\mathbf{B} & \cdots & a_{1n}\mathbf{B} \\ a_{21}\mathbf{B} & a_{22}\mathbf{B} & \cdots & a_{2n}\mathbf{B} \\ \vdots & \ddots & & \\ a_{m1}\mathbf{B} & a_{m2}\mathbf{B} & \cdots & a_{mn}\mathbf{B} \end{pmatrix}$$

is an $(mp) \times (nq)$ matrix. Formally, the matrix tensor product is a function

$$\otimes : \mathbb{C}^{m \times n} \times \mathbb{C}^{p \times q} \longrightarrow \mathbb{C}^{mp \times nq} \tag{1.1.29}$$

An example may be useful to clarify the introduced operation.

Example 1.1.1. Let

$$\mathbf{A} = \begin{pmatrix} a_{00} & a_{01} \\ a_{10} & a_{11} \end{pmatrix} \quad \mathbf{B} = \begin{pmatrix} b_{00} & b_{01} & b_{02} \\ b_{10} & b_{11} & b_{12} \\ b_{20} & b_{21} & b_{22} \end{pmatrix}$$

The tensor product $\mathbf{A} \otimes \mathbf{B}$ is obtained taking the scalar product of each element

of \mathbf{A} with the entire matrix \mathbf{B} :

$$\begin{aligned} \mathbf{A} \otimes \mathbf{B} &= \begin{pmatrix} a_{00} \cdot \begin{pmatrix} b_{00} & b_{01} & b_{02} \\ b_{10} & b_{11} & b_{12} \\ b_{20} & b_{21} & b_{22} \end{pmatrix} & a_{01} \cdot \begin{pmatrix} b_{00} & b_{01} & b_{02} \\ b_{10} & b_{11} & b_{12} \\ b_{20} & b_{21} & b_{22} \end{pmatrix} \\ a_{10} \cdot \begin{pmatrix} b_{00} & b_{01} & b_{02} \\ b_{10} & b_{11} & b_{12} \\ b_{20} & b_{21} & b_{22} \end{pmatrix} & a_{11} \cdot \begin{pmatrix} b_{00} & b_{01} & b_{02} \\ b_{10} & b_{11} & b_{12} \\ b_{20} & b_{21} & b_{22} \end{pmatrix} \end{pmatrix} \\ &= \begin{pmatrix} a_{00}b_{00} & a_{00}b_{01} & a_{00}b_{02} & a_{01}b_{00} & a_{01}b_{01} & a_{01}b_{02} \\ a_{00}b_{10} & a_{00}b_{11} & a_{00}b_{12} & a_{01}b_{10} & a_{01}b_{11} & a_{01}b_{12} \\ a_{00}b_{20} & a_{00}b_{21} & a_{00}b_{22} & a_{01}b_{20} & a_{01}b_{21} & a_{01}b_{22} \\ a_{10}b_{00} & a_{10}b_{01} & a_{10}b_{02} & a_{11}b_{00} & a_{11}b_{01} & a_{11}b_{02} \\ a_{10}b_{10} & a_{10}b_{11} & a_{10}b_{12} & a_{11}b_{10} & a_{11}b_{11} & a_{11}b_{12} \\ a_{10}b_{20} & a_{10}b_{21} & a_{10}b_{22} & a_{11}b_{20} & a_{11}b_{21} & a_{11}b_{22} \end{pmatrix} \end{aligned}$$

△

Property 1.1.2. The tensor product satisfies some properties which are exploited in the following:

- (I) $(\mathbf{A}_1 \otimes \mathbf{B}_1)(\mathbf{A}_2 \otimes \mathbf{B}_2)(\mathbf{A}_3 \otimes \mathbf{B}_3) = (\mathbf{A}_1\mathbf{A}_2\mathbf{A}_3 \otimes \mathbf{B}_1\mathbf{B}_2\mathbf{B}_3)$.
- (II) $\mathbf{A} \otimes (\mathbf{B} + \mathbf{C}) = \mathbf{A} \otimes \mathbf{B} + \mathbf{A} \otimes \mathbf{C}$.
- (III) $(\mathbf{A} \otimes \mathbf{B})^\dagger = \mathbf{A}^\dagger \otimes \mathbf{B}^\dagger$.
- (IV) $(\mathbf{A} \otimes \mathbf{B})^{-1} = \mathbf{A}^{-1} \otimes \mathbf{B}^{-1}$.
- (V) et \mathbf{A} be an $m \times m$ matrix and \mathbf{B} be a $p \times p$ matrix, then $\text{tr}(\mathbf{A} \otimes \mathbf{B}) = \text{tr}(\mathbf{A}) \cdot \text{tr}(\mathbf{B})$ and $\det(\mathbf{A} \otimes \mathbf{B}) = (\det(\mathbf{A}))^p \cdot (\det(\mathbf{B}))^m$.
- (VI) Let $|a\rangle, |b\rangle, |c\rangle, |d\rangle \in \mathbb{C}^n$, then

$$(|a\rangle \langle b|) \otimes (|c\rangle \langle d|) = (|a\rangle \otimes |c\rangle)(\langle b| \otimes \langle d|) = |ac\rangle \langle bd|$$

Theorem 1.1.6. Suppose \mathbf{A} is an $m \times m$ matrix with eigenvalues $\lambda_1, \dots, \lambda_n$ and associated eigenvectors $|\psi_1\rangle, \dots, |\psi_2\rangle$ and \mathbf{B} a $p \times p$ matrix with eigenvalues ζ_1, \dots, ζ_n and associated eigenvectors $|\phi_1\rangle, \dots, |\phi_2\rangle$. Then $\mathbf{A} \otimes \mathbf{B}$ has mp eigenvalues $\{\lambda_i \zeta_j\}$ and associated eigenvectors $\{|\psi_i \phi_j\rangle\}$

Proof. $|\psi_i\phi_j\rangle$ is an eigenvector of $\mathbf{A} \otimes \mathbf{B}$:

$$(\mathbf{A} \otimes \mathbf{B}) |\psi_i\phi_j\rangle = (\mathbf{A} \otimes \mathbf{B})(|\psi_i\rangle |\phi_j\rangle) = \mathbf{A} |\psi_i\rangle \otimes \mathbf{B} |\phi_j\rangle = \lambda_i \zeta_j |\psi_i\phi_j\rangle$$

$\lambda_i \zeta_j$ is the associated eigenvalue. Since there are mp eigenvectors, the vectors $|\psi_i\phi_j\rangle$ represent all and only the eigenvectors. \square

1.2 Quantum mechanics for quantum computation

When things get extremely small, classical mechanics fails to provide a faithful description of Nature. Quantum mechanics arose in the first decades of XXth century to explain experiments and observations which could not be understood applying classical physics. While a simple and engineer-oriented strongly recommended introduction to quantum mechanics can be found in [6], here just the concepts required by the quantum computing world are illustrated.

There are several “interpretations” of quantum mechanics, that is, the way which the mathematical formalism has to be understood. Here, the most common one is adopted, the **Copenhagen interpretation**, with a matrix formalism.

1.2.1 Fundamental postulates

The Copenhagen interpretation of quantum mechanics is founded on some postulates, which, by definition, cannot be proven theoretically but just accepted from experimental results. There is not a unique universally adopted set of postulates, and the choice depends on the author and the scenario. Here, a possible set is presented which is thought to be suitable for the quantum computation field. Other possible descriptions can be found in [5, 7, 8].

1.2.1.1 Wave function and superposition

Postulate 1.1. *Each physical system is associated with a complex Hilbert space \mathbb{H} . A pure state of the system is represented by a normalized vector $|\psi\rangle \in \mathbb{H}$, known as the **wavefunction**, which contains everything that can be known about the system before an observation. The linear combination of two states, that is their **superposition**, is a possible state of the system.*

Suppose that $\{|e_i\rangle\}, 1 \leq i \leq n$ represent a set of possible states of a system, for instance different locations (states) of a particle (system). Then a \mathbb{H}^n space is associated with the system and the superposition postulate says that the wavefunction before any observation is

$$|\psi\rangle = \sum_{i=1}^n c_i |e_i\rangle \quad (1.2.1)$$

where $c_i \in \mathbb{C}$ are complex weights known as **complex amplitudes**. The square

norm of the latter gives the **probability** that, after observation, that system collapses to a specific state: the wavefunction is a probability wave. According to this interpretation of the wavefunction, it is clear that

$$\sum_{i=1}^n |c_i|^2 = 1 \tag{1.2.2}$$

since the system must be found in *a* state. Coming back to the previous example, before observation, the particle is in a **linear combination** of all possible locations, like a wave. The complex numbers c_i say in which superposition the particle is currently in. Analogously, the wave function $|\psi\rangle$ can be thought as the **superposition** of n waves $|e_i\rangle$, each one contributing with intensity c_i .

Eventually, since, if observed, the particle must be found somewhere, the sum of the probabilities associated with all possible locations must be unitary.

There are two essential remarks about superposition which must be discussed. The first one is that the fact that the probability amplitudes are complex number is of striking importance. While classical probability allows only for real numbers between zero and one, quantum mechanics has probability amplitudes which can be positive, negative or complex. These amplitudes, before measurements, can interact and cancel each other out, giving rise to the phenomenon of **interference**³, which is one of the most important concepts in quantum mechanics and quantum information processing. The second remark is that superposition cannot be fully understood in classical terms. In the following, an experimental example is proposed to try to help the visualization of the phenomenon, but it is better to accept superposition as a new ontological category distinctive of quantum mechanics: it is a complex linear combination of different states.

This fact that a system is in a superposition of all possible states before an observation is performed and, then, when the observation is carried out, it decays to a specific state is rather counter-intuitive. Nevertheless, countless experiments have shown that the predictions of quantum mechanics are accurate, as the well known double-slit experiment. The arrangement prescribes the presence of a wall with two splits, behind which a screen is placed. Quantum particles, like electrons or photons, are fired against the wall, *one by one*, so that they cannot interact with each other. If no observation is performed before the wall, the particles arrive at the screen describing an interference plot, as reported in Figure 1.2. This can only be explained admitting the single particle which is fired lives in a superposition

³Give a look at [9].

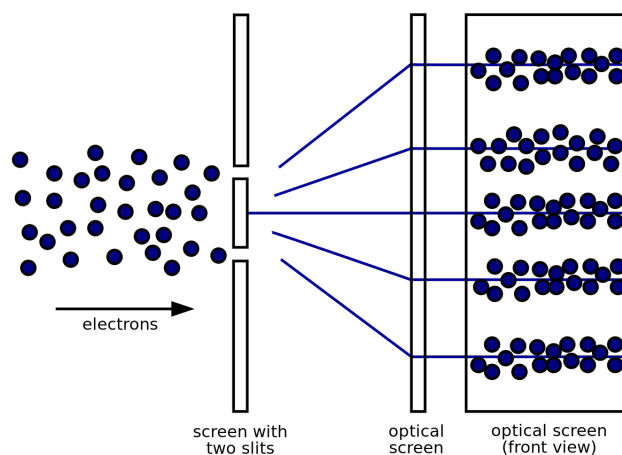


Figure 1.2: Double slit experiment with electrons. Note that electrons are fired one by one. Adapted from [10].

of states and, like a wave, can move through both slits simultaneously, giving rise to an interference path. Nevertheless, it is *not* an actual wave, since, if observed while moving through the wall, it will undoubtedly behave like a classical particle, that is, like a marble, it will move through a *single* slit.

In conclusion, a quantum system does live in a superposition of states.

1.2.1.2 Observables

Consider a generic system which can be found in several states, for instance a particle moving along a line. There are several *questions* which can be posed to the system: Which is your velocity? Which is your mass? Which is your position? and so on. Each question posed to the system, that is, each physical quantity which can be measured (or observed) is an **observable** of the system.

Postulate 1.2. *To each physical observable there corresponds a Hermitian operator acting on \mathbb{H} .*

Some observables and the related operators are reported in table 1.1, which are derived by similitude. In general the application of an operator to a ket changes the state. Nevertheless, according to definition 1.1.11 there are special states (that is ket) which are not changed by the action of the operator. These are the eigenstates of the operator.

Observable	Hermitian operator
Position	$\hat{\mathbf{r}} = \mathbf{r}$
Momentum	$\mathbf{p} = -i\hbar\nabla$
Kinetic energy	$\mathbf{T} = -\frac{\hbar^2}{2m}\nabla^2$
Potential energy	\mathbf{V}
Hamiltonian	$\mathbf{H} = \mathbf{V} + \mathbf{T}$
Angular momentum	$\mathbf{L} = -\mathbf{r} \times i\hbar\nabla$
Spin	$\mathbf{S} = \frac{\hbar}{2}\boldsymbol{\sigma}$
Total angular momentum	$\mathbf{J} = \mathbf{L} + \mathbf{S}$

Table 1.1: Main observables and related quantum operators.

1.2.1.3 Measurements

Postulate 1.3. *The only possible outcome of an observable a is one of the eigenvalues of the associated Hermitian operator \mathbf{A} . After the measurement is carried out, the state of the system **collapses** immediately to the eigenstate of \mathbf{A} associated with the measured eigenvalue.*

Property 1.2.1. The expectation value $\langle \mathbf{A} \rangle$ of a is

$$\langle \mathbf{A} \rangle = \langle \psi | \mathbf{A} | \psi \rangle \quad (1.2.3)$$

Proof. Let $\{|\lambda_i\rangle\}$ be the eigenvectors of \mathbf{A} and $\{\lambda_i\}$ the associated eigenvalues. Since \mathbf{A} is Hermitian, according to theorem 1.1.4

$$\mathbf{A} = \sum_i \lambda_i |\lambda_i\rangle\langle\lambda_i|$$

Expanding $|\psi\rangle$ in terms of the eigenvectors $|\lambda_i\rangle$ of \mathbf{A}

$$|\psi\rangle = \sum_i c_i |\lambda_i\rangle$$

then

$$\langle \psi | \mathbf{A} | \psi \rangle = \sum_{i,j} c_j^* c_i \langle \lambda_j | \mathbf{A} | \lambda_i \rangle = \sum_{i,j} c_j^* c_i \lambda_i \delta_{i,j} = \sum_i \lambda_i |c_i|^2$$

According to the interpretation of the wavefunction, $|c_i|^2$ represents the probability p_i that the outcome of the measurement operation is λ_i . Since the eigenvalues λ_i represent all and only the possible outcomes, the previous expression is in the form

$$\sum_i p_i \lambda_i$$

which is the well known definition of the expectation value of a random variable with a finite number of finite outcomes λ_i occurring with probabilities p_i , respectively. \square

As previously stated, any possible outcome λ_i is found with a probability $|c_i|^2$, which can be expressed as

$$|c_i|^2 = \langle \psi | \mathbf{P}_i | \psi \rangle \quad (1.2.4)$$

where

$$\mathbf{P}_i = |\lambda_i\rangle\langle\lambda_i| \quad (1.2.5)$$

is the projection operator, which *projects* $|\psi\rangle$ to the eigenstate associated with the eigenvector $|\lambda_i\rangle$

$$\frac{\mathbf{P}_i |\psi\rangle}{\sqrt{\langle \psi | \mathbf{P}_i | \psi \rangle}} \quad (1.2.6)$$

Proof. The probability is easily shown

$$\langle \psi | \mathbf{P}_i | \psi \rangle = \left(\sum_k c_k^* \langle \lambda_k | \right) |\lambda_i\rangle\langle\lambda_i| \left(\sum_k c_k |\lambda_k\rangle \right) = c_i^* c_i = |c_i|^2$$

If the measured outcome is λ_i , the system must collapse to state λ_i , which is an eigenvector of \mathbf{A} :

$$\frac{\mathbf{P}_i |\psi\rangle}{\sqrt{\langle \psi | \mathbf{P}_i | \psi \rangle}} = \frac{c_i |\lambda_i\rangle}{\sqrt{|c_i|^2}} \sim |\lambda_i\rangle$$

since a quantum state is defined up to a general phase factor. \square

In summary, given an observable a , the possible outcomes of a measurement are the eigenvalues of the associated Hermitian operator \mathbf{A} . As soon as the measurement is carried out, the system is no longer in a superposition of states but collapses to the eigenstate associated with the measured eigenvalue. The probability with which a specific outcome is found is obtained resorting to the projection operator, which is built starting from the eigenvectors of \mathbf{A} .

Example 1.2.1. Let the system be described by the state vector

$$|\psi\rangle = c_0 |e_0\rangle + c_1 |e_1\rangle$$

where $|e_0\rangle$ and $|e_1\rangle$ realize an orthonormal basis. Let a be an observable which acts on the system and let \mathbf{A} be the associated Hermitian operator. Suppose that

$$\mathbf{A} |\lambda\rangle = \lambda |\lambda\rangle$$

so that the eigenvalue is λ when the system is in state $|\lambda\rangle$. With which probability would one obtain the value λ ?

The first step is to build the projection operator

$$\mathbf{P}_\lambda = |\lambda\rangle\langle\lambda|$$

Next, according to Equation 1.2.4, one can evaluate the probability as

$$\begin{aligned} p_\lambda &= \langle\psi|\mathbf{P}_\lambda|\psi\rangle = |\langle\lambda|\psi\rangle|^2 = |c_0\langle\lambda|e_0\rangle + c_1\langle\lambda|e_1\rangle|^2 = \\ &= |c_0\langle\lambda|e_0\rangle|^2 + |c_1\langle\lambda|e_1\rangle|^2 + 2\operatorname{Re}\{c_0c_1^*\langle\lambda|e_0\rangle\langle\lambda|e_1\rangle^*\} \end{aligned}$$

where the last term is an interference term. △

The previous discussion holds true for a closed system where the possible outcomes of a measurement are strictly orthogonal (being the eigenvectors of a Hermitian operator). In this case, the measurement is said to be **projective**⁴. If, on the other hand, the system is open⁵, one has to define a more general operator instead of the simple projection operator.

Definition 1.2.1. The measurement operator \mathbf{M} is defined such that the probability of measuring ζ is

$$p(\zeta) = \langle\psi|\mathbf{M}_\zeta^\dagger\mathbf{M}_\zeta|\psi\rangle \quad (1.2.7)$$

and the state, immediately after the measurement, collapses to

$$|\zeta\rangle = \frac{\mathbf{M}_\zeta|\psi\rangle}{\sqrt{p(\zeta)}} \quad (1.2.8)$$

Moreover, since the total probability must be unitary, the measurement operators must satisfy the completeness relation

$$\sum_{\zeta} \mathbf{M}_\zeta^\dagger\mathbf{M}_\zeta = \mathbb{I} \quad (1.2.9)$$

Example 1.2.2. Let

$$|0\rangle = \begin{pmatrix} 1 \\ 0 \end{pmatrix} \quad |1\rangle = \begin{pmatrix} 0 \\ 1 \end{pmatrix}$$

and assume

$$|\psi\rangle = \alpha|0\rangle + \beta|1\rangle$$

⁴More details in [11]

⁵In short, a closed quantum system is an idealized isolated system while an open system is a system which interacts with the environment.

which are the (orthogonal) eigenstates of the operator σ_z and so they realize an orthonormal basis of \mathbb{H}^2 . When a measurement is performed, the state vector is projected to one of the basis vectors.

The measurement operators can be formally defined as follows.

$$\mathbf{M}_0 = \begin{pmatrix} a & b \\ c & d \end{pmatrix}$$

since

$$\begin{aligned} p(0) &= \langle 0 | \begin{pmatrix} a^* & c^* \\ b^* & d^* \end{pmatrix} \cdot \begin{pmatrix} a & b \\ c & d \end{pmatrix} | 0 \rangle = |a|^2 + |c|^2 = 1 \\ p(1) &= \langle 1 | \begin{pmatrix} a^* & c^* \\ b^* & d^* \end{pmatrix} \cdot \begin{pmatrix} a & b \\ c & d \end{pmatrix} | 1 \rangle = |b|^2 + |d|^2 = 0 \end{aligned}$$

and the operator must be Hermitian, it follows that

$$\mathbf{M}_0 = \begin{pmatrix} 1 & 0 \\ 0 & 0 \end{pmatrix} = |0\rangle\langle 0| = \mathbf{P}_0$$

Analogously

$$\mathbf{M}_1 = \begin{pmatrix} 0 & 0 \\ 0 & 1 \end{pmatrix} = |1\rangle\langle 1| = \mathbf{P}_1$$

which coincide with the projection operators. This is a general result: when the system is closed, the measurement operators coincide with the projection operators.

The probability can be computed as

$$p(0) = \langle \psi | \mathbf{M}_0^\dagger \mathbf{M}_0 | \psi \rangle = \langle \psi | 0 \rangle \langle 0 | 0 \rangle \langle 0 | \psi \rangle = \alpha^* \cdot 1 \cdot \alpha = |\alpha|^2$$

and immediately after the measurement, the system collapses to

$$\frac{\mathbf{M}_0 |\psi\rangle}{\sqrt{p(0)}} = \frac{\alpha}{|\alpha|} \sim |0\rangle$$

△

There is an interesting aspect concerning quantum system measurements which is still missing. Consider, for the sake of concreteness, a marble traveling according

to a given trajectory. It is definitely reasonable to ask the marble about its velocity *and* its position at the same instant of time. In the same fashion, a car can be found to travel at 50 km h^{-1} when it is in Corso Duca degli Abruzzi 24, in Torino. There is nothing strange about that. Nevertheless, this is no longer the case for quantum systems.

Theorem 1.2.1. *Let a and b be two observables and \mathbf{A} and \mathbf{B} the associated Hermitian operators. The variances are defined as*

$$\begin{aligned}\sigma_A^2 &= \langle \mathbf{A}^2 \rangle - \langle \mathbf{A} \rangle^2 \\ \sigma_B^2 &= \langle \mathbf{B}^2 \rangle - \langle \mathbf{B} \rangle^2\end{aligned}$$

The Heisenberg's uncertainty principle states that

$$\sigma_A^2 \sigma_B^2 \geq \left(\frac{1}{2i} \langle [\mathbf{A}, \mathbf{B}] \rangle \right)^2 \quad (1.2.10)$$

The proof of this principle is reported in all classical quantum mechanics book, as [12, p.112]. At first sight, the inequality may seem trivially satisfied by the fact that $i^2 = -1$. However, the following property holds true.

Property 1.2.2. The expected value of the commutator of two Hermitian operators is always purely imaginary.

Proof. Let \mathbf{A} and \mathbf{B} be two Hermitian operators. Then by definition

$$[\mathbf{A}, \mathbf{B}] = \mathbf{A}\mathbf{B} - \mathbf{B}\mathbf{A}$$

the Hermitian conjugate is

$$[\mathbf{A}, \mathbf{B}]^\dagger = (\mathbf{A}\mathbf{B})^\dagger - (\mathbf{B}\mathbf{A})^\dagger = \mathbf{B}^\dagger \mathbf{A}^\dagger - \mathbf{A}^\dagger \mathbf{B}^\dagger = \mathbf{B}\mathbf{A} - \mathbf{A}\mathbf{B} = -[\mathbf{A}, \mathbf{B}]$$

where the definition of Hermitian operator has been exploited. Since

$$[\mathbf{A}, \mathbf{B}]^\dagger = -[\mathbf{A}, \mathbf{B}] \quad (1.2.11)$$

the commutator of two Hermitian operators is said to be *anti-Hermitian*. Now, the expectation value of an anti-Hermitian operator is known to be imaginary. As a matter of fact, let \mathbf{C} be an anti-Hermitian operator $\mathbf{C}^\dagger = -\mathbf{C}$ with eigenvalues

c_i and associated eigenvectors $|c_i\rangle$. Then

$$\begin{aligned}\mathbf{C} |c_i\rangle &= c_i |c_i\rangle \\ \langle c_i| \mathbf{C}^\dagger &= -\langle c_i| \mathbf{C} = -c_i^* \langle c_i|\end{aligned}$$

so

$$\langle c_i| \mathbf{C} |c_i\rangle = c_i \langle c_i|c_i\rangle = -c_i^* \langle c_i|c_i\rangle \implies c_i = -c_i^* \implies \text{Re}\{c_i\} = 0$$

which means that the eigenvalues are imaginary. It follows that if \mathbf{C} is anti-Hermitian, then $i\mathbf{C}$ must be Hermitian. Repeating the step proposed in the proof of property 1.2.1, one immediately gets that the expectation value of an anti-Hermitian operator can be written as the sum of its eigenvalues. Consequently, the expectation value of an anti-Hermitian operator is imaginary. \square

The Heisenberg's principle states that the commutator of two operators says how good a simultaneous measure of the two associated observables can possibly be. If the two operators have non-zero commutator, i.e., they *do not commute*, Nature enforces a limit to the accuracy with which the observables can be simultaneously known.

Example 1.2.3. Consider a particle in a unidimensional reference system described by the wavefunction $|\psi\rangle$ and imagine one wants to measure the position and the momentum of the particle. From table 1.1

$$[\mathbf{x}, \mathbf{p}] |\psi\rangle = -i\hbar x \frac{\partial}{\partial x} |\psi\rangle + i\hbar \frac{\partial}{\partial x} (x |\psi\rangle) = \frac{\hbar}{i} \left[x \frac{\partial |\psi\rangle}{\partial x} - x \frac{\partial |\psi\rangle}{\partial x} - |\psi\rangle \right] = i\hbar |\psi\rangle$$

from which

$$[\mathbf{x}, \mathbf{p}] = i\hbar$$

so the two operators do **not** commute and it is not possible to know the position and the velocity of a quantum particle simultaneously with arbitrary accuracy. The Heisenberg's principle sets an upper limit to the accuracy:

$$\sigma_x^2 \sigma_p^2 \geq \left(\frac{\hbar}{2}\right)^2 \implies \sigma_x \sigma_p \geq \frac{\hbar}{2}$$

The point is that the wavefunction $|\psi\rangle$ can be written in many orthonormal bases, corresponding to different observables. When $|\psi\rangle$ is thought as a wave, it can be decomposed into sinusoids, whose position is totally undermined but whose

wavelength is well known. This is the momentum basis⁶. On the other hand, when $|\psi\rangle$ is thought as a particle, it is decomposed into the position basis, which is made of “peaks”, that is, of vectors which are zero everywhere but in a point. In this case, the position is well known, while the momentum is undermined. This is usually summarized saying that non commuting operators do not have a complete set of eigenfunctions. \triangle

Example 1.2.4. Consider a spin- $\frac{1}{2}$ particle and suppose one wants to determine the spin vector. The Hermitian operators associated with the three components of the vector are the Pauli matrices. As stated in §1.1.12, Pauli matrices do **not** commute, so it is **not** possible to measure the three components of the spin vector simultaneously. \triangle

1.2.1.4 Schrödinger equation

Postulate 1.4. *The time evolution of a state is ruled by the Schrödinger equation:*

$$i\hbar \frac{\partial |\psi\rangle}{\partial t} = \mathcal{H} |\psi\rangle \quad (1.2.12)$$

where \mathcal{H} is the Hamiltonian, that is, the Hermitian operator associated with the total energy of the system.

The case in which the Hamiltonian is time independent is of particular interest. The following result holds true.

Property 1.2.3. If the Hamiltonian is time independent, the Schrödinger equation is formally solved as

$$|\psi(t)\rangle = \exp\left(-\frac{\mathcal{H}t}{\hbar}\right) |\psi(0)\rangle \triangleq \mathbf{U}(t) |\psi(0)\rangle \quad (1.2.13)$$

⁶The relation between momentum p and wavelength λ is given by the well known De Broglie's equation $\lambda = \frac{h}{p}$.

where the **time evolution operator** is

$$U(t) = \exp\left(-\frac{\mathcal{H}t}{\hbar}\right) \quad (1.2.14)$$

Proof. First, the Hamiltonian is an operator, which is represented on a proper basis by a matrix. The matrix exponential is defined as

$$e^{\mathbf{A}} = \sum_{k=0}^{\infty} \frac{\mathbf{A}^k}{k!} = \mathbb{I} + \mathbf{A} + \frac{\mathbf{A}^2}{2!} + \frac{\mathbf{A}^3}{3!} + \dots$$

Next, assuming \mathbf{A} is time independent, the derivative of the matrix exponential is

$$\begin{aligned} \frac{de^{\mathbf{A}t}}{dt} &= \lim_{\delta \rightarrow 0} \frac{e^{\mathbf{A}(t+\delta)} - e^{\mathbf{A}t}}{\delta} = e^{\mathbf{A}t} \left[\lim_{\delta \rightarrow 0} \frac{e^{\mathbf{A}\delta} - \mathbb{I}}{\delta} \right] \\ &= e^{\mathbf{A}t} \left[\lim_{\delta \rightarrow 0} \frac{1}{\delta} \left(\mathbf{A}\delta + \frac{\mathbf{A}^2\delta^2}{2!} + \dots \right) \right] = e^{\mathbf{A}t} \mathbf{A} = \mathbf{A}e^{\mathbf{A}t} \end{aligned}$$

where the last equality is obvious from the definition of matrix exponential.

Replacing 1.2.13 in 1.2.12 yields

$$\begin{aligned} i\hbar \frac{\partial |\psi\rangle}{\partial t} &= \mathcal{H} |\psi\rangle \\ i\hbar \frac{\partial (e^{-\mathcal{H}t/\hbar} |\psi(0)\rangle)}{\partial t} &= \mathcal{H} e^{-\mathcal{H}t/\hbar} |\psi(0)\rangle \\ i\hbar |\psi(0)\rangle \left(-\frac{i\mathcal{H}}{\hbar} \right) e^{-\mathcal{H}t/\hbar} &= \mathcal{H} e^{-\mathcal{H}t/\hbar} |\psi(0)\rangle \\ \mathcal{H} e^{-\mathcal{H}t/\hbar} |\psi(0)\rangle &= \mathcal{H} e^{-\mathcal{H}t/\hbar} |\psi(0)\rangle \end{aligned}$$

□

The time evolution operator is obviously **unitary** since

$$UU^\dagger = \exp\left(-\frac{\mathcal{H}t}{\hbar}\right) \exp\left(+\frac{\mathcal{H}t}{\hbar}\right) = \mathbb{I} \quad (1.2.15)$$

and so the time evolution preserves the total unitary probability of the wavefunction.

1.2.2 The wavefunction and the state vector

It is more rigorous to refer to the ket $|\psi\rangle$ as the **state-vector** of the system, rather than the wavefunction. However, starting from the ket, one can extract a complex scalar function relative to a specific basis [13]. Let \mathbb{H} be a Hilbert space spanned by the complete basis set of the position operator $|r_i\rangle$. The state vector, being an inhabitant of the same Hilbert space, can be written with respect to the position eigenbasis as

$$|\psi\rangle = \sum_i \langle r_i|\psi\rangle |r_i\rangle \quad (1.2.16)$$

If the basis set tends to a *continuous* basis set, then

$$|\psi\rangle = \sum_i \langle r_i|\psi\rangle |r_i\rangle \longrightarrow \int \langle r|\psi\rangle |r\rangle dr \quad (1.2.17)$$

The expression $\langle r|\psi\rangle$ means that $|\psi\rangle$ is written in the position eigenbasis, without explicitly identify the eigenvector $|r_i\rangle$: for different $|r_i\rangle$, the inner product outputs different numbers. In practice, $|\psi\rangle$ is expressed as a function of $|r\rangle$. The **wavefunction** is customarily defined as the following complex scalar function

$$\psi(\mathbf{r}) = \langle r|\psi\rangle \quad (1.2.18)$$

so that

$$|\psi\rangle = \int \psi(\mathbf{r}) |r\rangle dr \quad (1.2.19)$$

The inner product of two state vectors expressed with respect to the position eigenbasis can be written as

$$\langle \phi|\psi\rangle = \int \langle \phi|r\rangle \langle r|r\rangle \langle r|\psi\rangle dr = \int \phi^*(\mathbf{r})\psi(\mathbf{r}) dr \quad (1.2.20)$$

Finally, consider the linear operator \mathbf{A} acting on the ket $|\psi\rangle$. Since $\mathbf{A}|\psi\rangle$ is a vector, it can be expanded in the position eigenbasis as Equation 1.2.18, obtaining

$$\mathbf{A}\psi(\mathbf{r}) = \langle r|\mathbf{A}|\psi\rangle \quad (1.2.21)$$

Thus, the expectation value of \mathbf{A} is simply

$$\langle \psi|\mathbf{A}|\psi\rangle = \int \psi^*(\mathbf{r})\mathbf{A}\psi(\mathbf{r})dr \quad (1.2.22)$$

1.2.3 Assembled systems, entanglement and superposition

So far, only single-component systems have been discussed. It is clear that a system made of a single component cannot be actually useful to perform some quantum computation. It would be somehow similar to have a single bit to perform classic electronic computation. So, it is mandatory to deal with multipartite systems, that is, with systems made of many components. Suppose, for instance, a system is made of two elements: the first one lives in the Hilbert space \mathbb{H}_1^n which has an orthonormal basis $\{e_{1,i}\}$ and the second one lives in the Hilbert space \mathbb{H}_2^m which has an orthonormal basis $\{e_{2,i}\}$. The whole system is an inhabitant of

$$\mathbb{H} = \mathbb{H}_1 \otimes \mathbb{H}_2 \in \mathbb{C}^{nm} \quad (1.2.23)$$

and is described by the wavefunction

$$|\psi\rangle = \sum_{i,j} c_{i,j} |e_{1,i}\rangle \otimes |e_{2,j}\rangle = \sum_{i,j} c_{i,j} |e_{1,i}, e_{2,j}\rangle \quad (1.2.24)$$

The result is trivially extended to systems composed of N elements.

For the sake of clearness, consider two independent particles, each one being allowed only two points:

$$|\psi_a\rangle = a_0 |x_0\rangle + a_1 |x_1\rangle \in \mathbb{H}_1^2 \quad (1.2.25)$$

$$|\psi_b\rangle = b_0 |x_0\rangle + b_1 |x_1\rangle \in \mathbb{H}_2^2 \quad (1.2.26)$$

Now, suppose to “merge” the two quantum systems in a single quantum system. The latter belongs to

$$\mathbb{H} = \mathbb{H}_1 \otimes \mathbb{H}_2 \in \mathbb{C}^4 \quad (1.2.27)$$

One would be tempted to say that *each* generic state vector of the assembled system can be rewritten as as the tensor product of two state vectors, one coming from the first quantum system, the other from the second. That is

$$|\psi\rangle = |\psi_a\rangle \otimes |\psi_b\rangle$$

However, this is **not true**. For example, let

$$|\psi\rangle = |x_0\rangle \otimes |y_0\rangle + |x_1\rangle \otimes |y_1\rangle \quad (1.2.28)$$

this is a legal inhabitant of $\mathbb{H} = \mathbb{H}_1 \otimes \mathbb{H}_2$ but it turns out that it cannot be

rewritten as the tensor product of two state vectors. As a matter of fact

$$|\psi_a\rangle \otimes |\psi_b\rangle = a_0b_0|x_0y_0\rangle + a_0b_1|x_0y_1\rangle + a_1b_0|x_1y_0\rangle + a_1b_1|x_1y_1\rangle \quad (1.2.29)$$

In order to satisfy Equation 1.2.28, one would have to solve

$$\begin{cases} a_0b_0 = a_1b_1 = 1 \\ a_0b_1 = a_1b_0 = 0 \end{cases} \quad (1.2.30)$$

which, clearly, does not actually admit any solution. Consequently, there are states which cannot be rewritten as the tensor product of states belonging to subsystems. These states are known as entangled states.

Definition 1.2.2. A state is said to be **entangled** if it cannot be written as the tensor product of two states. Otherwise, it is said to be **separable**.

Entangled states cannot be classically described. They represent a peculiar characteristic of quantum systems and their exploitation is a powerful resource for quantum computation. Nonetheless, it is definitely not trivial to classify entangled state. Some hints are reported in [5], even if nowadays, no method is known when the system is composed of three or more components.

Going a little bit deeper in the entanglement business may help the understanding of the topics which are presented in next chapters. It is clear the the dimension of the set of separable states $\mathbb{H}_1 \cdots \mathbb{H}_N$ is

$$\sum_{i=1}^N \dim \mathbb{H}_i \quad (1.2.31)$$

while

$$\dim \mathbb{H} = \dim (\mathbb{H}_1 \otimes \mathbb{H}_2 \otimes \cdots \otimes \mathbb{H}_N) = \prod_{i=1}^N \dim \mathbb{H}_i \quad (1.2.32)$$

In general

$$\prod_{i=1}^N \dim \mathbb{H}_i \gg \sum_{i=1}^N \dim \mathbb{H}_i \quad (1.2.33)$$

which means that most states in a multipartite system are entangled. As hinted in Equation 1.2.24, the most general state vector of \mathbb{H} is expressed as a linear combination of some complex coefficients and the tensor product of the basis vectors of $\mathbb{H}_1 \cdots \mathbb{H}_N$. In other words, the basis vectors of \mathbb{H} are given by the tensor product of the basis vectors of the subsystem. The point is that $|\psi\rangle \in \mathbb{H}$ can be any

arbitrary superposition of the basis vectors: many of these superpositions cannot be expressed taking the tensor product of the basis vectors of the subsystems. This means that an entangled state is a legitimate state of the system as a whole, but it is **impossible to attribute to the subsystems a definite pure state**.

The measurement of entangled states deserves some extra words. Consider again the case described by Equation 1.2.28 and suppose to perform a measurement on the first particle. Suppose also that the particle is found, immediately after the measurement, to live in $|x_0\rangle$. Then, *necessarily*, the second particle *must* collapse to state $|y_0\rangle$. In other words, a measurement performed on a particle causes the wavefunction of the whole system to collapse so that also the second particle collapses to an unequivocally defined state. No matter the actual distance in space between the two particles.

1.2.4 Mixed states and density matrix formalism

In many cases of interest, it happens that a quantum system is not just in state $|\psi\rangle$, but is in state $|\psi_i\rangle$ with probability p_i , which are properly normalized. It is of fundamental importance to avoid confusion between the probabilistic behaviour of $|\psi\rangle$ (the outcome of a measurement is a certain state with a probability which is the square of the related complex amplitude) with the stochastic nature of the system which has a certain (semi-classical) probability to be in a given state. The prefix *semi* is added since, according to [14], the values p_i cannot truly be understood as classical probabilities. Indeed, in classical probability, one can assign probabilities only to mutually exclusive events. On the other hand, the states $|\psi_i\rangle$ are distinguishable but not necessarily exclusive. As a matter of fact, there exist states which are linear superpositions of other states. Thus, the $|\psi_i\rangle$ are, in general, not an orthogonal basis of \mathbb{H}^n .

A well-known example is a collection of independent spins- $\frac{1}{2}$ (an *ensemble*). At any instant of time, different spins have different “orientations” (i.e, in a different state) and the total nuclear magnetization is the sum of the contributions from the individual spins. In these cases, the state is said to be **mixed**, in contrast with the **pure** states. When dealing with mixed states, the most suitable approach is to describe the system not by means of a simple state vector $|\psi\rangle$ as for pure states, but by means of a so-called density operator. How is this operator defined?

As known from property 1.2.1, the expectation value of an operator \mathbf{A} for the fraction p_i of the ensemble which is in state $|\psi_i\rangle$ is

$$\langle \mathbf{A} \rangle = \langle \psi_i | \mathbf{A} | \psi_i \rangle \quad (1.2.34)$$

Since $|\psi_i\rangle$ appears with probability p_i , the expectation value of \mathbf{A} is naturally written as

$$\langle \mathbf{A} \rangle = \sum_i p_i \langle \psi_i | \mathbf{A} | \psi_i \rangle \quad (1.2.35)$$

The state vector can be expressed according to an orthonormal basis as

$$|\psi\rangle = \sum_i c_i |e_i\rangle \quad (1.2.36)$$

which allows to rewrite the previous expression as

$$\langle \mathbf{A} \rangle = \sum_{n,m} \overline{c_n c_m^*} \langle e_m | \mathbf{A} | e_n \rangle \quad (1.2.37)$$

There are three remarks which are in order. First, the kets $|e_m\rangle$ and $|e_n\rangle$ are not necessarily eigenvectors of \mathbf{A} . Second, the probability p_i is “embedded” in the average value $\overline{c_n c_m^*}$. Third, it is interesting to highlight that, for a given basis set, the terms $\langle e_m | \mathbf{A} | e_n \rangle$ are constants and, so, the expected value of \mathbf{A} depends only on the products $c_n c_m^*$. The latter can be conveniently arranged to form a matrix.

Definition 1.2.3. The **density matrix** is the matrix representation of the density operator ρ , such that

$$\rho_{nm} = \overline{c_n c_m^*} \quad (1.2.38)$$

The general expression for the density matrix is

$$\rho = \sum_i p_i |\psi_i\rangle\langle\psi_i| \quad (1.2.39)$$

The physical state is completely described by the associated density matrix.

1.2.4.1 Properties of the density operator

Theorem 1.2.2. *Let a be an observable and \mathbf{A} the associated Hermitian operator. Assume the state of the system is described by the density matrix ρ . Then the expectation value⁷ of \mathbf{A} is*

$$\langle \mathbf{A} \rangle = \text{tr}(\rho \mathbf{A}) \quad (1.2.40)$$

Proof. Let Ω be the matrix associated with an operator with respect to a basis $|e_i\rangle$. The trace of Ω is, by definition, the sum of the elements of the main diagonal, that is

$$\text{tr}(\Omega) = \sum_i \langle e_i | \Omega | e_i \rangle$$

Since the expectation value of \mathbf{A} is

$$\langle \mathbf{A} \rangle = \sum_i p_i \langle \psi_i | \mathbf{A} | \psi_i \rangle$$

exploiting the completeness relation, the previous equation can be rewritten as

$$\sum_i p_i \langle \psi_i | \mathbf{A} | \psi_i \rangle = \sum_i p_i \langle \psi_i | \mathbf{A} \mathbb{I} | \psi_i \rangle = \sum_{i,k} p_i \langle \psi_i | \mathbf{A} | e_k \rangle \langle e_k | | \psi_i \rangle$$

⁷Strictly speaking, the right hand side is not the expectation value, but the statistical average contribution of each ensemble member to the final macroscopic result.

Since $\langle e_k | \psi_i \rangle$ is just a number

$$\sum_{i,k} p_i \langle \psi_i | \mathbf{A} | e_k \rangle \langle e_k | \psi_i \rangle = \sum_{i,k} p_i \langle e_k | \psi_i \rangle \langle \psi_i | \mathbf{A} | e_k \rangle$$

exploiting the definition of trace and the linearity

$$\langle \mathbf{A} \rangle = \sum_i p_i \text{tr}(|\psi_i\rangle\langle\psi_i| \mathbf{A}) = \text{tr} \left(\sum_i p_i |\psi_i\rangle\langle\psi_i| \mathbf{A} \right) = \text{tr}(\boldsymbol{\rho} \mathbf{A}) \quad (1.2.41)$$

□

It is clear that the elements on the main diagonal are the probabilities to find the system in a basis state. Since the sum of probabilities must be unitary, one can imagine that the density matrix has unit trace. As a matter of fact, the following property holds true.

Property 1.2.4. The **trace** of a density matrix is unitary.

$$\text{tr}(\boldsymbol{\rho}) = 1 \quad (1.2.42)$$

Proof.

$$\begin{aligned} \text{tr}(\boldsymbol{\rho}) &= \text{tr} \left(\sum_i p_i |\psi_i\rangle\langle\psi_i| \right) = \sum_{i,k} p_i \langle e_k | \psi_i \rangle \langle \psi_i | e_k \rangle \\ &= \sum_i p_i \langle \psi_i | \left(\sum_k |e_k\rangle\langle e_k| \right) | \psi_i \rangle = \sum_i p_i \langle \psi_i | \psi_i \rangle \end{aligned}$$

□

Property 1.2.5. The density matrix is a **Hermitian** operator.

$$\boldsymbol{\rho} = \boldsymbol{\rho}^\dagger \quad (1.2.43)$$

Proof. The proof follows immediately from the fact that p_i is real and $|\psi_i\rangle\langle\psi_i| = |\psi_i\rangle\langle\psi_i|^\dagger$. □

Property 1.2.6. The density matrix is **positive semi-definite**. Consequently, all its eigenvalues are non-negative.

Proof. For a generic vector $|\zeta\rangle$

$$\langle \zeta | \boldsymbol{\rho} | \zeta \rangle = \sum_i p_i \langle \zeta | \psi_i \rangle \langle \psi_i | \zeta \rangle = \sum_i p_i |\langle \psi_i | \zeta \rangle|^2 \geq 0$$

□

Finally, in case of a **pure state**

$$\rho = |\psi\rangle\langle\psi| \quad (1.2.44)$$

Theorem 1.2.3. *A state ρ is pure if and only if $\rho^2 = \rho$.*

Proof. According to property 1.2.5, ρ is Hermitian and so its eigenvectors are orthogonal (Cf. theorem 1.1.3).

If $\rho^2 = \rho$ then ρ is a pure state Assume ρ admits the following spectral decomposition

$$\rho = \sum_i \lambda_i |\lambda_i\rangle\langle\lambda_i|$$

since

$$\rho^2 = \rho \implies \sum_i \lambda_i |\lambda_i\rangle\langle\lambda_i| = \sum_i \lambda_i^2 |\lambda_i\rangle\langle\lambda_i|$$

it must be true that $\lambda_i = \lambda_i^2$, that is

$$\lambda_i = \begin{cases} 0 \\ 1 \end{cases}$$

Since, according to property 1.2.4

$$\text{tr}(\rho) = \sum_i \lambda_i = 1$$

it follows that $\lambda_\chi = 1$ for some χ and $\lambda_i = 0$ for $i \neq \chi$. This implies that ρ is a pure state $|\lambda_\chi\rangle\langle\lambda_\chi|$.

If ρ is a pure state then $\rho^2 = \rho$ Let

$$\rho = |\psi\rangle\langle\psi|$$

then

$$\rho^2 = |\psi\rangle\langle\psi| |\psi\rangle\langle\psi| = |\psi\rangle \langle\psi|\psi\rangle \langle\psi| = \rho$$

□

1.2.4.2 Time evolution

The following theorem describes the time evolution of a system represented by a density matrix.

Theorem 1.2.4. *The temporal evolution of a system described by a density matrix ρ is given by the **Liouville - von Neumann equation***

$$i\hbar \frac{d\rho}{dt} = [\mathcal{H}, \rho] \quad (1.2.45)$$

Proof. Each $|\psi_i\rangle$ follows the Schrödinger equation

$$i\hbar \frac{d|\psi_i\rangle}{dt} = \mathcal{H}|\psi_i\rangle$$

the Hermitian conjugate is

$$-i\hbar \frac{d\langle\psi_i|}{dt} = \langle\psi_i| \mathcal{H}$$

consequently, the time derivative of the density matrix is simply

$$\begin{aligned} i\hbar \frac{d\rho}{dt} &= i\hbar \sum_i p_i \frac{d}{dt} (|\psi_i\rangle\langle\psi_i|) = i\hbar \sum_i p_i \left(\frac{d|\psi_i\rangle}{dt} \langle\psi_i| + |\psi_i\rangle \frac{d\langle\psi_i|}{dt} \right) \\ &= i\hbar \sum_i p_i (\mathcal{H}|\psi_i\rangle\langle\psi_i| - |\psi_i\rangle\langle\psi_i| \mathcal{H}) = \mathcal{H}\rho - \rho\mathcal{H} = [\mathcal{H}, \rho] \end{aligned}$$

□

As it is routinely done for pure states, also the time evolution of mixed states described by density matrices is represented by means of the time evolution operator

$$\rho(t) = U \left(\sum_i p_i |\psi_i\rangle\langle\psi_i| \right) U^\dagger = U\rho U^\dagger \quad (1.2.46)$$

where U is defined in Equation 1.2.14.

1.2.4.3 Density operator of a subsystem

Statistical quantum mechanics often deals with subsystems, considering exclusively one of the parts which realize the composite system. In practice, starting from a composite system $\mathcal{H} = \mathcal{H}_a \otimes \mathcal{H}_b$, it is necessary to eliminate the subsystem b in order to focus on a , which is the subsystem of interest.

The first step is the introduction of the partial trace.

Definition 1.2.4. The **partial trace** of operator \mathbf{A} over \mathcal{H}_b is an operator acting only on \mathcal{H}_a defined as

$$\mathbf{A}_a = \text{tr}_b(\mathbf{A}) = \sum_k (\mathbb{I} \otimes \langle k|) \mathbf{A} (\mathbb{I} \otimes |k\rangle) \quad (1.2.47)$$

The partial trace, as the standard trace, does not depend on the basis.

The partial trace can be used to somehow forget about the second subsystem and retrieve the density matrix of the first subsystem from that of the composite system.

Property 1.2.7. The density operator describing the subsystem belonging to \mathcal{H}_a is obtained from the density operator of the composite system $\mathcal{H} = \mathcal{H}_a \otimes \mathcal{H}_b$, *tracing out* the subsystem \mathcal{H}_b .

$$\rho_a = \text{tr}_b(\rho) = \sum_k (\mathbb{I} \otimes \langle k|) \rho (\mathbb{I} \otimes |k\rangle) \quad (1.2.48)$$

Example 1.2.5. Let the basis vectors of a two dimensional space be

$$|0\rangle = \begin{pmatrix} 1 \\ 0 \end{pmatrix} \quad |1\rangle = \begin{pmatrix} 0 \\ 1 \end{pmatrix}$$

and suppose that the wavefunction of the composite system is

$$|\psi\rangle = \frac{|10\rangle + |00\rangle}{\sqrt{2}} = \frac{|1\rangle + |0\rangle}{\sqrt{2}} \otimes |0\rangle$$

Hence, the system is not entangled. The overall density matrix is

$$\rho = |\psi\rangle\langle\psi| = \frac{1}{2} (|10\rangle\langle 10| + |10\rangle\langle 00| + |00\rangle\langle 10| + |00\rangle\langle 00|) = \frac{1}{2} \begin{pmatrix} 1 & 0 & 1 & 0 \\ 0 & 0 & 0 & 0 \\ 1 & 0 & 1 & 0 \\ 0 & 0 & 0 & 0 \end{pmatrix}$$

The density matrix relative to the first subsystem is computed according to Equation 1.2.48:

$$\rho_a = (\mathbb{I} \otimes \langle 0|) \rho (\mathbb{I} \otimes |0\rangle) + (\mathbb{I} \otimes \langle 1|) \rho (\mathbb{I} \otimes |1\rangle)$$

The first term on the right hand side becomes

$$\begin{aligned} (\mathbb{I} \otimes \langle 0|) \rho (\mathbb{I} \otimes |0\rangle) &= \frac{1}{2} (\mathbb{I} |1\rangle\langle 1| \mathbb{I}) \otimes (\langle 0|0\rangle \langle 0|0\rangle) + \frac{1}{2} (\mathbb{I} |1\rangle\langle 0| \mathbb{I}) \otimes (\langle 0|0\rangle \langle 0|0\rangle) \\ &\quad + \frac{1}{2} (\mathbb{I} |0\rangle\langle 1| \mathbb{I}) \otimes (\langle 0|0\rangle \langle 0|0\rangle) + \frac{1}{2} (\mathbb{I} |0\rangle\langle 0| \mathbb{I}) \otimes (\langle 0|0\rangle \langle 0|0\rangle) \\ &= \frac{1}{2} (|0\rangle\langle 0| + |0\rangle\langle 1| + |1\rangle\langle 0| + |1\rangle\langle 1|) \end{aligned}$$

The second term on the right hand side becomes

$$\begin{aligned} (\mathbb{I} \otimes \langle 1|) \rho (\mathbb{I} \otimes |1\rangle) &= \frac{1}{2} (\mathbb{I} |1\rangle\langle 1| \mathbb{I}) \otimes (\langle 1|0\rangle \langle 0|1\rangle) + \frac{1}{2} (\mathbb{I} |1\rangle\langle 0| \mathbb{I}) \otimes (\langle 1|0\rangle \langle 0|1\rangle) \\ &\quad + \frac{1}{2} (\mathbb{I} |0\rangle\langle 1| \mathbb{I}) \otimes (\langle 1|0\rangle \langle 0|1\rangle) + \frac{1}{2} (\mathbb{I} |0\rangle\langle 0| \mathbb{I}) \otimes (\langle 1|0\rangle \langle 0|1\rangle) \\ &= 0 \cdot (|0\rangle\langle 0| + |0\rangle\langle 1| + |1\rangle\langle 0| + |1\rangle\langle 1|) \end{aligned}$$

The density matrix is therefore

$$\rho_a = \frac{1}{2} \begin{pmatrix} 1 & 1 \\ 1 & 1 \end{pmatrix}$$

Finally, it is trivial to get the density matrix of subsystem b

$$\rho_b = \begin{pmatrix} 1 & 0 \\ 0 & 0 \end{pmatrix}$$

and to prove that

$$\rho = \rho_a \otimes \rho_b$$

△

Example 1.2.6. Suppose, now, that the composite system is entangled, let, for instance, the wavefunction be

$$|\psi\rangle = \frac{|01\rangle - |10\rangle}{\sqrt{2}}$$

The corresponding density matrix is

$$\rho = |\psi\rangle\langle\psi| = \frac{1}{2} (|01\rangle\langle 01| - |01\rangle\langle 10| - |10\rangle\langle 01| + |10\rangle\langle 10|) = \frac{1}{2} \begin{pmatrix} 0 & 0 & 0 & 0 \\ 0 & 1 & -1 & 0 \\ 0 & -1 & 1 & 0 \\ 0 & 0 & 0 & 0 \end{pmatrix}$$

The density matrix relative to the first subsystem is computed according to Equation 1.2.48:

$$\rho_a = (\mathbb{I} \otimes \langle 0|) \rho (\mathbb{I} \otimes |0\rangle) + (\mathbb{I} \otimes \langle 1|) \rho (\mathbb{I} \otimes |1\rangle)$$

The first term on the right hand side becomes

$$\begin{aligned} (\mathbb{I} \otimes \langle 0|) \rho (\mathbb{I} \otimes |0\rangle) &= \frac{1}{2} (\mathbb{I} |0\rangle\langle 0| \mathbb{I}) \otimes (\langle 0|1\rangle \langle 1|0\rangle) + \frac{1}{2} (\mathbb{I} |0\rangle\langle 1| \mathbb{I}) \otimes (\langle 0|1\rangle \langle 0|0\rangle) \\ &\quad + \frac{1}{2} (\mathbb{I} |1\rangle\langle 0| \mathbb{I}) \otimes (\langle 0|0\rangle \langle 1|0\rangle) + \frac{1}{2} (\mathbb{I} |1\rangle\langle 1| \mathbb{I}) \otimes (\langle 0|0\rangle \langle 0|0\rangle) \\ &= \frac{1}{2} |1\rangle\langle 1| \end{aligned}$$

The second term on the right hand side becomes

$$\begin{aligned} (\mathbb{I} \otimes \langle 1|) \rho (\mathbb{I} \otimes |1\rangle) &= \frac{1}{2} (\mathbb{I} |0\rangle\langle 0| \mathbb{I}) \otimes (\langle 1|1\rangle \langle 1|1\rangle) + \frac{1}{2} (\mathbb{I} |0\rangle\langle 1| \mathbb{I}) \otimes (\langle 1|1\rangle \langle 0|1\rangle) \\ &\quad + \frac{1}{2} (\mathbb{I} |1\rangle\langle 0| \mathbb{I}) \otimes (\langle 1|0\rangle \langle 1|1\rangle) + \frac{1}{2} (\mathbb{I} |1\rangle\langle 1| \mathbb{I}) \otimes (\langle 1|0\rangle \langle 0|1\rangle) \\ &= \frac{1}{2} |0\rangle\langle 0| \end{aligned}$$

The density matrix is therefore

$$\rho_a = \frac{1}{2} \begin{pmatrix} 1 & 0 \\ 0 & 1 \end{pmatrix} = \frac{1}{2} \mathbb{I}$$

and represents the so-called **maximally mixed state**: all the information about the subsystem a is clearly lost. This is a general result, because the partial trace acting on pure entangled states produces maximally mixed states.

Finally, it is trivial to get the density matrix of subsystem b

$$\rho_b = \frac{1}{2} \begin{pmatrix} 1 & 0 \\ 0 & 1 \end{pmatrix} = \frac{1}{2} \mathbb{I}$$

and to prove that

$$\rho \neq \rho_a \otimes \rho_b$$



1.2.4.4 Measurements

The measurement operation on a density matrix can be understood in similarity [14] to the measurement of pure states described in postulate 1.3.

Theorem 1.2.5. *Let M_i be the measurement operators defined in 1.2.1. The probability of measuring ρ_ζ is*

$$p(\rho_\zeta) = \text{tr} \left(M_\zeta^\dagger M_\zeta \rho \right) \quad (1.2.49)$$

and the state, immediately after the measurement, collapses to

$$\rho_\zeta = \frac{M_\zeta^\dagger \rho M_\zeta}{p(\zeta)} \quad (1.2.50)$$

Proof. When dealing with pure states

$$p(\zeta) = \langle \psi | M_\zeta^\dagger M_\zeta | \psi \rangle$$

in case of mixed states, the previous equation can be rewritten as

$$p(\rho_\zeta) = \sum_i p_i \langle \psi_i | M_\zeta^\dagger M_\zeta | \psi_i \rangle$$

exploiting the definition of the trace operator it follows immediately that

$$p(\rho_\zeta) = \sum_i p_i \text{tr} \left(M_\zeta^\dagger M_\zeta | \psi_i \rangle \langle \psi_i | \right) = \text{tr} \left(M_\zeta^\dagger M_\zeta \sum_i p_i | \psi_i \rangle \langle \psi_i | \right) = \text{tr} \left(M_\zeta^\dagger M_\zeta \rho \right)$$

Next, a pure state collapses, after measurement, to

$$|\zeta\rangle = \frac{M_\zeta | \psi \rangle}{\sqrt{p(\zeta)}} \quad (1.2.51)$$

in analogy, a mixed state collapses to

$$\sum_i p_i \frac{M_\zeta | \psi_i \rangle \langle \psi_i | M_\zeta^\dagger}{\sqrt{p(\zeta)}} = \frac{M_\zeta^\dagger \rho M_\zeta}{p(\zeta)}$$

□

Example 1.2.7. Suppose a projective measurement is carried out so that

$$M_\zeta = P_\zeta = |\lambda_\zeta\rangle \langle \lambda_\zeta|$$

The state, immediately after the measurement, changes to

$$\begin{aligned} \frac{\mathbf{M}_\zeta^\dagger \boldsymbol{\rho} \mathbf{M}_\zeta}{p(\zeta)} &= \frac{|\zeta\rangle\langle\zeta| \boldsymbol{\rho} |\zeta\rangle\langle\zeta|}{\sum_i p_i \langle\psi_i| |\zeta\rangle\langle\zeta| |\zeta\rangle\langle\zeta| |\psi_i\rangle} = \frac{|\zeta\rangle\langle\zeta| \sum_i p_i |\psi_i\rangle\langle\psi_i| |\zeta\rangle\langle\zeta|}{\sum_i p_i |\langle\psi_i|\zeta\rangle|^2} \\ &= \frac{|\zeta\rangle \sum_i p_i |\langle\psi_i|\zeta\rangle|^2 \langle\zeta|}{\sum_i p_i |\langle\psi_i|\zeta\rangle|^2} \sim |\zeta\rangle\langle\zeta| \end{aligned}$$

It is clear that the measurement forces the mixed state to collapse to a pure state $|\zeta\rangle\langle\zeta|$. △

1.2.4.5 Separable and inseparable states

Pure states can be classified in separable and entangled states. A generalization holds for mixed states.

Definition 1.2.5. A state $\boldsymbol{\rho}$ is

- **Uncorrelated** if it can be written as

$$\boldsymbol{\rho} = \boldsymbol{\rho}_1 \otimes \boldsymbol{\rho}_2 \otimes \cdots \otimes \boldsymbol{\rho}_N \quad (1.2.52)$$

- **Separable** if it can be written as

$$\boldsymbol{\rho} = \sum_i p_i \boldsymbol{\rho}_1^i \otimes \boldsymbol{\rho}_2^i \otimes \cdots \otimes \boldsymbol{\rho}_N^i \quad (1.2.53)$$

where $\boldsymbol{\rho}_j^i$ are mixed states of the respective subsystems.

- **Inseparable** otherwise.

1.2.4.6 Fidelity

It is often interesting to evaluate how close two density matrices are to each other. For instance, one may be willing to compare the density matrix obtained as a result of an experiment with the theoretically expected one. For this purpose, it is customary to define the following figure of merit [15].

Definition 1.2.6. Let $\boldsymbol{\rho}_1$ and $\boldsymbol{\rho}_2$ be two density matrix. The fidelity is defined as

$$F(\boldsymbol{\rho}_1, \boldsymbol{\rho}_2) = \left(\text{tr} \left(\sqrt{\sqrt{\boldsymbol{\rho}_1} \boldsymbol{\rho}_2 \sqrt{\boldsymbol{\rho}_1}} \right) \right)^2 \quad (1.2.54)$$

where the square root of the density matrix is

$$\sqrt{\rho} = \sum_i \sqrt{p_i} |\psi_i\rangle\langle\psi_i| \quad (1.2.55)$$

if

$$\rho = \sum_i p_i |\psi_i\rangle\langle\psi_i| \quad (1.2.56)$$

is the spectral decomposition of ρ .

The fidelity is always a non negative number equal or smaller than 1. The equality holds only when the two density matrices are equal.

Chapter 2

Theory of quantum computing

Quantum computing is the art of using the force of quantum mechanics to perform computations. It is a field that requires the cooperation of scientists from different backgrounds: theoretical and experimental physics, chemistry, mathematics, electronic engineering, computer science. The first question that arises naturally when approaching this new world is: why quantum computing?

After many decades devoted to the research and development of technology, architecture and software, the standard, classical, computation has reached incredible results. The always inflating number of applications that are leveraging high performance integrated systems has increased the pressure and diversified the requirements on both IC architectures design and on technological evolution. Nowadays electronic systems are high performance, low-power and low-cost. The predictions of Moore's law have been met for several decades but standard CMOS circuits are expected to be no longer able to satisfy nowadays increasing demand for systems with even higher performances and lower power consumption. This commits to looking for new solutions. The research has taken two main paths: More-Moore and More-Than-Moore.

More-Moore is the micro and nano-electronic approach to evolution: the miniaturisation as the via to increase transistor density and keep Moore's Law effectiveness alive, introducing completely new structures, as FD-SOI, Fin-FET and GAA-FET, while countless smart solutions have been investigated, discovered and exploited in the history of electronics to improve the performances, using superior technologies and boosting data flow speed. The beyond-CMOS era which is beginning in this time partially follows the lines of this tradition: new solutions, not-CMOS based, are being tested to improve performances, increase the density and reduce the power consumption of electronic systems. The after-Moore nano-electronic is moving towards magnetic and molecular solutions.

More-Than-Moore means diversification: the digital integrated circuit is no longer able to satisfy the needs of nowadays society. Multi-functional diversified systems are required by the market and the expectations in terms of pervasiveness and effectiveness of electronics pave the way to the realization of systems which

are interacting with people and the environment. In this field, the world of MEMS finds its natural place.

Both paths brought radical innovations. However, quantum computing is not just an innovation, it is expected to be an actual change of paradigm. Not only it demands the exploitation of new technologies¹, but it also requires a completely new way of approaching computer science and logic.

The beginning of the quantum computation era dates back the 1980s, when Charles Bennet and Paul Benioff published their first papers and Richard Feynman was involved about the feasibility of quantum computer. In the same years, Deutsch proposed the first quantum algorithm, showing the power of quantum superposition.

In the 1990s, Peter Shor and Lov Grover presented their famous algorithms, which demonstrated the advantages of quantum computation over the classical one. In 1998 the first experimental demonstration of a quantum algorithm became possible thanks to a working two-qubit NMR quantum computer, used to solve Deutsch's problem².

During the first and second decade of the third millennium, new technologies are introduced: superconducting quantum dots, trapped ions, nuclear magnetic resonance, molecular magnets and many others. The availability, in recent years, of experimental quantum processors renewed the interest towards this field.

There are at least two main reasons for which quantum computing is expected to broaden the computation horizons.

Firstly, rough computational power. While a classical computer is in one state every moment, the superposition principle of quantum mechanics allows a quantum computer to be in a superposition of states every instant of time. Proper handling of complex probability amplitudes brings a formidable improvement of parallel processing. Moreover, entanglement proves to be a compelling resource for quantum computation. These properties can be exploited, for instance, in search algorithms and for cryptography.

Secondly, quantum computing speaks the same language Nature does: quantum mechanics. Physical systems may be extremely complex, preventing a classical computer to perform reliable simulations. The hardware of quantum computers

¹A highly recommended reading where the different technologies are presented, the feasibility of quantum computing is discussed starting from DiVincenzo criteria and, then, the possibilities provided by nano-magnets are analyzed in great details is [16].

²A short but interesting summary of the early history of quantum computing can be found in the introduction of [17].

is represented by quantum systems: molecules, magnets, superconductors. Simulating a complex quantum system with a quantum computer means to exploit Nature to simulate itself: quantum computing is spontaneously suitable to handle the complexity of physical systems. For instance, quantum chemistry is expected to be one of the most promising application areas of quantum computing.

Nevertheless, quantum computation is not expected, at least in the short time, to replace classical computation. It will probably provide new computational power to tackle challenging complex problems in specific fields of applications. Quantum computing is still at its dawn and, at the time of writing, the so-called quantum supremacy, that is the ability of a quantum computer to solve a problem a classical computer cannot solve efficiently, is still under debate. Moreover, the research for useful quantum algorithms is still ongoing. As far as the hardware is concerned, the quest for reliable and scalable qubits, characterized by long decoherence times is not over and it is still not known which of the many hardware solutions under research will be identified as the reference one.

One of the plausible scenarios is that future quantum processors will be used for research applications and be remotely available for consumers. When the classical processor will recognize a task which a quantum processor would solve more efficiently, it will exploit the latter, connecting to the remote server.

In the first part of this chapter, the general concepts of quantum computing are introduced, using, as far as possible, a graphical approach. The second part is devoted to the discussion of Grover's search algorithm.

2.1 Introduction to quantum computing

2.1.1 Bits and qubits

A classical bit is a classical unit of information, describing a two-dimensional system. Instead of representing bits as 0 and 1, as every electronic engineer or computer scientist is used to do, it is more convenient to adopt a vector notation: bit 0 is associated with state $|0\rangle$ and has a 1 in the zero's row and a 0 in the one's row; conversely, bit 1 is associated with state $|1\rangle$ and has a 0 in the zero's row and a 1 in the one's row.

$$|0\rangle = \begin{pmatrix} 1 \\ 0 \end{pmatrix} \quad |1\rangle = \begin{pmatrix} 0 \\ 1 \end{pmatrix} \quad (2.1.1)$$

A classical bit can be only either 0 or 1. This is no longer true for quantum systems: the superposition principle states that a quantum system can be found in a superposition of states.

Definition 2.1.1. A quantum bit is a unit of information describing a two dimensional quantum system. It is represented by a vector belonging to \mathbb{H}^2 , whose basis vectors are classical bits.

$$|\psi\rangle = c_0 |0\rangle + c_1 |1\rangle = \begin{pmatrix} c_0 \\ c_1 \end{pmatrix} \quad (2.1.2)$$

where c_0 and c_1 are complex number with the property that $|c_0|^2$ is the probability that the qubit collapses to $|0\rangle$ immediately after the measurement and $|c_1|^2$ is the probability that the qubit collapses to $|1\rangle$. Consequently, $|c_0|^2 + |c_1|^2 = 1$.

It has to be remarked that even if a qubit exists in infinitely many superpositions of $|0\rangle$ and $|1\rangle$, the quantity of information which can be obtained through measurement is the same as the one which can be extracted from a classical bit. As a matter of fact, when a measurement is carried out, according to postulate 1.3, the qubit is projected to one of the basis vectors and becomes, *definitely*, either $|0\rangle$ or $|1\rangle$.

There is one aspect which deserves an additional remark. It is customary to say that the outcome of a measurement is “zero” or “one” and that, after the measurement, the system must be found either in state-zero or state-one. It has to be clear that *zero* and *one* are just labels which are associated with specific

outcomes, whose actual value depends on the physical system which implements the qubits. The following example may be of help.

Example 2.1.1. As it will be clear reading the coming chapters, a possibility to implement qubits is represented by spin states of spin- $\frac{1}{2}$ nuclei. Since the Hermitian operators associated with the three components of the spin do not commute, it is possible to measure only one component. Routinely, the component along the so-called quantization axis is measured. This is conventionally associated with the z-component of the spin. Assume the wavefunction describing the spin of the nucleus is

$$|\psi\rangle = c_0 |\downarrow\rangle + c_1 |\uparrow\rangle$$

where $|\downarrow\rangle$ and $|\uparrow\rangle$ represent the *up* and *down* spin states. The Hermitian operator associated with the z-component of the spin is

$$\sigma_z = \frac{\hbar}{2} \begin{pmatrix} 1 & 0 \\ 0 & -1 \end{pmatrix}$$

The eigenvalues are $+\frac{\hbar}{2}$ and $-\frac{\hbar}{2}$. The associated eigenvectors are

$$\begin{aligned} +\frac{\hbar}{2} &\longrightarrow |\uparrow\rangle = \frac{\hbar}{2} \begin{pmatrix} 1 \\ 0 \end{pmatrix} \\ -\frac{\hbar}{2} &\longrightarrow |\downarrow\rangle = \frac{\hbar}{2} \begin{pmatrix} 0 \\ 1 \end{pmatrix} \end{aligned}$$

Note the following aspects:

- The wavefunction is written with respect to the eigenbasis of σ_z .
- The possible measurement outcomes are $\pm\frac{\hbar}{2}$ which are the eigenvalues of σ_z .
- The eigenvalue $+\frac{\hbar}{2}$ can be arbitrarily³ associated with logic 0 and the corresponding eigenstate $|\uparrow\rangle$ to $|0\rangle$. The probability to obtain this outcome is $|c_0|^2$.
- The eigenvalue $-\frac{\hbar}{2}$ can be arbitrarily associated with logic 1 and the corresponding eigenstate $|\downarrow\rangle$ to $|1\rangle$. The corresponding probability is $|c_1|^2$.

△

³The actual sign convention for the NMR will be discussed in the following.

2.1.2 Multi-qubit systems

As outlined in §1.2.3, a quantum computer with a single qubit would be useless. A multi-qubit system is usually referred to as a **quantum register**.

Consider a classical register and, for the sake of definiteness, assume it has a parallelism of 1 B. It is clear that the state of the register is unequivocally defined specifying the state of each bit. For instance

$$R = 01001101 \quad (2.1.3)$$

Adopting the vector formalism introduced in the previous section, R can be rewritten as

$$R = \begin{pmatrix} 1 \\ 0 \end{pmatrix} \otimes \begin{pmatrix} 0 \\ 1 \end{pmatrix} \otimes \begin{pmatrix} 1 \\ 0 \end{pmatrix} \otimes \begin{pmatrix} 1 \\ 0 \end{pmatrix} \otimes \begin{pmatrix} 0 \\ 1 \end{pmatrix} \otimes \begin{pmatrix} 0 \\ 1 \end{pmatrix} \otimes \begin{pmatrix} 1 \\ 0 \end{pmatrix} \otimes \begin{pmatrix} 0 \\ 1 \end{pmatrix} \quad (2.1.4)$$

which is a $2^8 = 256$ row vector, numbered from 00000000 to 11111111 with all 0 entries but a single 1 in correspondence of 01001101. That is all the story for a classical register: every possible state of R is the tensor product of the states of the single bits. As a consequence, it is sufficient to indicate the state of each bit, that is, to write eight real numbers (0 or 1).

Now, consider eight qubits. The state of each qubit is

$$q_i = a_i |0\rangle + b_i |1\rangle \quad (2.1.5)$$

If these eight qubits realize a quantum register of one qubyte, the state of the register can be written as

$$|Q\rangle = \begin{pmatrix} a_0 \\ b_0 \end{pmatrix} \otimes \begin{pmatrix} a_1 \\ b_1 \end{pmatrix} \otimes \begin{pmatrix} a_2 \\ b_2 \end{pmatrix} \otimes \begin{pmatrix} a_3 \\ b_3 \end{pmatrix} \otimes \begin{pmatrix} a_4 \\ b_4 \end{pmatrix} \otimes \begin{pmatrix} a_5 \\ b_5 \end{pmatrix} \otimes \begin{pmatrix} a_6 \\ b_6 \end{pmatrix} \otimes \begin{pmatrix} a_7 \\ b_7 \end{pmatrix} \quad (2.1.6)$$

In this case, Q is written as the tensor product of $n = 8$ qubits, that is, specifying $2n = 16$ complex numbers. However, from the basic properties of the tensor product, it is well known that the space generated by the tensor product of n two-dimensional complex vectors is not $2n$ but it is 2^n . Wherefore, a *generic state* of Q must be specified determining $2^8 = 256$ complex numbers. What has happened? The answer is **entanglement** and **superposition**. The quantum register is forced by nobody to live only in tensor product states, but it is free to live in every *superposition* of these states. These superpositions are not necessarily

decomposable into a tensor product form. In other words, they may be entangled states.

The most comfortable way to figure out this superposition is probably the following one. Consider that n qubits generate a 2^n complex vector space, whose basis vectors are all possible strings of n qubits. The n -qubit quantum register can live in every superposition of these basis vectors. For instance, coming back the previous eight qubit example, the basis vectors are:

$$\begin{aligned} |e_0\rangle &= |00000000\rangle \\ |e_1\rangle &= |00000001\rangle \\ |e_2\rangle &= |00000010\rangle \\ &\dots \\ |e_{255}\rangle &= |11111111\rangle \end{aligned} \tag{2.1.7}$$

and a generic state of Q can be written as

$$|Q\rangle = \sum_{i=0}^{2^n-1} c_i |e_i\rangle \tag{2.1.8}$$

In conclusion, all tensor products of n qubits are proper states of an n qubit register, but not all states of an n qubit register can be written as the tensor product of n qubits.

2.1.3 Matrix formalism for classical logic gates

As classical bits can be expressed according to a vector formalism, so classical logic gates can be represented by matrices. In particular, a logic gate which receives n input bits and provides m output bits is a $2^m \times 2^n$ matrix.

2.1.3.1 NOT gate

The truth table is

a	$\neg a$
0	1
1	0

when the input is $|0\rangle$ the output must be $|1\rangle$ and viceversa. This can be written as

$$\mathbf{NOT} = |1\rangle\langle 0| + |0\rangle\langle 1| = \begin{pmatrix} 0 & 1 \\ 1 & 0 \end{pmatrix} \quad (2.1.9)$$

This way of writing matrices is quite useful and deserves some attention. One can read it as:

- When $|0\rangle$ enters, $|1\rangle$ exits

$$\mathbf{NOT} |0\rangle = |1\rangle\langle 0| |0\rangle + |0\rangle\langle 1| |0\rangle = |1\rangle$$

- When $|1\rangle$ enters, $|0\rangle$ exits

$$\mathbf{NOT} |1\rangle = |1\rangle\langle 0| |1\rangle + |0\rangle\langle 1| |1\rangle = |0\rangle$$

2.1.3.2 AND gate

The truth table is

a	b	$a \wedge b$
0	0	0
0	1	0
1	0	0
1	1	1

The matrix is

$$\mathbf{AND} = |0\rangle\langle 00| + |0\rangle\langle 01| + |0\rangle\langle 10| + |1\rangle\langle 11| = \begin{pmatrix} 1 & 1 & 1 & 0 \\ 0 & 0 & 0 & 1 \end{pmatrix} \quad (2.1.10)$$

2.1.3.3 NAND gate

The truth table is

a	b	$\neg(a \wedge b)$
0	0	1
0	1	1
1	0	1
1	1	0

The matrix is

$$\mathbf{NAND} = |1\rangle\langle 00| + |1\rangle\langle 01| + |1\rangle\langle 10| + |0\rangle\langle 11| = \begin{pmatrix} 0 & 0 & 0 & 1 \\ 1 & 1 & 1 & 0 \end{pmatrix} \quad (2.1.11)$$

It is clear that a NAND gate is equivalent to an AND gate followed by a NOT gate. As a matter of fact, the same matrix can be found as

$$\mathbf{NAND} = \mathbf{NOT}[\mathbf{AND}] = \begin{pmatrix} 0 & 1 \\ 1 & 0 \end{pmatrix} \begin{pmatrix} 1 & 1 & 1 & 0 \\ 0 & 0 & 0 & 1 \end{pmatrix} = \begin{pmatrix} 0 & 0 & 0 & 1 \\ 1 & 1 & 1 & 0 \end{pmatrix} \quad (2.1.12)$$

2.1.4 Parallel and sequential operations

In the previous section, the NAND gate is obtained as the cascade of an AND gate and a NOT gate, giving a first hint about how to deal with sequential operations.

2.1.4.1 Sequential operations

If the algorithm requires to apply operator A and, then, operator B to state $|\psi\rangle$, one has to compute the outer product of the two matrices and apply the result to the vector describing the system state according to the following order:

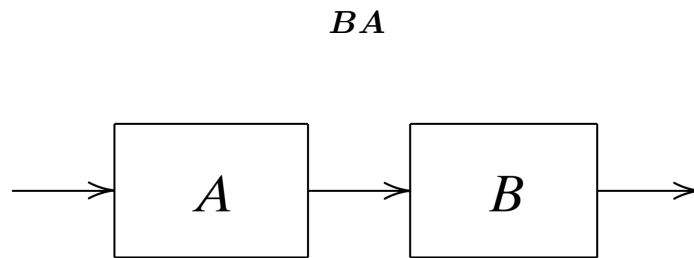
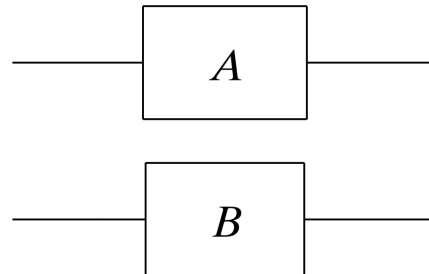


Figure 2.1: Sequential operations: B is applied *after* A . Adapted from [18].

2.1.4.2 Parallel operations

If the algorithm requires to apply operator A and operator B in parallel, one has to compute the tensor product of the two matrices:



$$A \otimes B$$

Figure 2.2: Parallel operations: A and B are applied in parallel. Adapted from [18].

2.1.4.3 Mixed operations

Assume that the first step consists of operator A receiving n input bits and providing m output bits. During the second step, operator B acts on $p < m$ bits and provides q output bits; the other $m - p$ bits are unaffected during the second step. The matrix representation is

$$(B \otimes \mathbb{I}_{m-p})A \tag{2.1.13}$$

where \mathbb{I}_{m-p} is the $2^{m-p} \times 2^{m-p}$ identity matrix. The corresponding circuit is reported in Figure 2.3.

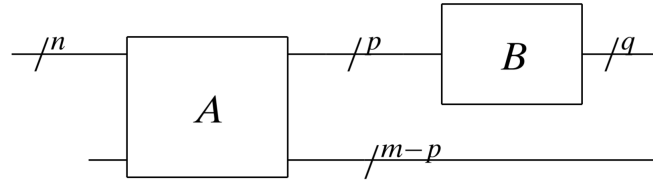


Figure 2.3: Mixed operations. Adapted from [18].

2.1.5 Bloch sphere

A beautiful graphical tool to visualize one-qubit states and operations is the Bloch sphere.

2.1.5.1 Pure states

Property 2.1.1. Given a generic qubit in the form

$$|\psi\rangle = c_0 |0\rangle + c_1 |1\rangle \quad (2.1.14)$$

it can be rewritten as

$$|\psi\rangle = \cos\left(\frac{\theta}{2}\right) |0\rangle + e^{i\phi} \sin\left(\frac{\theta}{2}\right) |1\rangle = \begin{pmatrix} \cos\left(\frac{\theta}{2}\right) \\ e^{i\phi} \sin\left(\frac{\theta}{2}\right) \end{pmatrix} \quad (2.1.15)$$

where the *longitude* $0 \leq \phi \leq 2\pi$ and the *latitude* $0 \leq \theta \leq \pi$.

Proof. Since c_0 and c_1 are complex numbers, Equation 2.1.14 can be written in polar form as

$$|\psi\rangle = r_0 e^{i\phi_0} |0\rangle + r_1 e^{i\phi_1} |1\rangle$$

A quantum state is defined up to a phase, consequently, without loss of generality, it is customary to choose the global phase such that c_0 is real, that is $|\psi\rangle$ is multiplied by $e^{-i\phi_0}$

$$e^{-i\phi_0} |\psi\rangle = r_0 |0\rangle + r_1 e^{i(\phi_1 - \phi_0)} |1\rangle$$

Since

$$|c_0|^2 + |c_1|^2 = 1 \implies r_0^2 + r_1^2 = 1$$

renaming

$$r_0 = \cos\left(\frac{\theta}{2}\right) \quad r_1 = \sin\left(\frac{\theta}{2}\right) \quad \phi = \phi_1 - \phi_0$$

one gets

$$|\psi\rangle = \cos\left(\frac{\theta}{2}\right) |0\rangle + e^{i\phi} \sin\left(\frac{\theta}{2}\right) |1\rangle$$

where the factor $1/2$ for θ is chosen, in analogy with the definition of spherical coordinates, so that each qubit is mapped once on the sphere. \square

The Cartesian coordinates can be retrieved as

$$\begin{aligned}x &= \cos \phi \sin \theta \\y &= \sin \phi \sin \theta \\z &= \cos \theta\end{aligned}\tag{2.1.16}$$

Each pure state is represented by a point on the surface on the sphere, spanned by the unit **Bloch vector**

$$\hat{\mathbf{b}}(\theta, \phi) = \begin{pmatrix} \cos \phi \sin \theta & \sin \phi \sin \theta & \cos \theta \end{pmatrix}'\tag{2.1.17}$$

The Bloch sphere for a generic state vector $|\psi\rangle$ is reported in Figure 2.4. The

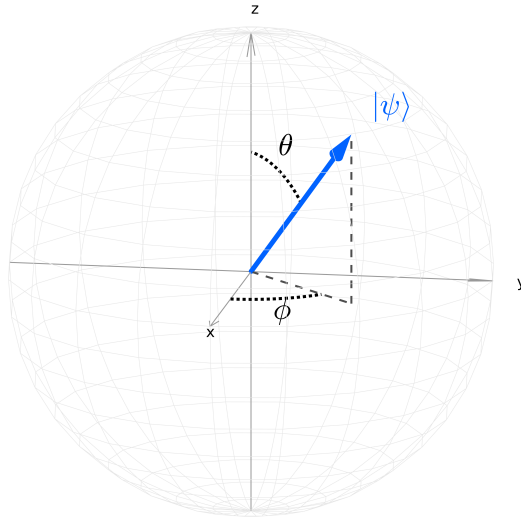


Figure 2.4: Bloch sphere.

North pole is the state $|0\rangle$, while the South pole is the state $|1\rangle$: they represent the classical bit 0 and 1. As one can see, the state $|\psi\rangle$ is a linear combination of both states: it is not $|0\rangle$, it is not $|1\rangle$, it is not $|0\rangle$ and $|1\rangle$ simultaneously, it is not $|0\rangle$ or $|1\rangle$. It is a *superposition* of $|0\rangle$ and $|1\rangle$, whose nature is described, in the Bloch sphere formalism, by means of the longitude ϕ and the latitude θ . When the qubit is measured according to the *standard basis*, that is, the eigenbasis of σ_z , it collapses either to the North pole or to the South pole, i.e., to a classical bit. The probability of which pole the state will collapse to depends solely on the *latitude*. Therefore, the probability is not affected by a change of phase of the qubit, i.e., by a rotation of the latter about \hat{z} .

2.1.5.2 Mixed states

As extensively detailed in §1.2.4, mixed states are described according to the density matrix formalism. The following property is useful to understand how mixed states are represented in the Bloch sphere.

Property 2.1.2. Every density matrix $\rho \in \mathbb{H}^{2 \times 2}$ can be written as

$$\rho = \frac{1}{2} (\mathbb{I} + n_x \sigma_x + n_y \sigma_y + n_z \sigma_z) = \frac{1}{2} \begin{pmatrix} 1 + n_z & n_x - i n_y \\ n_x + i n_y & 1 - n_z \end{pmatrix} \quad (2.1.18)$$

The generalized Bloch vector

$$\mathbf{n} = \begin{pmatrix} n_x & n_y & n_z \end{pmatrix}' \quad (2.1.19)$$

spans all points of the **Bloch ball**.

Proof. The density matrix associated with a pure state can be rewritten as

$$\begin{aligned} |\psi\rangle\langle\psi| &= \begin{pmatrix} \cos\left(\frac{\theta}{2}\right) \\ e^{i\phi} \sin\left(\frac{\theta}{2}\right) \end{pmatrix} \begin{pmatrix} \cos\left(\frac{\theta}{2}\right) & e^{-i\phi} \sin\left(\frac{\theta}{2}\right) \end{pmatrix} \\ &= \begin{pmatrix} \cos^2\left(\frac{\theta}{2}\right) & \sin\left(\frac{\theta}{2}\right) \cos\left(\frac{\theta}{2}\right) e^{-i\phi} \\ \sin\left(\frac{\theta}{2}\right) \cos\left(\frac{\theta}{2}\right) e^{+i\phi} & \sin^2\left(\frac{\theta}{2}\right) \end{pmatrix} \\ &= \frac{1}{2} (\mathbb{I} + \cos\phi \sin\theta \sigma_x + \sin\phi \sin\theta \sigma_y + \cos\theta \sigma_z) \\ &= \frac{1}{2} (\mathbb{I} + b_x \sigma_x + b_y \sigma_y + b_z \sigma_z) \end{aligned}$$

where $\hat{\mathbf{b}}$ is the Bloch vector of Equation 2.1.17.

A mixed state is

$$\rho = \sum_i p_i |\psi_i\rangle\langle\psi_i| = \sum_i p_i \rho_i$$

Since each contributing pure state density matrix ρ_i can be represented by a unit Bloch vector $\hat{\mathbf{b}}_i$, also the overall mixed state density matrix can be represented by a vector

$$\mathbf{n} = \sum_i p_i \hat{\mathbf{b}}_i$$

It is obvious that $|\mathbf{n}| \leq 1$ since $|\hat{\mathbf{b}}_i| = 1, \forall i$. □

Once the density matrix is assigned, the components of the generalized Bloch

vector are immediately computed from Equation 2.1.18 as

$$\begin{aligned}n_x &= 2 \operatorname{Re}\{\rho_{01}\} \\n_y &= 2 \operatorname{Im}\{\rho_{10}\} \\n_z &= \rho_{00} - \rho_{11}\end{aligned}\tag{2.1.20}$$

An example is reported in Figure 2.5: it is interesting to see that the generalized Bloch vector does not point to the surface of the unit Bloch sphere (in pale gray in the figure), since it has a magnitude smaller than one.

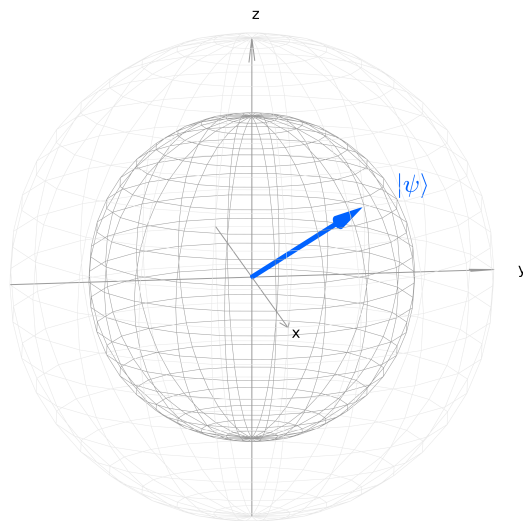


Figure 2.5: Bloch ball for a mixed state.

2.1.6 Quantum gates

The whole world of classical digital electronics is founded on the application of logic gates to classical bits: complex processors are built properly combining logic gates. In analogy with this world, when a simple operator is applied on a qubit to change the state of the latter, in the quantum computing jargon one would say that a quantum gate (**qugate**) has been applied to the qubit. Elaborated quantum circuits are obtained composing quantum gates. The action of a quantum gate \mathbf{U} on a qubit $|\psi_{in}\rangle$ can be expressed as

$$|\psi_{out}\rangle = \mathbf{U} |\psi_{in}\rangle \quad (2.1.21)$$

In a classical computer, the information travels around the circuit, moving from the processor to the memory back and forth and reaching the I/O devices. On the other hand, in a quantum processor, the quantum bits which carry the information are stored in a quantum register. Properly designed external stimuli are applied to the latter to produce the desired gate operation. Hence, the information does not travel around but sits in a specific register and successive gates are applied one after the other to the register.

Every quantum gate must be characterized by the following requirements.

Definition 2.1.2. A quantum gate is a linear unitary reversible operator.

Unitarity The unitary property of quantum mechanics requires that the norm of the state vector is preserved during every evolution. After all, it is reasonable to require that no probability leak can occur. As stated in property 1.2.3, the time evolution of a quantum state is described by the unitary operator

$$\mathbf{U} = \exp\left(-\frac{\mathcal{H}t}{\hbar}\right)$$

Since a quantum gate acting on the state vector of a closed quantum system prompts an evolution of the latter, it must be a unitary time operator \mathbf{U} , where the Hamiltonian depends on the actual physical processes by which it is implemented.

Reversibility Every unitary gate satisfies

$$\mathbf{U}^\dagger \mathbf{U} = \mathbb{I} \quad (2.1.22)$$

which ensures that it can always be undone. As a matter of fact, a reversible logic gate has always a unique input associated with a unique output. Therefore, knowing the output, it is always possible to retrieve the input and vice versa. A simple example of a reversible gate in the classical NOT gate, while, for instance, the AND gate is not reversible.

Linearity The linearity ensures that the action of a quantum gate on a generic state vector is unmistakably determined once the action on the basis vectors is stated. This means, for example, that a one-qubit gate is fully defined describing its action on $|0\rangle$ and $|1\rangle$ (according to the standard convention of using the eigenbasis of σ_z).

The fundamental quantum gates are presented in the following, distinguishing between one-qubit and multi-qubit qugates.

2.1.6.1 One-qubit quantum gates

The \mathbb{I} gate This gate maps state $|0\rangle$ to state $|0\rangle$ and $|1\rangle$ to state $|1\rangle$:

$$\mathbb{I} : \begin{cases} |0\rangle \longrightarrow |0\rangle \\ |1\rangle \longrightarrow |1\rangle \end{cases} \quad (2.1.23)$$

Consequently

$$\mathbb{I} = |0\rangle\langle 0| + |1\rangle\langle 1| = \begin{pmatrix} 1 & 0 \\ 0 & 1 \end{pmatrix} \quad (2.1.24)$$

As it is possible to appreciate in Figure 2.6, the \mathbb{I} gate leaves $|\psi_1\rangle = c_0 |0\rangle + c_1 |1\rangle$

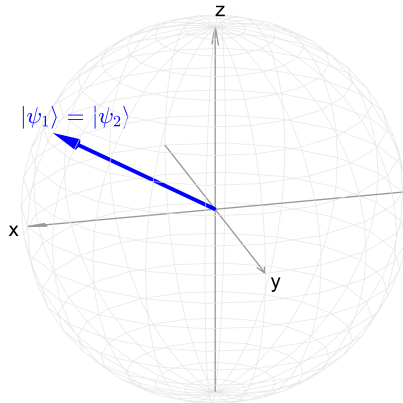


Figure 2.6: Identity gate.

unaffected

$$|\psi_2\rangle = \mathbb{I}|\psi_1\rangle = |0\rangle\langle 0|\psi_1\rangle + |1\rangle\langle 1|\psi_1\rangle = c_0|0\rangle + c_1|1\rangle = |\psi_1\rangle \quad (2.1.25)$$

The \mathbf{X} gate This gate maps state $|0\rangle$ to state $|1\rangle$ and $|1\rangle$ to state $|0\rangle$:

$$\mathbf{X} : \begin{cases} |0\rangle \longrightarrow |1\rangle \\ |1\rangle \longrightarrow |0\rangle \end{cases} \quad (2.1.26)$$

Consequently

$$\mathbf{X} = |1\rangle\langle 0| + |0\rangle\langle 1| = \begin{pmatrix} 0 & 1 \\ 1 & 0 \end{pmatrix} = \sigma_x \quad (2.1.27)$$

As it is possible to appreciate in Figure 2.7, the \mathbf{X} gate introduces a rotation of π about \hat{x} and implements the logic NOT operation⁴

$$|\psi_2\rangle = \mathbf{X}|\psi_1\rangle = |1\rangle\langle 0|\psi_1\rangle + |0\rangle\langle 1|\psi_1\rangle = c_0|1\rangle + c_1|0\rangle \quad (2.1.28)$$

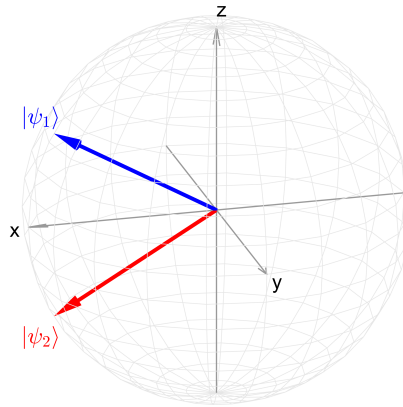


Figure 2.7: The \mathbf{X} gate.

The \mathbf{Y} gate This gate maps state $|0\rangle$ to state $i|1\rangle$ and $|1\rangle$ to state $-i|0\rangle$:

$$\mathbf{Y} : \begin{cases} |0\rangle \longrightarrow i|1\rangle \\ |1\rangle \longrightarrow -i|0\rangle \end{cases} \quad (2.1.29)$$

⁴Some authors, as [19], state that the \mathbf{X} gate is not an actual NOT gate since it does not map every qubit to the antipodes of the Bloch sphere. In any case, the important thing is to understand the operation performed by this gate, then one can call it as they prefer.

Consequently

$$\mathbf{Y} = i |1\rangle\langle 0| - i |0\rangle\langle 1| = \begin{pmatrix} 0 & -i \\ i & 0 \end{pmatrix} = \sigma_y \quad (2.1.30)$$

As it is possible to appreciate in Figure 2.8, the \mathbf{Y} gate introduces a rotation of π about \hat{y}

$$|\psi_2\rangle = \mathbf{Y} |\psi_1\rangle = i |1\rangle \langle 0|\psi_1\rangle - i |0\rangle \langle 1|\psi_1\rangle = i (c_0 |1\rangle - c_1 |0\rangle) \quad (2.1.31)$$

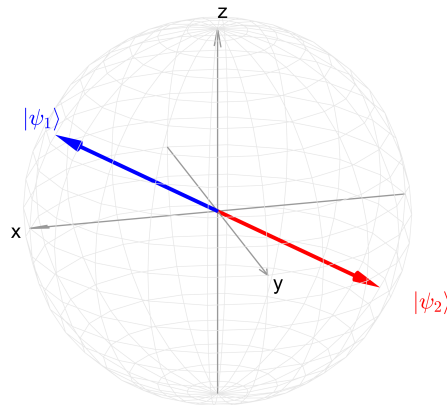


Figure 2.8: The \mathbf{Y} gate.

The \mathbf{Z} gate This gate maps state $|0\rangle$ to state $|0\rangle$ and $|1\rangle$ to state $-|1\rangle$:

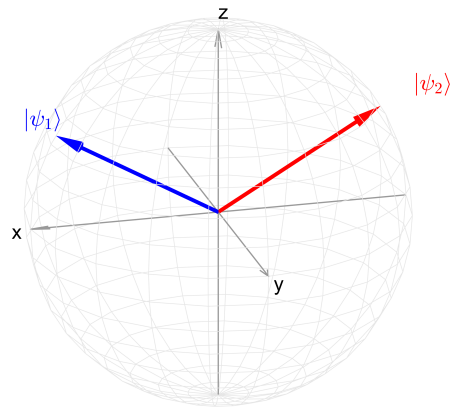
$$\mathbf{Z} : \begin{cases} |0\rangle \longrightarrow |0\rangle \\ |1\rangle \longrightarrow -|1\rangle \end{cases} \quad (2.1.32)$$

Consequently

$$\mathbf{Z} = |0\rangle\langle 0| - |1\rangle\langle 1| = \begin{pmatrix} 1 & 0 \\ 0 & -1 \end{pmatrix} = \sigma_z \quad (2.1.33)$$

As it is possible to appreciate in Figure 2.9, the \mathbf{Z} gate introduces a rotation of π about \hat{z}

$$|\psi_2\rangle = \mathbf{Z} |\psi_1\rangle = |0\rangle \langle 0|\psi_1\rangle - |1\rangle \langle 1|\psi_1\rangle = c_0 |0\rangle - c_1 |1\rangle \quad (2.1.34)$$


 Figure 2.9: The \mathbf{Z} gate.

The \mathbf{T} gate This gate maps state $|0\rangle$ to state $|0\rangle$ and $|1\rangle$ to state $e^{i\frac{\pi}{4}}|1\rangle$:

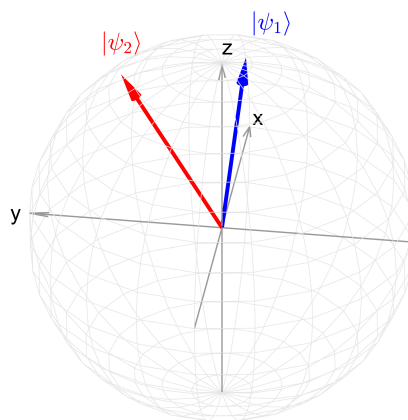
$$\mathbf{T} : \begin{cases} |0\rangle \longrightarrow |0\rangle \\ |1\rangle \longrightarrow e^{i\frac{\pi}{4}}|1\rangle \end{cases} \quad (2.1.35)$$

Consequently

$$\mathbf{T} = |0\rangle\langle 0| + e^{i\frac{\pi}{4}}|1\rangle\langle 1| = \begin{pmatrix} 1 & 0 \\ 0 & e^{i\frac{\pi}{4}} \end{pmatrix} \quad (2.1.36)$$

As it is possible to appreciate in Figure 2.10, the \mathbf{T} gate introduces a rotation of $\frac{\pi}{4}$ about \hat{z}

$$|\psi_2\rangle = \mathbf{T}|\psi_1\rangle = |0\rangle\langle 0|\psi_1\rangle + e^{i\frac{\pi}{4}}|1\rangle\langle 1|\psi_1\rangle = c_0|0\rangle + c_1e^{i\frac{\pi}{4}}|1\rangle \quad (2.1.37)$$


 Figure 2.10: The \mathbf{T} gate.

The S gate This gate maps state $|0\rangle$ to state $|0\rangle$ and $|1\rangle$ to state $e^{i\frac{\pi}{2}}|1\rangle$:

$$\mathbf{S} : \begin{cases} |0\rangle \longrightarrow |0\rangle \\ |1\rangle \longrightarrow e^{i\frac{\pi}{2}}|1\rangle \end{cases} \quad (2.1.38)$$

Consequently

$$\mathbf{S} = |0\rangle\langle 0| + e^{i\frac{\pi}{2}}|1\rangle\langle 1| = \begin{pmatrix} 1 & 0 \\ 0 & e^{i\frac{\pi}{2}} \end{pmatrix} = \mathbf{T}^2 \quad (2.1.39)$$

As it is possible to appreciate in Figure 2.11, the S gate introduces a rotation of $\frac{\pi}{2}$ about \hat{z}

$$|\psi_2\rangle = \mathbf{S}|\psi_1\rangle = |0\rangle\langle 0|\psi_1\rangle + e^{i\frac{\pi}{2}}|1\rangle\langle 1|\psi_1\rangle = c_0|0\rangle + i|1\rangle \quad (2.1.40)$$

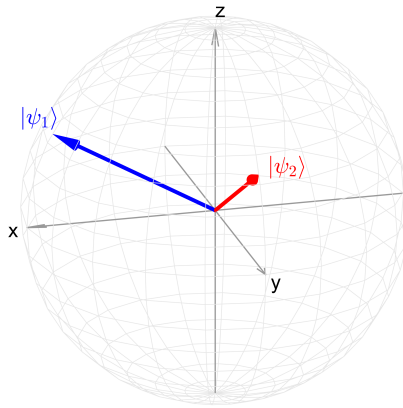


Figure 2.11: The S gate.

The H gate The Hadamard transformation is a fundamental unitary operation which maps state $|0\rangle$ to state $\frac{1}{\sqrt{2}}(|0\rangle + |1\rangle)$ and $|1\rangle$ to state $\frac{1}{\sqrt{2}}(|0\rangle - |1\rangle)$:

$$\mathbf{S} : \begin{cases} |0\rangle \longrightarrow \frac{1}{\sqrt{2}}(|0\rangle + |1\rangle) \\ |1\rangle \longrightarrow \frac{1}{\sqrt{2}}(|0\rangle - |1\rangle) \end{cases} \quad (2.1.41)$$

Consequently

$$\mathbf{H} = \frac{|0\rangle + |1\rangle}{\sqrt{2}}\langle 0| + \frac{|0\rangle - |1\rangle}{\sqrt{2}}\langle 1| = \frac{1}{\sqrt{2}} \begin{pmatrix} 1 & 1 \\ 1 & -1 \end{pmatrix} \quad (2.1.42)$$

As it is possible to appreciate in Figure 2.12, the \mathbf{H} gate sends $|0\rangle$ (and obviously $|1\rangle$) to a superposition state. As a matter of fact, if \mathbf{H} is applied to a generic state

$$|\psi_2\rangle = \mathbf{H} |\psi_1\rangle = \frac{|0\rangle + |1\rangle}{\sqrt{2}} \langle 0|\psi_1\rangle + \frac{|0\rangle - |1\rangle}{\sqrt{2}} \langle 1|\psi_1\rangle = \frac{c_0 + c_1}{\sqrt{2}} |0\rangle + \frac{c_0 - c_1}{\sqrt{2}} |1\rangle \quad (2.1.43)$$

In the specific case of $|0\rangle$

$$|\psi_2\rangle = \mathbf{H} |0\rangle = \frac{1}{\sqrt{2}} (|0\rangle + |1\rangle) \quad (2.1.44)$$

The Hadamard transformation is routinely employed in quantum algorithms to

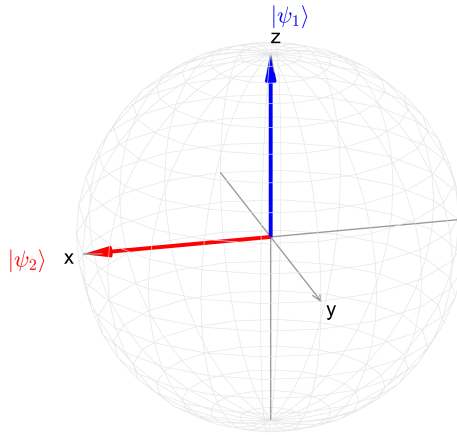


Figure 2.12: The \mathbf{H} gate.

send an initial fiduciary state $|00 \cdots 0\rangle$ to a superposition of all basis states. Let

$$\mathbf{H}_1 \otimes \mathbf{H}_2 \otimes \cdots \otimes \mathbf{H}_n = \mathbf{H}^{\otimes n} \quad (2.1.45)$$

Applying $\mathbf{H}^{\otimes n}$ to the initial fiduciary state

$$\mathbf{H}^{\otimes n} |00 \cdots 0\rangle = \frac{1}{\sqrt{2^n}} \sum_{x=0}^{2^n-1} |x\rangle \quad (2.1.46)$$

one obtains a superposition of all basis states, as expected.

Example 2.1.2. Consider a three-qubit system and suppose it is initialized to

the fiduciary state $|\psi_1\rangle = |000\rangle$. Next, $\mathbf{H}^{\otimes 3}$ is applied to the initial state.

$$\begin{array}{ccc}
 |0\rangle & \longrightarrow \boxed{H} \longrightarrow & \frac{|0\rangle+|1\rangle}{\sqrt{2}} \\
 \\
 |0\rangle & \longrightarrow \boxed{H} \longrightarrow & \frac{|0\rangle+|1\rangle}{\sqrt{2}} \\
 \\
 |0\rangle & \longrightarrow \boxed{H} \longrightarrow & \frac{|0\rangle+|1\rangle}{\sqrt{2}} \\
 \\
 |\psi_1\rangle & & |\psi_2\rangle
 \end{array}$$

The output state is the tensor product of the three output qubits

$$\begin{aligned}
 |\psi_2\rangle &= \mathbf{H}^{\otimes 3} |000\rangle = \left(\frac{|0\rangle + |1\rangle}{\sqrt{2}} \right) \otimes \left(\frac{|0\rangle + |1\rangle}{\sqrt{2}} \right) \otimes \left(\frac{|0\rangle + |1\rangle}{\sqrt{2}} \right) \\
 &= \frac{|000\rangle + |001\rangle + |010\rangle + |011\rangle + |100\rangle + |101\rangle + |110\rangle + |111\rangle}{\sqrt{2^3}} \\
 &= \frac{1}{\sqrt{2^3}} \sum_{x=0}^7 |x\rangle
 \end{aligned}$$

Therefore, it is the superposition of all possible eigenstates. As it is clear from this example, these eigenstates represent all the possible bit strings one can write using n bits. The use of the Hadamard transformation, is one of the most important tools of quantum computing.

Each basis vector has a probability

$$p_i = \left(\frac{1}{\sqrt{8}} \right)^2 = \frac{1}{8}$$

to be the outcome when a projective measurement is performed. △

Generic one-bit gates As reported in [20], the most general form of a one qubit gate is

$$U(\theta, \phi, \lambda) = \begin{pmatrix} \cos(\frac{\theta}{2}) & -e^{i\lambda} \sin(\frac{\theta}{2}) \\ e^{i\phi} \sin(\frac{\theta}{2}) & e^{i\lambda+i\phi} \cos(\frac{\theta}{2}) \end{pmatrix} \quad (2.1.47)$$

Other useful qugates are the ones which allow to perform arbitrary rotations about a specific axis:

- A rotation of α about \hat{x} :

$$\mathbf{R}_x(\alpha) = \exp\left(-i\frac{\alpha}{2}\boldsymbol{\sigma}_x\right) = \begin{pmatrix} \cos\left(\frac{\alpha}{2}\right) & -i\sin\left(\frac{\alpha}{2}\right) \\ -i\sin\left(\frac{\alpha}{2}\right) & \cos\left(\frac{\alpha}{2}\right) \end{pmatrix} = \cos\left(\frac{\alpha}{2}\right)\mathbb{I} - i\sin\left(\frac{\alpha}{2}\right)\mathbf{X} \quad (2.1.48)$$

In particular, note that a rotation of π about \hat{x} is

$$\mathbf{R}_x(\pi) = -i\mathbf{X} \sim \mathbf{X} \quad (2.1.49)$$

where the last equality follows from the fact that a quantum state is defined up to a phase contribution.

- A rotation of α about \hat{y} :

$$\mathbf{R}_y(\alpha) = \exp\left(-i\frac{\alpha}{2}\boldsymbol{\sigma}_y\right) = \begin{pmatrix} \cos\left(\frac{\alpha}{2}\right) & -\sin\left(\frac{\alpha}{2}\right) \\ \sin\left(\frac{\alpha}{2}\right) & \cos\left(\frac{\alpha}{2}\right) \end{pmatrix} = \cos\left(\frac{\alpha}{2}\right)\mathbb{I} - i\sin\left(\frac{\alpha}{2}\right)\mathbf{Y} \quad (2.1.50)$$

In particular, note that a rotation of π about \hat{y} is

$$\mathbf{R}_y(\pi) = -i\mathbf{Y} \sim \mathbf{Y} \quad (2.1.51)$$

- A rotation of α about \hat{z} :

$$\mathbf{R}_z(\alpha) = \exp\left(-i\frac{\alpha}{2}\boldsymbol{\sigma}_z\right) = \begin{pmatrix} e^{-i\frac{\alpha}{2}} & 0 \\ 0 & e^{+i\frac{\alpha}{2}} \end{pmatrix} = \cos\left(\frac{\alpha}{2}\right)\mathbb{I} - i\sin\left(\frac{\alpha}{2}\right)\mathbf{Z} \quad (2.1.52)$$

In particular, note that a rotation of π about \hat{z} is

$$\mathbf{R}_z(\pi) = -i\mathbf{Z} \sim \mathbf{Z} \quad (2.1.53)$$

2.1.6.2 Multi-qubit and controlled quantum gates

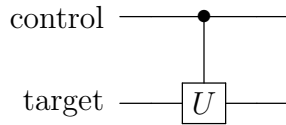
Generic controlled gate A generic two-qubit controlled gate is a gate which acts on the target qubit if and only if the control qubit is in state $|1\rangle$. It is a kind of *if-then-else* gate. Let

$$\mathbf{U} = \begin{pmatrix} u_0 & u_1 \\ u_2 & u_3 \end{pmatrix} \quad (2.1.54)$$

the associated controlled \mathbf{CU} gate is

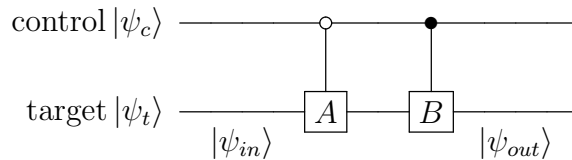
$$\mathbf{CU} = |0\rangle\langle 0| \otimes \mathbb{I} + |1\rangle\langle 1| \otimes \mathbf{U} = \begin{pmatrix} 1 & 0 & 0 & 0 \\ 0 & 1 & 0 & 0 \\ 0 & 0 & u_0 & u_1 \\ 0 & 0 & u_2 & u_3 \end{pmatrix} = \begin{pmatrix} \mathbb{I} & \mathbf{0} \\ \mathbf{0} & \mathbf{U} \end{pmatrix} \quad (2.1.55)$$

where $\mathbf{0}$ is a matrix of zeros. The circuit symbol is



The behavior of a controlled gate is trivial if the control qubit is in state $|0\rangle$ or in state $|1\rangle$. What does it happen when the control qubit is a linear combination of $|0\rangle$ and $|1\rangle$? Well, the controlled gate acts on the superposition state and the control actions are performed in parallel: the “degree” of each action depends on the amplitude of the corresponding eigenstate in the input superposition state.

Example 2.1.3. Consider the following quantum circuit



where the \mathbf{A} gate is applied to the target bit if the control bit is in $|0\rangle$, while the \mathbf{B} gate is applied if the target bit is in $|1\rangle$. The corresponding matrix is

$$\begin{pmatrix} \mathbf{A} & \mathbf{0} \\ \mathbf{0} & \mathbf{B} \end{pmatrix} = \begin{pmatrix} A_{11} & A_{12} & 0 & 0 \\ A_{21} & A_{22} & 0 & 0 \\ 0 & 0 & B_{11} & B_{12} \\ 0 & 0 & B_{21} & B_{22} \end{pmatrix}$$

Suppose the target qubit is in a generic state

$$|\psi_t\rangle = t_0|0\rangle + t_1|1\rangle$$

When the control qubit is in state $|0\rangle$, the output state is

$$|\psi_{out}\rangle = |0\rangle \otimes \mathbf{A}(t_0 |0\rangle + t_1 |1\rangle)$$

while, when it is in state $|1\rangle$, the output becomes

$$|\psi_{out}\rangle = |1\rangle \otimes \mathbf{B}(t_0 |0\rangle + t_1 |1\rangle)$$

Suppose, now, that the input is a general superposition state

$$|\psi_{in}\rangle = a |00\rangle + b |01\rangle + c |10\rangle + d |11\rangle$$

Then, the gate acts on each input eigenstate proportionally:

$$\begin{aligned} a |00\rangle &\longrightarrow a |0\rangle \otimes \mathbf{A} |0\rangle \\ b |01\rangle &\longrightarrow b |0\rangle \otimes \mathbf{A} |1\rangle \\ c |10\rangle &\longrightarrow c |1\rangle \otimes \mathbf{B} |0\rangle \\ d |11\rangle &\longrightarrow d |1\rangle \otimes \mathbf{B} |1\rangle \end{aligned}$$

Thanks to linearity, the proper control actions are performed, in the correct proportions

$$|\psi_{out}\rangle = |0\rangle \otimes \mathbf{A}(a |0\rangle + b |1\rangle) + |1\rangle \otimes \mathbf{B}(c |0\rangle + d |1\rangle)$$

△

The extension to multi-qubit controlled quantum gate is trivial.

The CNOT gate The controlled NOT gate, also known as **CX** gate, is an important quantum gate which flips the second qubit (the **target qubit**) if and only if the first qubit (the **control qubit**) is in state $|1\rangle$. Otherwise, the target qubit is unaffected.

$$\mathbf{CX} : \begin{cases} |00\rangle \longrightarrow |00\rangle \\ |01\rangle \longrightarrow |01\rangle \\ |10\rangle \longrightarrow |11\rangle \\ |11\rangle \longrightarrow |10\rangle \end{cases} \quad (2.1.56)$$

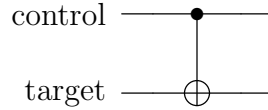
Consequently

$$\begin{aligned}
 \mathbf{CX} &= |00\rangle\langle 00| + |01\rangle\langle 01| + |11\rangle\langle 10| + |10\rangle\langle 11| \\
 &= |0\rangle\langle 0| \otimes \mathbf{I} + |1\rangle\langle 1| \otimes \mathbf{X} = \begin{pmatrix} 1 & 0 & 0 & 0 \\ 0 & 1 & 0 & 0 \\ 0 & 0 & 0 & 1 \\ 0 & 0 & 1 & 0 \end{pmatrix} \quad (2.1.57)
 \end{aligned}$$

Since the target qubit is flipped only if the control qubit is in state $|1\rangle$, the operation performed by the \mathbf{CX} gate corresponds to the logic **XOR** operation, even if, differently from the classical XOR logic gate, it is reversible since the control qubit is “conserved” and provided in output:

$$|x\rangle |y\rangle \xrightarrow{\mathbf{CX}} |x\rangle |x \oplus y\rangle \quad (2.1.58)$$

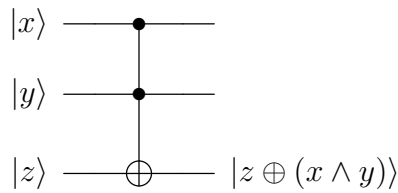
The circuital symbol is



The Toffoli gate The Toffoli or Controlled-Controlled-NOT gate, also known as \mathbf{CCX} , flips the target qubit if and only if both control qubits are in state $|1\rangle$. The corresponding matrix is derived as

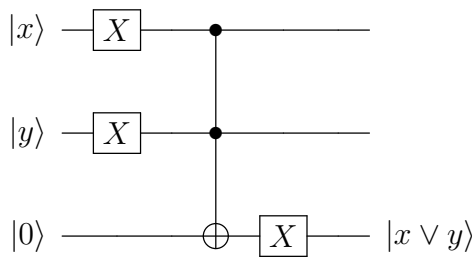
$$\begin{aligned}
 \mathbf{CCX} &= (|00\rangle\langle 00| + |01\rangle\langle 01| + |10\rangle\langle 10|) \otimes \mathbf{I} + |11\rangle\langle 11| \otimes \mathbf{X} \\
 &= \begin{pmatrix} 1 & 0 & 0 & 0 & 0 & 0 & 0 & 0 \\ 0 & 1 & 0 & 0 & 0 & 0 & 0 & 0 \\ 0 & 0 & 1 & 0 & 0 & 0 & 0 & 0 \\ 0 & 0 & 0 & 1 & 0 & 0 & 0 & 0 \\ 0 & 0 & 0 & 0 & 1 & 0 & 0 & 0 \\ 0 & 0 & 0 & 0 & 0 & 1 & 0 & 0 \\ 0 & 0 & 0 & 0 & 0 & 0 & 0 & 1 \\ 0 & 0 & 0 & 0 & 0 & 0 & 1 & 0 \end{pmatrix} \quad (2.1.59)
 \end{aligned}$$

The circuit symbol is

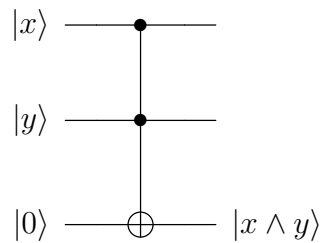


Using basic logic theorems, it is straightforward to realize that classical AND and OR operations can be performed resorting to the Toffoli gate, even if the latter is reversible, while the former are not.

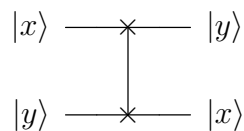
The OR gate:



The AND gate:



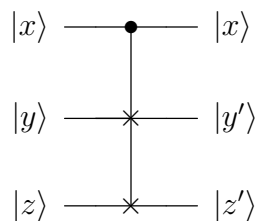
The SWAP gate The SWAP gate swaps two qubits:



The corresponding matrix is

$$U_{\text{SWAP}} = |00\rangle\langle 00| + |01\rangle\langle 10| + |10\rangle\langle 01| + |11\rangle\langle 11| = \begin{pmatrix} 1 & 0 & 0 & 0 \\ 0 & 0 & 1 & 0 \\ 0 & 1 & 0 & 0 \\ 0 & 0 & 0 & 1 \end{pmatrix} \quad (2.1.60)$$

The Fredkin gate The Fredkin gate is a Controlled-SWAP gate, which swaps the two target qubits if and only if the control qubit is in state $|1\rangle$:

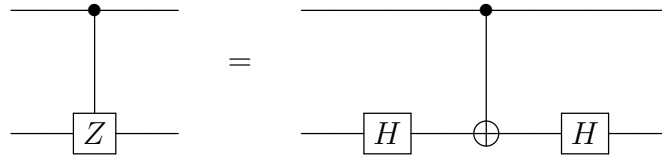


The corresponding matrix is

$$U_{\text{Fredkin}} = |0\rangle\langle 0| \otimes \mathbb{I}^{\otimes 2} + |1\rangle\langle 1| \otimes U_{\text{SWAP}} = \begin{pmatrix} 1 & 0 & 0 & 0 & 0 & 0 & 0 & 0 \\ 0 & 1 & 0 & 0 & 0 & 0 & 0 & 0 \\ 0 & 0 & 1 & 0 & 0 & 0 & 0 & 0 \\ 0 & 0 & 0 & 1 & 0 & 0 & 0 & 0 \\ 0 & 0 & 0 & 0 & 1 & 0 & 0 & 0 \\ 0 & 0 & 0 & 0 & 0 & 0 & 1 & 0 \\ 0 & 0 & 0 & 0 & 0 & 1 & 0 & 0 \\ 0 & 0 & 0 & 0 & 0 & 0 & 0 & 1 \end{pmatrix} \quad (2.1.61)$$

2.1.6.3 Some useful equivalences

Controlled-Z gate The Controlled-Z gate can be obtained using two Hadamard gates and a CNOT gate:



The Pauli decomposition Defining the phase gate as

$$\Phi(\delta) \triangleq \begin{pmatrix} e^{i\delta} & 0 \\ 0 & e^{i\delta} \end{pmatrix} \quad (2.1.62)$$

every unitary gate U can be rewritten as the product of the phase gate and a special unitary gate V :

$$U = \Phi(\delta) \times V \quad (2.1.63)$$

It is easy to show [19] that a special unitary gate can always be rewritten as the product of three rotation gates

$$V = R_z(\alpha)R_y(\beta)R_z(\gamma) \quad (2.1.64)$$

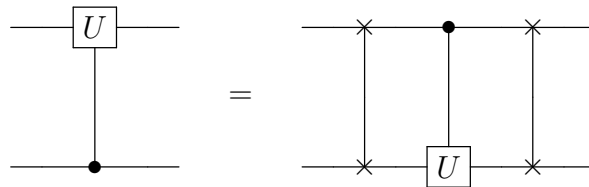
for some angles α , β and γ . Consequently, every unitary gate can be expressed as

$$U = \Phi(\delta)R_z(\alpha)R_y(\beta)R_z(\gamma) \quad (2.1.65)$$

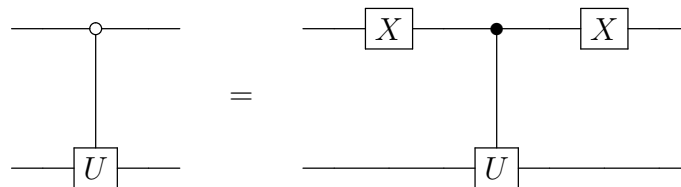
Standard decompositions for controlled and controlled-controlled quantum gates are well known and can be found in almost every book on quantum computing,

as [21, 5, 19].

Flipped control qubit According to the hardware configuration of the quantum processor, it often happens that a correlation can be arranged only among some qubits. In these cases, it can be useful to flip the control and target qubit of a controlled quantum gate. The following equivalence holds true:



Control on $|0\rangle$ If the action of the controlled gate on the target qubit is prompted by a control qubit in state $|0\rangle$, one can adopt the following circuit:



Other interesting equivalences can be found in [22].

2.1.6.4 Universal set of quantum gates

A universal set of quantum gates is a set from which every quantum circuit can be implemented. The following **universality theorem** ensures that every quantum circuit can be decomposed in elementary quantum gates.

Theorem 2.1.1. *The set of **single qubit gates** and **CNOT gate** is universal: any unitary gate acting on an n -qubit register can be implemented with single qubit gates and CNOT gates.*

The proof can be found in the original paper [21] and in [5]. It has to be remarked that this is not the only possible set of universal quantum gates. According to the hardware implementation, the physical realization of some quantum gates can be more or less simple. Some possibilities are presented in [19].

2.1.7 No-cloning theorem

A striking difference with respect to classical computing is that quantum information cannot be copied exactly.

Theorem 2.1.2. *There is no deterministic quantum procedure by which an unknown arbitrary pure quantum state can be cloned exactly.*

Proof. Suppose ad absurdum that there exists a unitary transformation which is able to clone a quantum state:

$$|\psi\rangle |0\rangle \xrightarrow{U_{\text{clone}}} |\psi\rangle |\psi\rangle$$

which means that the quantum state of the first qubit is replicated on the second qubit. In particular, for the basis vectors $|0\rangle$ and $|1\rangle$, the action of U_{clone} is

$$\begin{aligned} |00\rangle &\xrightarrow{U_{\text{clone}}} |00\rangle \\ |10\rangle &\xrightarrow{U_{\text{clone}}} |11\rangle \end{aligned}$$

Now, consider the expected action of the cloning gate on the following superposition states

$$\begin{aligned} \frac{|0\rangle + |1\rangle}{\sqrt{2}} \otimes |0\rangle &\xrightarrow{U_{\text{clone}}} \frac{|0\rangle + |1\rangle}{\sqrt{2}} \otimes \frac{|0\rangle + |1\rangle}{\sqrt{2}} \\ \frac{|0\rangle - |1\rangle}{\sqrt{2}} \otimes |0\rangle &\xrightarrow{U_{\text{clone}}} \frac{|0\rangle - |1\rangle}{\sqrt{2}} \otimes \frac{|0\rangle - |1\rangle}{\sqrt{2}} \end{aligned}$$

Nevertheless, because of linearity, the actual action of U_{clone} is

$$\begin{aligned} \frac{|0\rangle + |1\rangle}{\sqrt{2}} \otimes |0\rangle &\xrightarrow{U_{\text{clone}}} \frac{|00\rangle + |11\rangle}{\sqrt{2}} \\ \frac{|0\rangle - |1\rangle}{\sqrt{2}} \otimes |0\rangle &\xrightarrow{U_{\text{clone}}} \frac{|00\rangle - |11\rangle}{\sqrt{2}} \end{aligned}$$

One should agree upon the fact that the obtained states *are not* clones of the input state. Thus, if U_{clone} copies the basis states, it does not clone non-orthogonal states and vice versa. \square

There is a final remark which is of interest. The no-cloning theorem states that it is not possible to copy *unknown arbitrary* states. If, on the other hand, states are limited to $|0\rangle$ and $|1\rangle$, qubits can be copied, as highlighted in [5].

2.2 Quantum algorithms

At this time, it is interesting to understand why one should use a quantum computer and which are the main advantages compared to classical computation. The discussion of quantum algorithms, that is, the algorithms which are tailored to be executed on a quantum processor, is not the main core of this research. Some recommended readings addressing this topic are [16, 18, 19, 23]. Nevertheless, the basic tricks exploited by quantum algorithms are detailed in the following and a well-known example is presented, following a graphical, non standard-approach.

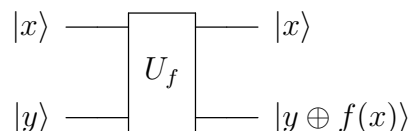
As hinted in the introduction of this chapter, the research for useful quantum algorithms is still ongoing, but the embedded computational power and the fields in which it is expected to outperform classical computers when the hardware will be ready, are becoming well known to the scientific community. In [19], some interesting applications are reviewed, ranging from the simulation of quantum systems, to quantum chemistry and mathematics.

2.2.1 Quantum parallelism and interference

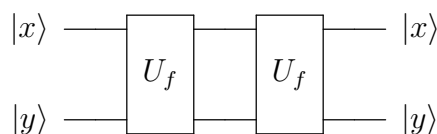
A quantum computer has several shots in its locker to solve a problem. The first one is a technique known as **quantum parallelism**. Suppose that there exists a linear unitary operator U_f whose action is:

$$|x\rangle |y\rangle \xrightarrow{U_f} |x\rangle |y \oplus f(x)\rangle \quad (2.2.1)$$

which implements a function f . In quantum computing jargon, U_f is routinely addressed as the **oracle**.



This construction ensures that U_f is unitary and thus reversible. As a matter of fact, it is trivial to see that U_f is its own inverse:



Now, assume the first qubit is sent to a superposition state applying a Hadamard gate

$$\mathbf{H}^{\otimes n} |x\rangle = \frac{1}{\sqrt{2}} \sum_{x=0}^{2^n-1} |x\rangle \quad (2.2.2)$$

When the input is a superposition of 2^n states, being \mathbf{U}_f a **linear** operator, it computes 2^n values $f(x_k)$, $1 \leq k \leq n$ *simultaneously*.

$$\mathbf{U}_f \left(\frac{1}{\sqrt{2^n}} \sum_{x=0}^{2^n-1} |x\rangle |y\rangle \right) = \frac{1}{\sqrt{2^n}} \sum_{x=0}^{2^n-1} |x\rangle |y \oplus f(x)\rangle \quad (2.2.3)$$

This seems to be an exponential speedup obtained almost for free: calling a single time the oracle, all the 2^n possible outcomes of the function are computed. Unluckily, things are not so simple. The point is that, even if the quantum state produced by the oracle function is actually a superposition of all possible outcomes, when a measurement is performed, the system collapses to a *single* state. What is worse, all outputs have the same probability to be measured, namely $1/2^n$, and, at this point, it is not possible to choose a specific vector at will. In other words, the probability to pick up the desired output is just $1/2^n$.

However, quantum parallelism *is* a powerful tool. As a matter of fact, quantum algorithms are tailored such that, once this superposition is obtained, some special operations are performed to increase the probability of the desired outcome and reduce the probability of the others. The aforementioned “special operations” resort on the quantum interference, that is, the fact that the **probability amplitudes** are complex numbers and can be properly combined to increase or reduce the probability of a specific outcome. It will be clearer when analysing an actual quantum algorithm.

A generic quantum algorithm can be divided in four main steps:

1. **Prepare superposition:** the input qubits are sent to a superposition state, often adopting the Hadamard gate.
2. **Manipulate:** some operations, depending on the specific algorithm, are performed on the superposition state.
3. **Consolidate:** the output superposition is consolidated, that is, exploiting the quantum interference the desired output is given a larger probability.
4. **Measure.**

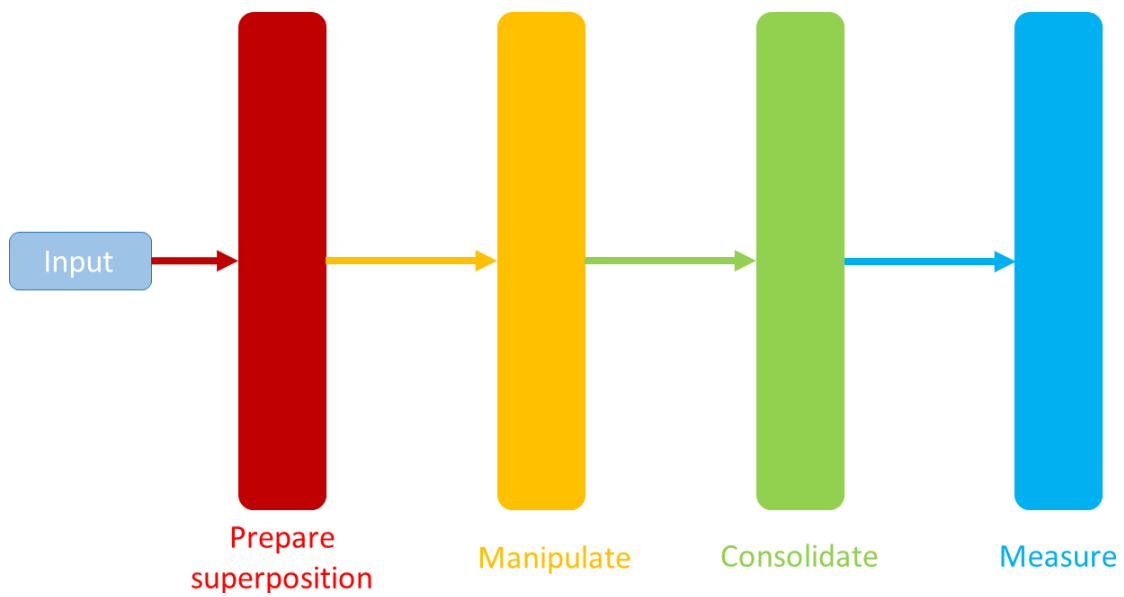


Figure 2.13: Schematic representation of a quantum algorithm.

It is interesting to highlight that, even if the probability of the desired outcome is increased, it is still a probability, meaning that there is no certainty to get the proper answer. After all, quantum mechanics is all about probability. However, as suggested in [24], one can always verify the answer: for many problems, verifying the solution is much easier than finding it.

2.2.2 Grover’s search algorithm

Search is a pervasive task in many fields. Such a task is particularly demanding when the problem is **unstructured**, which means that the discovery that a specific possibility is incorrect does not allow to learn anything useful about the solution of the problem. It is a classical *look-for-a-needle-in-a-haystack* problem. A simple example of an unstructured search problem is a standard telephone directory: instead of looking for the number given the name (this is a structured problem), one can look for the name given the number. The fact that a certain number is not the searched one does not allow to advance any hypothesis on where the desired number is.

A classical algorithm tackles the problem with a generate-and-test approach: all possible solutions are generated and then tested, one by one. It is obvious that if there are $N = 2^n$ elements, it will take, on average, $\mathcal{O}(N/2)$ iterations of the algorithm to find the searched result. Nevertheless, if one is very unlucky, they will find the solution on the N -th repetition. Hence, the cost of the classical algorithm is $\mathcal{O}(N)$. The quantum counterpart, Grover’s search algorithm, can achieve the same result with a $\mathcal{O}(\sqrt{N})$ cost. This is a quadratic, and so **polynomial, speedup**. Other well-known quantum algorithms, such as Deutsch-Jozsa algorithm, allow gaining a more impressive exponential speed-up with respect to their classical counterpart. Nevertheless, Grover’s search algorithm has a significantly larger range of possible applications.

For the sake of simplicity, in the following, it will be given for granted that a solution to the problem exists and is unique. Grover’s search algorithm can be easily extended to deal with problems which may have many solutions or no solution at all. For further details, the reader is suggested to look at [19, 25, 26].

2.2.2.1 The oracle

The word *oracle* comes from the Latin verb *orare* and refers to an omniscient person uttering predictions and knowing answers to all questions. In computer science, the oracle is a mathematical tool useful to evaluate the complexity of an algorithm. It is a kind of black-box to which one provides an input and asks whether or not it is the searched solution. In mathematical terms, assuming that one has to find a target item amongst $N = 2^n$ candidates, each of them labelled by a proper index x in the range $0 \leq x \leq N - 1$ and that the searched element

corresponds to the label s , the oracle function is defined as

$$f(x) = \begin{cases} 0 & \text{if } x \neq s \\ 1 & \text{if } x = s \end{cases} \quad (2.2.4)$$

Thus, if $x = s$ the oracle says *yes*, otherwise it says *no*.

The oracle is probably one of the most counter-intuitive concepts of this section, for people without a background in computer science. As a matter of fact, one could argue that the solution s has to be known to realize the oracle function, which, in turns, is used to find s . It seems meaningless. Two remarks are needed. The first one is that the oracle is used to compare the costs of different implementations of an algorithm, even if parts of the latter are not thoroughly understood. One evaluates the cost in units of the number of calls to the oracle: an algorithm which addresses the oracle fewer times, has a lower cost. The second remark is that when dealing with real problems, the oracle is replaced by a testing procedure which does not have an explicit foreknowledge of the solution, but only an *implicit* one, via the properties that a valid solution must have. There is a substantial difference between a circuit which can *recognize* a solution and which *knows* the solution in advance.

2.2.2.2 Geometrical interpretation

As previously stated, one of the main tricks of quantum computation is the proper exploitation of **quantum parallelism**. If the solution state $|s\rangle$ is completely unknown, a reasonable starting state is an equal superposition of all possible search solutions:

$$|E\rangle = H^{\otimes n} |0\rangle = \frac{1}{\sqrt{N}} \sum_{x \in \{0,1\}^n} |x\rangle \quad (2.2.5)$$

Even if obvious, it is worth highlighting that the possible solutions coincide with the computational basis states and so they are mutually orthogonal. It is clear that if it is known in advance that some state $|x\rangle$ cannot be a legal solution to the problem, the initial superposition can be arranged by making sure $|x\rangle$ is not included, in order to speed up the algorithm. Nevertheless, here the worst case in which the initial state has to be an equal mixture of all possible outcomes is dealt with.

At the time being, if a measurement is performed, the system has a probability

$$p_s = \left(\frac{1}{\sqrt{N}} \right)^2 = \frac{1}{N} \quad (2.2.6)$$

to collapse to the searched solution. The aim, now, is to *increase the probability* of getting $|E\rangle \rightarrow |s\rangle$ while reducing the probability that the outcome is any other undesired state. This is the realm of **quantum interference** and Grover's algorithm makes advantage of the latter through two expedients:

1. Reflection about $|s\rangle$ via the application of the oracle operator.
2. Reflection about $|E\rangle$ via the application of the diffusion operator.

The starting state Pure quantum states have always unitary magnitude and the latter is not changed when quantum gates are applied. Consequently, a nice pictorial way of representing a quantum state is on a unitary circle, as the one reported in Figure 2.14. The initial state is $|E\rangle$, which is an equal superposition of all basis states. Note that $|E\rangle$ is close to be orthogonal to the solution state vector $|s\rangle$. Clearly, this is due to the fact that the component of $|E\rangle$ in the direction of $|s\rangle$ has a magnitude of $1/\sqrt{N}$, which is small, when N is large. If $|\bar{E}\rangle$ is obtained from $|E\rangle$ removing $|s\rangle$ and denoting with δ the angle between $|E\rangle$ and $|\bar{E}\rangle$, it is just a matter of trivial trigonometry to realize that

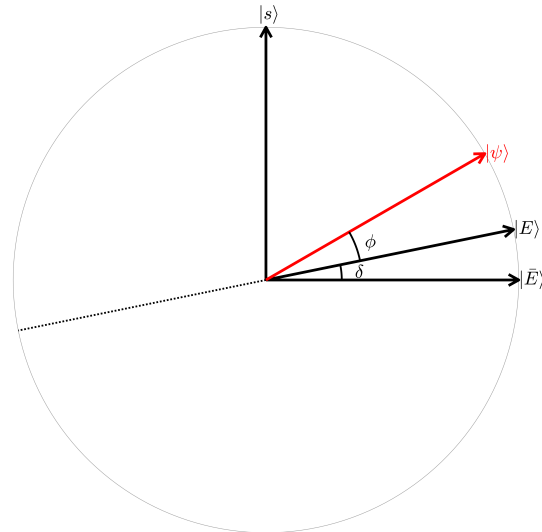


Figure 2.14: Initial state.

$$\sin(\delta) = \frac{1}{\sqrt{N}} \longrightarrow \delta = \text{asin}\left(\frac{1}{\sqrt{N}}\right) \approx \frac{1}{\sqrt{N}} \quad (2.2.7)$$

The aim is to rotate $|E\rangle$ so that it will end up to be as close as possible to the solution $|s\rangle$. At the end, when a measurement is performed, the probability that the system will collapse to $|s\rangle$ must be very high.

Finally, consider that the symbol $|\psi\rangle$ is adopted to represent a generic state at a certain step of the algorithm.

Reflection about $|s\rangle$ The main problem is that, unfortunately, the solution $|s\rangle$

is not known. Thus, the desired rotation cannot be achieved in a single step. A possibility comes from elementary geometry which states that two consecutive reflections about different axes result in a rotation.

Now, suppose that it is possible somehow to perform a reflection of $|\psi\rangle$ about $|s\rangle$. Letting θ be the angle between $|\psi\rangle$ and $|s\rangle$, 2θ is the total angle between $|\psi\rangle$ and $|\psi_1\rangle$, as reported in Figure 2.15. How to perform this reflection will be clear in the following, when discussing the circuitual implementation.

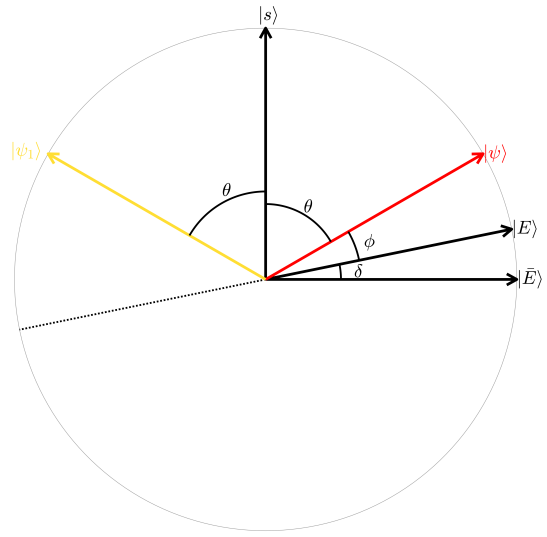


Figure 2.15: Reflection about $|s\rangle$.

Reflection about $|E\rangle$ Now, imagine that also a reflection about the initial state $|E\rangle$ is feasible. Since the angle between $|\psi_1\rangle$ and the extension of $|E\rangle$ is $\pi - (2\theta + \phi)$, the overall angle between the original $|\psi\rangle$ and $|\psi_2\rangle$ is $\alpha = 2\theta + 2\phi$. Since the angle between $|E\rangle$ and $|\bar{E}\rangle$ can be expressed as $\delta = \frac{\pi}{2} - \theta - \phi$, the rotation angle becomes

$$\alpha = 2\theta + 2\phi = \pi - 2\delta \quad (2.2.8)$$

At this point, a rotation of an angle 2δ has been achieved. As a matter of fact, it has to be remarked that $|\psi_2\rangle$ is closer to $-|s\rangle$ than $-|\psi\rangle$ of an angle 2δ .

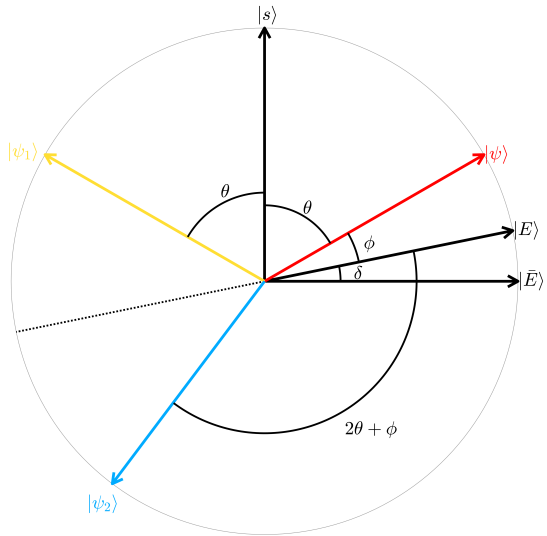


Figure 2.16: Reflection about $|E\rangle$.

Get rid of the π factor It is well known that a *global* phase factor makes no difference at the end of a quantum computation. Hence

$$|\psi_2\rangle \sim -|\psi_2\rangle \quad (2.2.9)$$

Consequently, the state $|\psi_2\rangle$ can be multiplied by a phase factor -1 , getting $|\psi_3\rangle$.

At this time, it should be evident that the consecutive reflections about $|s\rangle$ and $|E\rangle$ have the effect of rotating $|\psi\rangle$ a 2δ angle closer to the solution $|s\rangle$. Thus, this procedure can be repeated several times (say M times) to force the initial state to get closer and closer to $|s\rangle$. If the total angle between $|E\rangle$ and $|s\rangle$ is

$$\Theta \triangleq \frac{\pi}{2} - \delta \tag{2.2.10}$$

the required number of iterations is computed dividing Θ by the angle of each rotation and taking the closest integer

$$M = \text{round} \left(\frac{\Theta}{2\delta} \right) = \text{round} \left(\frac{\pi}{4\delta} - \frac{1}{2} \right) \tag{2.2.11}$$

Since $\delta \sim 1/\sqrt{N}$, the previous expression can be approximated as

$$M \sim \frac{\pi\sqrt{N}}{4} \tag{2.2.12}$$

It has to be noted the promised **quadratic speedup** with respect to the classical counterpart.

Measurement In the final step, the maximum angle between $|\psi_f\rangle$ and the searched solution $|s\rangle$ is δ , as it is clear from Figure 2.18. Consequently, the system collapses to $|s\rangle$ with a probability which is equal to the square of the probability amplitude of $|s\rangle$ in $|\psi_f\rangle$:

$$p_s = \cos^2(\delta) = 1 - \sin^2(\delta) \sim 1 - \frac{1}{N} \tag{2.2.13}$$

The probability to get a wrong result is very small. Anyway, it is also possible to check if the obtained outcome is wrong: it is enough to use the oracle operator and discover whether the algorithm has provided a proper solution or not.

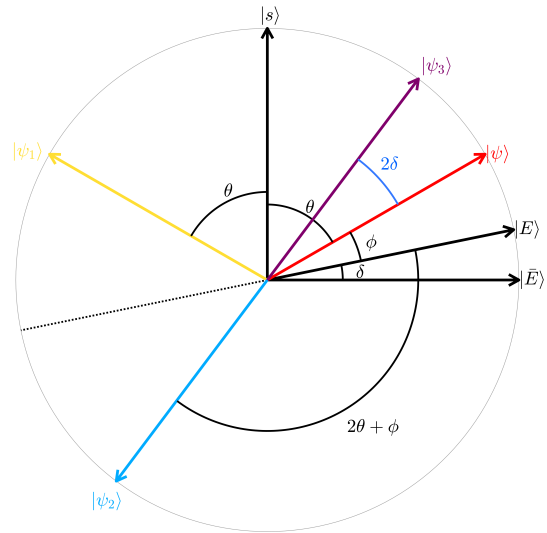


Figure 2.17: The rotation of 2δ .

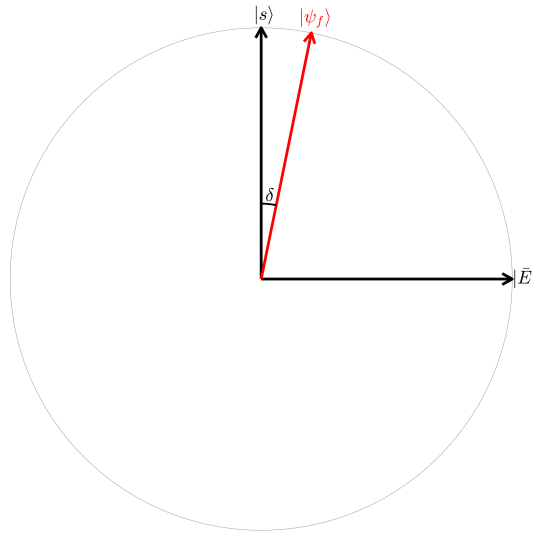


Figure 2.18: The final step.

2.2.2.3 Quantum circuit

In order to develop a circuital implementation of the discussed algorithm, it is necessary to focus on a specific case, so to be able to define a specific oracle function. Suppose the Grover's algorithm has to find the state $|10\rangle$: this is just an example useful to provide an actual quantum circuit which can be simulated on a quantum simulator. As detailed in section §2.2.2.1, in real-world implementations, the oracle is replaced by a proper testing procedure. From the previous discussion, it follows that there are three main steps which have to be converted in quantum circuits:

1. Initial superposition.
2. Oracle.
3. Diffusion operator.

When there are only two qubits, and so $N = 4$, the δ angle is

$$\delta = \arcsin\left(\frac{1}{2}\right) = \frac{\pi}{6} \quad (2.2.14)$$

Consequently, the number of rotations is just

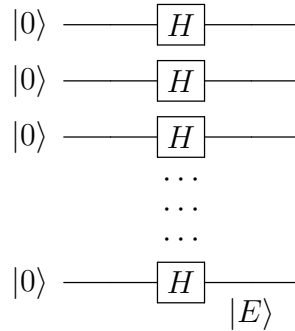
$$M = \text{round}\left(\frac{\pi}{4\delta} - \frac{1}{2}\right) = \text{round}\left(\frac{3}{2} - \frac{1}{2}\right) = \text{round}(1) = 1 \quad (2.2.15)$$

which means that after one rotation the initial state $|E\rangle$ coincides exactly with the solution $|s\rangle$. Hence, one can reasonably expect to find out that the probability of getting the desired state when a measurement is performed is 100%.

Initial superposition As discussed several times, an equal superposition of all possible basis vectors can be achieved applying a Hadamard gate to each qubit, previously initialized to $|0\rangle$:

$$|E\rangle = H^{\otimes n} |0\rangle = \frac{1}{\sqrt{N}} \sum_{x \in \{0,1\}^n} |x\rangle \quad (2.2.16)$$

The corresponding circuit for the n -qubit case is



and the quantum circuit for the 2-qubit case can be trivially derived.

The oracle operator The oracle operator is a unitary operator associated with the oracle function $f(x)$ presented in section §2.2.2.1. As discussed in section §2.2.1, it has the following form:

$$|x\rangle |y\rangle \xrightarrow{U_f} |x\rangle |y \oplus f(x)\rangle \quad (2.2.17)$$

where $|y\rangle$ is an extra qubit, known to the scientific community as the **ancilla qubit**.

The intent of this step is to perform a reflection about $|s\rangle$. In practice, this means to leave the $|s\rangle$ state alone and take every other computational basis state $|x\rangle$ to $-|x\rangle$. This operation can be implemented by the following operator

$$2 |s\rangle\langle s| - \mathbb{I} \quad (2.2.18)$$

Example 2.2.1. Assume that $N = 4$, the computational basis vectors are

$$|00\rangle |01\rangle |10\rangle |11\rangle$$

Suppose that the desired state is $|s\rangle = |10\rangle$, then the previous operator becomes

$$2|10\rangle\langle 10| - \mathbb{I}$$

The effect of this operator on the basis vectors is

$$\begin{aligned} |00\rangle &\longrightarrow (2|10\rangle\langle 10| - \mathbb{I})|00\rangle = 0|00\rangle - |00\rangle = -|00\rangle \\ |01\rangle &\longrightarrow (2|10\rangle\langle 10| - \mathbb{I})|01\rangle = 0|01\rangle - |01\rangle = -|01\rangle \\ |10\rangle &\longrightarrow (2|10\rangle\langle 10| - \mathbb{I})|10\rangle = 2|10\rangle - |10\rangle = +|10\rangle \\ |11\rangle &\longrightarrow (2|10\rangle\langle 10| - \mathbb{I})|11\rangle = 0|11\rangle - |11\rangle = -|11\rangle \end{aligned}$$

△

Since the global phase of a quantum state can be ignored, it should be clear that the same outcome is obtained if **only** $|s\rangle$ is subjected to a sign change, while all other basis states are left untouched. This operation can be obviously implemented by the following operator

$$-(2|s\rangle\langle s| - \mathbb{I}) = \mathbb{I} - 2|s\rangle\langle s| \tag{2.2.19}$$

This operator can be obtained from the oracle. As a matter of fact, assume that the ancilla qubit is initialized in state $|1\rangle$ and then a Hadamard gate is applied, so that

$$|y\rangle = |1\rangle \xrightarrow{H} \frac{|0\rangle - |1\rangle}{\sqrt{2}} \triangleq |-\rangle \tag{2.2.20}$$

The application of the oracle operator, when the n input qubits are in state $|x\rangle$ and the ancilla is in state $|-\rangle$, leads to

$$\begin{aligned} U_f(|x\rangle |y\rangle) &= |x\rangle \otimes |y \oplus f(x)\rangle = \frac{|x\rangle |0 \oplus f(x)\rangle - |x\rangle |1 \oplus f(x)\rangle}{\sqrt{2}} \\ &= (-1)^{f(x)} |x\rangle |-\rangle = \begin{cases} +\frac{|x\rangle(|0\rangle - |1\rangle)}{\sqrt{2}} & \text{if } x \neq s \\ -\frac{|x\rangle(|0\rangle - |1\rangle)}{\sqrt{2}} & \text{if } x = s \end{cases} \end{aligned} \tag{2.2.21}$$

In practical terms, the oracle operator has to **change the sign of the ancilla**

qubit if and only if the input n qubits (all qubits apart from the ancilla qubit) are in state $|x\rangle = |s\rangle$.

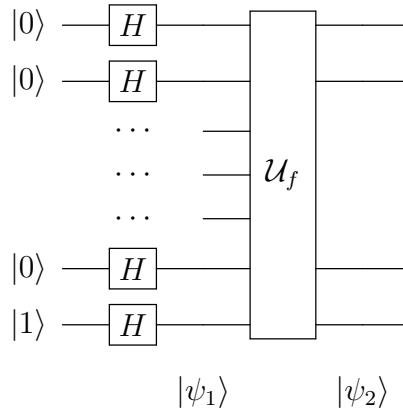
Letting

$$|\psi_1\rangle = |E\rangle \otimes |-\rangle \tag{2.2.22}$$

the application of the oracle function leads to

$$|\psi_2\rangle = \mathbf{U}_f |\psi_1\rangle = \frac{1}{\sqrt{N}} \sum_{x \in \{0,1\}^n} (-1)^{f(x)} |x\rangle |-\rangle \tag{2.2.23}$$

The quantum circuit obtained so far can be represented as follows:

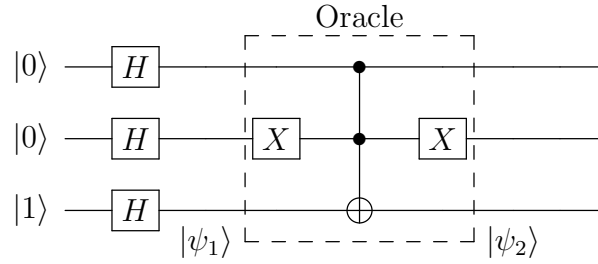


Consider again the case under analysis, that is, when $|s\rangle = |10\rangle$ and $n = 2$. The oracle function must change the sign of the ancilla qubit if and only if the top qubit is in state $|1\rangle$ and the bottom one is in $|0\rangle$. The Toffoli gate, presented in section §2.1.6.2, flips the target qubit when both control qubits are in state $|1\rangle$. In this regard, it is interesting to note that flipping the $|-\rangle$ is equivalent to multiply it by -1 :

$$|-\rangle = \frac{|0\rangle - |1\rangle}{\sqrt{2}} \xrightarrow{\mathbf{X}} \frac{|1\rangle - |0\rangle}{\sqrt{2}} = -|-\rangle \tag{2.2.24}$$

As a consequence, it is possible to build the oracle operator up with just a Toffoli gate, provided that the second qubit is properly flipped by an \mathbf{X} gate. The

resulting quantum circuit is



Clearly, the target qubit of the Toffoli gate, that is the ancilla qubit, is flipped only if the input to the oracle is

$$|\psi_1\rangle = |10\rangle |-\rangle \tag{2.2.25}$$

While the first \mathbf{X} gate is needed to flip $|0\rangle \rightarrow |1\rangle$ the second control qubit, so that the Toffoli gate can flip the target qubit when the input is $|10\rangle$, the second \mathbf{X} gate is mandatory to send back the second qubit to its initial state. This allows to get the desired $|\psi_2\rangle$, that is, to get a -1 coefficient in front of state $|10\rangle$.

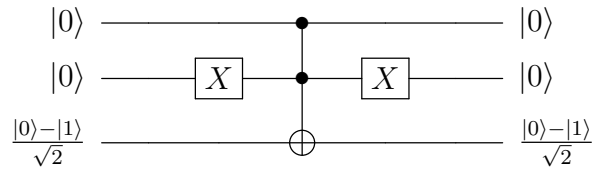
It is useful to analyze the working principle of this quantum circuit investigating all possible cases. The input Hadamard gates create the following state:

$$|\psi_1\rangle = |E\rangle |-\rangle = \frac{|00\rangle + |01\rangle + |10\rangle + |11\rangle}{2} \otimes \frac{|0\rangle - |1\rangle}{\sqrt{2}} \tag{2.2.26}$$

Since the quantum gates are linear operators, it is possible to understand their action imagining that, downstream of the Hadamard gates, instead of a single oracle working on a superposition of four basis states, there are four **parallel oracles**, each of them acting on a single basis state. Then, the overall output state vector $|\psi_2\rangle$ is the averaged sum of the four state vectors produced by the four parallel oracles.

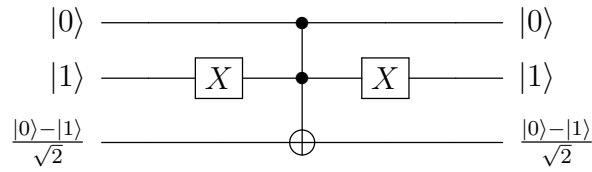
Input $|00\rangle$ The application of the oracle operator produces

$$|\psi_{1a}\rangle = |00\rangle \otimes \frac{|0\rangle - |1\rangle}{\sqrt{2}} \rightarrow |00\rangle \otimes \frac{|0\rangle - |1\rangle}{\sqrt{2}} = |\psi_{2a}\rangle \tag{2.2.27}$$



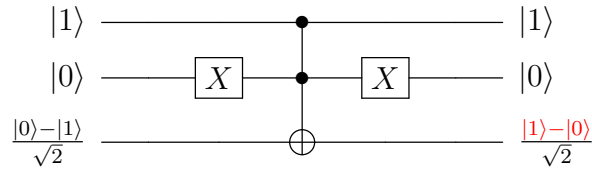
Input |01⟩ The application of the oracle operator produces

$$|\psi_{1b}\rangle = |01\rangle \otimes \frac{|0\rangle - |1\rangle}{\sqrt{2}} \longrightarrow |01\rangle \otimes \frac{|0\rangle - |1\rangle}{\sqrt{2}} = |\psi_{2b}\rangle \quad (2.2.28)$$



Input |10⟩ The application of the oracle operator produces

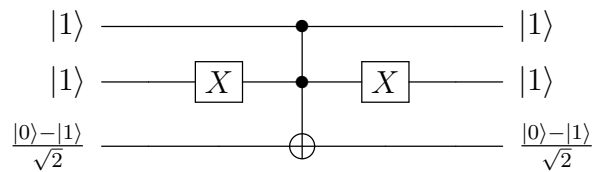
$$|\psi_{1c}\rangle = |10\rangle \otimes \frac{|0\rangle - |1\rangle}{\sqrt{2}} \longrightarrow |10\rangle \otimes \frac{|1\rangle - |0\rangle}{\sqrt{2}} = -|10\rangle \otimes \frac{|0\rangle - |1\rangle}{\sqrt{2}} = |\psi_{2c}\rangle \quad (2.2.29)$$



As expected, when the input coincides with the target state, the output sign is changed thanks to the flip of the ancilla qubit.

Input |11⟩ The application of the oracle operator produces

$$|\psi_{1d}\rangle = |11\rangle \otimes \frac{|0\rangle - |1\rangle}{\sqrt{2}} \longrightarrow |11\rangle \otimes \frac{|0\rangle - |1\rangle}{\sqrt{2}} = |\psi_{2d}\rangle \quad (2.2.30)$$



The overall output state vector can be computed exploiting the linearity of

quantum mechanics

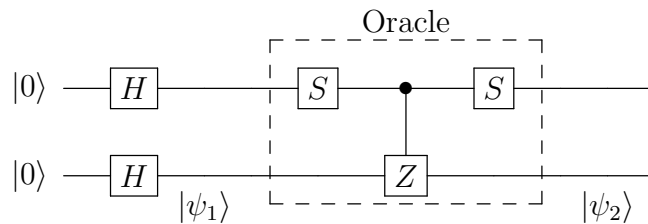
$$\begin{aligned}
 |\psi_2\rangle &= \frac{|\psi_{2a}\rangle + |\psi_{2b}\rangle + |\psi_{2c}\rangle + |\psi_{2d}\rangle}{2} \\
 &= \frac{|00\rangle + |01\rangle - |10\rangle + |11\rangle}{2} \otimes \frac{|0\rangle - |1\rangle}{\sqrt{2}}
 \end{aligned}
 \tag{2.2.31}$$

There is one subtle point which is worth some extra words. One should note that with the proposed quantum circuit, the ancilla is fixed to state $|-\rangle$ (apart from a possible phase factor) regardless of the values assumed by the input qubits. At first sight, one may misleadingly be brought to think it is just a chance. On the contrary, it is a mandatory prerequisite to exploit quantum interference, usually known as **clean computation**. As a matter of fact, it is quite obvious that if the circuit forced the ancilla qubit to change as a function of the input qubits, the output state would look like

$$|\psi_2\rangle \propto \sum_x |x\rangle |g(x)\rangle
 \tag{2.2.32}$$

In this case, it would be impossible to get any sort of cancellation/sum between terms with different values of $g(x)$.

Finally, while the proposed oracle is somehow *general*, some optimized circuits can be derived for some specific cases. For instance, a possible implementation which does not require the extra ancilla qubit is



Exploiting the linearity of quantum mechanics as previously explained, it is trivial to prove that this circuit is fully equivalent to the previous one.

The diffusion operator The purpose of this step is to perform a reflection about $|E\rangle$. At first glance, this job seems more demanding than the reflection about $|s\rangle$, since $|E\rangle$ is a superposition state. Nevertheless, it is well known that the effect of the application of a Hadamard gate $\mathbf{H}^{\otimes n}$ to a superposition state is

to send it back to $|00 \dots 0\rangle$. For instance

$$|0\rangle \xrightarrow{\mathbf{H}} \frac{|0\rangle + |1\rangle}{\sqrt{2}} \xrightarrow{\mathbf{H}} |0\rangle \quad (2.2.33)$$

Thus, the basic intuition is to use the Hadamard gates to send $|E\rangle \rightarrow |00 \dots 0\rangle$, perform a simple reflection about $|00 \dots 0\rangle$ and, eventually, send the obtained result back to a superposition state applying again the Hadamard gates.

More rigorously, since a reflection about $|E\rangle$ can be written as

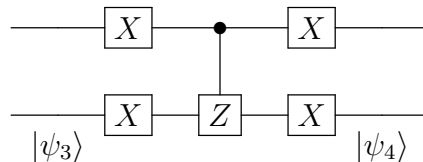
$$|E\rangle\langle E| - \mathbb{I} \quad (2.2.34)$$

and since, by construction, $|E\rangle = \mathbf{H}^{\otimes n} |00 \dots 0\rangle$, then

$$|E\rangle\langle E| - \mathbb{I} = \mathbf{H}^{\otimes n} (|00 \dots 0\rangle\langle 00 \dots 0| - \mathbb{I}) \mathbf{H}^{\otimes n} \quad (2.2.35)$$

which means that the core of the reflection operator has to perform, as expected, a simple reflection about $|00 \dots 0\rangle$, or, that is the same up to a global phase factor, a change of sign of state $|00 \dots 0\rangle$ only.

Which circuit can implement this reflection? It is well known that the \mathbf{Z} gate add a -1 factor to $|1\rangle$ while it leaves $|0\rangle$ unaffected. Adding a control qubit, the action of the \mathbf{Z} gate on the target qubit is fulfilled only if the control is in state $|1\rangle$. In the case $n = 2$, the effect of the controlled- \mathbf{Z} gate is to add a -1 phase factor when the input is in state $|11\rangle$. In order to get the desired sign change for the state $|00\rangle$ instead of $|11\rangle$ it is enough to add a couple of \mathbf{X} gates:

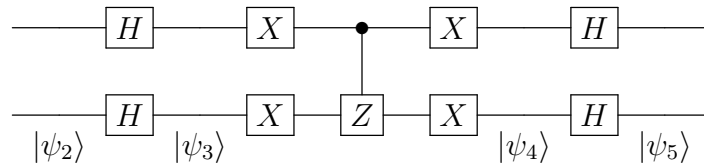


The downstream \mathbf{X} gates are added to get a clean computation, so that $|\psi_4\rangle$ is equal to $|\psi_2\rangle$ apart from a possible phase factor. As previously detailed, thanks to this ploy, the quantum interference can be exploited and the desired cancellation and sum of probability is achieved. It is straightforward to see that the behaviour

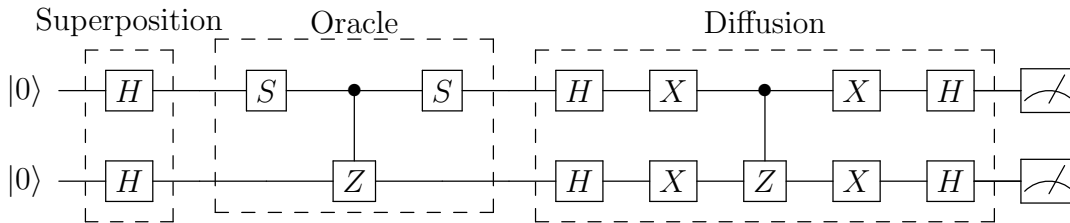
of the quantum circuit is:

$$\begin{aligned}
 |00\rangle &\longrightarrow -|00\rangle \\
 |01\rangle &\longrightarrow +|01\rangle \\
 |10\rangle &\longrightarrow +|10\rangle \\
 |11\rangle &\longrightarrow +|11\rangle
 \end{aligned}
 \tag{2.2.36}$$

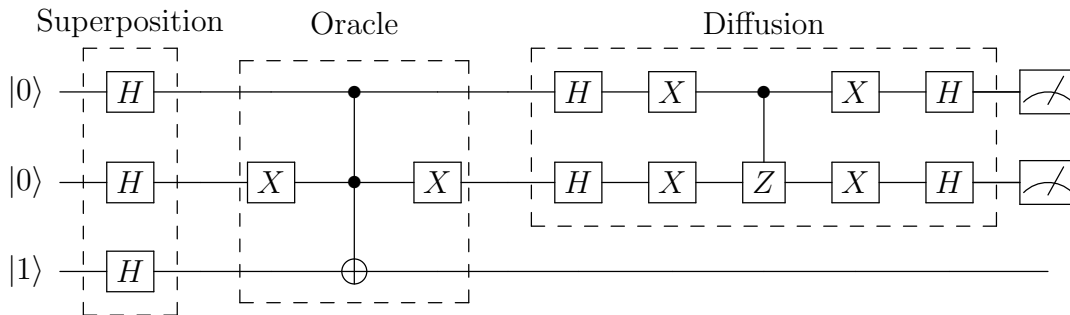
Consequently, the desired phase change of $|00\rangle$ is achieved. In order to obtain the inversion about $|E\rangle$, Equation 2.2.35 says that it is enough to add some Hadamard gates upstream and downstream the circuit which performs the phase inversion of $|00\rangle$. For the 2-qubit case, one gets



The overall quantum circuit Cascading the two quantum circuits, one obtains:



where the measurement operators have been added at the end of the circuit. Obviously, a fully equivalent circuit can be obtained using the other oracle operator proposed:



Note the extra qubit for the ancilla, initialized to $|1\rangle$.

2.3 Quantum assembly

The astonishing development of digital electronics has been made possible by the introduction of several levels of abstraction. The increasing complexity of electronic systems committed to looking for fast and rational ways of detailing how transistors have to be combined to realize processing units. It would not be possible to describe a processor starting from the exhaustive physical behaviour of transistors. Hardware description languages, such as VHDL and Verilog, are well known to electronic engineers and allow the design of a circuit without having a deep knowledge of the physics behind the hardware.

Quantum assembly (QASM) is the quantum counterpart of a hardware description language for standard digital electronics. An important caveat is that the name *is* misleading: QASM is much more similar to VHDL or Verilog, than it is to classical assembly language. It is not a programming language; on the contrary, it is a *description of quantum hardware and quantum operations*, which does not require to know the details of the physics (for instance, it does not depend on how qubits are physically stored, initialized, measured and so on), but which is designed to control a physical system.

A basic intuition about the working principle of a quantum computer is schematically reported in Figure 2.19. The classical computer, which is the master of the

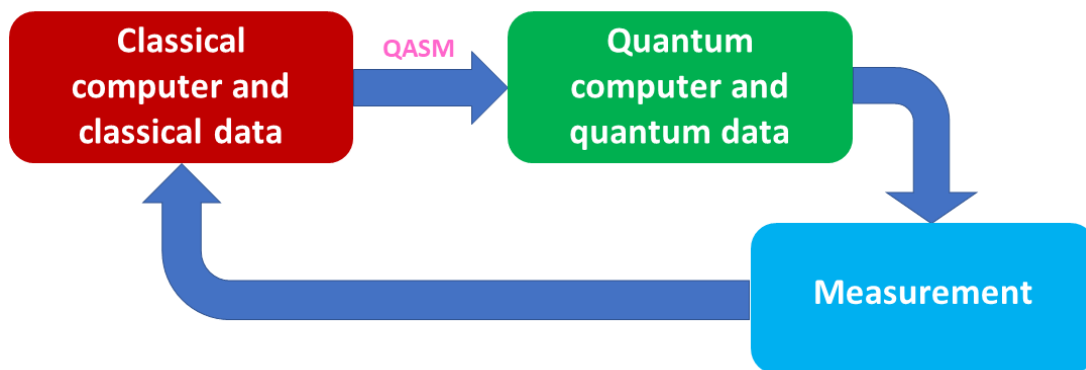


Figure 2.19: Schematic representation of a quantum computer.

system, stores classical bits and executes some given algorithm. When it needs some quantum capability to speed up the execution, it wakes the quantum processor up, sending some QASM instructions. The quantum processor plays the role of the slave and performs the required quantum operations. At the end, a measurement is carried out and the output, which is classical, is provided back to the classical computer.

2.3.1 Syntax

The presentation of a detailed description of QASM would be thoroughly redundant and useless, since several good user manuals are already available on the internet. Moreover, the syntax is simple and self-evident. The interested reader is suggested to consult [27], which is a very good and exhaustive reference text. Here, just the main features are reported.

QASM is a case sensitive language, where statements are separated by semicolons and comments are introduced by a pair of forward slashes and terminated by a new line. The order in which statements are presented is the order in which they are applied.

The first line must always be `OPENQASM M.m`, where `M` is the major version and `m` the minor version. The statement `include "filename"` has the same effect of copying and pasting the contents of the file "filename".

Storage elements There are two kinds of storage elements:

- **Classical register:** the statement `creg name [size]` declares an array of bits with the given size and name.
- **Quantum register:** the statement `qreg name [size]` declares an array of qubits with the given size and name.

Qubits are initialized in $|0\rangle$ and bits in 0. To access a particular bit/qubit in a register, one uses the statement `name [i]`. Numeration starts from 0.

Quantum gate

- **One-qubit gates:** the statement `name_gate q[i]` applies the gate `name_gate` to the i -th qubit of the q quantum register.
- **CNOT:** the statement `CX q[i], q[j]` applies a CNOT gate which flips the target qubit `q[j]` only if the control qubit `q[i]` is in state $|1\rangle$.
- **Custom gates:** new unitary gates can be introduced using the following subroutine:

```
1  gate name(params) qargs
2  {
3      //body
4  }
```

where `params` is an optional comma-separated list of parameter names and `qargs` is a comma-separated list of qubit arguments.

Measurement and reset

- **Measurement:** the statement `measure q[i] -> c[j]` measures the qubit `q[i]` and save the result in the classical bit `c[i]`. The measurement is performed in the computational Z-basis, which means that it is a projective measurement on the eigenstates of σ_z .
- **Reset:** the statement `reset q[i]` initializes qubit `q[i]` to state $|0\rangle$.

2.3.2 Grover's search algorithm QASM

The QASM for an implementation of the Grover's search algorithm for the $|10\rangle$ case discussed in section §2.2.2.3 is reported in the following. It is a simple example useful to see how quantum circuits are described in quantum assembly.

```
1 // Grover's search algorithm: 10 case
2
3 OPENQASM 2.0;
4 include "qelib1.inc";
5
6 qreg q[2];
7 creg c[2];
8
9 // Initial superposition
10
11 h q[0];
12 h q[1];
13
14
15 // Oracle operator
16
17 s q[0];
18 id q[1];
19
20 id q[0];
21 h q[1];
22
23 cx q[0], q[1]; //q[0] is the control and q[1] the target
24
25 id q[0];
26 h q[1];
27
28 s q[0];
29 id q[1];
30
31
32 // Grover diffusion operator
33
34 h q[0];
```

```
35  h q[1];
36
37  x q[0];
38  x q[1];
39
40  id q[0];
41  h q[1];
42
43  cx q[0], q[1];
44
45  id q[0];
46  h q[1];
47
48  x q[0];
49  x q[1];
50
51  h q[0];
52  h q[1];
53
54
55  // Measurement: from qubits to classical bits
56
57  measure q[0] -> c[1];
58  measure q[1] -> c[0];
```

The identity gates have been added just for clarity, so that it is possible to identify immediately the different parts of the quantum circuit. Finally, the fact that qubit `q[0]` is mapped to bit `c[1]` and `q[1]` is mapped to bit `c[0]` depends exclusively on the chosen convention for the order in which bits are shown by the simulator.

2.3.3 Simulation of Grover’s search algorithm

The quantum assembly description proposed in section §2.3.2 can be provided as input to a QASM simulator. A cloud-available quantum service is **IBM Q experience** [1], which has been used to obtain the circuit reported in Figure 2.20.

IBM Q experience allows to run the code on an actual quantum processor or on a quantum simulator. The result provided by the latter can be analyzed in Figure 2.21. As expected, the result is $|10\rangle$. The interesting point is that, as

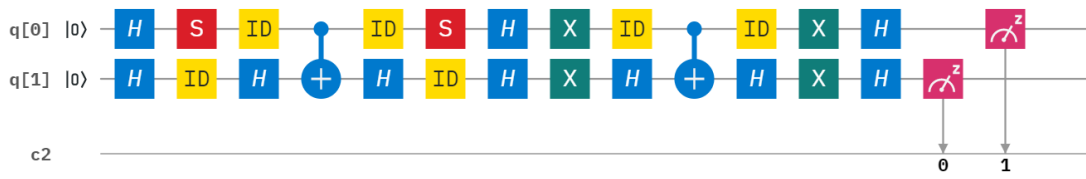


Figure 2.20: Grover's quantum circuit.

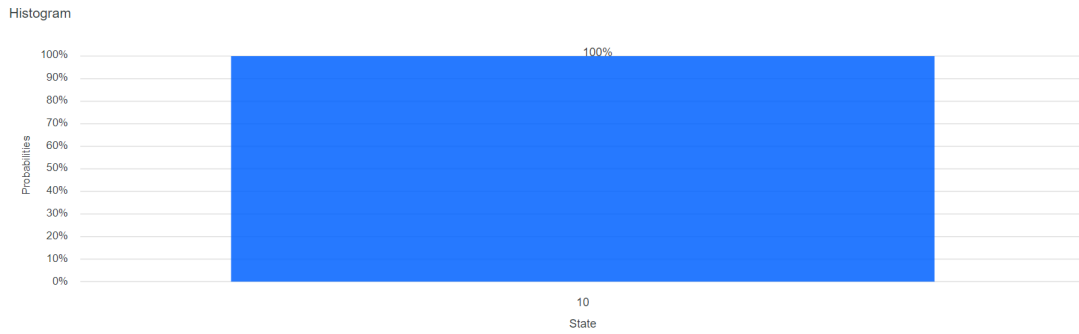


Figure 2.21: Simulation for $|10\rangle$ case.

discussed in section §2.2.2.3, when dealing with just two qubits, a single iteration is enough to obtain the desired result with 100% probability. Indeed, the histogram presented in Figure 2.21 is in total agreement with the theoretical derivation.

Part II

Nuclear magnetic resonance physical theory

Chapter 3

Introduction to magnetism

The purpose of this chapter is to provide the fundamental tools to understand the nuclear magnetic resonance. First, the general concepts of magnetism are introduced from a classical point of view. Second, the quantum mechanical interpretation is proposed, analyzing the differences among electronic and nuclear magnetism.

3.1 Classical magnetism

3.1.1 The fundamental concepts

An electric current flowing in the $+\hat{z}$ direction generates a magnetic field \mathbf{H} which lies in the x - y plane. The magnitude of \mathbf{H} is given by the Biot-Savart law:

$$|\mathbf{H}| = \frac{I}{2\pi r} \quad [\text{A m}^{-1}] \quad (3.1.1)$$

where r is the distance from the center of the current. Conversely, an electric current flowing in a closed loop causes a magnetic field to arise in the perpendicular plane, whose magnitude is

$$H = \frac{I}{2r} \quad (3.1.2)$$

The direction of the field is obtained using the well known right-hand rule, as reported in Figure 3.1.

The term magnetic field is commonly adopted both for the \mathbf{H} field and the \mathbf{B} field. In order to describe how the two fields are related, it is necessary to introduce another vector quantity: the magnetization \mathbf{M} .

Definition 3.1.1. The **magnetization** field is defined as

$$\mathbf{M} = \frac{d\mathbf{m}}{dV} \quad [\text{A m}^{-1}] \quad (3.1.3)$$

where $d\mathbf{m}$ is the elementary magnetic moment and dV is the infinitesimal volume

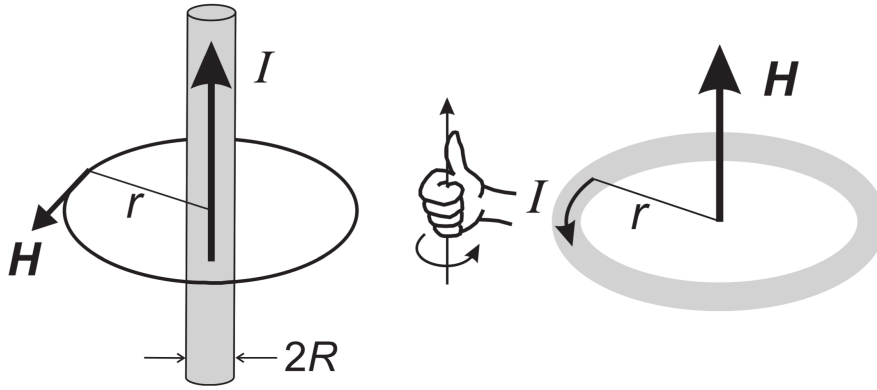


Figure 3.1: The direction of the magnetic field. Adapted from [28].

element. The magnetization defines the magnetic properties of the material and its magnitude is the volume density of the magnetic moment.

The three fields are related according to

$$\mathbf{B} = \mu_0 (\mathbf{H} + \mathbf{M}) \quad [\text{T}] \quad (3.1.4)$$

where μ_0 is the vacuum magnetic permeability.

Definition 3.1.2. The **magnetic permeability** in a homogeneous medium can be defined as

$$\mu = \mu_m \mu_0 \quad (3.1.5)$$

where μ_m is the adimensional relative magnetic permeability.

It is clear that if $\mu_m = 1$, then $\mu = \mu_0$. The quantity which measures how far μ_m is from unit is the magnetic susceptibility.

Definition 3.1.3. The **magnetic susceptibility** is defined as

$$\chi = \mu_m - 1 \quad (3.1.6)$$

The magnetization can be expressed as

$$\mathbf{M} = \chi \mathbf{H} \quad (3.1.7)$$

According to the developed formalism, it is possible to classify magnetic substances.

Diamagnetic substances Isotropic diamagnetic substances are characterized by a magnetic permeability which is constant and less than one. Consequently:

$$\mu_m < 1 \longrightarrow \chi < 0 \quad (3.1.8)$$

and the magnetization \mathbf{M} has opposite direction with respect to the field \mathbf{H} .

Paramagnetic substances Isotropic paramagnetic substances are characterized by a magnetic permeability which is constant and larger than one. Consequently:

$$\mu_m > 1 \longrightarrow \chi > 0 \quad (3.1.9)$$

and the magnetization \mathbf{M} has the same direction the field \mathbf{H} .

Ferromagnetic substances In ferromagnetic substances, both the permeability and the susceptibility depend on the value of the magnetic field and the magnetic history of the sample. Indeed, ferromagnetic substances are characterized by hysteresis and retain a residual magnetization even when the external field is switched off. The hysteresis is not discussed here, since it is not fundamental for aim of this research, but can be found in every book about magnetism, as [29, 30].

In both isotropic paramagnetic and diamagnetic substances, the following simple relation holds true

$$\mathbf{B} = \mu_0 \mu_m \mathbf{H} = \mu \mathbf{H} \quad (3.1.10)$$

In the following, the focus will be on diamagnetic substances and the magnetic field will be mainly identified with \mathbf{B} -field, also to avoid confusion with the Hadamard gate (\mathbf{H}), the system Hamiltonian (\mathcal{H}) and the Hilbert space (\mathbb{H}).

3.1.2 The magnetic moment

It is always possible to isolate a positive or a negative charge. This is a consequence of the existence, in Nature, of the fundamental positive charge of the proton and the fundamental negative charge of the electron. On the contrary, it is not possible to obtain an isolated magnetic pole. However, **fictitious** positive $p^+ = -p$ and negative $p^- = -p$ magnetic charges can be defined.

Definition 3.1.4. According to Gilbert model, the **magnetic dipole** is formed by a fictitious positive magnetic charge (north) and an fictitious negative magnetic charge (south) at a fictitious distance d . The magnetic dipole **moment** m points from the south pole to the north pole, has units of $[\text{Am}^2]$ and has expression

$$m = p d \quad [\text{Am}^2] \quad (3.1.11)$$

The magnetic field B points from the north pole to the south pole.

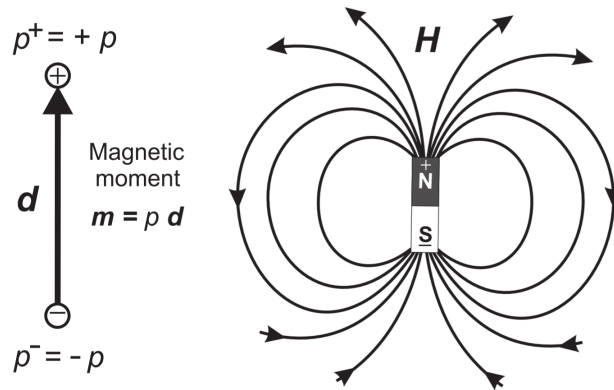


Figure 3.2: The magnetic moment and the magnetic field. Adapted from [28].

A closed current loop generates a magnetic field which can be shown to be equal to that of a dipole. This is known as the Ampère model of the magnetic moment. It is interesting to remark that classical magnetism traces all magnetic phenomena back to moving charges. Consequently, the Ampère model is physically correct, while the Gilbert model is not physically accurate, but can be sometimes useful to get an intuitive understanding the problem. The associated magnetic dipole moment has magnitude given by

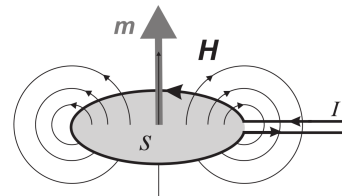


Figure 3.3: The magnetic moment of a current loop. From [28].

$$|m| = I \cdot S \quad [\text{Am}^2] \quad (3.1.12)$$

where I is the current and S the area enclosed by the loop, while the direction is given by the right-hand rule, as clear from Figure 3.3. The proof can be found in [28].

3.1.2.1 The magnetic moment of a rotating electron

The magnetic moment generated by a rotating electron is proportional to the classical angular momentum, due to the rotation of a particle with mass m_e and charge $q = -e$:

$$\mathbf{m} = -\frac{e}{2m_e}\mathbf{l} = -\frac{\mu_B}{\hbar}\mathbf{l} \quad (3.1.13)$$

where μ_B is the **Bohr magneton** and is defined as

$$\mu_B = \frac{e\hbar}{2m_e} \sim 9.274 \times 10^{-24} \text{ J T}^{-1} \sim 5.788 \times 10^{-5} \text{ eV T}^{-1} \quad (3.1.14)$$

Equivalently

$$\mathbf{m} = \gamma\mathbf{l} \quad (3.1.15)$$

where γ is the **electron gyromagnetic ratio**, defined as

$$\gamma = \frac{q}{2m_e} = -\frac{e}{2m_e} = -\frac{\mu_B}{\hbar} = -8.794 \times 10^{10} \frac{\text{rad}}{\text{s} \cdot \text{T}} \quad (3.1.16)$$

The minus sign, which arises from the negative charge of the electron, implies that **the angular momentum and the magnetic moment of an electron are antiparallel.**

Proof. Consider a charge q which is rotating around a current loop, whose area is $S = r^2\pi$. The resulting current is

$$I = \frac{q\omega}{2\pi}$$

According to Equation 3.1.12, the magnitude of the magnetic moment is

$$|\mathbf{m}| = \frac{qr^2}{2}\omega$$

Since the vector angular frequency $\boldsymbol{\omega}$ and \mathbf{m} have the same direction, the previous

equation can be rewritten in vector form as

$$\mathbf{m} = \frac{qr^2}{2}\boldsymbol{\omega}$$

Replacing $\boldsymbol{\omega} = (\mathbf{r} \times \mathbf{v})/r^2$ in the previous equation one gets

$$\mathbf{m} = \frac{q}{2}(\mathbf{r} \times \mathbf{v})$$

The classical angular momentum is

$$\mathbf{l} = \mathbf{r} \times \mathbf{p} = m\mathbf{r} \times \mathbf{v}$$

where \mathbf{p} is the linear momentum. Replacing $q = -e$ one obtains

$$\mathbf{m} = -\frac{e}{2m_e}\mathbf{l}$$

□

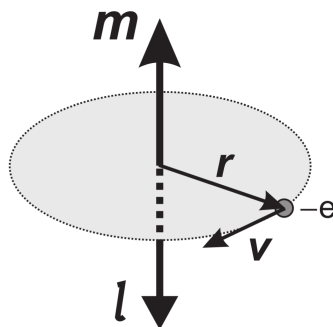


Figure 3.4: The rotating electron. From [28].

3.1.2.2 The energy and the force of a magnetic dipole in a magnetic field

The potential energy of a magnetic dipole in a field \mathbf{B} is

$$E = -\mathbf{m} \cdot \mathbf{B} \quad [\text{J}] \quad (3.1.17)$$

The energy is minimized when the magnetic moment is parallel to the magnetic field, while it is maximized when they are anti-parallel. Hence, the energetically favored configuration is with \mathbf{m} and \mathbf{B} parallel.

The force acting on an infinitesimal loop with dipole moment \mathbf{m} in a field \mathbf{B} is the negative gradient of the potential energy:

$$\mathbf{F} = \nabla (\mathbf{m} \cdot \mathbf{B}) \quad [\text{N}] \quad (3.1.18)$$

This relation is obtained using the Ampère model of the current loop. As previously stated, the (nonphysical) Gilbert model can help in understanding some phenomena at an intuitive level. The force derived using the latter has the following expression

$$\mathbf{F} = (\mathbf{m} \nabla) \mathbf{B} \quad (3.1.19)$$

The two expressions turn out to be equivalent is $\mathbf{m} \times \nabla \times \mathbf{B} = 0$, as shown is [31].

Example 3.1.1. Suppose there is a non-homogeneous magnetic field increasing along $+\hat{z}$ and that a magnetic dipole is oriented along $+\hat{z}$, as in Figure 3.5. According to Equation 3.1.19, the force experienced by the magnetic dipole is

$$F_z = m_z \frac{\partial B_z}{\partial z} \hat{z} \quad (3.1.20)$$

From which one understands that:

- A magnetic moment parallel to the magnetic field perceives a force toward increasing field.
- A magnetic moment antiparallel to the magnetic field perceives a force toward decreasing field.

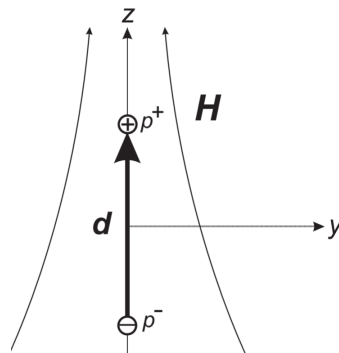


Figure 3.5: The magnetic moment in a non-homogeneous field. From [28].

3.1.2.3 Torque and classical precession

Consider a magnetic moment in a homogeneous magnetic field \mathbf{B} . The two fictitious charges experience an equal but opposite force $\mathbf{F} = p\mathbf{B}$ and so the net force is zero. However, there is a net torque \mathbf{T} acting on the dipole.

$$\boldsymbol{\tau} = \mathbf{m} \times \mathbf{B} \quad (3.1.21)$$

Proof. From the definition of torque

$$\boldsymbol{\tau} = \mathbf{r} \times \mathbf{F}$$

replacing $\mathbf{F} = p\mathbf{B}$

$$\boldsymbol{\tau} = \mathbf{r} \times \mathbf{F} = \mathbf{r} \times p\mathbf{B} = \mathbf{m} \times \mathbf{B}$$

□

The everyday experience is that a compass needle, which can be seen as a magnetic dipole, turns into the direction of the applied field. Indeed, the torque of Equation 3.1.21 does line up a *static* magnetic moment with the magnetic field \mathbf{B} . The picture, however, is different if the magnetic moment arises from an **angular momentum**, as the orbital angular momentum of a rotating electron or the spin moment. As well known from Newton's mechanics, the effect of a torque is to force the angular momentum \mathbf{l} to move according to

$$\frac{d\mathbf{l}}{dt} = \boldsymbol{\tau} = \mathbf{m} \times \mathbf{B} \quad (3.1.22)$$

Proof.

$$\frac{d\mathbf{l}}{dt} = \frac{d\mathbf{r}}{dt} \times m\mathbf{v} + m\mathbf{r} \times \frac{d\mathbf{v}}{dt} = \mathbf{v} \times \mathbf{p} + \mathbf{r} \times \mathbf{F} = \boldsymbol{\tau}$$

Since \mathbf{p} and \mathbf{v} are parallel and so their cross product is zero. □

The so-called **equation of motion** of a magnetic moment \mathbf{m} in a field \mathbf{B} can be immediately derived from Equation 3.1.22 and reads:

$$\frac{d\mathbf{m}}{dt} = \gamma \mathbf{m} \times \mathbf{B} = \gamma \boldsymbol{\tau} \quad (3.1.23)$$

The magnetic moment **precesses** about the magnetic field \mathbf{B} and the phenomenon is usually referred to as the **Larmor precession**. Qualitatively, Equation 3.1.23

says that the rate of change of \mathbf{m} depends on the field \mathbf{B} and its motion is perpendicular to both \mathbf{m} and \mathbf{B} .

More quantitatively, the magnitude of \mathbf{m} remains constant as time flows, that is, its time derivative is zero:

$$\frac{d|\mathbf{m}|}{dt} = \frac{dm}{dt} = 0 \quad (3.1.24)$$

Proof.

$$2m \frac{dm}{dt} = \frac{dm^2}{dt} = \frac{d\mathbf{m}\mathbf{m}}{dt} = 2\mathbf{m} \frac{d\mathbf{m}}{dt} = 2\mathbf{m} (\gamma \mathbf{m} \times \mathbf{B}) = 0 \implies \frac{dm}{dt} = 0$$

Where $\mathbf{m} (\gamma \mathbf{m} \times \mathbf{B}) = 0$ since \mathbf{m} is perpendicular to $\mathbf{m} \times \mathbf{B}$. □

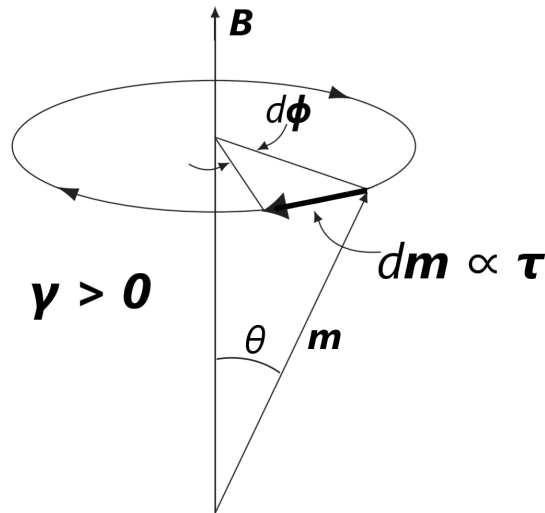


Figure 3.6: The precession of the magnetic moment for positive γ . Adapted from [32].

So, the magnitude of \mathbf{m} is constant as expected, but its direction is not: the vector \mathbf{m} performs a rotation about \mathbf{B} . As a matter of fact, Equation 3.1.23 states clearly that the differential increment $d\mathbf{m}$ is **perpendicular** to the plane defined by \mathbf{m} and \mathbf{B} , thus forcing \mathbf{m} in a rotation around a circular path.

Consider Figure 3.6¹. Let $d\phi$ be the angle by which \mathbf{m} precesses in the time interval dt and θ the angle between \mathbf{B} and \mathbf{m} . The component of \mathbf{m} perpendicular to \mathbf{B} is

$$m_{\perp} = m \sin(\theta) \quad (3.1.25)$$

¹A caveat: as it will be clear as the theory is developed, the sense of rotation depends on the sign of the gyromagnetic ratio γ , which can be *positive* for particles different from the electron. Figure 3.6 is drawn assuming $\gamma > 0$, because this will be the most common case of interest.

The infinitesimal increment dm can be expressed as

$$dm = m_{\perp}d\Phi = m \sin(\theta)d\Phi \quad (3.1.26)$$

Moreover, from Equation 3.1.23, one gets that

$$dm = |\gamma| \cdot |\mathbf{m} \times \mathbf{B}|dt = |\gamma|mB \sin(\theta)dt \quad (3.1.27)$$

From which the frequency of precession has magnitude

$$\omega = |\boldsymbol{\omega}| \triangleq \left| \frac{d\Phi}{dt} \right| = |\gamma|B \quad (3.1.28)$$

The sign of the vector precession frequency is clear from the geometry of Figure 3.6.

A magnetic moment

$$\mathbf{m} = \gamma \mathbf{l} \quad (3.1.29)$$

in a static magnetic field

$$\mathbf{B} = B\hat{\mathbf{z}} \quad (3.1.30)$$

describes a precession about \mathbf{B} at a vector frequency

$$\boldsymbol{\omega} = -\gamma\mathbf{B} \quad [\text{rad s}^{-1}] \quad (3.1.31)$$

known as the **Larmor frequency**. The magnitude is

$$\omega = |\boldsymbol{\omega}| = |\gamma|B \quad (3.1.32)$$

There is some confusion in the scientific literature about the sign convention for the Larmor frequency. The most reasonable solution seems to define the *vector* frequency as a quantity with sign, while the magnitude ω of $\boldsymbol{\omega}$ is always assumed to be positive. This research is written according to this convention. Many authors define a sign for ω and extend it to $\boldsymbol{\omega}$, but it is not rigorous to give a sign to the magnitude of a vector.

As a consequence:

- If the gyromagnetic ratio γ is **positive**, then ω is negative and the precession occurs **clockwise** at a frequency $\omega = \gamma B$.
- If the gyromagnetic ratio γ is **negative**, then ω is positive and the precession occurs **anti-clockwise** at a frequency $\omega = |\gamma|B$.

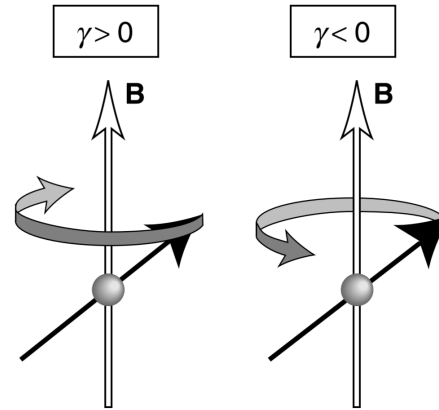


Figure 3.7: The sign of the precession. Adapted from [33].

It is interesting to highlight that Equation 3.1.31 does not depend on the angle θ between \mathbf{m} and \mathbf{B} . Thus, it does not depend on m_{\perp} : this is a remarkable aspect which has to be kept in mind and which justifies the fact that the quantum mechanical approach delivers the same result. As it will be clear in the following, in quantum mechanics the component of \mathbf{m} perpendicular to \mathbf{B} remains undetermined when a measurement (on the standard basis) is carried out. Nevertheless, independently of m_{\perp} , the magnetic moment precesses at ω .

Moreover, θ does **not change** when a static field \mathbf{B} is applied. Wherefore, the energy of the system is unchanged: it remains constant, during precession, at a value which is not necessarily the minimum one. Actually, this is not the whole truth, since eventually the magnetic moment will collapse to the direction of the applied field and the energy of the system *will be* minimized; but this is quite a complex story which is treated in details for the NMR case in section §4.3. For the time being, it is enough to stick to the fact that the energy is constant when a *static* field is applied.

3.2 Quantum mechanical interpretation of magnetism

This section is devoted to present the basic concepts to understand how quantum mechanics treats the magnetic phenomena.

Magnetism is intimately connected with angular momentum of particles. Consequently, the first step towards the quantum mechanics understanding of magnetism is to deal with the quantum mechanics picture of angular momentum.

3.2.1 The angular momentum in the quantum mechanics picture

Suppose the instantaneous position of a classical particle is

$$\mathbf{r} = x\hat{\mathbf{x}} + y\hat{\mathbf{y}} + z\hat{\mathbf{z}} \quad (3.2.1)$$

and the linear momentum is

$$\mathbf{p} = p_x\hat{\mathbf{x}} + p_y\hat{\mathbf{y}} + p_z\hat{\mathbf{z}} \quad (3.2.2)$$

Then, the classical angular momentum is a vector with components

$$\mathbf{l} = \mathbf{r} \times \mathbf{p} = (yp_z - zp_y)\hat{\mathbf{x}} + (zp_x - xp_z)\hat{\mathbf{y}} + (xp_y - yp_x)\hat{\mathbf{z}} \quad (3.2.3)$$

The magnitude has the traditional expression of the magnitude of a vector

$$l^2 = l_x^2 + l_y^2 + l_z^2 \quad (3.2.4)$$

with $|l_k| \leq l$.

According to postulate 1.2, a Hermitian operator is associated with each physical observable. The quantum mechanical **operators** for angular momentum can be constructed replacing the position and the linear momentum by the operators of table 1.1. In the position representation one gets:

$$\mathbf{l}_x = \frac{\hbar}{i} \left(y \frac{\partial}{\partial z} - z \frac{\partial}{\partial y} \right) \quad \mathbf{l}_y = \frac{\hbar}{i} \left(z \frac{\partial}{\partial x} - x \frac{\partial}{\partial z} \right) \quad \mathbf{l}_z = \frac{\hbar}{i} \left(x \frac{\partial}{\partial y} - y \frac{\partial}{\partial x} \right) \quad (3.2.5)$$

Letting \mathbf{l}^2 be the quantum operator associated with the magnitude of the angular

momentum, it is trivial to see that the following commutation relations hold:

$$\begin{aligned}
 [\mathbf{l}_x, \mathbf{l}_y] &= i\hbar \mathbf{l}_z \\
 [\mathbf{l}_y, \mathbf{l}_z] &= i\hbar \mathbf{l}_x \\
 [\mathbf{l}_z, \mathbf{l}_x] &= i\hbar \mathbf{l}_y \\
 [\mathbf{l}^2, \mathbf{l}_k] &= 0 \quad k = x, y, z
 \end{aligned}
 \tag{3.2.6}$$

These relations are at the real basis of the theory of the angular momentum. Thus, an observable can be considered an angular momentum if the associated Hermitian operator satisfies these commutation relations.

Since \mathbf{l}_x , \mathbf{l}_y and \mathbf{l}_z do not commute with each other, according to theorem 1.2.1, it is not possible to specify more than one component of the angular momentum. On the other hand, since \mathbf{l}^2 commutes with all three components, one is allowed to determine the magnitude of the angular momentum and one of its components, for instance the one along the \hat{z} axis, as reported in Figure 3.8. The bluish cone is used to represent pictorially the fact the magnitude of the angular momentum (the side of the cone) and its \hat{z} projection (the height of the cone) are determined, while the orientation of the angular momentum is unknown, since the \hat{x} and \hat{y} components are undetermined. This representation is known to the scientific community as the *vector model*. However, it is important to note that \mathbf{l} is *not* a vector, but a quantum mechanical operator. For instance, the commutation relations can be rewritten in a compact fashion as

$$\mathbf{l} \times \mathbf{l} = i\hbar \mathbf{l}
 \tag{3.2.7}$$

The cross product of \mathbf{l} with itself is not zero and so \mathbf{l} cannot be an actual vector.

3.2.1.1 The eigenvalues and eigenstates of the angular momentum

The simultaneous eigenstates of \mathbf{l}^2 and \mathbf{l}_z are specified by two quantum numbers: l and m_l . The full derivation and the theoretical justification are quite involved and can be found in quantum mechanics books, as the recommended [34, Chapter 4]. The interesting point, however, is the result. Starting from the unique hypothesis that the angular momentum is a Hermitian operator which satisfies the

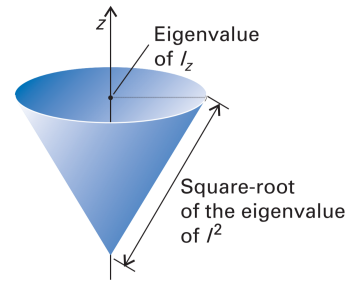


Figure 3.8: The angular momentum and its projection along \hat{z} . From [34].

commutation relations of equations 3.2.6, it is possible to show that:

1. The magnitude of the angular momentum can assume only the values

$$\hbar\sqrt{l(l+1)} \quad (3.2.8)$$

with $l = 0, \frac{1}{2}, 1, \frac{3}{2}, \dots$.

2. The component of the angular momentum along an arbitrary \hat{z} direction is limited to the $2l + 1$ values

$$m_l \hbar \quad (3.2.9)$$

with $m_l = -l, -l + 1, \dots, l - 1, l$.

There is one interesting remark about this result. For orbital angular momenta, the quantum numbers follow the previously introduced notation: l and m_L . In this case, angular momenta can be classically understood as generated by a particle rotating around a specified centre and it can be shown that cyclic boundary conditions must be applied to the wavefunction. The consequence is that the quantum number l can take only *integral* values. On the other hand, when intrinsic angular momenta are considered, the quantum numbers are denoted as s and m_s . Moreover, s can take both integral and half-integral values, since no cyclic boundary condition is applied. Finally, a general angular momentum, which can be both intrinsic and orbital, is usually specified with quantum numbers j and m_j .

3.2.1.2 The spin

Some elementary particles present an **intrinsic** angular momentum, known as *spin*. The word spin is misleading because it conveys the wrong idea that the angular momentum is originated by the spinning of a particle. On the other hand, it is much better to accept that a particle can *have* an intrinsic angular moment. After all, a particle can have, for instance, mass and charge. Why should not it have spin?

Spin is a purely quantum mechanical effect and has no classical counterpart. The first experiment to prove the existence of the spin was carried out in 1921 by Otto Stern and Walther Gerlach, but the actual understanding of spin is due to George Uhlenbeck and Samuel Goudsmit, who, in 1927, attributed the result of the

experiment to the spin of the electron. In the experiment, a beam of silver atoms

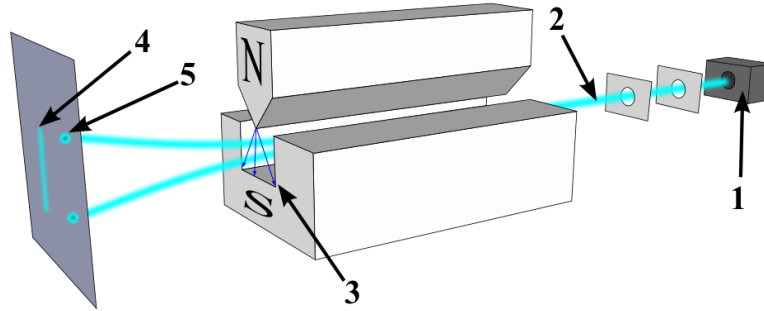


Figure 3.9: The Stern-Gerlach experimental setup: (1) furnace, (2) beam of silver atoms, (3) inhomogeneous magnetic field, (4) classically expected result, (5) observed result. From [35].

is directed through a magnetic field which is inhomogeneous along the \hat{z} direction, as illustrated in Figure 3.9. Silver has 47 electrons and, as it will be clearer in the following, the outer $5s$ electron is unpaired and gives rise to a spin-only magnetic moment. Ideal classical magnetic dipoles cannot change their orientation relative to the magnetic field because of the necessity to conserve energy and angular momentum, as explained in [28]. According to Equation 3.1.20, the force acting on the dipole is

$$\mathbf{F} = |\mathbf{m}| \cos \theta \frac{\partial B_z}{\partial z} \hat{z} \quad (3.2.10)$$

where θ is the angle between \mathbf{m} and the \hat{z} axis. Since the dipoles are initially randomly oriented, one would observe a continuous distribution on the screen. On the contrary, after the inspection of the detector screen, only two separated Ag spots are observed. The magnetic field, acting on the spin, exerts a force which drives the atoms towards the two spots: since the electron spin can have only two observable discrete \hat{z} orientations, parallel or antiparallel to the magnetic field, all atoms end in only two spots. It should be clear from this discussion that Stern-Gerlach experiment can be explained only admitting the existence in Nature of this peculiar intrinsic angular momentum, known as spin.

Spin is an angular momentum and, so, it is described by the same operators discussed for the general angular momentum. Consequently, the commutation relations 3.2.6 still hold true. As mentioned above, the spin quantum number s can take also half-integral values. More formally, it is conventionally defined as $s = \frac{k}{2}$, $k \in \mathbb{N}$ and particles with

- Half-integer spin are known as **fermions**.

- Integer spin are known as **bosons**.

According to Equation 3.2.8, the magnitude of the total spin angular momentum, usually denoted as capital S , is

$$S = \hbar\sqrt{s(s+1)} \quad (3.2.11)$$

Similarly, the component of the spin angular momentum along an arbitrary \hat{z} direction is limited to the $2s + 1$ values

$$m_s\hbar \quad (3.2.12)$$

with $m_s = -s, -s + 1, \dots, s - 1, s$.

Spin- $\frac{1}{2}$ systems The case in which $s = \frac{1}{2}$ is of peculiar interest. For instance, electrons have $s = \frac{1}{2}$, but also several nuclei used in NMR quantum computing are characterized by the same spin quantum number. In this case, $m_s = \pm\frac{1}{2}$ and the observable projections along \hat{z} are simply $s_z = \pm\frac{\hbar}{2}$. The possible basis states can be denoted as

$$|\uparrow\rangle = \begin{pmatrix} 1 \\ 0 \end{pmatrix} \quad |\downarrow\rangle = \begin{pmatrix} 0 \\ 1 \end{pmatrix} \quad (3.2.13)$$

and constitute an orthonormal basis set. They represent, respectively, a state in which the spin is *parallel* and *antiparallel* to an external applied magnetic field \mathbf{B} which defines the quantization axis \hat{z} . The spin operators are \mathbf{s}_x , \mathbf{s}_y and \mathbf{s}_z . Conventionally, the latter is chosen to be the diagonal one: it must have $\pm\frac{\hbar}{2}$ eigenvalues and $|\uparrow\rangle$ and $|\downarrow\rangle$ as eigenvectors. All the properties [36] of the spin- $\frac{1}{2}$ operators are expressed by the **Pauli matrices** presented in section §1.1.12. As a matter of fact, the matrix representation of the spin operators is

$$\begin{aligned} \mathbf{s}_k &= \frac{\hbar}{2}\boldsymbol{\sigma}_k, \quad k = x, y, z \\ \mathbf{s}^2 &= \mathbf{s}_x^2 + \mathbf{s}_y^2 + \mathbf{s}_z^2 = \frac{3\hbar^2}{4} \begin{pmatrix} 1 & 0 \\ 0 & 1 \end{pmatrix} \end{aligned} \quad (3.2.14)$$

It is interesting to remark that, by construction, the eigenvalues and eigenvectors of \mathbf{s}_z are

$$\begin{aligned} +\frac{\hbar}{2} &\longleftrightarrow |\uparrow\rangle \\ -\frac{\hbar}{2} &\longleftrightarrow |\downarrow\rangle \end{aligned} \tag{3.2.15}$$

while both eigenvectors of \mathbf{s}^2 operator are associated with the eigenvalue $\frac{3\hbar^2}{4}$ whose square root is equal to S . As expected, the measurable outcomes are the eigenvalues of the Hermitian operators, as stated by postulate 1.2. It is well known that postulate 1.1 requires that the superposition of two states is a state of the system. Indeed, a general spin wavefunction can be written as

$$|\psi\rangle = c_0 |\uparrow\rangle + c_1 |\downarrow\rangle \tag{3.2.16}$$

that is, as the **superposition** of the two basis eigenstates. It is clear that, according to postulate 1.3, $|c_0|^2$ is the probability that, after a measurement, the system collapses to $|\uparrow\rangle$, while $|c_1|^2$ is the probability that, after a measurement, the system collapses to $|\downarrow\rangle$. Note the strong similarity with the definition of **qubit**.

3.2.1.3 Angular momenta of composite system

Consider a system in which there are two separated sources of angular momentum, \mathbf{j}_1 and \mathbf{j}_2 . It can be a single particle which is characterized by both spin and orbital angular momenta, or a couple of particles with an angular momentum each. It turns out [34] that the operators for independent sources of angular momentum commute with each other, so that the operators \mathbf{j}_1^2 , \mathbf{j}_2^2 , j_{1z} and j_{2z} can be specified simultaneously. The total angular momentum is

$$\mathbf{j} = \mathbf{j}_1 + \mathbf{j}_2 \tag{3.2.17}$$

which can easily be shown to satisfy the commutation relations 3.2.6 so that it is an actual angular momentum.

A fast computation shows that \mathbf{j}^2 commutes with \mathbf{j}_z but not with j_{1z} and j_{2z} . This means that there are two possibilities when one wants to specify a composite system:

1. The **uncoupled picture**: the quantum numbers $j_1, j_2, m_{j_1}, m_{j_2}$ are specified while j is unknown. In this case, the total angular momentum is undetermined and there is no information about the orientations of the two momenta.
2. The **coupled picture**: the quantum numbers j_1, j_2, j, m_j are specified while m_{j_1} and m_{j_2} are unknown. In this case, the total angular momentum is determined but there is no information about the two components. The derivation of the allowed values of j can be proved [34] to follow the **Clebsch-Gordon series**:

$$j = j_1 + j_2, j_1 + j_2 - 1, \dots, |j_1 - j_2| \quad (3.2.18)$$

A possible pictorial representation is the so-called vector model, reported in Figure 3.10. In the **coupled** case, the vector \mathbf{j} has a well defined length given by

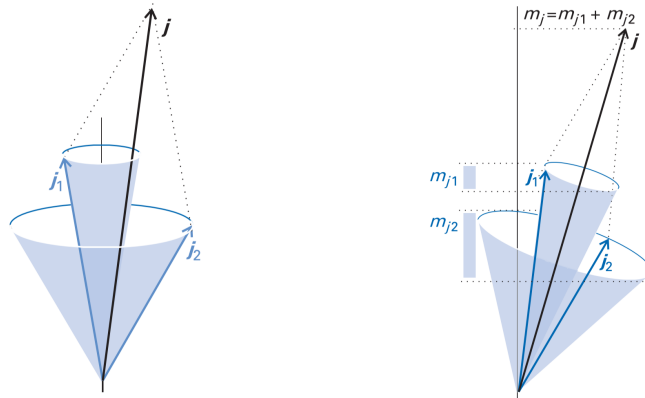


Figure 3.10: The vector model: the uncoupled picture on the left and the coupled picture on the right. Adapted from [35].

$\hbar\sqrt{j(j+1)}$. It lies on a cone since j_x and j_y cannot be determined. Moreover, the lengths of the two contributing angular momenta are known and given by $\hbar\sqrt{j_1(j_1+1)}$ and $\hbar\sqrt{j_2(j_2+1)}$. As far as the projections along \hat{z} are concerned, m_{j_1} and m_{j_2} are not specified, while $m_j = m_{j_1} + m_{j_2}$ is known.

On the other hand, in the **uncoupled** picture, both m_{j_1} and m_{j_2} are known, while j is undetermined. As a consequence, the magnitude of the total angular momentum is not specified and, so, the relative orientations of \mathbf{j}_1 and \mathbf{j}_2 are not known. Note that, however, the projection along \hat{z} is well defined.

3.2.2 Microscopic magnetism

There are three sources of magnetism at microscopic level:

- The orbital magnetic moment of circulating electrons.
- The intrinsic magnetic moment of electrons.
- The intrinsic magnetic moment of atomic nuclei.

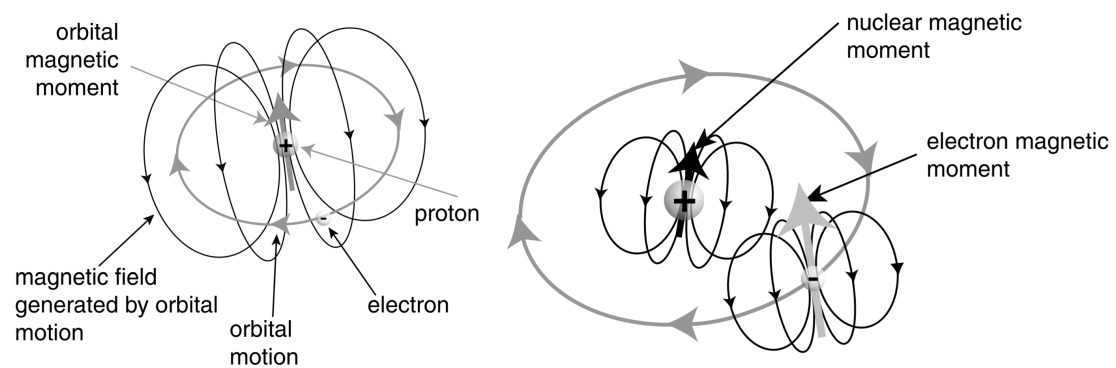


Figure 3.11: The microscopic sources of magnetism in a Hydrogen atom. Adapted from [33].

The first two belong to the field of electron magnetism, while the latter is a nuclear magnetic phenomenon.

3.2.2.1 Electron magnetism

The electron shows two well defined sources of angular momentum: the first is associated with the orbital motion around the nucleus, the second is the spin.

According to the semi-classical model discussed in section §3.1.2.1, the magnetic moment associated with the **orbital angular momentum** is

$$\mathbf{m} = -\frac{\mu_B}{\hbar}\mathbf{l} = \gamma\mathbf{l}$$

Moving to the quantum mechanics interpretation, one has to replace the observables with the corresponding Hermitian operators. As extensively analysed in section §3.2.1, the three components of the angular momentum operator cannot be specified simultaneously. It is customary to identify the $\hat{\mathbf{z}}$ axis as the quantization axis of the system: the **operator** which corresponds to the projection of the orbital magnetic moment to the $\hat{\mathbf{z}}$ axis is

$$m_z = -\frac{\mu_B}{\hbar}l_z = \gamma l_z \quad (3.2.19)$$

and the possible outcomes are

$$m_z = -\frac{\mu_B}{\hbar}\hbar m_l = -\mu_B \cdot m_l \quad (3.2.20)$$

The orbital magnetic moment is also responsible for diamagnetism. In a non rigorous way, one could say that when an external field \mathbf{B} is applied, the electron speeds up or slows down so that, according to Lenz's law, the change in the magnetic moment is opposite to the direction of \mathbf{B} . This effect corresponds to an extra magnetic moment antiparallel to the field. Diamagnetism is a universal phenomenon, but, being typically much weaker than paramagnetism, it is observed only when the latter is absent. Note that this description is just qualitative and the reader is invited to consult dedicated texts as [37] for a proper discussion.

The **spin** is an angular momentum and so it is reasonably associated with a magnetic moment. In analogy with Equation 3.1.13, one can write the spin magnetic moment as

$$\mathbf{m} \propto \gamma\mathbf{s} \implies \mathbf{m} = g \cdot \gamma\mathbf{s} \quad (3.2.21)$$

The dimensionless proportionality constant, known as **g-factor**, comes from the quantum electrodynamics theory and has value

$$g = 2.002319304 \quad (3.2.22)$$

usually approximated with 2, when discussing magnetism.

Since the three components of the spin operator do not commute, one usually deals with the \hat{z} component

$$\mathbf{m}_z = g \cdot \gamma \mathbf{s}_z = -\frac{g\mu_B}{\hbar} \mathbf{s}_z \quad (3.2.23)$$

whose possible outcomes are

$$m_z = -g \cdot \mu_B m_s \quad (3.2.24)$$

It is interesting to highlight that the spin angular momentum accounts for paramagnetism. Consequently, the latter usually occurs in atoms or molecules with unpaired electrons, since Pauli principle forces electrons in pairs to have opposing spins.

The total magnetic moment of an electron is

$$\mathbf{m} = -\frac{\mu_B}{\hbar} (\mathbf{l} + g \cdot \mathbf{s}) \quad (3.2.25)$$

and has a \hat{z} component given by

$$m_z = -\mu_B (m_l + g \cdot m_s) \quad (3.2.26)$$

In this regard, note that the total angular momentum, defined, according to Equation 3.2.17, as

$$\mathbf{j} = \mathbf{s} + \mathbf{l} \quad (3.2.27)$$

is *not* parallel to the total magnetic moment because of the g -factor in the definition of the magnetic moment associated with the spin angular momentum.

The two magnetic moments interact with each other giving rise to the so-called **spin-orbit coupling**. In an elementary and rough way, this coupling can be grasped as follows. From the electron's point of view, the nucleus revolves around it. Being the nucleus a charged particle, the motion is equivalent to a current loop which gives rise to a magnetic field which influences the spin of the electron. The energy associated with the spin-orbit coupling is such that [36, 34]:

- It depends on the Z number of the nucleus. Hence, the spin-orbit coupling is stronger for heavy atoms.
- It is minimized if the two moments are *antiparallel*.

Many electron atom When several electrons are present in the same atom, one has to evaluate the total momenta of the system, in order to compute the corresponding magnetic moment. The approach to follow depends on the relative strength of the spin-orbit coupling and the Coulomb interactions among electrons. When the latter prevails, as it is usually the case for systems of interest in magnetism, the **Russel-Saunders** coupling (or LS coupling) is applicable [34, 36]. In this case, the orbital angular momenta l_i couple into a resultant total orbital angular momentum L and the spin angular momenta s_i couple into a resultant total spin angular momentum S . The weak spin-orbit interaction, eventually, couples L and S into a total angular momentum J . The corresponding quantum numbers are evaluated according to an appropriate application of the Clebsh-Gordon series. For the two-electron case:

$$\begin{aligned} S &= s_1 + s_2, s_1 + s_2 - 1, \dots, |s_1 - s_2| \\ L &= l_1 + l_2, l_1 + l_2 - 1, \dots, |l_1 - l_2| \\ J &= L + S, L + S - 1, \dots, |L - S| \end{aligned} \quad (3.2.28)$$

When, on the other hand, the spin-orbit coupling is very strong, as it is in heavy atoms, the orbital and spin angular momenta of each single electron couple to give a combined angular momentum j_i . J is obtained coupling all the j_i . This is known as the **jj -coupling**.

Magnetism is usually concerned with the ground state, that is, the lowest-energy state. There is an empirical prescription, the so-called **Hund's rule**, which can be used to determine the ground state for systems which obey to the Russel-Saunders coupling [36]:

1. The energy level with the highest value of total spin angular momentum quantum number S lies lowest in energy. The physical reason is that, in order to minimize the Coulomb repulsion, the electrons tend to occupy different degenerate orbitals. It turns out, moreover, that energy is minimized if they have parallel spin.
2. For a given S , the energy level with the highest value of total orbital angular momentum quantum number L lies lowest in energy. The justification is that electrons orbit in the same sense whenever possible. Indeed, in this case they will meet less often than if they orbit in opposite directions. The mutual repulsion is thus minimized.

3. For atoms with less than half-filled shells, the level with the *lowest* value of J lies lowest in energy ($J = |L - S|$). When a shell is more than half full, the level with the *highest* value of J lies lowest in energy ($J = L + S$). When the shell is exactly half full, $L = 0$ and $J = S$. This turns out to be a consequence of the spin-orbit coupling.

Example 3.2.1. Consider a carbon atom which has six electrons. The electronic configuration is

$$1s^2 2s^2 2p^2$$

Which is the total angular momentum j for the ground state? First of all, the core electrons can be neglected in the computation since the angular momentum of a closed shell always turns out to be zero. Then, since $s_k = 1/2$ and $l_k = 1$ with $k = 1, 2$, according to equations 3.2.28, the allowed values are

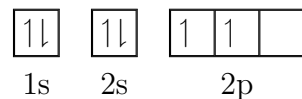
$$S = 1, 0$$

$$L = 2, 1, 0$$

The first Hund's rule requires to select $S = 1$, which means that the two electrons must be in two separated $2p$ orbitals. This granted, the second Hund's rule forces to choose the orbitals with m_l equal to 0 and 1, so that

$$L = 0 + 1 = 1$$

The corresponding configuration is



Since the $2p$ shell is less than half filled, the total angular momentum quantum number is

$$J = |1 - 1| = 0 \implies M_j = 0$$

where M_j is the \hat{z} projection of the total angular momentum. Consequently, the carbon ground state is non-magnetic [36].

△

Zeeman energy The application of a magnetic field affects the energy levels of atoms. As it is clear from the above discussion, electrons possess magnetic moments as a consequence of orbital and spin angular momenta. These moments

interact with an applied \mathbf{B} field.

As previously remarked, the total angular momentum \mathbf{J} is not collinear to the total magnetic moment \mathbf{m} because of the g -factor in the expression of the spin magnetic moment. It can be shown [36, 34] that, because of the spin-orbit coupling, the spin and orbital angular momenta precess about \mathbf{J} . Consequently, also the total magnetic moment \mathbf{m} precesses, as reported in Figure 3.12. This motion has the effect to average to zero all components of \mathbf{m} which are not parallel to \mathbf{J} . The *average* value of the total magnetic moment can be shown [34] to be

$$\mathbf{m} = g_J \cdot \gamma \mathbf{J} \quad (3.2.29)$$

where g_J is the Landé g -factor [34], whose expression is

$$g_J = 1 + \frac{J(J+1) + S(S+1) - L(L+1)}{2J(J+1)} \quad (3.2.30)$$

Note that when $J = 0$, the Landé g -factor is undetermined, but the magnetic

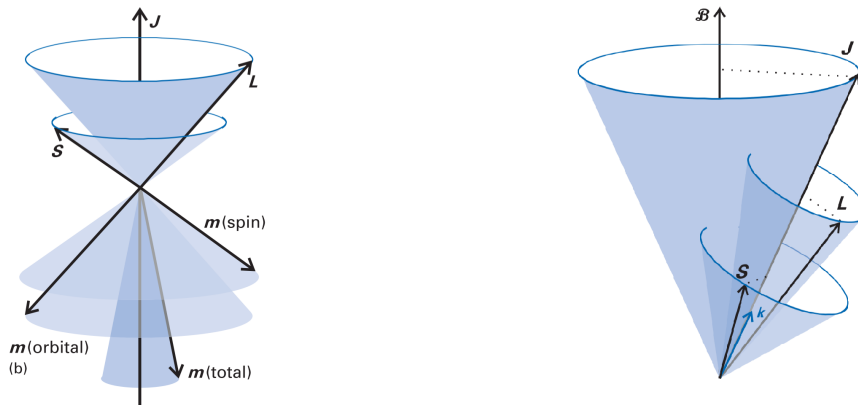


Figure 3.12: The precession of \mathbf{L} and \mathbf{S} about \mathbf{J} on the left and the precession of \mathbf{J} about \mathbf{B} on the right. Adapted from [35].

moment is zero [38].

According to Equation 3.1.17, when a magnetic dipole is placed in static magnetic field, the classical energy can be computed as

$$E = -\mathbf{m} \cdot \mathbf{B}$$

As reported in table 1.1, the quantum mechanical operator associated with the total energy is the **Hamiltonian** of the system:

$$\mathcal{H} = -\mathbf{m} \cdot \mathbf{B} = -\gamma(\mathbf{L} + 2\mathbf{S}) \cdot \mathbf{B} \sim -g_J \cdot \gamma \mathbf{J} \cdot \mathbf{B} \quad (3.2.31)$$

The consequence is the splitting of the energy levels. Let \hat{z} be the axis of orientation of the static field \mathbf{B} . Then the Hamiltonian can be rewritten as

$$\mathcal{H} = -g_J \cdot \gamma \mathbf{J}_z \mathbf{B} \quad (3.2.32)$$

The energy levels E_{M_J} can be easily found [39] replacing the eigenvalues of the operator \mathbf{J}_z in the previous equation

$$E_{M_J} = g_J \cdot \mu_B M_J B \quad (3.2.33)$$

where B is the magnitude of \mathbf{B} . The energy levels are clearly equidistant and the energy differences between two adjacent ones is

$$\Delta E = |E_{M_J} - E_{M_{J-1}}| = g_J \mu_B B \quad (3.2.34)$$

The phenomenon will be analyzed in greater details for the simple (and useful) case of spin- $\frac{1}{2}$ systems. Finally, as represented in Figure 3.12, according to a semi-classical model, the total angular momentum \mathbf{J} precesses about \mathbf{B} , similarly to the classical precession described in section §3.1.2.3.

3.2.2.2 Nuclear magnetism

Nowadays physics states that everything in the Universe is made up of three elementary particles:

- **Quarks:** up and down, charm and strange and top and bottom.
- **Leptons:** electron and electron neutrino, muon and muon neutrino, tau and tau neutrino.
- **Bosons:** they are particles responsible for mediating the action of forces. The photons for the electromagnetic force, the gluons for the strong nuclear force and the vector bosons for the weak nuclear force.

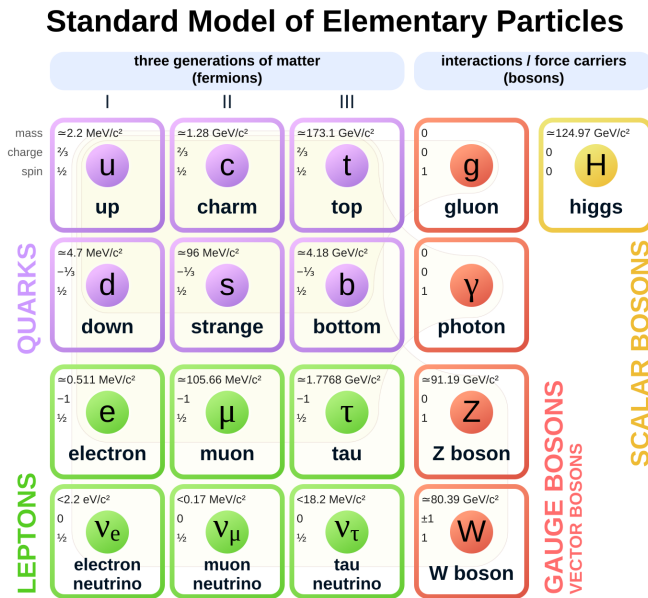


Figure 3.13: The elementary particles according to the standard model. From [40].

The proton is a fermion, since it is a spin- $\frac{1}{2}$ particle. Until the 1980s, it was thought that the three quarks that make up a proton, two up and one down, had spin such that one is in the opposite direction of the other two. The proton’s spin would arise naturally as

$$\frac{1}{2} + \frac{1}{2} - \frac{1}{2} = \frac{1}{2} \tag{3.2.35}$$

It was later experimentally discovered that the three above mentioned quarks only contributed about 30% to the proton’s spin. At the time of writing, the exact origin of the proton spin is still an open question. However, it is thought to

be due to the spin of gluons which mediate the strong nuclear force and to some orbital angular momentum. Clearly, the same issue exists for neutrons.

This is the realm of particle physics, which falls outside the scope of this research, for which it is definitely enough to know that both neutrons and protons possess spin, with $s = \frac{1}{2}$. Nonetheless, it is considered important to warn the reader of the ongoing debate about the spin of these particles.

The nucleus consists of protons and neutrons and it is characterized by:

- **Atomic number Z** : it is the number of protons. It determines the chemical properties of the atom.
- **Mass number A** : the total number of nucleons. Nuclei with the same atomic number but different mass numbers are called isotopes.
- **Spin number I** : It is the quantum number associated with the *total* angular momentum of the nucleus², which depends on the total spin angular momentum and total orbital angular momentum of the nucleons which make it up. The value of I in the lowest energy nuclear state is called the ground state nuclear spin.

The determination of the nuclear spin ground state is by no means trivial and no generic relation does exist which is able to give satisfactory results for all nuclei. One of the models adopted is the **shell model** in which nucleons fill nuclear energy shells as electrons fill atomic shells. Then, the total nuclear angular momentum (the nuclear spin) is computed according to the LS-coupling or, more commonly, to the jj-coupling. Some generic practical rules can be derived:

- If the nucleus has an **even** number of protons and an **even** number of neutrons, the ground spin quantum number is **zero**.
- If the nucleus has an **odd** number of protons and an **odd** number of neutrons, the ground spin quantum number takes an **integer** value.
- If the nucleus has an **even** number of protons and an **odd** number of neutrons or, vice versa, an **odd** number of protons and an **even** number of neutrons, the ground spin quantum number takes a **half integer** value.

The nuclear spins of magnetic isotopes are reported in Figure 3.14.

A nucleus with non-zero spin must exhibit a magnetic moment. In analogy with the magnetism of the electron, one defines the **nuclear magneton** as

²Note that the total angular momentum when the nucleus is regarded as an individual particle is conventionally named *spin* and the symbol I is used instead of J .

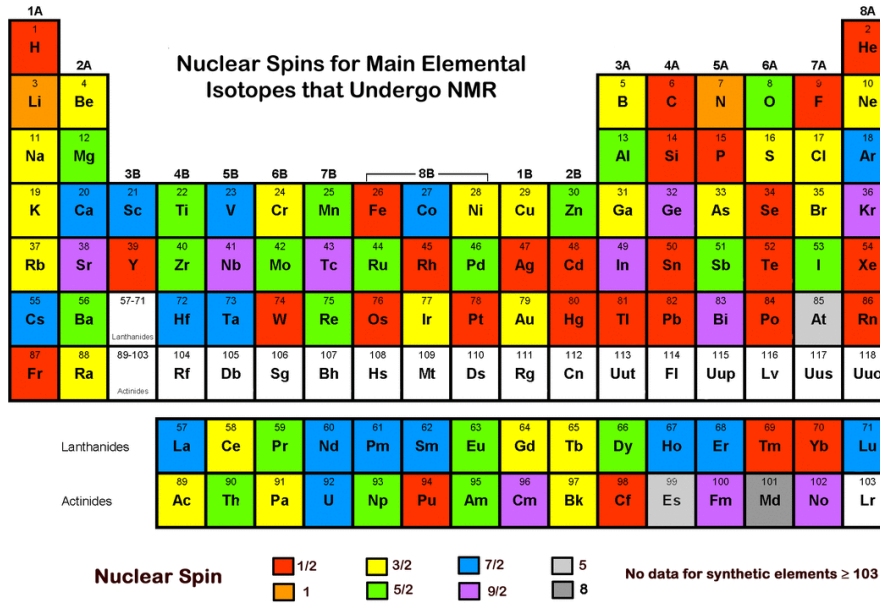


Figure 3.14: The nuclear spins. From [41].

$$\mu_N = \frac{q\hbar}{2m_p} = 5.051 \times 10^{-27} \text{ J T}^{-1} \quad (3.2.36)$$

The magnetic moment is proportional to the total angular momentum Hermitian operator \mathbf{I} :

$$\mathbf{m} \propto \frac{\mu_N}{\hbar} \mathbf{I} \quad (3.2.37)$$

Calling the proportionality constant as **nuclear g -factor**, one can write

$$\mathbf{m} = g_n \cdot \frac{\mu_N}{\hbar} \mathbf{I} = \gamma_n \mathbf{I} \quad (3.2.38)$$

where γ_n is the nuclear gyromagnetic ratio:

$$\gamma_n = g_n \cdot \frac{\mu_N}{\hbar} \quad \left[\frac{\text{rad}}{\text{s} \cdot \text{T}} \right] \quad (3.2.39)$$

The nuclear g -factor, which is embedded in the definition of γ_n , can be either positive or negative. The gyromagnetic ratio, thus, has a sign:

- If γ_n is positive, then \mathbf{m} and \mathbf{I} are parallel³.

³Note that \mathbf{m} and \mathbf{I} are actually quantum operators, so the property of being parallel refers to the vector model or to the related observables.

- If γ_n is negative, then \mathbf{m} and \mathbf{I} are anti-parallel.

The spin operator \mathbf{I} is obviously an angular momentum operator and so its three components do not commute and cannot be specified simultaneously. Moreover

- Its magnitude can assume only the values

$$\hbar\sqrt{I(I+1)} \quad (3.2.40)$$

where the spin quantum number can be $I = 0, \frac{1}{2}, 1, \frac{3}{2}, \dots$.

- Its component along an arbitrary $\hat{\mathbf{z}}$ direction is limited to the $2I + 1$ values

$$m_I\hbar \quad (3.2.41)$$

with $m_I = -I, -I + 1, \dots, I - 1, I$.

Zeeman effect In analogy with the case of the electron, the $2I + 1$ states are degenerate when no field is present. When a strong magnetic field⁴ \mathbf{B}_0 is applied along the $\hat{\mathbf{z}}$ axis, the Hamiltonian of the system is

$$\mathcal{H} = -\gamma_n B_0 \mathbf{I}_z \quad (3.2.42)$$

and $2I + 1$ well defined energy eigenstates arise

$$E_{m_I} = -\hbar\gamma_n m_I B_0 \quad (3.2.43)$$

The energy difference between two adjacent energy levels is

$$\Delta E = \hbar|\gamma_n|B_0 \quad (3.2.44)$$

According to the Planck-Einstein relation

$$\Delta E = hf \quad (3.2.45)$$

a radiation of frequency

$$\omega = |\gamma_n|B_0 \quad (3.2.46)$$

⁴Henceforth, a static magnetic field will be denoted with the symbol \mathbf{B}_0 .

is needed to stimulate the transition to the state of higher energy. Note that this is exactly the same expression for the Larmor frequency obtained in section §3.1.2.3 from a classical model.

3.2.2.3 Some remarks on microscopic magnetism

The **magneton** can be regarded as the unit of measurement of magnetic effects, to some extent. In this regard, one should note that the Bohr magneton, that is, the electron magneton is

$$\mu_B = \frac{e\hbar}{2m_e} \sim 9.274 \times 10^{-24} \text{ J T}^{-1} \sim 5.788 \times 10^{-5} \text{ eV T}^{-1}$$

while the nuclear magneton is

$$\mu_N = \frac{q\hbar}{2m_p} \sim 5.051 \times 10^{-27} \text{ J T}^{-1} \sim 3.152 \times 10^{-8} \text{ eV T}^{-1}$$

which means that

$$\frac{\mu_B}{\mu_N} \sim 1836 \quad (3.2.47)$$

Hence, the magnetic phenomena related to the electron are roughly three orders of magnitude larger than those related to the nucleus. Consequently, the energy separation between energy levels is three orders of magnitude larger, in the case of the electron. Assuming a field $B_0 = 10 \text{ T}$, the Larmor frequency can be in the order⁵ of 100 MHz for a nucleus and 280 GHz for an electron. The corresponding energy differences between adjacent energy levels are in the order of

$$\begin{aligned} \Delta E_e &\sim 1.159 \times 10^{-3} \text{ eV} \\ \Delta E_N &\sim 4.429 \times 10^{-7} \text{ eV} \end{aligned} \quad (3.2.48)$$

There are approximately three-four orders of magnitude between the energy required to promote an electron to an higher energy state and that required to promote a nucleus⁶.

When discussing the magnetic property of materials and molecules, one usually neglects the contribution coming from the nuclear magnetism. Consequently,

⁵Considering ^{13}C , $f = 107.084 \text{ MHz}$

⁶Even if obvious, it is worth underlying that the discussion is focused on the *ground state* and the considered energy levels are the $2J + 1$ (or $2I + 1$) levels which split when a magnetic field is applied, because of the Zeeman effect.

the difference among diamagnetic, paramagnetic and ferromagnetic behaviour depends on the electronic magnetism. It turns out that most substances do not have a magnetic moment in the electronic ground state, because electrons pair up according to the Pauli principle. However, the majority of materials is weakly diamagnetic in ground state [33] because of the electron orbital currents induced by the applied field. The following chapters will mainly focus on nuclear magnetism in diamagnetic substances, when the electronic magnetism can be, more or less, ignored. At first sight, this statement could appear to be quite senseless, since, as discussed at the beginning of this section, electronic magnetism is significantly larger than nucleus's. However, the point is that it *is* larger, but the fields which, as will be clear in the following, are applied to provide the ΔE_N , do not affect the electronic magnetism. Eventually, the latter can be considered as a time independent contribution to the bulk magnetic field of the sample. Except for the chemical shift, which will be discussed later on.

Chapter 4

Nuclear magnetic resonance

In the previous chapter, the phenomena related to magnetism have been introduced from a classical and a quantum mechanical point of view. In particular, the semi-classical precession of an ideal magnetic dipole has been discussed. Then, the behaviour of the orbital and spin angular momenta has been analysed, highlighting the differences between nuclear and electronic magnetism. The latter gives birth to an interesting physical phenomenon, the nuclear magnetic resonance, which can be exploited to build a quantum processor up. In this chapter, the behaviour of the spin angular momentum in presence of an applied field is analysed in greater details, relating it to the semi-classical picture of the precession, which is of help to understand how to realize quantum gates. In particular, it is known that nuclei with $I > \frac{1}{2}$ are characterized by short decoherence times, resulting to be unsuitable for quantum computation. Hence, this chapter mainly focuses on spin- $\frac{1}{2}$ nuclear systems.

The first part is devoted to the analysis of a single spin- $\frac{1}{2}$ in a magnetic field, while the second part discusses the behaviour of an ensemble of spins.

4.1 Single spin

Consider a nucleus whose spin quantum number is $I = \frac{1}{2}$, for instance ^{13}C . In analogy with Equation 3.2.14, all the properties of the nuclear spin- $\frac{1}{2}$ operators are expressed by the **Pauli matrices** presented in section §1.1.12. As a matter of fact, the matrix representation of the spin operators is

$$\begin{aligned} \mathbf{I}_k &= \frac{\hbar}{2} \boldsymbol{\sigma}_k, & k = x, y, z \\ \mathbf{I}^2 &= \mathbf{I}_x^2 + \mathbf{I}_y^2 + \mathbf{I}_z^2 = \frac{3\hbar^2}{4} \begin{pmatrix} 1 & 0 \\ 0 & 1 \end{pmatrix} \\ \mathbf{I} &= \begin{pmatrix} \mathbf{I}_x & \mathbf{I}_y & \mathbf{I}_z \end{pmatrix}^t \end{aligned} \quad (4.1.1)$$

As discussed in section §3.2.2.2, when an external static field \mathbf{B}_0 is applied, the Hamiltonian of the system is

$$\mathcal{H} = -\gamma_n B_0 \mathbf{I}_z \quad (4.1.2)$$

Since $I = \frac{1}{2}$, only two energy eigenstates arise as a consequence of the Zeeman splitting. The associated basis states, known as **Zeeman eigenstates**, are the eigenvectors of $\boldsymbol{\sigma}_z$:

$$|\uparrow\rangle = \begin{pmatrix} 1 \\ 0 \end{pmatrix} \quad |\downarrow\rangle = \begin{pmatrix} 0 \\ 1 \end{pmatrix} \quad (4.1.3)$$

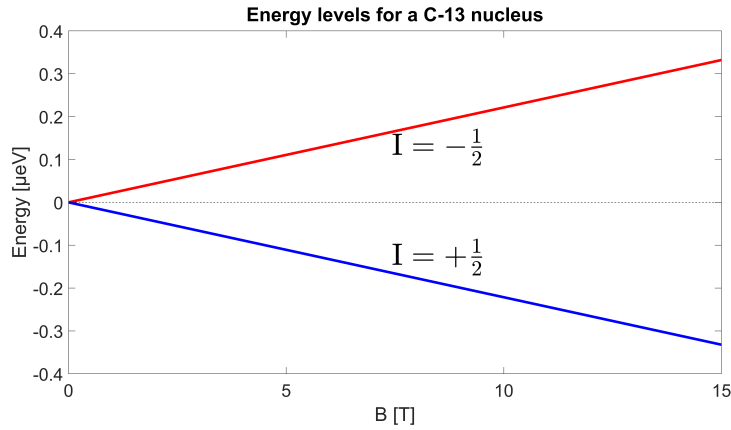
while the corresponding energy levels, that is, the eigenvalues of the Hamiltonian, are

$$\begin{aligned} E_{\uparrow} &= -\frac{\gamma_n \hbar B_0}{2} = -\frac{g_n \mu_N B_0}{2} \\ E_{\downarrow} &= +\frac{\gamma_n \hbar B_0}{2} = +\frac{g_n \mu_N B_0}{2} \end{aligned} \quad (4.1.4)$$

The energy difference between the two eigenstates is

$$\Delta E = \hbar |\gamma_n| B_0 \quad (4.1.5)$$

One should note that it is directly proportional to the magnitude of the applied field. The case of ^{13}C is reported in Figure 4.1, for typical values of B_0 . A spin-


 Figure 4.1: The Zeeman effect for a ^{13}C nucleus.

$\frac{1}{2}$ system can be in a generic superposition of the two basis states. The spin wavefunction, at time $t = 0$, can be written as

$$|\psi(0)\rangle = c_0 |\uparrow\rangle + c_1 |\downarrow\rangle \quad (4.1.6)$$

According to property 1.2.3, since the Hamiltonian is time independent, the time evolution is ruled by the time operator

$$\mathcal{U}(t) = \exp\left(-\frac{\mathcal{H}t}{\hbar}\right) = \mathbf{R}_z(-\gamma_n B_0 t) \quad (4.1.7)$$

Proof. Replacing the expression of \mathcal{H} and applying corollary 1.1.5.1, one gets

$$\begin{aligned} \mathcal{U}(t) &= \exp\left(i\frac{\gamma_n B_0 \mathbf{I}_z}{\hbar} t\right) = \cos\left(\frac{\gamma_n B_0 t}{2}\right) \cdot \mathbb{I} + i \sin\left(\frac{\gamma_n B_0 t}{2}\right) \cdot \boldsymbol{\sigma}_z \\ &= \begin{pmatrix} \cos\left(\frac{\gamma_n B_0 t}{2}\right) + i \sin\left(\frac{\gamma_n B_0 t}{2}\right) & 0 \\ 0 & \cos\left(\frac{\gamma_n B_0 t}{2}\right) - i \sin\left(\frac{\gamma_n B_0 t}{2}\right) \end{pmatrix} \\ &= \begin{pmatrix} e^{i\frac{\gamma_n B_0 t}{2}} & 0 \\ 0 & e^{-i\frac{\gamma_n B_0 t}{2}} \end{pmatrix} = \mathbf{R}_z(-\gamma_n B_0 t) \end{aligned}$$

The last equivalence follows directly from the definition of the rotation operator $\mathbf{R}_z(\alpha)$ introduced in section §2.1.6.1. \square

The wavefunction at time t is therefore

$$|\psi(t)\rangle = \mathbf{R}_z(-\gamma_n B_0 t) |\psi(0)\rangle = c_0 e^{i\frac{\gamma_n B_0 t}{2}} |\uparrow\rangle + c_1 e^{-i\frac{\gamma_n B_0 t}{2}} |\downarrow\rangle \quad (4.1.8)$$

Proof.

$$\begin{aligned}
 |\psi(t)\rangle &= \mathbf{R}_z(-\gamma_n B_0 t) |\psi(0)\rangle \\
 &= \begin{pmatrix} e^{i\frac{\gamma_n B_0}{2}t} & 0 \\ 0 & e^{-i\frac{\gamma_n B_0}{2}t} \end{pmatrix} \left[c_0 \begin{pmatrix} 1 \\ 0 \end{pmatrix} + c_1 \begin{pmatrix} 0 \\ 1 \end{pmatrix} \right] \\
 &= c_0 e^{i\frac{\gamma_n B_0}{2}t} |\uparrow\rangle + c_1 e^{-i\frac{\gamma_n B_0}{2}t} |\downarrow\rangle
 \end{aligned}$$

□

As time flows, the static field forces a change in the phase between the up and down spin eigenstates, but the probability to measure a specific outcome ($|\uparrow\rangle$ or $|\downarrow\rangle$) is **unchanged**. Even if this is a pure quantum mechanical effect, it

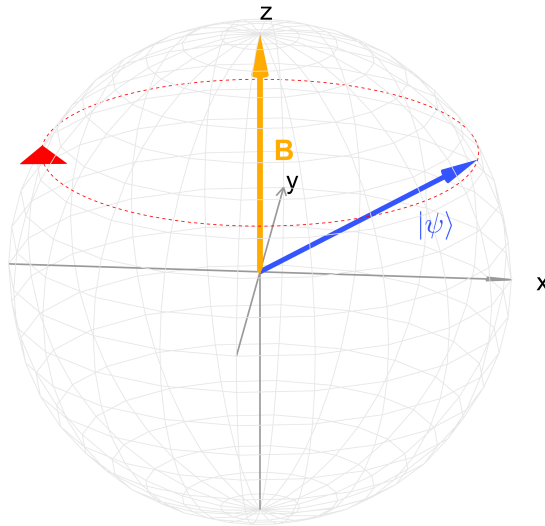


Figure 4.2: The spin precession assuming $\gamma_n > 0$.

is possible to give a pictorial representation of the phenomenon. The spin can be represented as an arrow **precessing** about the applied magnetic field at a frequency $\omega_0 = -\gamma \mathbf{B}_0$. This is a powerful tool to get a feel for the behaviour of the spin and fix the ideas, since it builds a bridge to the semi-classical precession of the magnetic moment, but it should not be overinterpreted. The latitude of the spin ($|\psi\rangle$) gives the probability with which the two Zeeman eigenstates can be measured, which is unaffected by the precession about \mathbf{B}_0 . When a measurement is carried out, the spin collapses to one of the two allowed eigenstates and it is represented by a vector lying along the \hat{z} axis. It should be obvious that it does not mean that the \hat{x} and \hat{y} components are zero. On the other hand, they are simply undefined, since the three components of the spin operator do not commute and cannot be measured simultaneously.

The product $\gamma_n B_0$ has the dimensions of an angular frequency. In section §3.1.2.3, this product is defined as the **Larmor frequency**¹ and associated with the precession of an ideal magnetic dipole about an external field:

$$\boldsymbol{\omega}_0 = -\gamma_n \mathbf{B}_0 \implies \omega_0 = |\gamma_n| B_0$$

It was pointed out that the classically derived expression for ω_0 does not depend on the component of the magnetic moment perpendicular to the applied field. This justifies the fact that the result obtained adopting the classical model agrees with the one provided by quantum mechanics, where the perpendicular component is not specified.

The sign of the precession As well known, the Hamiltonian is

$$\mathcal{H} = -\gamma_n B_0 \mathbf{I}_z = -\gamma_n B_0 \frac{\hbar \boldsymbol{\sigma}_z}{2}$$

and has eigenvalues and associated eigenvectors

$$E_{\downarrow} = +\frac{\gamma_n \hbar B_0}{2} \longrightarrow |\downarrow\rangle \quad E_{\uparrow} = -\frac{\gamma_n \hbar B_0}{2} \longrightarrow |\uparrow\rangle \quad (4.1.9)$$

Calling the ground state E_{ground} and the high energy state E_{high} :

- For a particle with $\gamma < \mathbf{0}$ and, so, with the magnetic moment antiparallel to the spin, the energy states are:

$$E_{\text{ground}} = E_{\downarrow} = -\frac{\hbar \omega_0}{2} \longrightarrow |\downarrow\rangle \quad E_{\text{high}} = E_{\uparrow} = +\frac{\hbar \omega_0}{2} \longrightarrow |\uparrow\rangle \quad (4.1.10)$$

The vector angular frequency $\boldsymbol{\omega}_0$ is positive and the spin precesses **anti-clockwise**. The electron and few nuclei, as ^{15}N and ^{29}Si , have negative gyromagnetic ratio.

- For a particle with $\gamma > \mathbf{0}$ and, so, with the magnetic moment parallel to the spin, the energy states are:

$$E_{\text{ground}} = E_{\uparrow} = -\frac{\hbar \omega_0}{2} \longrightarrow |\uparrow\rangle \quad E_{\text{high}} = E_{\downarrow} = +\frac{\hbar \omega_0}{2} \longrightarrow |\downarrow\rangle \quad (4.1.11)$$

The vector angular frequency $\boldsymbol{\omega}_0$ is negative and the spin precesses **clockwise**. Most nuclei have positive gyromagnetic ratio.

¹Here the Larmor frequency corresponding to the field \mathbf{B}_0 is denoted with the subscript 0, for the sake of clearness.

4.1.1 The radio-frequency field

In short, one can say that the application of a static field to a single spin- $\frac{1}{2}$ system has two effects: the rise of two well-defined energy levels and the spin precession about \mathbf{B}_0 . It is also known, from the previous discussion that, assuming $\gamma_n > 0^2$, the system energy is minimized when the spin is parallel to the applied field and maximized in the opposite case. However, it is clear that the spin does not live in one or the other energy state, but rather in a linear *superposition* of both.

In order to encode the information carried by a qubit on a spin- $\frac{1}{2}$, one has to find a tool which allows changing the “orientation” of the spin. In other words, one must be able to change the \hat{z} component of the spin, something which cannot be achieved by the simple and spontaneous precession about \mathbf{B}_0 . However, this requires to change the θ angle and, consequently, the energy of the system. What is needed, in practice, is an interaction that can favour the transitions between levels. According to Equation 4.1.5, the required energy is $\Delta E = \hbar|\gamma_n|B_0$.

The most commonly used coupling is an **alternating magnetic field** applied perpendicularly to the static field, for instance along the \hat{x} axis

$$\mathbf{B}_r(t) = -2 \cdot B_r \cos(\omega_r t - \phi) \hat{x} \quad (4.1.12)$$

where ω_r and ϕ are the angular frequency and the phase of \mathbf{B}_r , respectively. The minus sign is arbitrarily chosen to simplify the successive discussion about quantum gates, while the factor 2 allows the Hamiltonian to have a cleaner expression. The latter is

$$\mathcal{H}_r = 2 \cdot \gamma_n \cdot B_r \cos(\omega_r t - \phi) \mathbf{I}_x \quad (4.1.13)$$

Defining the angular frequency

$$\omega_* \triangleq \gamma_n \cdot B_r \quad (4.1.14)$$

the radio-frequency Hamiltonian can be rewritten as

$$\mathcal{H}_r = 2 \cdot \omega_* \cos(\omega_r t - \phi) \mathbf{I}_x \quad (4.1.15)$$

Since B_r is typically around 10^{-4} T, while B_0 is of the order of 10 T, it results that $\omega_r \ll \omega_0$ and so the contribution induced by the alternating field can be written as a *perturbation* of the main Hamiltonian \mathcal{H}_0 . It follows that the overall

²Henceforth, unless otherwise specified, γ_n will be always assumed positive, since this is the case of interest for molecules routinely adopted in quantum computation.

Hamiltonian is

$$\mathcal{H} = \mathcal{H}_0 + \mathcal{H}_r = -\omega_0 \mathbf{I}_z + 2 \cdot \omega_* \cos(\omega_r t - \phi) \mathbf{I}_x \quad (4.1.16)$$

The explicit time dependence makes it hard to solve the associated Schrödinger equation and find the time evolution operator. A special technique is introduced to simplify the job: the use of a **rotating coordinate system** S' . If $\gamma_n > 0$,

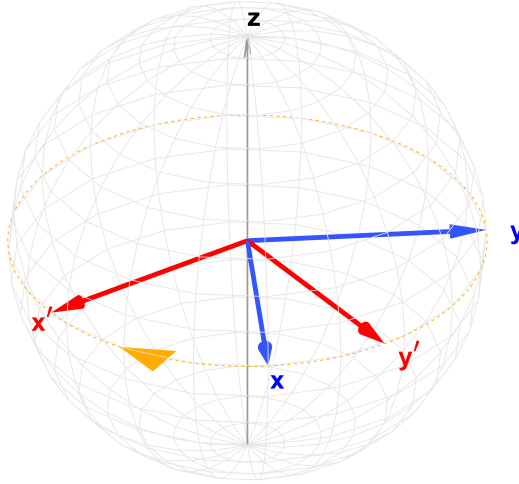


Figure 4.3: The rotating frame S' : $\boldsymbol{\omega} = -\omega \hat{\mathbf{z}}$ with $\omega > 0$.

then the static field \mathbf{B}_0 forces the spin to precess clockwise about $\hat{\mathbf{z}}$. The reference frame is chosen such that it rotates in the same sense of the spin. Consequently, the angular frequency which characterizes the rotation of the $\hat{\mathbf{x}}'$ and $\hat{\mathbf{y}}'$ is

$$\boldsymbol{\omega} = -\omega \hat{\mathbf{z}}, \quad \omega > 0 \quad (4.1.17)$$

The frame axes, as reported in Figure 4.3, are related as

$$\begin{aligned} \hat{\mathbf{x}}' &= \cos(\omega t) \hat{\mathbf{x}} - \sin(\omega t) \hat{\mathbf{y}} \\ \hat{\mathbf{y}}' &= \sin(\omega t) \hat{\mathbf{x}} + \cos(\omega t) \hat{\mathbf{y}} \\ \hat{\mathbf{z}}' &= \hat{\mathbf{z}} \end{aligned} \quad (4.1.18)$$

The analysis of the effects induced by the alternating magnetic field on the spin can be carried out adopting a semi-classical or a quantum mechanical model. The main aspects of both are presented in the following, since the first one is useful to have a pictorial understanding of what is going on, while the second one is extensively used to perform quantum computation. For a more rigorous and

detailed analysis, the reader is suggested to make reference to [42], which is one of the fundamental texts on NMR.

4.1.1.1 The classical picture

The radio frequency field introduced in Equation 4.1.12 can be broken in two rotating components, each of amplitude B_r :

$$\mathbf{B}_r(t) = \mathbf{B}_r^+(t) + \mathbf{B}_r^-(t) \quad (4.1.19)$$

where

$$\begin{aligned} \mathbf{B}_r^+(t) &= -B_r [\cos(\omega_r t - \phi)\hat{\mathbf{x}} - \sin(\omega_r t - \phi)\hat{\mathbf{y}}] \\ \mathbf{B}_r^-(t) &= -B_r [\cos(\omega_r t - \phi)\hat{\mathbf{x}} + \sin(\omega_r t - \phi)\hat{\mathbf{y}}] \end{aligned} \quad (4.1.20)$$

The component rotating **in the same sense** as the spin precession (negative for $\gamma > 0$ and positive for $\gamma < 0$) is known as the **resonant component**, while the component rotating **in the opposite sense** to the spin precession (positive for $\gamma > 0$ and negative for $\gamma < 0$) is referred to as the **non-resonant component**.

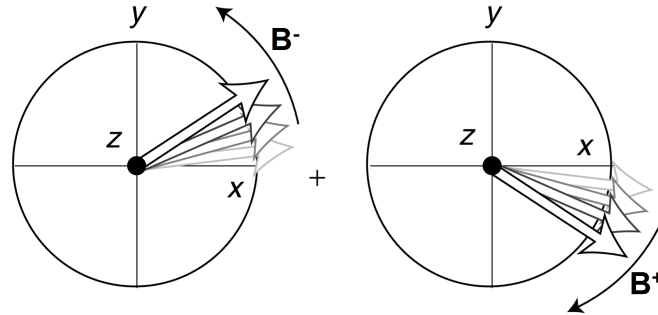


Figure 4.4: The resonant and the non-resonant components. Adapted from [33].

Near resonance, that is, when $\omega_r \sim \omega_0$, \mathbf{B}_r^+ rotates coherently with the Larmor precession, while \mathbf{B}_r^- rotates in the opposite sense. Consequently, if $\omega \sim \omega_0$, \mathbf{B}_r^+ is stationary in the rotating frame while \mathbf{B}_r^- rotates at twice the Larmor frequency. Therefore, only \mathbf{B}_r^+ will have an effective influence on the nuclear spins, provided that both fields have magnitude much smaller than that of the static field \mathbf{B}_0 . Hence, \mathbf{B}_r^- can be neglected. This is known as the **rotating wave approximation** in the scientific literature.

The equation of motion of the spin including both the effects of \mathbf{B}_0 and \mathbf{B}_r^+ can be written in the laboratory reference system S in analogy with Equation 3.1.23

as

$$\left(\frac{d\mathbf{m}}{dt}\right)_S = \gamma\mathbf{m} \times [\mathbf{B}_0 + \mathbf{B}_r^+(t)] \quad (4.1.21)$$

The time dependence of \mathbf{B}_r^+ can be eliminated using a coordinate system S' which rotates about $\hat{\mathbf{z}}$ at frequency $\boldsymbol{\omega} = -\omega\hat{\mathbf{z}}$, enforcing $\omega = \omega_r$. In this reference system, \mathbf{B}_r^+ is static. Moreover, since the axis of rotation coincides with the direction of \mathbf{B}_0 , also \mathbf{B}_0 is static.

The equation of motion of the magnetic moment in the rotating frame is

$$\left(\frac{d\mathbf{m}}{dt}\right)_{S'} = \gamma_n\mathbf{m} \times \mathbf{B}_{\text{eff}} \quad (4.1.22)$$

where

$$\mathbf{B}_{\text{eff}} \triangleq \left(B_0 - \frac{\omega_r}{\gamma_n}\right)\hat{\mathbf{z}} - B_r(\cos(\phi)\hat{\mathbf{x}}' + \sin(\phi)\hat{\mathbf{y}}') \quad (4.1.23)$$

Proof. The point is to compute the derivative of Equation 4.1.21 in the rotating coordinate system. It is known from basic kinematics that, if S is the laboratory reference system and S' is a system rotating at angular frequency $\boldsymbol{\omega}$ with respect to S , then the derivative of a generic vector \mathbf{a} is

$$\left(\frac{d\mathbf{a}}{dt}\right)_S = \left(\frac{d\mathbf{a}}{dt}\right)_{S'} + \boldsymbol{\omega} \times \mathbf{a}$$

For the proof, see for instance [43]. The derivative of the magnetic moment is therefore

$$\left(\frac{d\mathbf{m}}{dt}\right)_S = \left(\frac{d\mathbf{m}}{dt}\right)_{S'} + \boldsymbol{\omega} \times \mathbf{m}$$

Replacing Equation 4.1.21, one gets in the rotating frame

$$\left(\frac{d\mathbf{m}}{dt}\right)_{S'} = \left(\frac{d\mathbf{m}}{dt}\right)_S - \boldsymbol{\omega} \times \mathbf{m} = \gamma\mathbf{m} \times [\mathbf{B}_0 + \mathbf{B}_r^+(t)] - \boldsymbol{\omega} \times \mathbf{m}$$

The rotating magnetic field can be rewritten with respect to the rotating reference frame as

$$\begin{aligned} \mathbf{B}_r^+(t) &= -B_r [\cos(\omega_r t - \phi)\hat{\mathbf{x}} - \sin(\omega_r t - \phi)\hat{\mathbf{y}}] \\ &= -B_r \{ \cos(\phi) [\cos(\omega_r t)\hat{\mathbf{x}} - \sin(\omega_r t)\hat{\mathbf{y}}] + \sin(\phi) [\sin(\omega_r t)\hat{\mathbf{x}} + \cos(\omega_r t)\hat{\mathbf{y}}] \} \\ &= -B_r (\cos(\phi)\hat{\mathbf{x}}' + \sin(\phi)\hat{\mathbf{y}}') \end{aligned}$$

Replacing in the equation of motion

$$\begin{aligned}
 \left(\frac{d\mathbf{m}}{dt}\right)_{S'} &= \gamma\mathbf{m} \times [B_0\hat{\mathbf{z}} - B_r(\cos(\phi)\hat{\mathbf{x}}' + \sin(\phi)\hat{\mathbf{y}}')] + \mathbf{m} \times \boldsymbol{\omega} \\
 &= \mathbf{m} [(\gamma_n B_0 - \omega_r)\hat{\mathbf{z}} - \gamma_n B_r(\cos(\phi)\hat{\mathbf{x}}' + \sin(\phi)\hat{\mathbf{y}}')] \\
 &= \gamma_n \mathbf{m} \times \left[\left(B_0 - \frac{\omega_r}{\gamma_n} \right) \hat{\mathbf{z}} - B_r(\cos(\phi)\hat{\mathbf{x}}' + \sin(\phi)\hat{\mathbf{y}}') \right]
 \end{aligned}$$

□

The proposed classical model is interesting for a number of reasons. First of all, Equation 4.1.22 states that the magnetic moment precesses clockwise³ about the direction of \mathbf{B}_{eff} at an angular frequency, whose value, one resonance, is $\gamma_n B_r$. However, when the alternating field is far from resonance, that is, when

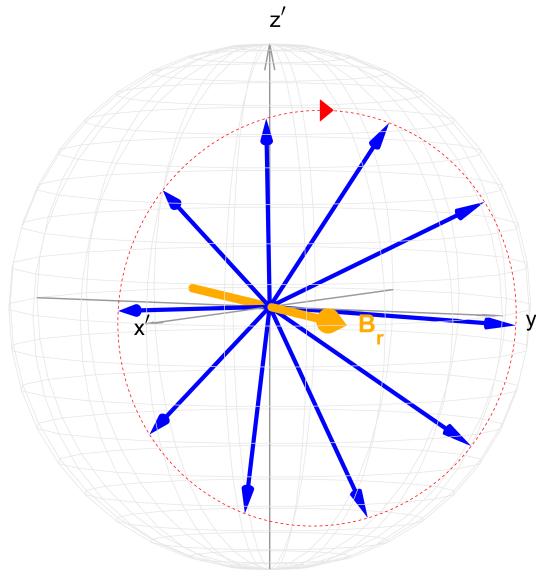


Figure 4.5: The precession of the spin on resonance in the rotating coordinate reference system for $\phi = 225^\circ$.

$$\xi \triangleq \omega - \omega_0 = \omega_r - \omega_0 \quad (4.1.24)$$

is large, the spin precesses in the rotating frame about an axis tilted away from

³As known from the discussion about the Larmor precession, if $\gamma_n > 0$, the spin precesses clockwise about \mathbf{B}_{eff} or anticlockwise about $-\mathbf{B}_{\text{eff}}$. The reason for the minus sign in Equation 4.1.12 is that with this choice, the spin performs a positive (anticlockwise) precession about an axis which describes a ϕ angle with $\hat{\mathbf{x}}'$.

the \hat{z} axis by a very **small angle** [44] given by

$$\alpha = \text{atan}\left(\frac{\omega_*}{\xi}\right) \quad (4.1.25)$$

As a matter of fact

$$\text{atan}\left(\frac{\omega_*}{\xi}\right) \sim 0 \quad (4.1.26)$$

when $|\xi| \gg \omega_*$. It follows that the effect of a radio frequency field on spins which are far off resonance is practically immaterial. On the other hand, if $\omega \sim \omega_0$, that is, near resonance, the **effective field** becomes

$$\mathbf{B}_{\text{eff}} \sim -B_r (\cos(\phi)\hat{\mathbf{x}}' + \sin(\phi)\hat{\mathbf{y}}') \quad (4.1.27)$$

and the spin precesses about \mathbf{B}_r^+ , which is stationary in the rotating frame, at frequency ω_* , as reported in Figure 4.5.

The main results obtained so far can be summarized as follows:

- When just a static field $\mathbf{B}_0 = B_0\hat{z}$ is applied to the system, the spin precesses about the \hat{z} axis at the Larmor frequency in the laboratory reference system, while it is constant in the rotating frame, given that the latter rotates at the Larmor frequency.
- When an alternating field $\mathbf{B}_r(t) = -2 \cdot B_r \cos(\omega_r t - \phi)\hat{\mathbf{x}}$ and a static field \mathbf{B}_0 are applied to the system, the spin follows a complex trajectory in the laboratory system, while it simply rotates about \mathbf{B}_r^+ in the rotating frame, assuming the resonance condition. An off-resonance field has a very small impact on the spin trajectory, since B_r is usually four-five orders of magnitude smaller than B_0 .

4.1.1.2 The quantum picture

The spin Hamiltonian reported in Equation 4.1.16 depends on time. In order to remove such dependence, the previous section presents the introduction of a rotating reference as a good solution. The quantum mechanical equivalent of the rotating coordinate transformation is a unitary transformation described by a unitary operator. It is clear that if the $\hat{\mathbf{x}}'$ and $\hat{\mathbf{y}}'$ axes rotate clockwise at angular frequency ω , a generic state vector $|\psi\rangle$ in S is mapped to the corresponding state vector $|\tilde{\psi}\rangle$ in S' by a unitary operator which describes an anticlockwise rotation

about \hat{z} :

$$|\tilde{\psi}\rangle = \mathbf{R}_z(\omega t) |\psi\rangle \quad (4.1.28)$$

The matrix representation, for the spin- $\frac{1}{2}$ case, is therefore

$$\mathbf{U}_R \triangleq \mathbf{R}_z(\omega t) = \exp\left(-i\frac{\omega\sigma_z}{2}t\right) = \begin{pmatrix} e^{-i\frac{\omega}{2}t} & 0 \\ 0 & e^{+i\frac{\omega}{2}t} \end{pmatrix} \quad (4.1.29)$$

The evolution of the state vector $|\tilde{\psi}\rangle$ is ruled by the Schrödinger equation, which, in the rotating frame, has the following expression

$$\frac{d|\tilde{\psi}\rangle}{dt} = -\frac{i}{\hbar}\tilde{\mathcal{H}}|\tilde{\psi}\rangle \quad (4.1.30)$$

where the rotating frame Hamiltonian is

$$\tilde{\mathcal{H}} = \mathbf{U}_R\mathcal{H}\mathbf{U}_R^\dagger - i\hbar\mathbf{U}_R\frac{d\mathbf{U}_R^\dagger}{dt} \quad (4.1.31)$$

Proof. The time derivative of the wavefunction in the rotating frame is

$$\frac{d|\tilde{\psi}\rangle}{dt} = \frac{d}{dt}(\mathbf{U}_R|\psi\rangle) = \frac{d\mathbf{U}_R}{dt}|\psi\rangle + \mathbf{U}_R\frac{d|\psi\rangle}{dt}$$

Replacing the Schrödinger equation in the previous expression one gets

$$\begin{aligned} \frac{d|\tilde{\psi}\rangle}{dt} &= \frac{d}{dt}(\mathbf{U}_R|\psi\rangle) = \frac{d\mathbf{U}_R}{dt}|\psi\rangle + \mathbf{U}_R\left[-\frac{i}{\hbar}\mathcal{H}|\psi\rangle\right] \\ &= \left[\frac{d\mathbf{U}_R}{dt} - \mathbf{U}_R\frac{i}{\hbar}\mathcal{H}\right]|\psi\rangle \\ &= -\frac{i}{\hbar}\left[i\hbar\frac{d\mathbf{U}_R}{dt} + \mathbf{U}_R\mathcal{H}\right]\mathbf{U}_R^\dagger\mathbf{U}_R|\psi\rangle \\ &= -\frac{i}{\hbar}\left[i\hbar\frac{d\mathbf{U}_R}{dt}\mathbf{U}_R^\dagger + \mathbf{U}_R\mathcal{H}\mathbf{U}_R^\dagger\right]\mathbf{U}_R|\psi\rangle \end{aligned}$$

Now consider that the time derivative of the identity operator is the zero operator

$$\frac{d\mathbb{I}}{dt} = \mathbf{0}$$

Then, since \mathbf{U}_R is unitary

$$\frac{d\mathbb{I}}{dt} = \frac{d\mathbf{U}\mathbf{U}^\dagger}{dt} = \frac{d\mathbf{U}}{dt}\mathbf{U}^\dagger + \mathbf{U}\frac{d\mathbf{U}^\dagger}{dt} = \mathbf{0} \implies \frac{d\mathbf{U}}{dt}\mathbf{U}^\dagger = -\mathbf{U}\frac{d\mathbf{U}^\dagger}{dt}$$

Replacing in the time derivative of $|\tilde{\psi}\rangle$

$$\frac{d|\tilde{\psi}\rangle}{dt} = -\frac{i}{\hbar} \left[\mathbf{U}_R \mathcal{H} \mathbf{U}_R^\dagger - i\hbar \mathbf{U}_R \frac{d\mathbf{U}_R^\dagger}{dt} \right] |\tilde{\psi}\rangle = -\frac{i}{\hbar} \tilde{\mathcal{H}} |\tilde{\psi}\rangle$$

□

When $\mathbf{U}_R = \mathbf{R}_Z(\omega t)$, the rotating frame Hamiltonian becomes

$$\tilde{\mathcal{H}} = \mathbf{R}_z(\omega t) \mathcal{H} \mathbf{R}_z(-\omega t) + \omega \mathbf{I}_z \quad (4.1.32)$$

Proof. Equation 4.1.31 is rewritten as

$$\tilde{\mathcal{H}} = \mathbf{R}_z(\omega t) \mathcal{H} \mathbf{R}_z(-\omega t) - i\hbar \mathbf{R}_z(\omega t) \frac{d\mathbf{R}_z(-\omega t)}{dt}$$

The derivative of the rotation operator is

$$\begin{aligned} \frac{d\mathbf{R}_z(-\omega t)}{dt} &= \frac{d}{dt} \left[\exp\left(i\omega t \frac{\sigma_z}{2}\right) \right] \\ &= i\omega \frac{\sigma_z}{2} \exp\left(i\omega t \frac{\sigma_z}{2}\right) \\ &= i\omega \frac{\sigma_z}{2} \mathbf{R}_z(-\omega t) \end{aligned}$$

and so

$$\tilde{\mathcal{H}} = \mathbf{R}_z(\omega t) \mathcal{H} \mathbf{R}_z(-\omega t) + \hbar\omega \frac{\sigma_z}{2}$$

□

As known from the classical model, the non-resonant field component which rotates in the opposite sense as the nuclear spin precession can be neglected, according to the **rotating wave approximation**. The resulting approximated Hamiltonian takes the following form

$$\tilde{\mathcal{H}} = \xi \mathbf{I}_z + \omega_* (\cos \phi \mathbf{I}_x + \sin \phi \mathbf{I}_y) \quad (4.1.33)$$

One should note that the Hamiltonian is now **time independent**.

Proof. The rotating operators satisfy [42, 33] the following useful properties

$$\begin{aligned} \mathbf{R}_z(\alpha) \mathbf{I}_x \mathbf{R}_z(-\alpha) &= \cos(\alpha) \mathbf{I}_x + \sin(\alpha) \mathbf{I}_y \\ \mathbf{R}_z(\alpha) \mathbf{I}_y \mathbf{R}_z(-\alpha) &= -\sin(\alpha) \mathbf{I}_x + \cos(\alpha) \mathbf{I}_y \\ \mathbf{R}_z(\alpha) \mathbf{I}_z \mathbf{R}_z(-\alpha) &= \mathbf{I}_z \end{aligned}$$

The approximated Hamiltonian, when only

$$\mathbf{B}_r^+(t) = -B_r [\cos(\omega_r t - \phi) \hat{\mathbf{x}} - \sin(\omega_r t - \phi) \hat{\mathbf{y}}]$$

is considered, takes the form

$$\begin{aligned} \mathcal{H} &= -\omega_0 \mathbf{I}_z + \omega_* [\cos(\omega_r t - \phi) \mathbf{I}_x - \sin(\omega_r t - \phi) \mathbf{I}_y] \\ &= -\omega_0 \mathbf{I}_z + \mathbf{R}_z(-\omega_r t + \phi) \mathbf{I}_x \mathbf{R}_z(\omega_r t - \phi) \end{aligned}$$

Moving to the rotating frame

$$\tilde{\mathcal{H}} = \xi \mathbf{I}_z + \mathbf{R}_z((\omega - \omega_r)t + \phi) \mathbf{I}_x \mathbf{R}_z((\omega_r - \omega)t - \phi)$$

If the rotating frame angular frequency coincides with that of the alternating field, that is, if

$$\omega \equiv \omega_r$$

then the Hamiltonian takes a simpler form

$$\begin{aligned} \tilde{\mathcal{H}} &= \xi \mathbf{I}_z + \mathbf{R}_z(\phi) \mathbf{I}_x \mathbf{R}_z(-\phi) \\ &= \xi \mathbf{I}_z + \omega_* (\cos \phi \mathbf{I}_x + \sin \phi \mathbf{I}_y) \end{aligned}$$

□

When the resonance condition is completely fulfilled, the Hamiltonian becomes

$$\tilde{\mathcal{H}} = \omega_* (\cos \phi \mathbf{I}_x + \sin \phi \mathbf{I}_y) \quad (4.1.34)$$

The matrix representation In order to see the effect of the non-resonant component of the magnetic field and be convinced that the rotating wave approximation is definitely reasonable, it is possible to write explicitly the rotating frame Hamiltonian matrix expression for the spin- $\frac{1}{2}$ case:

$$\tilde{\mathcal{H}} = \frac{\hbar}{2} \begin{pmatrix} -\omega_0 + \omega & \omega_* [e^{-i[(\omega-\omega_r)t+\phi]} + e^{-i[(\omega+\omega_r)t-\phi]}] \\ \omega_* [e^{i[(\omega-\omega_r)t+\phi]} + e^{i[(\omega+\omega_r)t-\phi]}] & \omega_0 - \omega \end{pmatrix} \quad (4.1.35)$$

Proof. Replacing Equation 4.1.16 in Equation 4.1.32, one gets

$$\tilde{\mathcal{H}} = \mathbf{R}_z(\omega t) [-\omega_0 \mathbf{I}_z + 2\omega_* \cos(\omega_r t - \phi) \mathbf{I}_x] \mathbf{R}_z(-\omega t) + \omega \mathbf{I}_z$$

which can be immediately rewritten as

$$\tilde{\mathcal{H}} = 2\omega_* \cos(\omega_r t - \phi) \mathbf{R}_z(\omega t) \mathbf{I}_x \mathbf{R}_z(-\omega t) + (\omega - \omega_0) \mathbf{I}_z$$

The first term on the right hand side is developed as

$$\begin{aligned} \mathbf{R}_z(\omega t) \mathbf{I}_x \mathbf{R}_z(-\omega t) &= \frac{\hbar}{2} \mathbf{R}_z(\omega t) \boldsymbol{\sigma}_x \mathbf{R}_z(-\omega t) \\ &= \frac{\hbar}{2} \begin{pmatrix} e^{-i\omega t/2} & 0 \\ 0 & e^{+i\omega t/2} \end{pmatrix} \begin{pmatrix} 0 & 1 \\ 1 & 0 \end{pmatrix} \begin{pmatrix} e^{+i\omega t/2} & 0 \\ 0 & e^{-i\omega t/2} \end{pmatrix} \\ &= \frac{\hbar}{2} \begin{pmatrix} 0 & e^{-i\omega t} \\ e^{+i\omega t} & 0 \end{pmatrix} \end{aligned}$$

The Hamiltonian becomes

$$\begin{aligned} \tilde{\mathcal{H}} &= \hbar \begin{pmatrix} 0 & \omega_* e^{-i\omega t} \cos(\omega_r t - \phi) \\ \omega_* e^{+i\omega t} \cos(\omega_r t - \phi) & 0 \end{pmatrix} + \frac{\hbar}{2} \begin{pmatrix} \omega - \omega_0 & 0 \\ 0 & \omega_0 - \omega \end{pmatrix} \\ &= \hbar \begin{pmatrix} \frac{\omega - \omega_0}{2} & \omega_* e^{-i\omega t} \cos(\omega_r t - \phi) \\ \omega_* e^{+i\omega t} \cos(\omega_r t - \phi) & \frac{\omega_0 - \omega}{2} \end{pmatrix} \end{aligned}$$

Replacing

$$\cos(\omega_r t - \phi) = \frac{e^{i(\omega_r t - \phi)} + e^{-i(\omega_r t - \phi)}}{2}$$

in the previous expression, one obtains Equation 4.1.35. \square

If the rotating frame angular frequency coincides with that of the alternating field, that is, if

$$\omega \equiv \omega_r \quad (4.1.36)$$

then the Hamiltonian takes a simpler form

$$\tilde{\mathcal{H}} = \frac{\hbar}{2} \begin{pmatrix} \xi & \omega_* [e^{-i\phi} + e^{-i(2\omega_r t - \phi)}] \\ \omega_* [e^{i\phi} + e^{i(2\omega_r t - \phi)}] & -\xi \end{pmatrix} \quad (4.1.37)$$

The terms oscillating rapidly with $2\omega_r$ derive from the non-resonant field component which rotates in the opposite sense with respect to the nuclear spin precession. If the time scale is sufficiently longer than $1/\omega_r$, then these terms are *averaged to zero* and can be safely neglected. This is, once more, the **rotating wave approximation**. The rotating frame Hamiltonian is now **time independent**

$$\tilde{\mathcal{H}} \approx \frac{\hbar}{2} \begin{pmatrix} \xi & \omega_* e^{-i\phi} \\ \omega_* e^{i\phi} & -\xi \end{pmatrix} = \frac{\hbar}{2} [\xi \sigma_z + \omega_* (\cos \phi \sigma_x + \sin \phi \sigma_y)] \quad (4.1.38)$$

where $\xi = 0$ when the resonance condition is met.

The time evolution operator Once the Hamiltonian is made time independent, the time evolution operator can be trivially obtained. Let the **generalized Rabi frequency** be

$$\Omega = \sqrt{\omega_*^2 + \xi^2} \quad (4.1.39)$$

The time evolution operator is

$$\tilde{U}(t) = \begin{pmatrix} \cos \frac{\Omega t}{2} - i \sin \frac{\Omega t}{2} \cdot \frac{\xi}{\Omega} & -i \sin \frac{\Omega t}{2} \cdot \frac{\omega_*}{\Omega} e^{-i\phi} \\ -i \sin \frac{\Omega t}{2} \cdot \frac{\omega_*}{\Omega} e^{i\phi} & \cos \frac{\Omega t}{2} + i \sin \frac{\Omega t}{2} \cdot \frac{\xi}{\Omega} \end{pmatrix} \quad (4.1.40)$$

When the resonance condition is fulfilled and so $\Omega \equiv \omega_*$, the operator

becomes

$$\tilde{U}(t) = \begin{pmatrix} \cos \frac{\omega_* t}{2} & -i \sin \frac{\omega_* t}{2} \cdot e^{-i\phi} \\ -i \sin \frac{\omega_* t}{2} \cdot e^{i\phi} & \cos \frac{\omega_* t}{2} \end{pmatrix} = \mathbf{R}_z(\phi) \mathbf{R}_x(\omega_* t) \mathbf{R}_z(-\phi) \quad (4.1.41)$$

Proof. The Hamiltonian of Equation 4.1.33, can be rewritten as

$$\tilde{\mathcal{H}} = \Omega \left(\frac{\xi}{\Omega} \mathbf{I}_z + \frac{\omega_* \cos(\phi)}{\Omega} \mathbf{I}_x + \frac{\omega_* \sin(\phi)}{\Omega} \mathbf{I}_y \right)$$

which allows the definition of the *unit* vector

$$\hat{\mathbf{n}} = \left(\frac{\xi}{\Omega} \hat{\mathbf{z}} + \frac{\omega_* \cos(\phi)}{\Omega} \hat{\mathbf{x}} + \frac{\omega_* \sin(\phi)}{\Omega} \hat{\mathbf{y}} \right)$$

Then, the Hamiltonian can be rewritten as

$$\tilde{\mathcal{H}} = \Omega \hat{\mathbf{n}} \mathbf{I} = \Omega (n_x \mathbf{I}_x + n_y \mathbf{I}_y + n_z \mathbf{I}_z)$$

Next, the time evolution operator is

$$\tilde{U}(t) = \exp\left(-\frac{i\tilde{\mathcal{H}}}{\hbar}t\right) = \exp\left(-\frac{i\Omega\hat{\mathbf{n}}\mathbf{I}}{\hbar}t\right) = \exp\left(-\frac{i\Omega\hat{\mathbf{n}}\boldsymbol{\sigma}}{2}t\right)$$

According to corollary 1.1.5.1, the previous exponential function can be rewritten as

$$\begin{aligned} \tilde{U}(t) &= \exp\left(-\frac{i\Omega\hat{\mathbf{n}}\boldsymbol{\sigma}}{2}t\right) = \cos \frac{\Omega t}{2} \mathbf{I} - i\hat{\mathbf{n}}\boldsymbol{\sigma} \sin \frac{\Omega t}{2} \\ &= \begin{pmatrix} \cos \frac{\Omega t}{2} & 0 \\ 0 & \cos \frac{\Omega t}{2} \end{pmatrix} - \sin \frac{\Omega t}{2} \cdot \left[\begin{pmatrix} \frac{i\xi}{\Omega} & 0 \\ 0 & -\frac{i\xi}{\Omega} \end{pmatrix} \right. \\ &\quad \left. + \begin{pmatrix} 0 & \frac{i\omega_* \cos \phi}{\Omega} \\ \frac{i\omega_* \cos \phi}{\Omega} & 0 \end{pmatrix} + \begin{pmatrix} 0 & \frac{\omega_* \sin \phi}{\Omega} \\ -\frac{\omega_* \sin \phi}{\Omega} & 0 \end{pmatrix} \right] \\ &= \begin{pmatrix} \cos \frac{\Omega t}{2} - i \sin \frac{\Omega t}{2} \cdot \frac{\xi}{\Omega} & -i \sin \frac{\Omega t}{2} \cdot \frac{\omega_*}{\Omega} [\cos \phi - i \sin \phi] \\ -i \sin \frac{\Omega t}{2} \cdot \frac{\omega_*}{\Omega} [\cos \phi + i \sin \phi] & \cos \frac{\Omega t}{2} + i \sin \frac{\Omega t}{2} \cdot \frac{\xi}{\Omega} \end{pmatrix} \\ &= \begin{pmatrix} \cos \frac{\Omega t}{2} - i \sin \frac{\Omega t}{2} \cdot \frac{\xi}{\Omega} & -i \sin \frac{\Omega t}{2} \cdot \frac{\omega_*}{\Omega} e^{-i\phi} \\ -i \sin \frac{\Omega t}{2} \cdot \frac{\omega_*}{\Omega} e^{i\phi} & \cos \frac{\Omega t}{2} + i \sin \frac{\Omega t}{2} \cdot \frac{\xi}{\Omega} \end{pmatrix} \end{aligned}$$

□

It is satisfying to see that the unitary operator $\tilde{U}(t) = \mathbf{R}_z(\phi)\mathbf{R}_x(\omega_*t)\mathbf{R}_z(-\phi)$ prescribes the same precession as the classical model: a positive anticlockwise precession of an angle ω_*t about an axis which describes a positive ϕ angle with \hat{x}' .

The approach to change the probability of the measurement outcome, that is, to “rotate” the spin vector about the xy -plane, is to apply a resonant field, with a proper phase ϕ and such that

$$\omega_*\tau = \theta \quad (4.1.42)$$

where θ is the desired rotation angle, τ the pulse width and ω_* the pulse amplitude, as one can see in Figure 4.6.

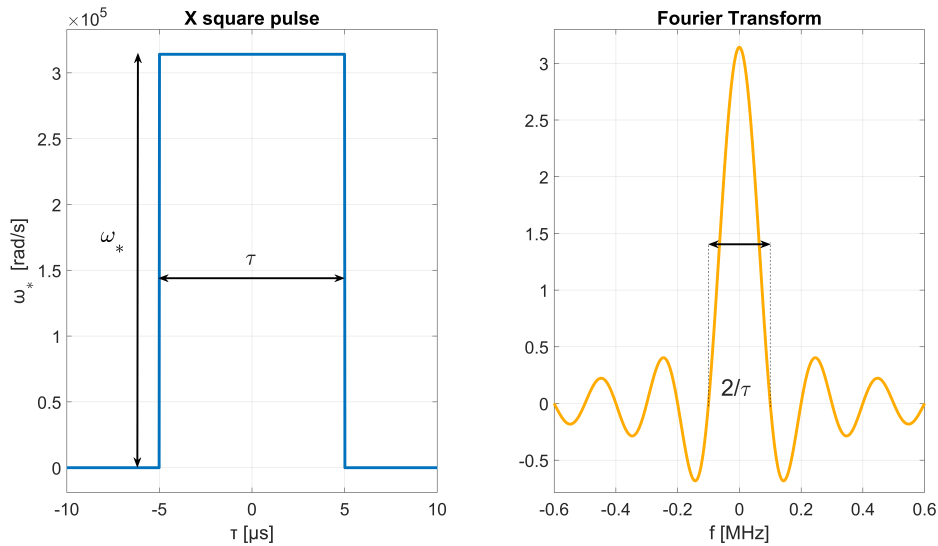


Figure 4.6: A π -pulse (or X-pulse) assuming $\tau = 10 \mu\text{s}$ on a ^{13}C nucleus spin and its Fourier transform. Note that the carrier is not represented for the sake of simplicity.

The Rabi oscillations It is interesting to study the behavior of the probabilities of the two possible outcomes when an alternating field is applied. Assume that the resonance condition is met and that the state of the system at time $t = 0$ is described by the following wavefunction in the rotating frame

$$|\tilde{\psi}(0)\rangle = \begin{pmatrix} c_0 \\ c_1 \end{pmatrix} \quad (4.1.43)$$

The state at time t is obtained applying the time operator to the state vector

$$\begin{aligned} |\tilde{\psi}(t)\rangle &= \begin{pmatrix} \cos \frac{\omega_* t}{2} & -i \sin \frac{\omega_* t}{2} \cdot e^{-i\phi} \\ -i \sin \frac{\omega_* t}{2} \cdot e^{i\phi} & \cos \frac{\omega_* t}{2} \end{pmatrix} \begin{pmatrix} c_0 \\ c_1 \end{pmatrix} \\ &= \begin{pmatrix} c_0 \cdot \cos \frac{\omega_* t}{2} - i c_1 \cdot \sin \frac{\omega_* t}{2} \cdot e^{-i\phi} \\ -i c_0 \cdot \sin \frac{\omega_* t}{2} \cdot e^{i\phi} + c_1 \cdot \cos \frac{\omega_* t}{2} \end{pmatrix} \end{aligned} \quad (4.1.44)$$

At resonance, as reported in Figure 4.7, the probabilities with which the system

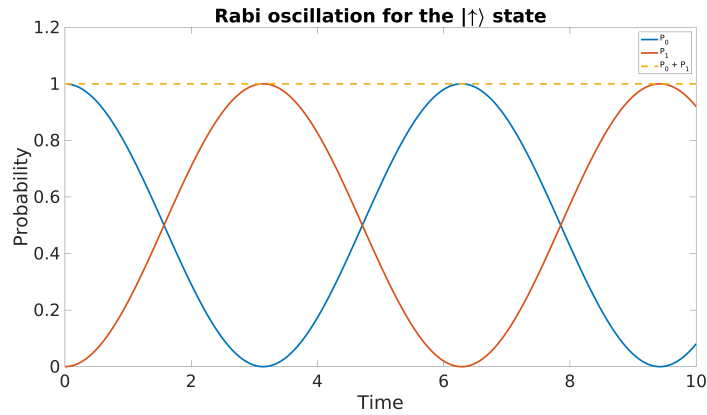


Figure 4.7: The Rabi oscillations for the $|\uparrow\rangle$ state.

is found in the ground or in the excited eigenstate of \mathcal{H}_0 oscillate at the **Rabi frequency** $\Omega = \omega_*$:

$$\begin{aligned} P_0 &= \left(c_0 \cos \frac{\omega_* t}{2} \right)^2 + \left(c_1 \sin \frac{\omega_* t}{2} \right)^2 \\ P_1 &= \left(c_0 \sin \frac{\omega_* t}{2} \right)^2 + \left(c_1 \cos \frac{\omega_* t}{2} \right)^2 \end{aligned} \quad (4.1.45)$$

Applying an alternating field for a specific amount of time allows the complete inversion of the probability of the outcome. There is one point which has to be remarked. When saying that the energy difference between the two Zeeman eigenstates is $\Delta E = \hbar|\gamma_n|B_0$, one could be brought to think that applying a resonant field, all spins will effectuate a transition to the higher energy state. This reasoning is clearly fallacious. First of all, the spins do not exist in one or the other state but in a linear superposition of both. Second, as clear from equations 4.1.44, the probability amplitudes are complex numbers: the coupling with the external radio frequency field generates complex oscillating coefficients and, thus, a sinusoidal behaviour of the probabilities. This is pictorially interpreted as the precession of the spin vector about the applied field.

4.1.2 The off-resonance field: the Bloch-Siegert effect

What does it happen when an off-resonance field is applied to a spin? In section 4.1.1.1, it is pointed out that the effect is almost negligible if the field is significantly off-resonance. The aim, now, is to make things more quantitative, following the quantum approach. In the proof of Equation 4.1.40, the unit vector $\hat{\mathbf{n}}$ is defined as

$$\hat{\mathbf{n}} = \left(\frac{\xi}{\Omega} \hat{\mathbf{z}} + \frac{\omega_* \cos(\phi)}{\Omega} \hat{\mathbf{x}} + \frac{\omega_* \sin(\phi)}{\Omega} \hat{\mathbf{y}} \right) \quad (4.1.46)$$

and the Hamiltonian is expressed as

$$\tilde{\mathcal{H}} = \Omega \hat{\mathbf{n}} \mathbf{I} \quad (4.1.47)$$

The generalized Rabi frequency can be rewritten as

$$\Omega = \sqrt{\omega_*^2 + \xi^2} = \xi \sqrt{1 + \epsilon^2} \quad (4.1.48)$$

where

$$\epsilon = \frac{\omega_*}{\xi} \quad (4.1.49)$$

The Hamiltonian becomes

$$\tilde{\mathcal{H}} = \xi \sqrt{1 + \epsilon^2} \hat{\mathbf{n}} \mathbf{I} \quad (4.1.50)$$

and the unit vector

$$\hat{\mathbf{n}} = \frac{1}{\sqrt{1 + \epsilon^2}} (\hat{\mathbf{z}} + \epsilon \cos(\phi) \hat{\mathbf{x}} + \epsilon \sin(\phi) \hat{\mathbf{y}}) \quad (4.1.51)$$

The time development operator is

$$\tilde{\mathbf{U}}(t) = \exp \left(-i \frac{\xi \sqrt{1 + \epsilon^2} \hat{\mathbf{n}} \boldsymbol{\sigma}}{2} t \right) \quad (4.1.52)$$

If the detuning ξ is significantly larger than ω_* , then $|\epsilon| \ll 1$ and

$$\hat{\mathbf{n}} \sim \hat{\mathbf{z}} \implies \tilde{\mathbf{U}}(t) \sim \exp \left(-i \frac{\xi \sqrt{1 + \epsilon^2} \boldsymbol{\sigma}_z}{2} t \right) \quad (4.1.53)$$

The rotation axis $\hat{\mathbf{n}}$ is just slightly tilted from the $\hat{\mathbf{z}}$. Therefore, the probability of finding the system in one or the other state is almost unaffected. However, the effect on the phase cannot be neglected when the long-term behaviour of the spin is taken into consideration.

When no alternating field is applied, the spin precesses according to

$$\tilde{U}(t) = \exp\left(-i\frac{\xi\sigma_z}{2}t\right) \quad (4.1.54)$$

given that the rotating field is characterized by the frequency ω . Comparing Equation 4.1.54 with Equation 4.1.53, it is clear that the effect of the off-resonance field is to cause a shift of the precession frequency

$$\xi(1 - \sqrt{1 + \epsilon^2}) \quad (4.1.55)$$

Even if this quantity is small, the phase shift

$$|t \cdot \xi(1 - \sqrt{1 + \epsilon^2})| \quad (4.1.56)$$

is not necessarily small because t can be large. This effect is known as **Bloch-Siegert effect** [45].

Example 4.1.1. Consider, as an example, to apply a radio frequency field such that

$$\theta = \omega_*\tau = \pi$$

with a pulse width

$$\tau = 2 \cdot \frac{2\pi}{\xi}$$

The amplitude is therefore

$$\omega_* = \frac{\xi}{4}$$

It follows that

$$\epsilon = \frac{\omega_*}{\xi} = 0.25$$

which is *not* much smaller than 1. As a consequence, $\hat{\mathbf{n}}$ is close but not coincident with $\hat{\mathbf{z}}$. Since the spin precesses about $\hat{\mathbf{n}}$, there is not only a shift in the reference phase

$$\left| \frac{4\pi}{\xi} \xi \left(1 - \sqrt{1 + \frac{1}{4}} \right) \right| \sim 22.16^\circ$$

but also a variation of probability, as clear from Figure 4.8. △

It is relevant that, once ξ is fixed⁴, increasing the pulse width τ results in a

⁴In actual implementations, the differences between the Larmor frequencies of separate nuclei depend on the specific molecule adopted.

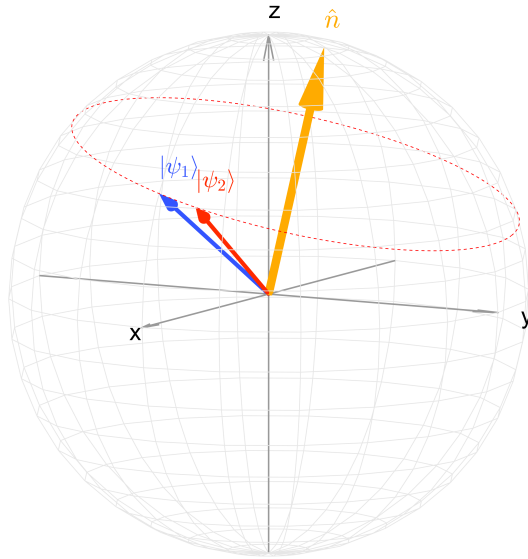


Figure 4.8: The Bloch-Siegert effect. Since $\xi > 0$, $|\psi_1\rangle$ precesses about \hat{n} according to the positive sense of rotation and evolves in $|\psi_2\rangle$. Note that the spin is observed from a reference frame which rotates at frequency $\omega = \omega_r \neq \omega_0$.

reduction of ω_* , which, in turns, lowers the value of ϵ , resulting in a minimized Bloch-Siegert effect. However, a very long τ , a kind of pulse known as **soft pulse** in the scientific literature, is not always a convenient choice, because the effect of spin-spin couplings (cf. chapter 5) may become not negligible. For clarity, the Bloch-Siegert effect is analysed in Figure 4.9 for the case presented in example 4.1.1, letting τ ranging from 0 to $8\pi/\xi$.

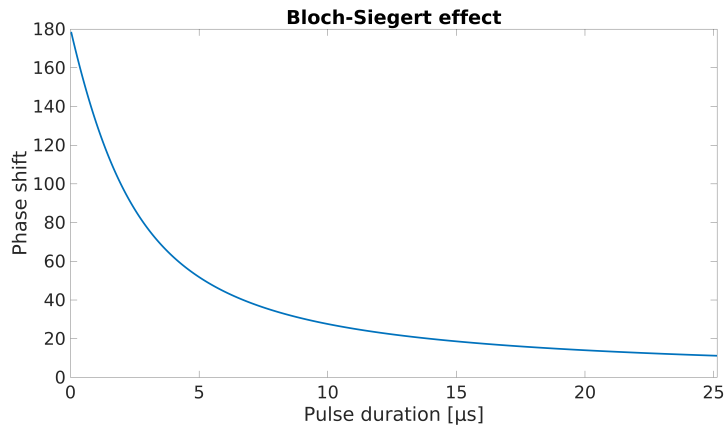


Figure 4.9: The Bloch-Siegert effect: the phase shift for the case presented in example 4.1.1, assuming $\tau \in [0, 8\pi/\xi]$. It is assumed that $\xi = 1 \text{ Mrad s}^{-1}$.

4.2 Spin ensemble

The description presented in the previous section, which adopts a vector model to detail the changes in the nuclear magnetization caused by the application of static and oscillating magnetic fields, is oversimplified. Liquid-state NMR is most suitably described by density operators, rather than state vectors.

Consider a sample of magnetically equivalent spin- $\frac{1}{2}$ subsystems, which, approximately, do not influence each other. Such a collection of a large number ($\sim 10^{22}$) of independent, identical subsystems is known as **ensemble**. At any instant of time, each spin has a different orientation. A very few of them are close to state $|\uparrow\rangle$ or to state $|\downarrow\rangle$, while the largest number is in a superposition of the two eigenstates of the central Hamiltonian. The overall nuclear magnetization results from the sum of the small contributions from the single spins. It is rather inconvenient to treat each spin individually and then add the results together. This kind of system is naturally described by the **density operator**, which is an elegant approach to represent the whole ensemble, without referring to the single spin states. Let

$$\rho = \sum_i p_i |\psi_i\rangle\langle\psi_i| = \begin{pmatrix} \overline{c_0 c_0^*} & \overline{c_0 c_1^*} \\ \overline{c_1 c_0^*} & \overline{c_1 c_1^*} \end{pmatrix} = \begin{pmatrix} \rho_\alpha & \rho_+ \\ \rho_- & \rho_\beta \end{pmatrix} \quad (4.2.1)$$

be the matrix representation of the density operator, where the overline denotes an average value. Some nomenclature is now useful: the *diagonal* elements are called **populations** while the *off-diagonal* elements are known as **coherences**.

Relationships and properties Let

$$|\psi\rangle = \begin{pmatrix} c_0 \\ c_1 \end{pmatrix} \quad (4.2.2)$$

be a generic state of a certain spin. The normalization condition requires that

$$c_0 c_0^* + c_1 c_1^* = 1 \quad (4.2.3)$$

Since this applies to all spins in the ensemble, it must be true that

$$\overline{c_0 c_0^*} + \overline{c_1 c_1^*} = 1 \implies \rho_\alpha + \rho_\beta = 1 \quad (4.2.4)$$

coherently with property 1.2.4 which requires every density matrix to have unitary trace. Moreover, the populations are by definition real and positive.

As far as the coherences are concerned, it follows from the construction of the density matrix that

$$\overline{c_0 c_1^*} = \{\overline{c_1 c_0^*}\}^* \implies \rho_+ = \rho_-^* \quad (4.2.5)$$

Thus, coherences come in conjugate pairs.

Physical interpretation The **populations** represent the *probability* of finding a member of the ensemble in one of the basis states when performing a measurement. It should be remarked the similarity with the case in which the state of a system is described by a simple state vector written as the linear superposition of the static Hamiltonian eigenstates

$$|\psi\rangle = c_0 |\uparrow\rangle + c_1 |\downarrow\rangle \quad (4.2.6)$$

and the probability of finding the spin in one or the other state is $|c_0|^2$ and $|c_1|^2$. The populations, consequently, do not indicate the actual fraction of spins which is in a peculiar state, since very few spins are effectively in one of the eigenstates, the vast majority being in a linear superposition of the latter.

Since the trace of a density matrix is unitary, only the difference in populations has a physical meaning:

- If $\rho_\alpha > \rho_\beta$ there is a net polarization of spins **along** the external field.
- If $\rho_\alpha < \rho_\beta$ there is a net polarization of spins **against** the external field.
- If $\rho_\alpha = \rho_\beta$ there is **no** net polarization in the direction of the field.

The **coherences** are related to the presence of a *transverse spin magnetization*. The off-diagonal terms can be generated only by spins which are in superposition states and not in some eigenstate. Nevertheless, this is not enough. Coherences do exist only if the transverse polarizations are also partially aligned. Conversely, if the polarization vectors of the subsystems are uniformly distributed in the transverse plane, no coherence can arise.

Eventually, it is useful to note that the phase of ρ_- denotes the angle of the transverse magnetization with respect to $+\hat{x}$. On the other hand, ρ_+ , being the complex conjugate of ρ_- , does not carry any useful additional information.

4.2.1 Thermal equilibrium

It is possible to prove [17, 33], resorting on quantum statistical mechanics, that in thermal equilibrium at temperature T :

- The **coherences** are identically zero.
- The **populations** follow the *Boltzmann distribution* and in the basis of the Hamiltonian eigenstates are expressed as

$$(\rho_0)_{mm} = \frac{e^{-\frac{E_m}{k_B T}}}{\sum_j e^{-\frac{E_j}{k_B T}}} \quad (4.2.7)$$

where E_j for $-I \leq j \leq I$ are the eigenvalues of the Hamiltonian and the denominator is known as the **partition function**

$$Z(T) = \sum_j e^{-\frac{E_j}{k_B T}} \quad (4.2.8)$$

The thermal equilibrium density matrix is therefore

$$\rho_0 = \frac{e^{-\frac{\mathcal{H}}{k_B T}}}{\sum_j e^{-\frac{E_j}{k_B T}}} = \frac{e^{-\frac{\mathcal{H}}{k_B T}}}{\text{tr}\left(e^{-\frac{\mathcal{H}}{k_B T}}\right)} \quad (4.2.9)$$

As thoroughly discussed, the laboratory frame Zeeman Hamiltonian for an ensemble of identical non interacting nuclei with spin quantum number I is

$$\mathcal{H} = -\omega_0 \mathbf{I}_z$$

When the high temperature limit holds true, that is for temperatures above 1 K, replacing the Hamiltonian, the density matrix acquires a simpler expression:

Let

$$\Delta \triangleq \frac{\hbar\omega_0}{k_B T} \quad (4.2.10)$$

then

$$\rho_0 = \left(\frac{1}{2I+1}\right) \mathbb{I} + \left(\frac{\Delta}{2I+1}\right) \frac{\sigma_z}{2} \quad (4.2.11)$$

Proof. Consider the numerator of Equation 4.2.7 and replace the expression of the Zeeman Hamiltonian. One gets

$$\exp\left(\frac{m_I \hbar \omega_0}{k_B T}\right), \quad m_I = -\frac{1}{2}, +\frac{1}{2}$$

As computed in section §3.2.2.3, the energy difference between the eigenvalues is small

$$\hbar \omega_0 \sim (1 \times 10^{-7} \text{ to } 1 \times 10^{-6}) \text{ eV}$$

while the thermal energy at room temperature (25 °C) is roughly

$$k_B T \sim 2.57 \times 10^{-2} \text{ eV} \quad (4.2.12)$$

As a consequence

$$\Delta = \frac{\hbar \omega_0}{k_B T} \sim (1 \times 10^{-5} \text{ to } 1 \times 10^{-4})$$

which means that the exponential function can be approximated with its Maclaurin series truncated to the first order

$$\exp\left(\frac{m_I \hbar \omega_0}{k_B T}\right) \sim 1 + \frac{m_I \hbar \omega_0}{k_B T}$$

Similarly, the denominator of Equation 4.2.7 is approximated as

$$\sum_{m_I=-I}^I e^{\frac{m_I \hbar \omega_0}{k_B T}} \sim 2I + 1$$

It follows that

$$(\rho_0)_{mm} \sim \frac{1 + \frac{m_I \hbar \omega_0}{k_B T}}{2I + 1}$$

and so the overall density matrix is

$$\rho_0 = \left(\frac{1}{2I + 1}\right) \mathbb{I} + \left(\frac{\Delta}{2I + 1}\right) \frac{\sigma_z}{2} \quad (4.2.13)$$

□

One should note that the first term on the right hand side of Equation 4.2.11 is simply the identity matrix. As well known, the latter commutes with all operators and so it does not evolve in time. This term describes a uniform background which is not acted upon by the applied magnetic field. On the other hand, the second term, which is a traceless matrix customarily referred to as the **deviation matrix**

$\Delta\rho$, is directly related to the operator \mathbf{I}_z .

$$\Delta\rho_0 = \frac{\Delta}{2I + 1} \frac{\sigma_z}{2} \quad (4.2.14)$$

It is this term which does interact with the applied field and does evolve in time.

The explicit matrix expression for the spin- $\frac{1}{2}$ case is

$$\rho_0 = \frac{1}{2} \begin{pmatrix} 1 & 0 \\ 0 & 1 \end{pmatrix} + \frac{\Delta}{4} \begin{pmatrix} 1 & 0 \\ 0 & -1 \end{pmatrix} \quad (4.2.15)$$

It is interesting to highlight that the Boltzmann distribution favors the lowest energy state, whose population is expected to be the highest one. However, since $\Delta \lll 1$, the low-energy state is just *slightly* more populated than the high-energy state. The population difference, at customary temperatures and fields, is only about one part in 10^5 ! The physical interpretation is that, at thermal equilibrium, there is only a very slight polarization of the spins along the direction of the applied field \mathbf{B}_0 , as one can appreciate in Figure 4.10.

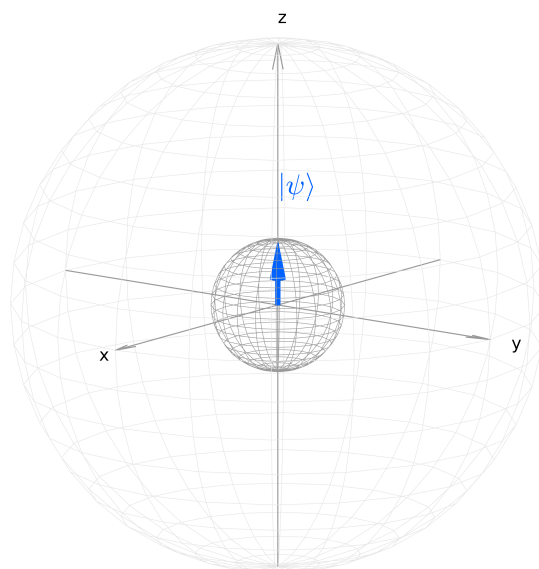


Figure 4.10: The thermal equilibrium density matrix, obtained for unrealistic $\Delta = 0.5$ for the sake of representation. As one can see, even for a Δ three orders of magnitude larger than the common one, the magnetization (represented by the Bloch vector) along the direction of the applied static field is weak.

4.2.2 The magnetization vector

As extensively discussed, the state of a single spin- $\frac{1}{2}$ is classically described by an arrow indicating the “orientation” of the spin angular momentum. The same approach is feasible for an ensemble of non-interacting spins. The **magnetization vector** \mathbf{M} is introduced as the vector indicating the net magnitude and direction of the ensemble magnetization. Equation 3.1.23, which describes the precession of a magnetic moment, has been derived for a single spin. Anyhow, considering a group of non-interacting spins, where the magnetic moment of the k -th spin is \mathbf{m}_k , the total magnetic moment is

$$\mathbf{m} = \sum_k \mathbf{m}_k \quad (4.2.16)$$

It is trivial to show [42] that 3.1.23 holds true also for the total magnetization

$$\frac{d\mathbf{M}}{dt} = \gamma \mathbf{M} \times \mathbf{B} \quad (4.2.17)$$

The point, now, is to find a meaningful way to provide a pictorial representation of the magnetization vector related to the density matrix. An obvious possibility is to use the Bloch vector as introduced in section §2.1.5.2. However, as seen in Figure 4.10, the Bloch vector does not have a convenient normalization. As a matter of fact, letting $\Delta \sim 10^{-5}$, the arrow would simply be not visible. As a consequence, the magnetization vector is conventionally defined [33] such that the thermal equilibrium magnetization vector is equal to a unit vector along the \hat{z} axis.

The magnetization vector is defined as

$$\mathbf{M} = M_x \hat{x} + M_y \hat{y} + M_z \hat{z} \quad (4.2.18)$$

where

$$\begin{aligned} M_x &= \frac{4 \operatorname{Re}\{\rho_{-}\}}{\Delta} \\ M_y &= \frac{4 \operatorname{Im}\{\rho_{-}\}}{\Delta} \\ M_z &= \frac{2(\rho_{\alpha} - \rho_{\beta})}{\Delta} \end{aligned} \quad (4.2.19)$$

Proof. Since the \hat{z} component of the Bloch vector at thermal equilibrium is

$$n_z = \rho_\alpha - \rho_\beta = \frac{\Delta}{2}$$

the \hat{z} component of the magnetization vector can be defined as

$$M_z = n_z \cdot \frac{2}{\Delta} = 1$$

In section §2.1.5.2 it is shown that a generic density matrix matrix can always be expressed as

$$\rho = \frac{1}{2} (\mathbb{I} + n_x \sigma_x + n_y \sigma_y + n_z \sigma_z)$$

which is rewritten as

$$\begin{aligned} \rho &= \frac{1}{2} \mathbb{I} + \frac{1}{2} \cdot \frac{2}{\Delta} \cdot \frac{\Delta}{2} (n_x \sigma_x + n_y \sigma_y + n_z \sigma_z) \\ &= \frac{1}{2} \mathbb{I} + \frac{\Delta}{4} \left(\frac{2}{\Delta} \cdot n_x \sigma_x + \frac{2}{\Delta} \cdot n_y \sigma_y + \frac{2}{\Delta} \cdot n_z \sigma_z \right) \\ &= \frac{1}{2} \mathbb{I} + \frac{\Delta}{4} (M_x \sigma_x + M_y \sigma_y + M_z \sigma_z) \end{aligned}$$

where

$$M_x = \frac{2 \cdot n_x}{\Delta} = \frac{4 \operatorname{Re}\{\rho_-\}}{\Delta}$$

$$M_y = \frac{2 \cdot n_y}{\Delta} = \frac{4 \operatorname{Im}\{\rho_-\}}{\Delta}$$

$$M_z = \frac{2 \cdot n_z}{\Delta} = \frac{2(\rho_\alpha - \rho_\beta)}{\Delta}$$

□

4.2.3 Free precession

In this section the spin ensemble free precession is analyzed in the idealized case in which the relaxation phenomena are neglected.

It is well known that a single spin, under the influence of a static field \mathbf{B}_0 , performs a precession about the $\hat{\mathbf{z}}$ axis at the Larmor frequency. In the laboratory frame

$$|\psi(t)\rangle = \mathbf{R}_z(-\omega_0 t) |\psi_0\rangle$$

The time evolution of a density operator, according to theorem 1.2.4, is ruled by the Liouville - von Neumann equation. If the Hamiltonian of the system is time independent, the Liouville - von Neumann equation can be solved introducing the familiar time evolution operator

$$\mathbf{U}(t) = \exp\left(-\frac{\mathcal{H}t}{\hbar}\right)$$

and the density operator evolves as

$$\boldsymbol{\rho}(t) = \mathbf{U}(t)\boldsymbol{\rho}(0)\mathbf{U}(t)^\dagger$$

Repeating the arguments proposed for the single spin, one gets

$$\boldsymbol{\rho}(t) = \mathbf{R}_z(-\omega_0 t)\boldsymbol{\rho}(0)\mathbf{R}_z(\omega_0 t) = \begin{pmatrix} \rho_\alpha(0) & e^{+i\omega_0 t}\rho_+(0) \\ e^{-i\omega_0 t}\rho_-(0) & \rho_\beta(0) \end{pmatrix} \quad (4.2.20)$$

The corresponding equations for the components of the magnetization vector are

$$\begin{aligned} M_x(t) &= M_x(0) \cos(\omega_0 t) + M_y(0) \sin(\omega_0 t) \\ M_y(t) &= M_y(0) \cos(\omega_0 t) - M_x(0) \sin(\omega_0 t) \\ M_z(t) &= M_z(0) \end{aligned} \quad (4.2.21)$$

Proof. The density matrix at time t is related to the density matrix at time $t = 0$ by

$$\boldsymbol{\rho}(t) = \mathbf{R}_z(-\omega_0 t)\boldsymbol{\rho}(0)\mathbf{R}_z(\omega_0 t) = \begin{pmatrix} \rho_\alpha(0) & e^{+i\omega_0 t}\rho_+(0) \\ e^{-i\omega_0 t}\rho_-(0) & \rho_\beta(0) \end{pmatrix}$$

The \hat{x} and \hat{y} components of the magnetization vector at time t are

$$M_x(t) = \frac{4 \operatorname{Re}\{\rho_-(t)\}}{\Delta} \quad M_y(t) = \frac{4 \operatorname{Im}\{\rho_-(t)\}}{\Delta}$$

Then

$$\begin{aligned} \rho_-(t) &= e^{-i\omega_0 t} \rho_-(0) = [\operatorname{Re}\{\rho_-(0)\} + i \operatorname{Im}\{\rho_-(0)\}] e^{-i\omega_0 t} \\ &= [\operatorname{Re}\{\rho_-(0)\} + i \operatorname{Im}\{\rho_-(0)\}] \cdot [\cos(\omega_0 t) - i \sin(\omega_0 t)] \\ &= \frac{\Delta}{4} \{ [M_x(0) \cos(\omega_0 t) + M_y(0) \sin(\omega_0 t)] + i [M_y(0) \cos(\omega_0 t) - M_x(0) \sin(\omega_0 t)] \} \end{aligned}$$

□

The magnetization vector performs a clockwise precession about the applied static field at the Larmor frequency, exactly as the magnetic moment of a single spin, pictured in Figure 4.2. Moreover, one should note that the \hat{z} component is constant, since there is no variation in the populations corresponding to the two eigenstates.

4.2.4 The radio-frequency field

As seen in section §4.1.1 for the case of a single spin, the customary approach to, classically speaking, rotate the spin vector is to apply a radio-frequency field (Equation 4.1.12). The effect of the latter on the ensemble overall magnetization is better understood in a rotating coordinate system, as the one introduced in Equation 4.1.18. The time evolution of the magnetization in the rotating frame can be described by the same classical model introduced in section §4.1.1.1, formally replacing the magnetic moment \mathbf{m} with the total magnetization \mathbf{M} . One gets that the latter turns out to precess clockwise about the direction of the effective magnetic field \mathbf{B}_{eff} in the rotating frame, as represented in Figure 4.5 for the single spin case.

On the other hand, the quantum mechanical interpretation requires some extra details. The evolution of the density operator $\rho(t)$ is ruled by the Liouville - von Neumann equation, which, in the rotating frame [46], has the following expression

$$\frac{d\tilde{\rho}}{dt} = -\frac{i}{\hbar} [\tilde{\mathcal{H}}, \tilde{\rho}] \quad (4.2.22)$$

where the rotating frame density matrix is

$$\tilde{\rho} = \mathbf{U}_R \rho \mathbf{U}_R^\dagger = \begin{pmatrix} \rho_\alpha & e^{-i\omega t} \rho_+ \\ e^{+i\omega t} \rho_- & \rho_\beta \end{pmatrix} = \begin{pmatrix} \tilde{\rho}_\alpha & \tilde{\rho}_+ \\ \tilde{\rho}_- & \tilde{\rho}_\beta \end{pmatrix} \quad (4.2.23)$$

and the rotating frame Hamiltonian is

$$\tilde{\mathcal{H}} = \mathbf{U}_R \mathcal{H} \mathbf{U}_R^\dagger - i\hbar \mathbf{U}_R \frac{d\mathbf{U}_R^\dagger}{dt} \quad (4.2.24)$$

Proof. The time derivative of the density operator in the rotating frame is

$$\frac{d\tilde{\rho}}{dt} = \frac{d\mathbf{U}_R \rho \mathbf{U}_R^\dagger}{dt} = \frac{d\mathbf{U}_R}{dt} \rho \mathbf{U}_R^\dagger + \mathbf{U}_R \frac{d\rho}{dt} \mathbf{U}_R^\dagger + \mathbf{U}_R \rho \frac{d\mathbf{U}_R^\dagger}{dt}$$

Replacing the Liouville - von Neumann equation in the previous expression one

gets

$$\begin{aligned}
 \frac{d\tilde{\rho}}{dt} &= \frac{dU_r}{dt} \rho U_R^\dagger - \frac{i}{\hbar} U_R [\mathcal{H}, \rho] U_R^\dagger + U_R \rho \frac{dU_R^\dagger}{dt} \\
 &= \frac{dU_r}{dt} U_R^\dagger U_R \rho U_R^\dagger - \frac{i}{\hbar} U_R [\mathcal{H}, \rho] U_R^\dagger + U_R \rho U_R^\dagger U_R \frac{dU_R^\dagger}{dt} \\
 &= \frac{dU_r}{dt} U_R^\dagger \tilde{\rho} - \frac{i}{\hbar} U_R [\mathcal{H}, \rho] U_R^\dagger + \tilde{\rho} U_R \frac{dU_R^\dagger}{dt}
 \end{aligned}$$

The commutator, which constitutes the second term on the right hand side, can be expanded as

$$\begin{aligned}
 U_R [\mathcal{H}, \rho] U_R^\dagger &= U_R [\mathcal{H} \rho - \rho \mathcal{H}] U_R^\dagger \\
 &= U_R \mathcal{H} U_R^\dagger U_R \rho U_R^\dagger - U_R \rho U_R^\dagger U_R \mathcal{H} U_R^\dagger \\
 &= U_R \mathcal{H} U_R^\dagger \tilde{\rho} - \tilde{\rho} U_R \mathcal{H} U_R^\dagger \\
 &= [U_R \mathcal{H} U_R^\dagger, \tilde{\rho}]
 \end{aligned}$$

As shown in the proof of Equation 4.1.31

$$\frac{dU}{dt} U^\dagger = -U \frac{dU^\dagger}{dt}$$

Replacing one gets

$$\begin{aligned}
 \frac{d\tilde{\rho}}{dt} &= -\frac{i}{\hbar} [U_R \mathcal{H} U_R^\dagger \tilde{\rho} - \tilde{\rho} U_R \mathcal{H} U_R^\dagger] - U \frac{dU^\dagger}{dt} \tilde{\rho} + \tilde{\rho} U \frac{dU^\dagger}{dt} \\
 &= -\frac{i}{\hbar} \left[U_R \mathcal{H} U_R^\dagger \tilde{\rho} - \tilde{\rho} U_R \mathcal{H} U_R^\dagger - i\hbar U \frac{dU^\dagger}{dt} \tilde{\rho} + i\hbar \tilde{\rho} U \frac{dU^\dagger}{dt} \right] \\
 &= -\frac{i}{\hbar} \left[U_R \mathcal{H} U_R^\dagger - i\hbar U \frac{dU^\dagger}{dt}, \tilde{\rho} \right] \\
 &= -\frac{i}{\hbar} [\tilde{\mathcal{H}}, \tilde{\rho}]
 \end{aligned}$$

□

One should remark that Equation 4.2.24 is identical to Equation 4.1.31. As a consequence, the analysis carried out in section §4.1.1.2 still holds and the time operator of Equation 4.1.40 can be used to describe the evolution of the density matrix.

Moreover, the thermal equilibrium density matrix has exactly the same expression both in the laboratory frame and in the rotating one.

Finally, the magnetization vector in the rotating frame is

$$\widetilde{\mathbf{M}} = \widetilde{M}_x \hat{\mathbf{x}}' + \widetilde{M}_y \hat{\mathbf{y}}' + \widetilde{M}_z \hat{\mathbf{z}}' \quad (4.2.25)$$

where the components \widetilde{M}_x , \widetilde{M}_y and \widetilde{M}_z are computed as prescribed by Equation 4.2.19, using the rotating frame density matrix instead of the laboratory frame density matrix.

4.2.4.1 Excitation of coherences

Consider again the thermal equilibrium density matrix in the rotating frame

$$\widetilde{\rho}_0 = \frac{1}{2} \mathbb{I} + \frac{\Delta}{2} \frac{\sigma_z}{2} \quad (4.2.26)$$

and suppose to apply a $\frac{\pi}{2}$ -pulse about the $\hat{\mathbf{x}}$ axis. After the pulse, the density operator is

$$\widetilde{\rho}(t) = \mathbf{R}_x(\pi/2) \widetilde{\rho}_0 \mathbf{R}_x(-\pi/2) = \frac{1}{2} \mathbb{I} - \frac{\Delta}{4} \sigma_y \quad (4.2.27)$$

In terms of the matrix representation

$$\begin{pmatrix} \frac{1}{2} + \frac{\Delta}{4} & 0 \\ 0 & \frac{1}{2} - \frac{\Delta}{4} \end{pmatrix} \xrightarrow{(\pi/2)_x} \begin{pmatrix} \frac{1}{2} & -\frac{\Delta}{4i} \\ \frac{\Delta}{4i} & \frac{1}{2} \end{pmatrix} \quad (4.2.28)$$

There is an interesting physical interpretation. The pulse leads to an equalization of the populations of the two eigenstates and converts the populations into coherences. As mentioned above, the coherences are related to the transverse magnetization. Indeed, it is trivial to see that the $\frac{\pi}{2}$ -pulse rotates the magnetization vector from $\hat{\mathbf{z}}$ (thermal equilibrium) to $-\hat{\mathbf{y}}'$:

$$\widetilde{\mathbf{M}} = \hat{\mathbf{z}} \xrightarrow{(\pi/2)_x} \widetilde{\mathbf{M}} = -\hat{\mathbf{y}}' \quad (4.2.29)$$

The equalization of populations means that there is no magnetization along the $\hat{\mathbf{z}}$ axis, while the rise of coherences denotes the presence of a magnetization in the transverse plane.

4.2.4.2 Inversion of populations

Now, suppose to apply a π -pulse about the $\hat{\mathbf{x}}$ axis. After the pulse, the density operator is

$$\widetilde{\rho}(t) = \mathbf{R}_x(\pi) \widetilde{\rho}_0 \mathbf{R}_x(-\pi) = \frac{1}{2} \mathbb{I} - \frac{\Delta}{4} \sigma_z \quad (4.2.30)$$

In terms of the matrix representation

$$\begin{pmatrix} \frac{1}{2} + \frac{\Delta}{4} & 0 \\ 0 & \frac{1}{2} - \frac{\Delta}{4} \end{pmatrix} \xrightarrow{(\pi/2)_x} \begin{pmatrix} \frac{1}{2} - \frac{\Delta}{4} & 0 \\ 0 & \frac{1}{2} + \frac{\Delta}{4} \end{pmatrix} \quad (4.2.31)$$

Once more, there is an interesting physical interpretation. The pulse promotes the inversion of populations, while no coherence is generated. Note that the higher energy state turns out to be more populated than the lower energy state. As a consequence, the magnetization vector is rotated from \hat{z} (thermal equilibrium) to $-\hat{z}$:

$$\widetilde{\mathbf{M}} = \hat{z} \xrightarrow{(\pi/2)_x} \widetilde{\mathbf{M}} = -\hat{z}' \quad (4.2.32)$$

4.3 Phenomenology of relaxation and decoherence

As mentioned in section §4.2.2, the magnetization vector satisfies the equation of motion 3.1.23, whose Cartesian components, in the laboratory frame, can be expressed as

$$\begin{aligned}\frac{dM_x(t)}{dt} &= \gamma_n [M_y(t)B_z(t) - M_z(t)B_y(t)] \\ \frac{dM_y(t)}{dt} &= \gamma_n [M_z(t)B_x(t) - M_x(t)B_z(t)] \\ \frac{dM_z(t)}{dt} &= \gamma_n [M_x(t)B_y(t) - M_y(t)B_x(t)]\end{aligned}\tag{4.3.1}$$

Considering Equation 4.1.23, it is trivial to get the rotating frame equations [46]

$$\begin{aligned}\frac{d\widetilde{M}_x(t)}{dt} &= -\xi\widetilde{M}_y(t) + \omega_* \sin(\phi)\widetilde{M}_z(t) \\ \frac{d\widetilde{M}_y(t)}{dt} &= +\xi\widetilde{M}_x(t) - \omega_* \cos(\phi)\widetilde{M}_z(t) \\ \frac{d\widetilde{M}_z(t)}{dt} &= \omega_* \cos(\phi)\widetilde{M}_y(t) - \omega_* \sin(\phi)\widetilde{M}_x(t)\end{aligned}\tag{4.3.2}$$

The solution of this linear system describes the evolution of the magnetization when both the static field and the alternating field are applied to the system.

Now, suppose that only the static field is applied. Then

$$\begin{aligned}\frac{d\widetilde{M}_x(t)}{dt} &= -\xi\widetilde{M}_y(t) \\ \frac{d\widetilde{M}_y(t)}{dt} &= +\xi\widetilde{M}_x(t) \\ \frac{d\widetilde{M}_z(t)}{dt} &= 0\end{aligned}\tag{4.3.3}$$

It can be shown that the solution is

$$\begin{aligned}\widetilde{M}_x(t) &= \widetilde{M}_x(0) \cos(\xi t) - \widetilde{M}_y(0) \sin(\xi t) \\ \widetilde{M}_y(t) &= \widetilde{M}_y(0) \cos(\xi t) + \widetilde{M}_x(0) \sin(\xi t) \\ \widetilde{M}_z(t) &= \widetilde{M}_z(0)\end{aligned}\tag{4.3.4}$$

The meaning of Equation 4.3.4 is straightforward. When no alternating field is present, the magnetization continues unceasingly to precess about the \hat{z} axis

in the rotating frame, at the frequency offset, forever and ever. However, the experimental behaviour is radically different.

The application of the radio-frequency field to the spin ensemble forces the state of the spin system to depart from the thermal equilibrium. If the spins were completely isolated from the outer world and if there were no interactions between them, the non-equilibrium condition would actually last forever. Yet, after *some time* the magnetization returns to the initial \hat{z} direction, re-establishing the thermal equilibrium condition. There are two phenomena which occur simultaneously and which are responsible for the recover of the equilibrium: the transverse relaxation and the longitudinal relaxation.

In this section, the description is tackled from a phenomenological point of view, according to the well-known **Bloch model**. The latter is built ad hoc to meet the experimental results and introduces two phenomenological time constants:

- The **longitudinal** relaxation time constant T_1 which describes the fact that the populations gradually drift towards the equilibrium values.
- The **transverse** relaxation time constant T_2 which describes the fact that the coherences gradually decay to zero.

It is interesting to highlight that the quantum information carried by a qubit encoded on a nuclear spin can be thought to be related to the θ and ϕ angles describing the position of the Bloch vector in the Bloch ball. Since relaxation phenomena cause randomization of both angles, there is a consequent **loss of quantum information**. Relaxation phenomena represent one of the main characteristics which have to be carefully considered when realizing hardware for quantum processors.

4.3.1 Transverse relaxation

It is experimentally observed that the transverse components of the nuclear magnetization disappear exponentially when the radio-frequency field is switched-off. In many simple cases, this phenomenon can be described including, in the previously introduced differential equations, some additional relaxation terms. Assuming

there is no alternating field:

$$\begin{aligned}\frac{d\widetilde{M}_x(t)}{dt} &= -\xi\widetilde{M}_y(t) - \frac{\widetilde{M}_x(t)}{T_2} \\ \frac{d\widetilde{M}_y(t)}{dt} &= +\xi\widetilde{M}_x(t) - \frac{\widetilde{M}_y(t)}{T_2}\end{aligned}\quad (4.3.5)$$

The solution of this linear system of differential equations yields

$$\begin{aligned}\widetilde{M}_x(t) &= \left[\widetilde{M}_x(0) \cos(\xi t) - \widetilde{M}_y(0) \sin(\xi t) \right] e^{-\frac{t}{T_2}} \\ \widetilde{M}_y(t) &= \left[\widetilde{M}_y(0) \cos(\xi t) + \widetilde{M}_x(0) \sin(\xi t) \right] e^{-\frac{t}{T_2}}\end{aligned}\quad (4.3.6)$$

where the alternating field is turned off at time $t = 0$. In practice, the transverse components of the magnetization vector decay at the same time as they precess, as represented in Figure 4.11. They are related to the coherences, which,

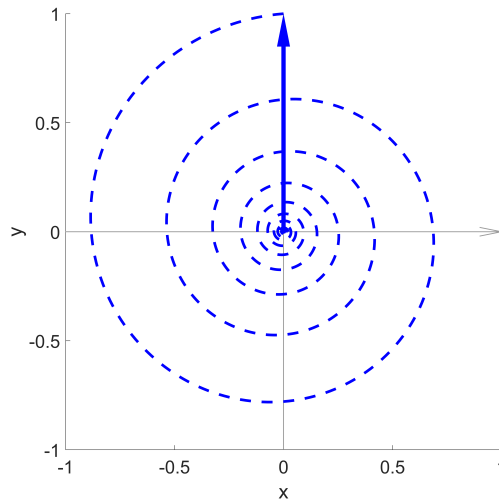


Figure 4.11: The transverse relaxation or decoherence. The magnetization in the transverse plane decays while precessing about the \hat{z} axis, as time goes on.

consequently, are subjected to an exponential decay:

$$\begin{aligned}\tilde{\rho}_-(t) &= [\tilde{\rho}_-(0)e^{i\xi t}] e^{-\frac{t}{T_2}} \\ \tilde{\rho}_+(t) &= [\tilde{\rho}_+(0)e^{-i\xi t}] e^{-\frac{t}{T_2}}\end{aligned}\quad (4.3.7)$$

There is a clear physical interpretation of this phenomenon. As mentioned above, the presence of a transverse magnetization requires spins to “have coherence”. Now, it should be clear from the previous discussion that the precession frequency of each spin is a direct consequence of the local magnetic field perceived by the

nucleus itself along the \hat{z} direction. This field depends, obviously, mainly on the external field \mathbf{B}_0 , but there are many other sources of local fields which superimpose to the external one and alter the resulting field. The consequence is that all spins feel the same *average* field. However, each particular spin feels a slightly different local field, which, as time flows, causes a gradual loss of coherence⁵. This is the reason for which this phenomenon is also known as *decoherence*. After some time, the spins distribute randomly and the transverse magnetization dies out.

4.3.2 Longitudinal relaxation

From experimental observations, it turns out that the longitudinal component of the magnetization tends to come back to the equilibrium value, when there is no longer an alternating field applied to the ensemble. Similarly to the transverse relaxation, the phenomenon can be described by the following differential equation

$$\frac{d\widetilde{M}_z(t)}{dt} = \frac{\widetilde{M}_{\text{eq}} - \widetilde{M}_z(t)}{T_1} \quad (4.3.8)$$

where M_{eq} is the thermal equilibrium magnetization. Note that with the definition given in section §4.2.2, $M_{\text{eq}} = 1$. The time-domain solution is

$$\widetilde{M}_z(t) = (\widetilde{M}_z(0) - \widetilde{M}_{\text{eq}})e^{-\frac{t}{T_1}} + \widetilde{M}_{\text{eq}} \quad (4.3.9)$$

where the radio frequency field is assumed to be switched off at time $t = 0$.

Proof. Equation 4.3.8 can be rewritten as

$$\left(\widetilde{M}_z - \widetilde{M}_{\text{eq}}\right)' = -\frac{1}{T_1} \cdot \left(\widetilde{M}_z - \widetilde{M}_{\text{eq}}\right)$$

Defining

$$\zeta(t) = \widetilde{M}_z - \widetilde{M}_{\text{eq}}$$

one gets

$$\frac{\zeta'}{\zeta} = -\frac{1}{T_1} \implies \ln(|\zeta|)' = -\frac{1}{T_1}$$

Using the Fundamental Theorem of Calculus

$$\ln(|\zeta|) = -\frac{t}{T_1} + C$$

⁵In [33], the author proposes a very useful comparison saying that the loss of spin coherence is conceptually similar to the loss of synchronization of several clocks, all started at the same time.

Taking the exponential of both members

$$\zeta(t) = \pm e^{-\frac{t}{T_1}} \cdot e^C \implies \pm \alpha e^{-\frac{t}{T_1}}$$

Replacing the definition of ζ , one finally gets

$$\widetilde{M}_z(t) = \pm \alpha e^{-\frac{t}{T_1}} + \widetilde{M}_{\text{eq}}$$

Exploiting the initial condition $M_z(t=0) = M(0)$, the solution of the associated Cauchy problem reads

$$\widetilde{M}_z(t) = (\widetilde{M}_z(0) - \widetilde{M}_{\text{eq}}) e^{-\frac{t}{T_1}} + \widetilde{M}_{\text{eq}}$$

□

The longitudinal component of magnetization is strictly related to the populations. There is a natural tendency for the system to re-establish the thermal equilibrium Boltzmann distribution making transitions preferably from the upper to the lower energy level. This process, differently with respect to the transversal relaxation, implies an exchange of energy between the system of nuclear spins and the lattice [33]. The behaviour of populations is described by the following equations

$$\begin{aligned} \widetilde{\rho}_\alpha(t) &= (\widetilde{\rho}_\alpha(0) - \widetilde{\rho}_\alpha^{\text{eq}}) e^{-\frac{t}{T_1}} + \widetilde{\rho}_\alpha^{\text{eq}} \\ \widetilde{\rho}_\beta(t) &= (\widetilde{\rho}_\beta(0) - \widetilde{\rho}_\beta^{\text{eq}}) e^{-\frac{t}{T_1}} + \widetilde{\rho}_\beta^{\text{eq}} \end{aligned} \tag{4.3.10}$$

where $\widetilde{\rho}^{\text{eq}}$ is the equilibrium population. Note that, as expected, as t approaches infinite, the two populations tend to their equilibrium values.

4.3.3 Relaxation phenomena

Longitudinal and transversal relaxations can usually be considered as two different phenomena occurring simultaneously. The two time constants are strictly related to each other: the individual spin polarizations cannot be rotated towards the \hat{z} axis, while maintaining transverse coherence. Thus, T_1 enforces an upper limit on the possible values of T_2 . It can be shown that it is always true that

$$T_2 \leq 2T_1 \tag{4.3.11}$$

Nevertheless, in most practical cases it turns out [33] that

$$T_2 \leq T_1 \quad (4.3.12)$$

Here, the equations describing the evolution of the three Cartesian components of the magnetization vector in the rotating frame are reported for the convenience of the reader

$$\begin{aligned} \widetilde{M}_x(t) &= \left[\widetilde{M}_x(0) \cos(\xi t) - \widetilde{M}_y(0) \sin(\xi t) \right] e^{-\frac{t}{T_2}} \\ \widetilde{M}_y(t) &= \left[\widetilde{M}_y(0) \cos(\xi t) + \widetilde{M}_x(0) \sin(\xi t) \right] e^{-\frac{t}{T_2}} \\ \widetilde{M}_z(t) &= (\widetilde{M}_z(0) - \widetilde{M}_{\text{eq}}) e^{-\frac{t}{T_1}} + \widetilde{M}_{\text{eq}} \end{aligned} \quad (4.3.13)$$

Example 4.3.1. Suppose that a $(\pi/2)_x$ pulse is applied to a thermal equilibrium system. The magnetization vector is rotated from the \hat{z} axis to the $-\hat{y}$ axis.

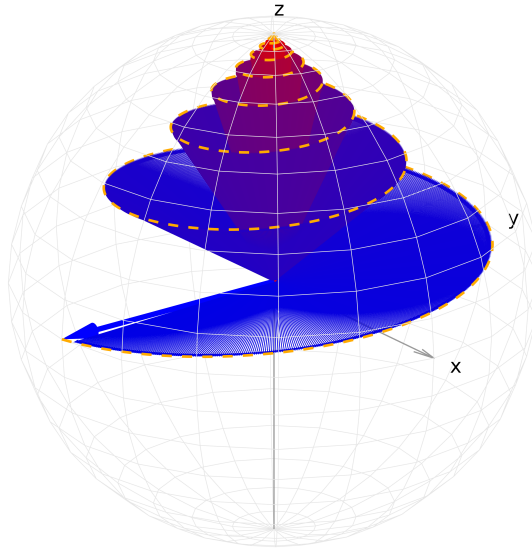


Figure 4.12: The evolution of the magnetization vector for $\xi = 2\pi \text{ rad s}^{-1}$ and $T_1 = T_2 = 2 \text{ s}$. At time $t = 0$ the magnetization vector lies along the $-\hat{y}$ axis (blue) and the alternating field is switched off, while the static field is maintained. As t approaches infinite, the magnetization performs a helicoidal motion about the \hat{z} axis. Eventually, it will be found to lie along the \hat{z} axis itself (red).

Assume that the time constants have values

$$T_1 = T_2 = 2 \text{ s}$$

and that the frequency shift is

$$\xi = 2\pi \text{ rad s}^{-1}$$

Let the radio frequency field be switched off at time $t = 0$: the evolution of the magnetization vector is obtained from Equation 4.3.13.

$$\begin{aligned}\widetilde{M}_x(t) &= \sin(\xi t)e^{-\frac{t}{T_2}} \\ \widetilde{M}_y(t) &= -\cos(\xi t)e^{-\frac{t}{T_2}} \\ \widetilde{M}_z(t) &= 1 - e^{-\frac{t}{T_1}}\end{aligned}\tag{4.3.14}$$

Since $M_{\text{eq}} = 1$ and $M_z(0) = 0$. The trajectory of the magnetization vector is pictured in Figure 4.12.



Chapter 5

Nuclear spin interactions

In the previous chapters, nuclear magnetic phenomena have been described for an ensemble on *non interacting* spins. If this were the whole story, NMR could not be used for quantum computation (how to implement a two-qubit gate?) and would have proved quite useless also for chemical applications. However, nuclear spins are well away from being isolated from each other and the surrounding environment. Indeed, nuclear spins feel several magnetic fields, due to the presence of electrons and other nuclei, which superimpose resulting in a **local field** which is, generally speaking, different in different nuclear sites. Distinct local fields mean distinct resonance frequencies, a phenomenon which allows gathering information on the internal interactions between the nucleus of interest and its neighbourhood.

The standard approach to describe the spin interactions is to write down the nuclear spin Hamiltonian, in the Zeeman eigenbasis, as the sum of \mathcal{H}_{ext} , which represents the interactions of the nucleus with the externally applied magnetic fields, and \mathcal{H}_{int} which takes into account the internal interactions of the nucleus with the surrounding environment:

$$\mathcal{H} = \mathcal{H}_{\text{ext}} + \mathcal{H}_{\text{int}} \quad (5.0.1)$$

The external Hamiltonian describes the contributions arising from the application of the static and radio-frequency fields

$$\mathcal{H}_{\text{ext}} = \mathcal{H}_0 + \mathcal{H}_r \quad (5.0.2)$$

and usually represents the main contributions to the overall Hamiltonian and the internal interactions can be dealt with according to the methodologies of the perturbation theory.

On the other hand, there are several internal interactions, whose peculiar nature depends on the specific physical system. For diamagnetic substances, it is usually reasonable [17, 33] to write

$$\mathcal{H}_{\text{int}} = \mathcal{H}_{cs} + \mathcal{H}_d + \mathcal{H}_j + \mathcal{H}_q \quad (5.0.3)$$

where \mathcal{H}_{cs} represents the chemical shift of the nucleus with the surrounding electrons, \mathcal{H}_d the direct dipolar spin-spin interaction, \mathcal{H}_j the indirect spin-spin coupling (customarily referred to as J-coupling) and \mathcal{H}_q the quadrupolar coupling between nuclei with spin quantum number $I > 1/2$ and the local electric field gradient. It has to be highlighted that the quadrupolar coupling is *not* present for spin- $\frac{1}{2}$ nuclei. Since it can be shown that it causes a reduction of the decoherence time, it is one of the main reasons for which NMR based quantum computers usually exploit only spin- $\frac{1}{2}$ nuclei. Hence, the quadrupolar coupling will not be addressed any further in the following.

While the contributions to the external Hamiltonian are thoroughly detailed in chapter 4, this chapter is dedicated to the discussion of the internal Hamiltonian, with a particular focus on chemical shift and J-coupling, which prove to be essential for the actual implementation of a quantum processor.

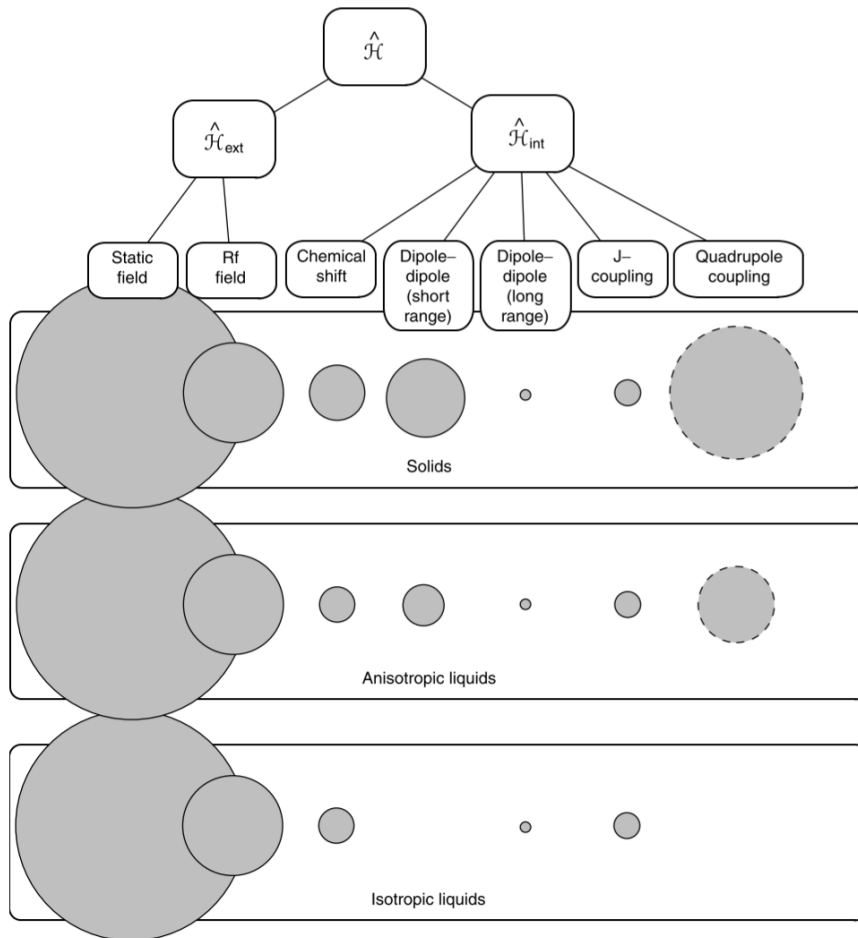


Figure 5.1: A summary of spin-interactions and their magnitudes. From [33].

5.1 Direct spin-spin coupling

A nucleus characterised by a non-zero spin is associated with a magnetic moment $\mathbf{m} = \gamma_n \mathbf{I}$. Every magnetic moment generates a magnetic field which “loops around” in the surrounding, according to the orientation of the former. This magnetic field can influence other spins and the interaction is obviously **mutual**: referring to figure, spin k interacts with the magnetic field generated by nucleus j and spin j interacts with the magnetic field generated by nucleus k . It is known

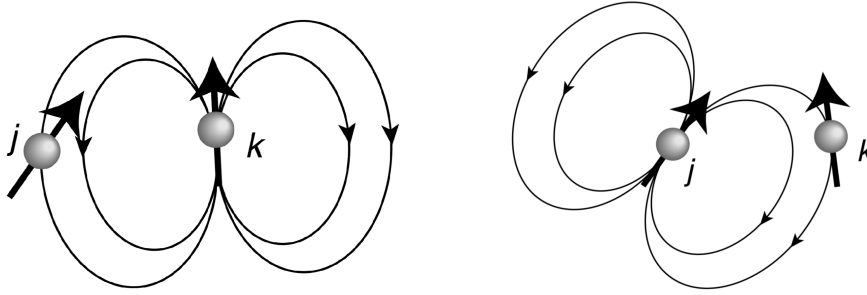


Figure 5.2: The direct spin-spin coupling: the magnetic field generated by spin k affects spin j and vice versa. Adapted from [33].

as *direct* spin-spin coupling or *dipolar* coupling, since it is not mediated by the electron cloud but takes place directly between the nuclei, because of direct field propagation, differently from the J-coupling.

Consider two nuclear magnetic moments \mathbf{m}_1 and \mathbf{m}_2 and let $\hat{\mathbf{r}} = \frac{\mathbf{r}}{r}$ be the adimensional unit vector which identifies the direction joining the two nuclei, then the Hamiltonian describing the system is [47, 42]

$$\mathcal{H}_d = -\frac{\mu_0}{4\pi} \frac{\gamma_1 \gamma_2}{r^3} \left(3\mathbf{I}_1^\dagger |\hat{\mathbf{r}}\rangle\langle\hat{\mathbf{r}}| \mathbf{I}_2 - (\mathbf{I}_1 \cdot \mathbf{I}_2) \right) \quad (5.1.1)$$

where \cdot denotes the inner product and the symbols \mathbf{I}_1 and \mathbf{I}_2 are used to identify a \mathbf{I} vector operator which acts only on spin 1 or on spin 2, that is

$$\begin{aligned} \mathbf{I}_1 &= \mathbf{I} \otimes \mathbb{I} \\ \mathbf{I}_2 &= \mathbb{I} \otimes \mathbf{I} \end{aligned} \quad (5.1.2)$$

The reader is reminded that the nuclear spin vector operator is defined according

to Equation 4.1.1 as

$$\mathbf{I} = \begin{pmatrix} \mathbf{I}_x \\ \mathbf{I}_y \\ \mathbf{I}_z \end{pmatrix}$$

Proof. From classical magnetism, the magnetic field generated by a magnetic dipole \mathbf{m}_2 is known to be

$$\mathbf{B}(\hat{\mathbf{r}}) = \frac{\mu_0}{4\pi r^3} (3(\mathbf{m}_2 \cdot \hat{\mathbf{r}})\hat{\mathbf{r}} - \mathbf{m}_2)$$

where \cdot denotes the inner product and $\hat{\mathbf{r}}$ is a unit vector:

$$\hat{\mathbf{r}} = \begin{pmatrix} r_x \\ r_y \\ r_z \end{pmatrix}$$

It is just a matter of trivial computation to realize that

$$(\mathbf{m}_2 \cdot \hat{\mathbf{r}})\hat{\mathbf{r}} = (\hat{\mathbf{r}}\hat{\mathbf{r}}^\dagger)\mathbf{m}_2$$

Consequently, the field can be rewritten as

$$\mathbf{B}(\hat{\mathbf{r}}) = \frac{\mu_0}{4\pi r^3} (3(\hat{\mathbf{r}}\hat{\mathbf{r}}^\dagger)\mathbf{m}_2 - \mathbf{m}_2)$$

or in braket notation as

$$\mathbf{B}(\hat{\mathbf{r}}) = \frac{\mu_0}{4\pi r^3} (3|\hat{\mathbf{r}}\rangle\langle\hat{\mathbf{r}}| |m_2\rangle - |m_2\rangle)$$

When a magnetic moment \mathbf{m}_1 interacts with the field originated by \mathbf{m}_2 , the resulting energy is

$$E = -\mathbf{m}_1 \cdot \mathbf{B}(\hat{\mathbf{r}}) = -\frac{\mu_0}{4\pi r^3} (3\langle m_1|\hat{\mathbf{r}}\rangle \langle\hat{\mathbf{r}}|m_2\rangle - \langle\hat{\mathbf{r}}|m_2\rangle)$$

In order to determine the system Hamiltonian, one has to replace the physical observables with the respective quantum mechanical operators:

$$\begin{aligned} |m_1\rangle &\longrightarrow \gamma_1 \mathbf{I}_1 \\ \langle m_2| &\longrightarrow \gamma_2 \mathbf{I}_2^\dagger \end{aligned}$$

The resulting equation is as in 5.1.1. □

One should note that the direct coupling interaction, described by the Hamiltonian of Equation 5.1.1 decays with the inverse cube of the distance between the two nuclei and is directly proportional to the product of the nuclear gyromagnetic ratios.

If no external static field \mathbf{B}_0 is applied, then there is not an “externally imposed” direction in space, meaning that all orientations are equivalent and, so, the complete dipolar Hamiltonian must be used to describe the direct coupling. On the other hand, when an externally applied field enforces a preferred direction in space (for instance, the \hat{z} direction along which a field \mathbf{B}_0 lies), the dipolar Hamiltonian is customarily simplified applying the so-called *secular approximation*, which is briefly presented in the next *further information*.

Further information 5.1. The secular approximation is routinely applied in the study of nuclear magnetic resonance when the system Hamiltonian can be written as the sum of two terms [33]

$$\mathcal{H} = \mathbf{A} + \mathbf{B} \quad (5.1.3)$$

where the symbol \mathbf{A} identifies a “large” Hermitian operator and \mathbf{B} a “small” one. Since \mathbf{A} is Hermitian, its eigenvectors realize a complete orthonormal basis. Let

$$\mathbf{A} |\psi_n\rangle = \lambda_n |\psi_n\rangle \quad (5.1.4)$$

where $|\psi_n\rangle$ are the eigenvectors of \mathbf{A} and λ_n the corresponding eigenvalues. The operator \mathbf{A} is obviously represented by a diagonal matrix in its eigenbasis:

$$\mathbf{A} = \begin{pmatrix} \bullet & 0 & 0 & \dots & 0 \\ 0 & \bullet & 0 & \dots & 0 \\ 0 & 0 & \bullet & \dots & 0 \\ \vdots & \ddots & & & \\ 0 & 0 & 0 & \dots & \bullet \end{pmatrix} \quad (5.1.5)$$

In general, \mathbf{B} does not commute with \mathbf{A} and so its matrix representation is *not* diagonal in the eigenbasis of \mathbf{A} . On the contrary, \mathbf{B} is expected to have finite values everywhere:

$$\mathbf{B} = \begin{pmatrix} \bullet & \bullet & \bullet & \dots & \bullet \\ \bullet & \bullet & \bullet & \dots & \bullet \\ \bullet & \bullet & \bullet & \dots & \bullet \\ \vdots & \ddots & & & \\ \bullet & \bullet & \bullet & \dots & \bullet \end{pmatrix} \quad (5.1.6)$$

The secular approximation consists in dropping all non-diagonal elements b_{mn} of \mathbf{B} in the eigenbasis of \mathbf{A} such that

$$|b_{mn}| \ll |\lambda_m - \lambda_n| \triangleq \delta_\lambda \quad (5.1.7)$$

that is, b_{mn} can be neglected if its magnitude is significantly smaller than the corresponding difference in the eigenvalues of the operator \mathbf{A} . In practice, the only non-diagonal elements of \mathbf{B} which survive the secular approximation are those which *connect* degenerate or near-degenerate eigenstates of \mathbf{A} . It is possible to express \mathbf{B} as

$$\mathbf{B} = \sum_n b_{nn} |\psi_n\rangle\langle\psi_n| + \sum_{\substack{n \neq m \\ |b_{mn}| \ll \delta_\lambda}} b_{nm} |\psi_m\rangle\langle\psi_n| \quad (5.1.8)$$

Additional information can be found in [33, 42]. \diamond

The dipolar Hamiltonian of Equation 5.1.1 can be rewritten as the sum of six matrices. The detailed justification is not reported because it requires some quite long computations which are not physically interesting, but can be found in [47]. For the purposes of this research, it is enough to know that

$$\mathcal{H}_d = \mathbf{A} + \mathbf{B} + \mathbf{C} + \mathbf{D} + \mathbf{E} + \mathbf{F} \quad (5.1.9)$$

where

$$\begin{aligned} \mathbf{A} &= \begin{pmatrix} \bullet & 0 & 0 & 0 \\ 0 & \bullet & 0 & 0 \\ 0 & 0 & \bullet & 0 \\ 0 & 0 & 0 & \bullet \end{pmatrix} & \mathbf{B} &= \begin{pmatrix} 0 & 0 & 0 & 0 \\ 0 & 0 & \bullet & 0 \\ 0 & \bullet & 0 & 0 \\ 0 & 0 & 0 & 0 \end{pmatrix} & \mathbf{C} &= \begin{pmatrix} 0 & \bullet & \bullet & 0 \\ 0 & 0 & 0 & \bullet \\ 0 & 0 & 0 & \bullet \\ 0 & 0 & 0 & 0 \end{pmatrix} \\ \mathbf{D} &= \begin{pmatrix} 0 & 0 & 0 & 0 \\ \bullet & 0 & 0 & 0 \\ \bullet & 0 & 0 & 0 \\ 0 & \bullet & \bullet & 0 \end{pmatrix} & \mathbf{E} &= \begin{pmatrix} 0 & 0 & 0 & \bullet \\ 0 & 0 & 0 & 0 \\ 0 & 0 & 0 & 0 \\ 0 & 0 & 0 & 0 \end{pmatrix} & \mathbf{F} &= \begin{pmatrix} 0 & 0 & 0 & 0 \\ 0 & 0 & 0 & 0 \\ 0 & 0 & 0 & 0 \\ \bullet & 0 & 0 & 0 \end{pmatrix} \end{aligned} \quad (5.1.10)$$

Consider for the sake of definiteness a two-spin- $\frac{1}{2}$ system with quantum numbers m_1 and m_2 . The Zeeman energy, when a static external field B_0 is applied, can be simply written as

$$E_Z = -m_1\gamma_1\hbar B_0 - m_2\gamma_2\hbar B_0 \quad (5.1.11)$$

where $m_i = \pm\frac{1}{2}$. Considering the Zeeman energy associated with each energy level

(refer to diagram reported in Figure 5.3), one should agree upon the fact that the matrix elements of \mathbf{C} , \mathbf{D} , \mathbf{E} and \mathbf{F} can usually be neglected, since the difference between the corresponding eigenvalues is of the order¹ of $|\sim 2\gamma_n \cdot \hbar B_0|$ and Equation 5.1.7 is expected to be satisfied. On the other hand, the terms of matrix \mathbf{B} are usually larger than the difference between the corresponding eigenvalues, which is roughly zero, since states $|\uparrow\downarrow\rangle$ and $|\downarrow\uparrow\rangle$ are near-degenerate.

The consequence of this long discussion is that the dipolar Hamiltonian, in the **homonuclear** case, can be written as

$$\mathcal{H}_d \sim -\frac{\mu_0}{4\pi} \frac{\gamma_1\gamma_2}{r^3} (\mathbf{A} + \mathbf{B}) = -\frac{\mu_0}{4\pi} \frac{\gamma_1\gamma_2}{r^3} \frac{3\cos^2(\theta) - 1}{2} (3\mathbf{I}_{1z}\mathbf{I}_{2z} - \mathbf{I}_1 \cdot \mathbf{I}_2) \quad (5.1.12)$$

Where θ is the angle between the vector $\hat{\mathbf{r}}$ joining the two spins and the field \mathbf{B}_0 (Figure 5.4). For additional details, one can consider [42, 47].

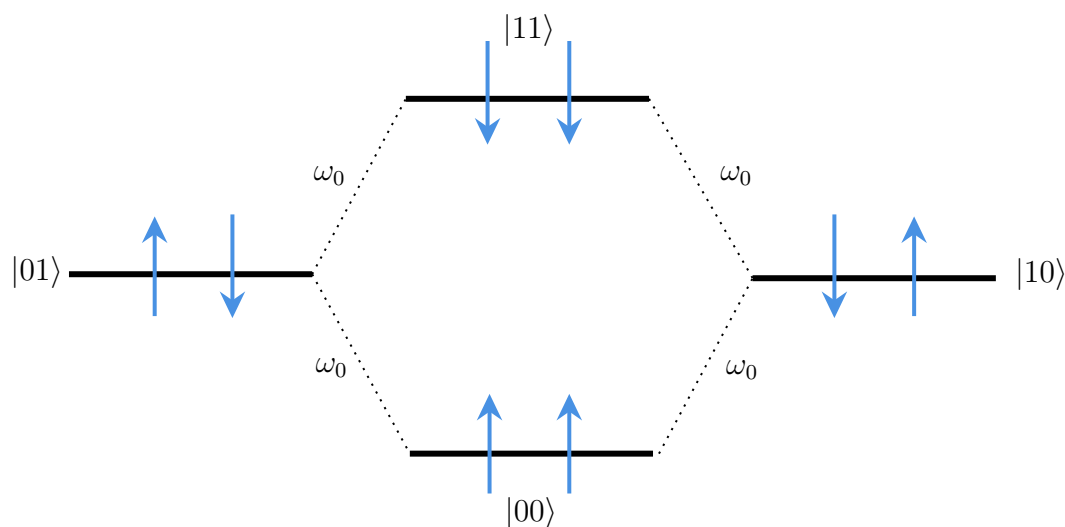


Figure 5.3: The Zeeman energy levels for a two-spin system. For the sake of simplicity, the two nuclei are assumed to have the same gyromagnetic ratio, so that $|01\rangle$ and $|10\rangle$ are degenerate.

When dealing with nuclei characterized by different gyromagnetic ratios or different chemical shifts (**heteronuclear** case), the corresponding spins precess with distinguishable frequencies [48].

¹The actual value depends on the gyromagnetic ratios.

As a consequence, from a semi-classical point of view, the \hat{x} and \hat{y} components of \mathbf{m}_2 can be seen as rapidly oscillating in the rotating frame of \mathbf{m}_1 , thus averaging to zero and vice versa. From a quantum mechanical perspective, the secular approximation usually kills also the elements of matrix \mathbf{B} , since energies associated with $|\uparrow\downarrow\rangle$ and $|\downarrow\uparrow\rangle$ can be quite different. The dipolar Hamiltonian, thus, can be expressed as

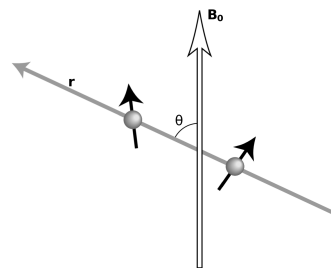


Figure 5.4: The θ angle. Adapted from [33].

$$\mathcal{H}_d \sim -\frac{\mu_0}{4\pi} \frac{\gamma_1 \gamma_2}{r^3} \frac{3 \cos^2(\theta) - 1}{2} \cdot 2\mathbf{I}_{1z} \mathbf{I}_{2z} \quad (5.1.13)$$

It has to be highlighted that the secular dipole-dipole coupling constant

$$d_{12} \triangleq -\frac{\mu_0}{4\pi} \frac{\gamma_1 \gamma_2}{r^3} \frac{3 \cos^2(\theta) - 1}{2} \quad (5.1.14)$$

presents an explicit dependence on the orientation of the spin pair with respect to the external field.

In an **isotropic liquid**, which is the main focus of this research, the dipole-dipole coupling can usually be safely neglected [33]. Indeed

- The *intramolecular* direct coupling averages to zero. The point is that the vector $\hat{\mathbf{r}}$ has only two ways to be oriented parallel to \mathbf{B}_0 , namely, in the same ($\theta = 0$) or in the opposite ($\theta = \pi$) direction, while there are infinite ways in which it can be oriented perpendicularly ($\theta = \pi/2$) to the magnetic field. In an ensemble of freely moving molecules, the different orientations of the vector $\hat{\mathbf{r}}$ average to zero the intramolecular coupling.
- The *short-distance intermolecular* direct coupling averages to zero because of rapid tumbling of molecules.
- The *long-distance intermolecular* direct coupling does not average to zero, but can be neglected thanks to the dependence on the inverse cube of $|\hat{\mathbf{r}}|$.

In the remainder of this text, the dipolar Hamiltonian will always be assumed to vanish

$$\mathcal{H}_d \sim 0 \quad (5.1.15)$$

5.2 Chemical shielding

The experimental evidence shows that the same isotopes in different molecular surroundings are characterized by different resonant frequencies. For instance, it is possible to identify three well-differentiated proton resonant frequencies in $\text{CH}_3\text{CH}_2\text{OH}$: they correspond to the three “kinds” of protons, the CH_3 group, the CH_2 group and the OH group. The reason is that the three kinds of protons experience slightly different *local* fields. The variation of the local fields on a submolecular distance scale is due to molecular electrons. At a very rough but intuitive level, this phenomenon, known to the scientific community as chemical shielding, can be seen as a three-step process:

1. The externally applied static field \mathbf{B}_0 induces circulating currents in molecular electron clouds.
2. The currents, in turn, give rise to an **induced** field \mathbf{B}_{ind} .
3. The nuclear spins sense a local field $\mathbf{B}_{\text{loc}} = \mathbf{B}_0 + \mathbf{B}_{\text{ind}}$.

As a rule of thumb, the local field is in the order of $\mathbf{B}_{\text{ind}} \sim 10^{-4} \cdot \mathbf{B}_0$, but the actual value depends on the nucleus of interest, the electronic structure of the molecule and the orientation of the latter with respect to the applied field.

The local field can alternatively be expressed as

$$\mathbf{B}_{\text{loc}} = (1 - \boldsymbol{\sigma})\mathbf{B}_0 \quad (5.2.1)$$

where $\boldsymbol{\sigma}$ is 3×3 tensor² known as the **shielding tensor** and defined as

$$\boldsymbol{\sigma} = \begin{pmatrix} \sigma_{xx} & \sigma_{xy} & \sigma_{xz} \\ \sigma_{yx} & \sigma_{yy} & \sigma_{yz} \\ \sigma_{zx} & \sigma_{zy} & \sigma_{zz} \end{pmatrix} \quad (5.2.2)$$

The local field is not necessarily oriented in the same direction as the applied field. Even if, in the general case, the shielding tensor is not symmetric, it can be shown that the observable first-order response is symmetric [49]. The symmetric part of $\boldsymbol{\sigma}$ can be diagonalized in a proper reference system, known as the **principal axes** coordinate system [50]. The chemical shielding principal axes are conventionally denoted using the capital letters $\hat{\mathbf{X}}$, $\hat{\mathbf{Y}}$ and $\hat{\mathbf{Z}}$ and defined by the following property: if the external field is applied along a principal axis of a certain nucleus, then

²Even if the same symbol is used, it is obvious that the shielding tensor has nothing to do with the Pauli matrices.

the induced field, at the same nucleus, has the same direction. In this reference system, the shielding tensor turns out to be diagonal

$$\boldsymbol{\sigma}_{\text{pas}} = \begin{pmatrix} \sigma_{XX} & 0 & 0 \\ 0 & \sigma_{YY} & 0 \\ 0 & 0 & \sigma_{ZZ} \end{pmatrix} \quad (5.2.3)$$

In order to relate the theoretical computations of the shielding tensor to NMR experiments, it proves useful to define the so called **isotropic chemical shielding** as the averaged trace of the shielding tensor

$$\sigma = \frac{1}{3} \text{tr}(\boldsymbol{\sigma}_{\text{pas}}) = \frac{1}{3} (\sigma_{XX} + \sigma_{YY} + \sigma_{ZZ}) = \frac{1}{3} \text{tr}(\boldsymbol{\sigma}) \quad (5.2.4)$$

where the last equality follows from the fact that the isotropic chemical shielding is independent of the chosen reference frame [50]. There are several conventions for the definition of the $\hat{\mathbf{X}}$, $\hat{\mathbf{Y}}$ and $\hat{\mathbf{Z}}$ axes. The choice has fallen on the Haeberlen’s [50], since it is the one adopted by ORCA [3, 2] which is one of the most known open source computational chemistry tools freely available to the scientific community. This convention defines the three components according to the following rule:

$$|\sigma_{YY} - \sigma| \leq |\sigma_{XX} - \sigma| \leq |\sigma_{ZZ} - \sigma| \quad (5.2.5)$$

A useful figure of merit is the **chemical shielding anisotropy** defined as

$$\sigma_{\text{aniso}} \triangleq \sigma_{ZZ} - \frac{\sigma_{XX} + \sigma_{YY}}{2} = \frac{3}{2} (\sigma_{ZZ} - \sigma) \quad (5.2.6)$$

which is a measure of the maximum deviation of the shielding from the isotropic value (according to 5.2.5). Finally, the difference between the $\hat{\mathbf{X}}$ and $\hat{\mathbf{Y}}$ principal values is quantified by the **bixiality** or **asymmetry**:

$$\eta = \frac{\sigma_{YY} - \sigma_{XX}}{\sigma_{ZZ} - \sigma} \quad (5.2.7)$$

Actually, what is routinely measured in NMR experiments, at least for the liquid state cases, is *not* the chemical shielding tensor, but just the shift in the resonance frequency caused by the variation of the local field with respect to the externally applied field. This shift, known as **chemical shift**, is usually evaluated with respect to a reference compound. If ω_{ref} is the Larmor frequency of the nuclei of interest in the reference compound and ω_{mol} is the one in the molecule under experiment, then the adimensional chemical shift constant is defined as

$$\delta = \frac{\omega_{\text{mol}} - \omega_{\text{ref}}}{\omega_{\text{ref}}} \quad (5.2.8)$$

Typical values for δ ranges from few to few hundreds of ppm (parts per million). For instance, the reference compound usually chosen for ^1H , ^{13}C and ^{29}Si is the tetramethylsilane $\text{Si}(\text{CH}_3)_4$ (abbreviated in TMS) which is chemically rather inert and gives NMR signals at frequencies far away from the typical ones of the previously mentioned nuclei. Conventionally, TMS spins are assumed to have zero chemical shift³ and are placed at the origin of the chemical shift scale, which increases *from right to left*, as clear from Figure 5.5, where some typical values are given with respect to TMS.

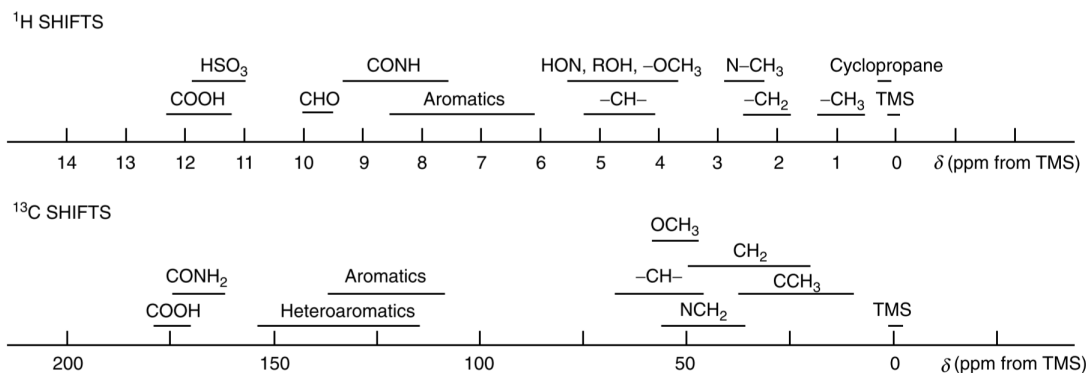


Figure 5.5: Chemical shift scale for ^1H and ^{13}C NMR experiments, with respect to TMS. From [33].

The relation between the chemical shift (experimentally measured) and the isotropic chemical shielding (theoretically computed) is

$$\delta = \frac{\sigma_{\text{ref}} - \sigma_{\text{mol}}}{1 - \sigma_{\text{ref}}} \sim \sigma_{\text{ref}} - \sigma_{\text{mol}} \quad (5.2.9)$$

Proof. Using the isotropic chemical shielding, the local magnetic field at the nucleus can be written as

$$\mathbf{B}_{\text{loc}} = (1 - \sigma)\mathbf{B}_0$$

³From an experimental point of view, a small amount of TMS is often added to the sample and the corresponding resonant frequency is assumed to occur at 0 ppm.

for both the molecule and the reference compound. The corresponding chemically shifted Larmor frequency is

$$\omega_0 = |\gamma_n| \cdot (1 - \sigma) B_0$$

Replacing in Equation 5.2.8, one gets

$$\begin{aligned} \delta &= \frac{\omega_{\text{mol}} - \omega_{\text{ref}}}{\omega_{\text{ref}}} = \frac{|\gamma_n| (1 - \sigma_{\text{mol}}) B_0 - |\gamma_n| (1 - \sigma_{\text{ref}}) B_0}{|\gamma_n| (1 - \sigma_{\text{ref}}) B_0} \\ &= \frac{\sigma_{\text{ref}} - \sigma_{\text{mol}}}{1 - \sigma_{\text{ref}}} \sim \sigma_{\text{ref}} - \sigma_{\text{mol}} \end{aligned} \tag{5.2.10}$$

□

It is worth highlighting that nuclei with *large* chemical shift are strongly *deshielded*, since as σ_{mol} gets smaller, δ increases. Another interesting aspect which has to be remarked is that the chemical shift ranges depend on the atomic number: nuclei with more electrons are characterized by a greater range of shielding.

5.2.1 The Hamiltonian of the chemical shielding

The nuclear spin interacts with the local field, which is different from the applied (along \hat{z}) field, because of the chemical shift. The corresponding Hamiltonian is

$$\mathcal{H} = -\gamma_n \mathbf{I} \cdot \mathbf{B}_{\text{loc}} = -\gamma_n \mathbf{I} \cdot (1 - \sigma) B_0 \hat{z} = \mathcal{H}_0 + \mathcal{H}_{cs} \quad (5.2.11)$$

from which the chemical-shift Hamiltonian is

$$\mathcal{H}_{cs} = +\gamma_n B_0 \mathbf{I} \cdot \sigma \hat{z} \quad (5.2.12)$$

It can be shown [33, 17] that applying the secular approximation, the previous expression reduces to

$$\mathcal{H}_{cs} \sim +\gamma_n B_0 \sigma_{zz} \mathbf{I}_z \quad (5.2.13)$$

and for an isotropic liquid it is enough to compute the isotropic chemical shielding

$$\mathcal{H}_{cs} \sim +\gamma_n B_0 \sigma \mathbf{I}_z \quad (5.2.14)$$

5.2.2 The origin of the chemical shielding

Chemical shifts are originated by the simultaneous interaction of nuclei with electrons and that of electrons with the applied magnetic field. The physics behind is not trivial and a full understanding requires advanced knowledge at least in quantum mechanics, molecular orbital theory, perturbation theory and group theory. Moreover, the computation of reliable chemical shifts, demanding detailed information about the electron density in the ground *and* excited states, is still nowadays a challenging task for computational chemistry software, which, in turn, requires the user to have some understanding of the computational theory beneath.

However, being the chemical shift one of the most relevant aspects of NMR, a basic understanding is mandatory for the engineer who desires to implement a NMR quantum computer. In the following, a semi-classical approach is proposed, which is an integrated and simplified review of Slichter’s interpretation [42] of Ramsey’s general theory of magnetic shielding [51, 52].

5.2.2.1 Time independent perturbation theory: some hints

When exact solutions to physical problems cannot be (efficiently) found, one has to look for methods of approximation. This is a necessary step because the Schrödinger equation can be solved exactly for very few quantum chemistry problems. There are basically two approaches: perturbation theory and self-consistent field procedures. While the second one is an iterative method routinely exploited by computational chemistry tools, in this section the main results of the first one are presented, since it proves more useful to get a physical understanding. The only simple case which is dealt with here is that of a quantum system characterized by many *non-degenerate* energy levels, for which the time *independent* perturbation theory can be applied. For a comprehensive treatment, the reader is referred to the specialized literature, as [34].

Suppose that the Hamiltonian of the unperturbed system is $\mathcal{H}^{(0)}$ and that $|\psi_n\rangle$ realize a complete orthonormal basis set of the corresponding Hilbert space. Assume that the solutions of the equations

$$\mathcal{H}^{(0)} |\psi_n^{(0)}\rangle = E_n^{(0)} |\psi_n^{(0)}\rangle \quad (5.2.15)$$

are known. Then, a *small* perturbation is applied to the system, such that the Hamiltonian of the perturbed system can be written as

$$\mathcal{H} = \mathcal{H}^{(0)} + \lambda\mathcal{H}^{(1)} + \lambda^2\mathcal{H}^{(2)} + \dots \quad (5.2.16)$$

where λ is an arbitrary parameter added to keep track of the order of the perturbation. Suppose that the perturbation is computed from the unperturbed state $|\psi_0^{(0)}\rangle$, which is not necessarily the ground state of the system. The perturbed state vector can be expanded as

$$|\psi_0\rangle = |\psi_0^{(0)}\rangle + \lambda |\psi_0^{(1)}\rangle + \lambda^2 |\psi_0^{(2)}\rangle + \dots \quad (5.2.17)$$

Similarly, the energy is

$$E_0 = E_0^{(0)} + \lambda E_0^{(1)} + \lambda^2 E_0^{(2)} + \dots \quad (5.2.18)$$

where $E_0^{(1)}$ is the first-order correction to the energy, $E_0^{(2)}$ the second-order correction and so on.

The perturbed Schrödinger equation which has to be solved is

$$\mathcal{H}|\psi_0\rangle - E_0|\psi_0\rangle = 0 \quad (5.2.19)$$

Replacing, collecting the terms with the same power of λ and equating to zero the coefficient of each power of λ^4 , one gets

$$\begin{aligned} \mathcal{H}^{(0)}|\psi_0^{(0)}\rangle &= E_0^{(0)}|\psi_0^{(0)}\rangle \\ \left[\mathcal{H}^{(0)} - E_0^{(0)}\right]|\psi_0^{(1)}\rangle &= \left[E_0^{(1)} - \mathcal{H}^{(1)}\right]|\psi_0^{(0)}\rangle \\ \left[\mathcal{H}^{(0)} - E_0^{(0)}\right]|\psi_0^{(2)}\rangle &= \left[E_0^{(2)} - \mathcal{H}^{(2)}\right]|\psi_0^{(0)}\rangle + \left[E_0^{(0)} - \mathcal{H}^{(1)}\right]|\psi_0^{(1)}\rangle \\ &\dots \end{aligned} \quad (5.2.20)$$

Once this background is built, it is simple to compute the corrections to the energy and the state vector.

⁴Since λ is an arbitrary parameter, the coefficient of each power of λ must be equated to zero separately.

First-order correction The first-order corrections to the state $|\psi_0^{(0)}\rangle$ are

- The first-order correction to the energy is

$$E_0^{(1)} = \langle \psi_0^{(0)} | \mathcal{H}^{(1)} | \psi_0^{(0)} \rangle \quad (5.2.21)$$

which is the first-order perturbation Hamiltonian averaged over the unperturbed state vector.

- The state vector corrected to first-order is

$$|\psi_0\rangle \sim |\psi_0^{(0)}\rangle + \sum_{n \neq 0} \frac{\langle \psi_n^{(0)} | \mathcal{H}^{(1)} | \psi_0^{(0)} \rangle}{E_0^{(0)} - E_n^{(0)}} |\psi_n^{(0)}\rangle \quad (5.2.22)$$

which is a linear superposition of all the unperturbed states of the systems.

Proof. The first step is the derivation of the first-order correction to the energy. The first-order correction to the wavefunction can be written as the linear combination of unperturbed state vectors, which constitute a complete orthonormal basis set

$$|\psi_0^{(1)}\rangle = \sum_n a_n |\psi_n^{(0)}\rangle$$

Replacing in the second equation of 5.2.20, one gets

$$\begin{aligned} \sum_n a_n [\mathcal{H}^{(0)} - E_0^{(0)}] |\psi_n^{(0)}\rangle &= [E_0^{(1)} - \mathcal{H}^{(1)}] |\psi_0^{(0)}\rangle \\ \sum_n a_n [E_n^{(0)} - E_0^{(0)}] |\psi_n^{(0)}\rangle &= [E_0^{(1)} - \mathcal{H}^{(1)}] |\psi_0^{(0)}\rangle \end{aligned}$$

The trick to get an expression for $E_0^{(1)}$ is to multiply everything by $\langle \psi_0^{(0)} |$:

$$\sum_n a_n [E_n^{(0)} - E_0^{(0)}] \langle \psi_0^{(0)} | \psi_n^{(0)} \rangle = 0 = E_0^{(1)} - \langle \psi_0^{(0)} | \mathcal{H}^{(1)} | \psi_0^{(0)} \rangle$$

from which Equation 5.2.21 follows immediately.

Turning, now, to the second topic of this derivation, a first-order perturbed state vector is

$$|\psi_0\rangle \sim |\psi_0^{(0)}\rangle + |\psi_0^{(1)}\rangle = |\psi_0^{(0)}\rangle + \sum_n a_n |\psi_n^{(0)}\rangle$$

and the scope is to find the coefficients a_n . The first step is to multiply everything in the second equation of 5.2.20 by a generic $\langle \psi_k^{(0)} |$ with $k \neq 0$

$$\begin{aligned} \sum_n a_n \langle \psi_k^{(0)} | [E_n^{(0)} - E_0^{(0)}] | \psi_n^{(0)} \rangle &= \langle \psi_k^{(0)} | [E_0^{(1)} - \mathcal{H}^{(1)}] | \psi_0^{(0)} \rangle \\ a_k [E_k^{(0)} - E_0^{(0)}] &= -\langle \psi_k^{(0)} | \mathcal{H}^{(1)} | \psi_0^{(0)} \rangle \end{aligned}$$

where the second line follows from the orthonormality of the eigenstates.

Since the state $|\psi_0^{(0)}\rangle$ is not degenerate by hypothesis, then

$$E_k^{(0)} - E_0^{(0)} \neq 0 \quad \forall k \neq 0$$

and the coefficient a_k can be written as

$$a_k = \frac{\langle \psi_k^{(0)} | \mathcal{H}^{(1)} | \psi_0^{(0)} \rangle}{E_0^{(0)} - E_k^{(0)}}$$

and so

$$|\psi_0\rangle \sim |\psi_0^{(0)}\rangle + \sum_{k \neq 0} \frac{\langle \psi_k^{(0)} | \mathcal{H}^{(1)} | \psi_0^{(0)} \rangle}{E_0^{(0)} - E_k^{(0)}} |\psi_k^{(0)}\rangle$$

from which it is clear that the perturbed state vector is approximated by “mixing” into $|\psi_0^{(0)}\rangle$ the other states of the system. \square

Second-order correction The second-order correction to the energy is

$$E_0^{(2)} = \langle \psi_0^{(0)} | \mathcal{H}^{(2)} | \psi_0^{(0)} \rangle + \sum_{k \neq 0} \frac{\langle \psi_k^{(0)} | \mathcal{H}^{(1)} | \psi_0^{(0)} \rangle \langle \psi_0^{(0)} | \mathcal{H}^{(1)} | \psi_k^{(0)} \rangle}{E_0^{(0)} - E_k^{(0)}} \quad (5.2.23)$$

The justification is similar to the first-order case and can be found in [34].

5.2.2.2 Perturbation Hamiltonian

The theory of chemical shift is initially worked out for a simple case of one electron in a molecule where there is only a single magnetic nucleus (and an undetermined number of non magnetic nuclei). The derivation can be split in three steps:

1. The calculation of the perturbation energy.
2. The determination of the current density induced by the external field.
3. The deduction of the magnetic field produced by this current at the nucleus of interest and the corresponding chemical shielding.

This section deals with the first step, but, first of all, the concept of vector potential must be introduced.

Further information 5.2. A generic vector function is a function which associates a vector (output) with another vector or with a scalar (input). Here, the focus is on $\mathbb{R}^3 \rightarrow \mathbb{R}^3$ maps which relate each point of the real three-dimensional space to a three-dimensional vector

$$\mathbf{G} = g_x \hat{\mathbf{x}} + g_y \hat{\mathbf{y}} + g_z \hat{\mathbf{z}} \quad (5.2.24)$$

The derivatives of a vector functions are described resorting to the **del** or **nabla** operator which is, in \mathbb{R}^3 , a three-dimensional vector defined as

$$\nabla = \frac{\partial}{\partial x} \hat{\mathbf{x}} + \frac{\partial}{\partial y} \hat{\mathbf{y}} + \frac{\partial}{\partial z} \hat{\mathbf{z}} \quad (5.2.25)$$

The **divergence** of a vector function is a scalar computed as the inner product of the nabla operator and the vector function itself

$$\nabla \cdot \mathbf{G} = \frac{\partial g_x}{\partial x} + \frac{\partial g_y}{\partial y} + \frac{\partial g_z}{\partial z} \quad (5.2.26)$$

The other possible derivative of a vector function is the **curl** of the function which is a vector defined as the cross product of the nabla operator and the vector function itself

$$\nabla \times \mathbf{G} = \begin{vmatrix} \hat{\mathbf{x}} & \hat{\mathbf{y}} & \hat{\mathbf{z}} \\ \frac{\partial}{\partial x} & \frac{\partial}{\partial y} & \frac{\partial}{\partial z} \\ g_x & g_y & g_z \end{vmatrix} \quad (5.2.27)$$

Finally, when the nabla operator is applied to a scalar function f , then it is known as the **gradient** of the function and the output is a vector defined as

$$\nabla f = \frac{\partial f}{\partial x} \hat{\mathbf{x}} + \frac{\partial f}{\partial y} \hat{\mathbf{y}} + \frac{\partial f}{\partial z} \hat{\mathbf{z}} \quad (5.2.28)$$

In order to build up the Schrödinger equation for a particle acted upon by a magnetic field, it turns out that it is mandatory to find a *magnetic vector potential* \mathbf{A} , measured in T m, which describes the magnetic field. By definition, the magnetic field is the curl of the vector potential

$$\mathbf{B} = \nabla \times \mathbf{A} \quad (5.2.29)$$

Example 5.2.1. For example, a potential

$$\mathbf{A}_0 = \frac{1}{2} B (-y \hat{\mathbf{x}} + x \hat{\mathbf{y}})$$

corresponds to a field

$$\mathbf{B} = \frac{1}{2} B \cdot \nabla \times (-y \hat{\mathbf{x}} + x \hat{\mathbf{y}}) = B \hat{\mathbf{z}}$$

that is, to a field uniformly applied along $\hat{\mathbf{z}}$. △

Example 5.2.2. Another useful example is the magnetic potential corresponding to the field produced by a single nucleus, whose magnetic dipole is \mathbf{m} (the expression is reported in the proof of Equation 5.1.1) which can be shown to be

$$\mathbf{A}_{\text{nuc}} = \frac{\mu_0}{4\pi r^3} \mathbf{m} \times \mathbf{r}$$

since $\mathbf{m} = \gamma_n \mathbf{I}$, the potential can be rewritten as

$$\mathbf{A}_{\text{nuc}} = \frac{\gamma_n \mu_0}{4\pi r^3} \mathbf{I} \times \mathbf{r}$$

△

It is well known that the curl of the gradient of an arbitrary scalar function f is always zero

$$\nabla \times \nabla f = 0 \quad (5.2.30)$$

As a consequence, the same magnetic field is obtained if an arbitrary vector ∇f

is added to the vector potential

$$\mathbf{B} = \nabla \times \mathbf{A} = \nabla \times (\mathbf{A} + \nabla f) \quad (5.2.31)$$

This property is known as **gauge invariance**. Accordingly, one can always select a proper gradient of a scalar function (a physicist would say a “gauge”) such that the divergence of the vector potential is zero. In this case, the gauge is said to be a **Coulomb gauge**. \diamond

The point, now, is to find an expression for the contribution $\mathbf{B}_{\text{ind}} = -\sigma\mathbf{B}_0$ to the local field which causes the resonant frequency shift. It has been stated several times that the energy of a magnetic dipole in a field \mathbf{B} is $E = -\mathbf{m} \cdot \mathbf{B}$. Hence, once the energy due to \mathbf{B}_{ind} is known, it is possible to derive an expression for \mathbf{B}_{ind} itself and, then, for $-\sigma$. It proves, thus, reasonable to compute the Hamiltonian of the system. In particular, a single electron under a potential energy V is associated with the energy

$$\mathcal{H}^{(0)} = \frac{p^2}{2m_e} + V \quad (5.2.32)$$

where the superscript refers to the absence of magnetic fields (i.e. the Hamiltonian is zero-order in the potential). When both the external field and the magnetic field originated by the nucleus are taken into consideration, the Hamiltonian has to be properly modified. Letting

$$\mathbf{A} = \mathbf{A}_0 + \mathbf{A}_{\text{nuc}} \quad (5.2.33)$$

it is possible to argue [34] that the new Hamiltonian⁵ can be obtained from \mathcal{H}_0 simply replacing \mathbf{p} with $\mathbf{p} + e\mathbf{A}$, where $q = -e$. It turns out that

$$\mathcal{H} = \frac{p^2}{2m_e} + V - \frac{q}{m_e} \mathbf{A} \cdot \mathbf{p} + \frac{q^2}{2m_e} A^2 = \frac{1}{2m_e} (\mathbf{p} - q(\mathbf{A}_0 + \mathbf{A}_{\text{nuc}}))^2 + V \quad (5.2.34)$$

Proof. The square of the momentum operator is $p^2 = \mathbf{p} \cdot \mathbf{p}$. Replacing $\mathbf{p} \rightarrow \mathbf{p} + e\mathbf{A}$, one gets

$$(\mathbf{p} + e\mathbf{A})(\mathbf{p} + e\mathbf{A}) = p^2 + e(\mathbf{p} \cdot \mathbf{A} + \mathbf{A} \cdot \mathbf{p}) + e^2 A^2$$

It is known from table 1.1 that the momentum operator is a differential operator. When the wavefunction is added

$$\mathbf{p} \cdot \mathbf{A}\psi = -i\hbar \nabla \cdot (\mathbf{A}\psi) = -i\hbar \mathbf{A} \cdot \nabla \psi = \mathbf{A} \cdot \mathbf{p}\psi$$

⁵Obviously, this rule applies to every potential \mathbf{A} and not only when the latter is the sum of the external potential and the nuclear one.

assuming a Coulomb gauge is chosen. Hence

$$(\mathbf{p} + e\mathbf{A})(\mathbf{p} + e\mathbf{A}) = p^2 + 2e\mathbf{A} \cdot \mathbf{p} + e^2 A^2$$

from which Equation 5.2.34 follows immediately. \square

Since there are two “sources of perturbation”, the external field and the nuclear field, it proves sensible to split the problem in two stages. The first step is the evaluation of the perturbation energy treating only \mathbf{A}_{nuc} as perturbation source. To this end, it is useful [42] to define a quantity which is a kind of generalized momentum operator which includes the external field potential

$$\boldsymbol{\chi} = \mathbf{p} + e\mathbf{A}_0 \quad (5.2.35)$$

Being the linear combination of two Hermitian operators, it is a Hermitian operator. The Hamiltonian becomes

$$\begin{aligned} \mathcal{H} &= \frac{\chi^2}{2m_e} + \frac{e}{2m_e}(\boldsymbol{\chi} \cdot \mathbf{A}_{\text{nuc}} + \mathbf{A}_{\text{nuc}} \cdot \boldsymbol{\chi}) + \frac{e^2}{2m_e}A_{\text{nuc}}^2 + V \\ &\sim \frac{\chi^2}{2m_e} + \frac{e}{2m_e}(\boldsymbol{\chi} \cdot \mathbf{A}_{\text{nuc}} + \mathbf{A}_{\text{nuc}} \cdot \boldsymbol{\chi}) + V \end{aligned} \quad (5.2.36)$$

where the second-order term in \mathbf{A}_{nuc} is dropped because the nuclear moment is very small compared with the electron moments. As a consequence, \mathbf{A}_{nuc} is reasonably treated according to a first-order perturbation theory.

The Hamiltonian presents a term which does not depend on \mathbf{A}_{nuc} , a term which is linear with \mathbf{A}_{nuc} and a term which is quadratic with \mathbf{A}_{nuc} . Defining

$$\begin{aligned} \mathcal{H}^{(0)} &= \frac{\chi^2}{2m_e} + V \\ \mathcal{H}^{(1)} &= \frac{e}{2m_e}(\boldsymbol{\chi} \cdot \mathbf{A}_{\text{nuc}} + \mathbf{A}_{\text{nuc}} \cdot \boldsymbol{\chi}) \\ \mathcal{H}^{(2)} &= \frac{e^2}{2m_e}A_{\text{nuc}}^2 \end{aligned} \quad (5.2.37)$$

one can write explicitly

$$\mathcal{H} = \mathcal{H}^{(0)} + \mathcal{H}^{(1)} + \mathcal{H}^{(2)} \sim \mathcal{H}^{(0)} + \mathcal{H}^{(1)} \quad (5.2.38)$$

Now, let \mathbf{j} be the electron current density which flows in the molecule when the external static field is applied. In other words, \mathbf{j} is the current due to the field \mathbf{B}_0 and the electrostatic potential V , but not to the nuclear field. Then, the magnetic

moment of the magnetic nucleus *couples* with the current \mathbf{j} , causing a shift in the energy of the nucleus itself. At first-order, the correction to the nuclear energy is

$$E_0^{(1)} = - \int \mathbf{A}_{\text{nuc}} \cdot \mathbf{j} d\tau \quad (5.2.39)$$

Proof. It is convenient to write the first-order correction to the energy reported in Equation 5.2.21 according to the methodology introduced in section §1.2.2

$$E_0^{(1)} = \langle \psi_0 | \mathcal{H}^{(1)} | \psi_0 \rangle = \frac{e}{2m_e} \int \psi_0^* (\boldsymbol{\chi} \cdot \mathbf{A}_{\text{nuc}} + \mathbf{A}_{\text{nuc}} \cdot \boldsymbol{\chi}) \psi_0 d\tau$$

where τ is the integration variable and ψ_0 is the exact unperturbed solution when the potential V and the field \mathbf{B}_0 act on the electron. The reader is reminded that at this level, only the nuclear field contribution is treated according to the perturbation theory, while the effects of the external field are “included” in ψ_0 . Hence, the first-order (in \mathbf{A}_{nuc}) correction to the energy is computed as the average value of the first-order Hamiltonian over the unperturbed ψ_0 . The subscript 0 is introduced to highlight that the state taken into consideration is the ground-state “modified” by the application of the external field.

It is known that an operator \mathbf{T} is Hermitian if and only if

$$\langle \phi | \mathbf{A} \psi \rangle = \langle \mathbf{A} \phi | \psi \rangle$$

which means

$$\int \phi^* \mathbf{A} \psi d\tau = \int (\mathbf{A} \phi)^* \psi d\tau$$

Consequently, exploiting the Hermiticity of $\boldsymbol{\chi}$, the fact that ψ_0 is a scalar function and the Coulomb gauge choice for \mathbf{A}_{nuc} , the first-order correction to the energy can be rewritten as

$$E_0^{(1)} = \frac{e}{2m_e} \int \mathbf{A}_{\text{nuc}} \cdot [(\boldsymbol{\chi} \psi_0)^* \psi_0 + \psi_0^* \boldsymbol{\chi} \psi_0] d\tau$$

Replacing the definition of $\boldsymbol{\chi}$, the term in brackets becomes

$$\begin{aligned} & \frac{e}{2m_e} [(\boldsymbol{\chi} \psi_0)^* \psi_0 + \psi_0^* \boldsymbol{\chi} \psi_0] \\ &= \frac{e}{2m_e} \{ \psi_0 [\mathbf{p} \psi_0 + e \mathbf{A}_0 \psi_0]^* + \psi_0^* [\mathbf{p} \psi_0 + e \mathbf{A}_0 \psi_0] \} \\ &= \frac{\hbar}{i} \frac{e}{2m_e} [-\psi_0 \nabla \psi_0^* + \psi_0^* \nabla \psi_0] + \frac{e^2 \mathbf{A}_0}{2m_e} [\psi_0^* \psi_0 + \psi \psi_0^*] \end{aligned}$$

At this point, it is interesting to note that the current density in presence of a magnetic field, whose corresponding potential is \mathbf{A} , can be shown [34, 42] to have expression

$$\mathbf{j} = - \left\{ \frac{\hbar}{i} \frac{e}{2m_e} [\psi^* \nabla \psi - \psi \nabla \psi^*] + \frac{e^2 \mathbf{A}}{m_e} \psi^* \psi \right\}$$

for an electron described by a wavefunction ψ . Hence, the first-order energy acquires the expression reported in Equation 5.2.39. \square

Inserting the expression of the nuclear potential, the first-order energy becomes

$$E_0^{(1)} = -\frac{\mu_0 \gamma_n}{4\pi} \int \frac{(\mathbf{I} \times \mathbf{r}) \cdot \mathbf{j}}{r^3} d\tau = -\frac{\mu_0 \gamma_n}{4\pi} \mathbf{I} \cdot \int \frac{\mathbf{r} \times \mathbf{j}}{r^3} d\tau \quad (5.2.40)$$

As previously stated, this expression represents the energy of a nuclear magnetic moment $\gamma_n \mathbf{I}$ interacting with the current due to the external field \mathbf{B}_0 and the electrostatic potential. This energy shift can be written as the inner product of the moment and a field \mathbf{B}_{ind} originated by the current

$$E_0^{(1)} = -\frac{\mu_0 \gamma_n}{4\pi} \mathbf{I} \cdot \int \frac{\mathbf{r} \times \mathbf{j}}{r^3} d\tau = -\mathbf{m} \mathbf{B}_{\text{ind}} \quad (5.2.41)$$

from which

$$\mathbf{B}_{\text{ind}} = \frac{\mu_0}{4\pi} \int \frac{\mathbf{r} \times \mathbf{j}}{r^3} d\tau \quad (5.2.42)$$

This is the very core of chemical shift: once the current \mathbf{j} is known, the field at the nucleus can be computed and the chemical shift obtained consequently. There is one interesting remark which can already be made. The sensitivity of the chemical shift depends on the inverse cube of r and so “nearby currents”, unless extremely small, are expected to have the greatest effect on the value of σ . The point, now, is to compute the current density.

5.2.2.3 Computation of the current density

At this point, the second part of the problem can be addressed. The current density \mathbf{j} , as mentioned above, depends exclusively on the external field \mathbf{B}_0 and the electrostatic potential. Now, it is the external field which is treated as a perturbation. Assuming that the molecular orbitals are non-degenerate, which is the common case, the corresponding wavefunctions can be shown to be real [42, 34]. Under this hypothesis, if the gauge of the vector potential is a Coulomb gauge, then the current density can be arbitrarily split in two contributions: a paramagnetic current density and a diamagnetic current density, which give opposite contributions to the induced field.

$$\mathbf{j} = \mathbf{j}_p + \mathbf{j}_d \quad (5.2.43)$$

Their expressions are

$$\begin{aligned} \mathbf{j}_d &= - \left(\frac{e^2}{m_e} \right) \mathbf{A}_0 \left(\psi_0^{(0)} \right)^2 \\ \mathbf{j}_p &= \frac{\hbar}{i} \frac{e}{2m_e} \sum_{n \neq 0} (a_n - a_n^*) \left(\psi_n^{(0)} \nabla \psi_0^{(0)} - \psi_0^{(0)} \nabla \psi_n^{(0)} \right) \end{aligned} \quad (5.2.44)$$

The diamagnetic current density depends only on the ground state ($\psi_0^{(0)}$), while the paramagnetic contribution is an admixture of ground and excited states.

Proof. The first step is to describe the electron acted upon by electrostatic potential *and* the external field by means of a Hamiltonian

$$\begin{aligned} \mathcal{H} &= \frac{1}{2m_e} (\mathbf{p} + e\mathbf{A}_0)^2 + V \\ &= \frac{p^2}{2m_e} + \frac{e}{2m_e} (\mathbf{p} \cdot \mathbf{A}_0 + \mathbf{A}_0 \cdot \mathbf{p}) + \frac{e^2}{2m_e} A_0^2 + V \end{aligned}$$

The external field can be regarded as a perturbation element. The unperturbed Hamiltonian (no external field applied) is clearly

$$\mathcal{H}^{(0)} = \frac{p^2}{2m_e} + V$$

and the solution of Schrödinger equations are assumed to be known when no external field is applied, as explained in section §5.2.2.1. According to the definition

introduced in the proof of Equation 5.2.39, the current density has expression

$$\mathbf{j} = - \left\{ \frac{\hbar}{i} \frac{e}{2m_e} [\psi^* \nabla \psi - \psi \nabla \psi^*] + \frac{e^2 \mathbf{A}_0}{m_e} \psi^* \psi \right\}$$

where the wavefunction is not necessarily real. What is routinely done at this point is the computation of the first-order (in \mathbf{B}_0) current density. It is clear that the terms that are first-order in \mathbf{A}_0 are also first-order in \mathbf{B}_0 . Consequently, the first-order correction to the Hamiltonian is

$$\mathcal{H}^{(1)} = \frac{e}{2m_e} (\mathbf{p} \cdot \mathbf{A}_0 + \mathbf{A}_0 \cdot \mathbf{p})$$

According to Equation 5.2.22 and section §1.2.2, the first-order perturbed wavefunction is

$$\psi_0 \sim \psi_0^{(0)} + \psi_0^{(1)} = \psi_0^{(0)} + \sum_{n \neq 0} \frac{\langle \psi_n^{(0)} | \mathcal{H}^{(1)} | \psi_0^{(0)} \rangle}{E_0^{(0)} - E_n^{(0)}} \psi_n^{(0)} = \psi_0^{(0)} + \sum_{n \neq 0} a_n \psi_n^{(0)}$$

The exact wavefunction ψ_0 is approximated as the sum of the unperturbed and the first-order perturbed wavefunctions. In other words, the switch-on of the external field causes the unperturbed ground-state $\psi_0^{(0)}$ to be distorted to $\psi_0 \sim \psi_0^{(0)} + \psi_0^{(1)}$, which takes into account both the electrostatic potential and the applied field.

Replacing in the definition of the current density, one gets

$$\begin{aligned} \mathbf{j} = \frac{\hbar}{i} \frac{e}{2m_e} \left\{ \psi_0^{(0)} \nabla \psi_0^{(0)*} - \psi_0^{(0)*} \nabla \psi_0^{(0)} + \sum_{n \neq 0} a_n \left(\psi_n^{(0)} \nabla \psi_0^{(0)*} - \psi_0^{(0)*} \nabla \psi_n^{(0)} \right) \right. \\ \left. - \sum_{n \neq 0} a_n^* \left(\psi_n^{(0)*} \nabla \psi_0^{(0)} - \psi_0^{(0)} \nabla \psi_n^{(0)*} \right) \right\} - \frac{e^2}{m_e} \left(\psi_0^{(0)} \right)^2 \mathbf{A}_0 \end{aligned}$$

Assuming, now, that the eigenfunctions $\psi_n^{(0)}$ and $\psi_0^{(0)}$ are real, the current density becomes

$$\mathbf{j} = \frac{\hbar}{i} \frac{e}{2m_e} \sum_{n \neq 0} (a_n - a_n^*) \left(\psi_n^{(0)} \nabla \psi_0^{(0)} - \psi_0^{(0)} \nabla \psi_n^{(0)} \right) - \frac{e^2}{m_e} \left(\psi_0^{(0)} \right)^2 \mathbf{A}_0$$

which can be arbitrarily split in the two contributions of Equation 5.2.44. \square

It is interesting to highlight that when the molecular orbitals are non-degenerate, the net current density is zero if no external field is applied. Another way of visualizing this physical phenomenon is to realize that under the same hypothesis, the

orbital angular momentum turns out to be null [34, 42]. According to the physical jargon, one would say that the angular momentum is **quenched**. On the other hand, when a magnetic field is applied, the wavefunctions get distorted, are no longer real [34] and the overall current density is, in general, not null. The orbital angular momentum gets “unquenched”.

Another aspect which deserves to be mentioned is that the current density shows an explicit dependence on the “shape” of the wavefunctions. Consequently, it will definitely not be a surprise that chemical shifts for different kinds of orbitals (i.e. s, p and so on) can be strongly mismatched. In the following two examples, just the main results for s and p orbitals are reported to highlight the noteworthy characteristics.

Example 5.2.3. The perturbation Hamiltonian $\mathcal{H}^{(1)}$ introduced in the proof of Equation 5.2.44, can be rewritten [42] to highlight the \hat{z} component of the angular momentum operator

$$\mathcal{H}^{(1)} = \frac{e}{2m_e} B_0 l_z = -\gamma_e B_0 l_z$$

Consider now an s orbital, which is spherically symmetric. It is known that $l_z \psi_0^{(0)} = 0$ and so

$$\psi_0 = \psi_0^{(0)} \longleftrightarrow a_n = 0 \quad \forall n \neq 0$$

As a matter of fact, an s orbital wavefunction can be expressed [53] as

$$\psi \sim e^{-r/\alpha} \quad \text{or} \quad \psi \sim (\beta - r)e^{-r/\alpha}$$

where α and β are two constants. In both cases, the application of the angular momentum operator gives a null result. As a consequence, the coefficients a_n are equal to zero and the overall current density has only the diamagnetic contribution

$$\mathbf{j} = \mathbf{j}_d = -\frac{e^2}{m_e} \mathbf{A}_0 \left(\psi_0^{(0)} \right)^2 = -\frac{e^2 B_0}{2m_e} (-y\hat{x} + x\hat{y}) \left(\psi_0^{(0)} \right)^2 \quad (5.2.45)$$

It is simple to realize that this current circles around the \hat{z} axis in such a way that it gives rise to an *induced* field which opposes the externally applied field and *shields* the nucleus, as shown in Figure 5.6. Hence, the diamagnetic character of this contribution to the current density. \triangle

Example 5.2.4. Consider a p-state and suppose that the surrounding of the nucleus is such that the three orbitals are non-degenerate, so that the orbital angular momentum, in absence of an external field, is quenched. By the way, this is a common case for atoms in molecules and solids and it is strictly related

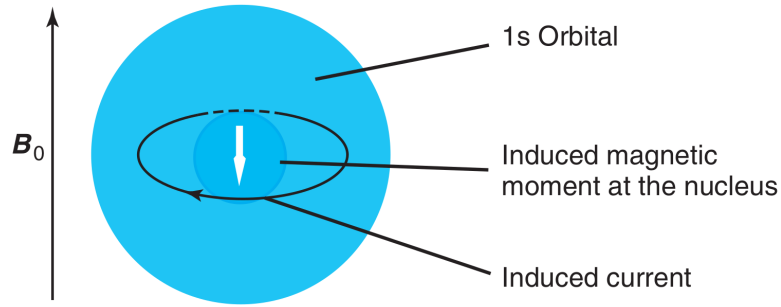


Figure 5.6: The shielding arising from the induced diamagnetic current. From [54].

to the fact that most substances are actually diamagnetic since atoms do not have permanent electronic magnetic moments. Suppose [42] that the ground-state wavefunction has the following shape

$$\psi_0^{(0)} = x f(r)$$

where $f(r)$ is a function with spherical symmetry. Since $l_z \psi_0^{(0)} \neq 0$ for a p-orbital, one would expect a non-null paramagnetic current contribution. As a matter of fact, it is possible to prove that

$$\begin{aligned} \mathbf{J}_p &= \frac{\hbar^2 e^2}{2m_e^2} \frac{B_0}{\Delta E_{0n}} (-y\hat{x} + x\hat{y}) f^2(r) \\ \mathbf{J}_d &= -\frac{e^2 B_0}{2m_e} (-y\hat{x} + x\hat{y}) x^2 f^2(r) \end{aligned}$$

where $\Delta E_{0n} = E_0 - E_n$. Both currents circulate about \hat{z} , but in opposite directions: \mathbf{J}_p gives rise to a magnetic field which reinforces \mathbf{B}_0 , while \mathbf{J}_d gives rise to a magnetic field which opposes \mathbf{B}_0 . △

5.2.2.4 Computation of the chemical shielding

Once the current density is known, it is possible to come back to the expression of the induced field (Equation 5.2.42) and, remembering that $\mathbf{B}_{\text{ind}} = -\sigma\mathbf{B}_0$, write down the following equations:

$$\begin{aligned}\mathbf{B}_{\text{ind}}^{\text{d}} &= -\sigma^{\text{d}}\mathbf{B}_0 = \frac{\mu_0}{4\pi} \int \frac{\mathbf{r} \times \mathbf{j}_{\text{d}}}{r^3} d\tau \\ \mathbf{B}_{\text{ind}}^{\text{p}} &= -\sigma^{\text{p}}\mathbf{B}_0 = \frac{\mu_0}{4\pi} \int \frac{\mathbf{r} \times \mathbf{j}_{\text{p}}}{r^3} d\tau\end{aligned}\tag{5.2.46}$$

from which the two contributions to the chemical shielding can be derived.

Diamagnetic chemical shielding The isotropic diamagnetic chemical shielding is given by the well known **Lamb formula**

$$\sigma^{\text{d}} = \left(\frac{e^2\mu_0}{12\pi m_e} \right) \left\langle \frac{1}{r} \right\rangle\tag{5.2.47}$$

which shows a strong dependence of the diamagnetic chemical shielding on the distance of the electron from the nucleus in question (for the choice of the Coulomb gauge mentioned above).

Proof. The first step is the computation of the cross product

$$\begin{aligned}\mathbf{r} \times \mathbf{j}_{\text{d}} &= -\frac{e^2 B_0}{2m_e} \left(\psi_0^{(0)} \right)^2 \mathbf{r} \times (-y\hat{\mathbf{x}} + x\hat{\mathbf{y}}) \\ &= -\frac{e^2 B_0}{2m_e} \left(\psi_0^{(0)} \right)^2 (-xz\hat{\mathbf{x}} - yz\hat{\mathbf{y}} + (x^2 + y^2)\hat{\mathbf{z}})\end{aligned}$$

It is evident that, in general, the induced field has components in all the three Cartesian directions, as expected. However, to evaluate the isotropic shielding, it is enough to know the diagonal terms σ_{xx} , σ_{yy} and σ_{zz} . Since the external field is assumed to be applied along the $\hat{\mathbf{z}}$ axis, only the z-component of the previous product is of interest

$$\sigma_{zz}^{\text{d}} = \frac{e^2\mu_0}{8\pi m_e} \int \frac{x^2 + y^2}{r^3} \left(\psi_0^{(0)} \right)^2 d\tau$$

By analogy, one immediately gets

$$\begin{aligned}\sigma_{xx}^d &= \frac{e^2\mu_0}{8\pi m_e} \int \frac{y^2 + z^2}{r^3} \left(\psi_0^{(0)}\right)^2 d\tau \\ \sigma_{yy}^d &= \frac{e^2\mu_0}{8\pi m_e} \int \frac{x^2 + z^2}{r^3} \left(\psi_0^{(0)}\right)^2 d\tau\end{aligned}$$

Since $\sigma = \frac{1}{3}(\sigma_{xx} + \sigma_{yy} + \sigma_{zz})$, one gets

$$\sigma^d = \frac{1}{3} \frac{e^2\mu_0}{8\pi m_e} \int \frac{2r^2}{r^3} \left(\psi_0^{(0)}\right)^2 d\tau = \left(\frac{e^2\mu_0}{12\pi m_e}\right) \left\langle \frac{1}{r} \right\rangle$$

□

Paramagnetic chemical shielding Differently from the diamagnetic shielding, the paramagnetic shielding arises when the applied field “mixes” excited states in the ground state. As a matter of fact, the isotropic paramagnetic shielding can be expressed as

$$\sigma^p = - \left(\frac{e^2\mu_0}{12\pi m_e^2}\right) \sum_{n \neq 0} \frac{\langle 0 | \mathbf{l} | n \rangle \langle n | r^{-3} \mathbf{l} | 0 \rangle}{\Delta E_{n0}} \quad (5.2.48)$$

where $\Delta_{n0} = E_n - E_0$ and the notation has been simplified introducing the symbols $|0\rangle = |\psi_0^{(0)}\rangle$ and $|n\rangle = |\psi_n^{(0)}\rangle$. It is interesting to highlight that σ^p is negative, thus forcing an increase in the local field.

Proof. As done for the derivation of the diamagnetic chemical shielding, one has to substitute the paramagnetic current density in Equation 5.2.46. It proves convenient to use the momentum operator \mathbf{p} :

$$\begin{aligned}\boldsymbol{\sigma}^p \mathbf{B}_0 &= -\frac{\mu_0}{4\pi} \int \frac{\mathbf{r} \times \mathbf{j}_p}{r^3} d\tau \\ &= -\frac{e\mu_0}{8\pi m_e} \sum_{n \neq 0} (a_n - a_n^*) \int \frac{\mathbf{r} \times \left(\psi_n^{(0)} \mathbf{p} \psi_0^{(0)} - \psi_0^{(0)} \mathbf{p} \psi_n^{(0)}\right)}{r^3} d\tau \\ &= -\frac{e\mu_0}{8\pi m_e} \sum_{n \neq 0} (a_n - a_n^*) \int \frac{\psi_n^{(0)} \mathbf{l} \psi_0^{(0)} - \psi_0^{(0)} \mathbf{l} \psi_n^{(0)}}{r^3} d\tau \\ &= -\frac{e\mu_0}{8\pi m_e} \sum_{n \neq 0} (a_n - a_n^*) \left\{ \left\langle n \left| \frac{\mathbf{l}}{r^3} \right| 0 \right\rangle - \left\langle 0 \left| \frac{\mathbf{l}}{r^3} \right| n \right\rangle \right\}\end{aligned}$$

where, as well known, $\mathbf{l} = \mathbf{r} \times \mathbf{p}$. Exploiting the hermiticity of the angular momentum operator

$$\left\langle 0 \left| \frac{\mathbf{l}}{r^3} \right| n \right\rangle = \left\langle n \left| \frac{\mathbf{l}}{r^3} \right| 0 \right\rangle^*$$

Next, since $|0\rangle$ and $|n\rangle$ are real states and the off-diagonal terms between real states of \mathbf{l} are imaginary [34], then

$$\left\langle n \left| \frac{\mathbf{l}}{r^3} \right| 0 \right\rangle^* = - \left\langle n \left| \frac{\mathbf{l}}{r^3} \right| 0 \right\rangle$$

Consequently,

$$\boldsymbol{\sigma}^p \mathbf{B}_0 = - \frac{e\mu_0}{4\pi m_e} \sum_{n \neq 0} (a_n - a_n^*) \left\langle n \left| \frac{\mathbf{l}}{r^3} \right| 0 \right\rangle$$

Remembering the expression of the first-order correction to the Hamiltonian presented in example 5.2.3, the mixing coefficient a_n can be rewritten as

$$a_n = \frac{\langle n | \mathcal{H}^{(1)} | 0 \rangle}{E_0^{(0)} - E_n^{(0)}} = \frac{\gamma_e B_0}{\Delta E_{n0}} \langle n | \mathbf{l}_z | 0 \rangle$$

Exploiting the same reasoning proposed before, one can write

$$\langle n | \mathbf{l}_z | 0 \rangle = \langle 0 | \mathbf{l}_z | n \rangle^* = - \langle 0 | \mathbf{l}_z | n \rangle$$

And so

$$\begin{aligned} a_n - a_n^* &= \frac{\gamma_e B_0}{\Delta E_{n0}} (\langle n | \mathbf{l}_z | 0 \rangle - \langle n | \mathbf{l}_z | 0 \rangle^*) \\ &= \frac{\gamma_e B_0}{\Delta E_{n0}} (\langle 0 | \mathbf{l}_z | n \rangle^* - \langle n | \mathbf{l}_z | 0 \rangle^*) \\ &= \frac{\gamma_e B_0}{\Delta E_{n0}} (- \langle 0 | \mathbf{l}_z | n \rangle - \langle 0 | \mathbf{l}_z | n \rangle) \\ &= - \frac{2\gamma_e B_0}{\Delta E_{n0}} \langle 0 | \mathbf{l}_z | n \rangle \end{aligned}$$

Once more, the resulting induced field will have components in all three directions. Anyway, in order to compute the isotropic shielding, it is enough to focus on the diagonal terms. Replacing, one gets

$$\sigma_{zz}^p = - \left(\frac{e^2 \mu_0}{4\pi m_e^2} \right) \sum_{n \neq 0} \frac{\langle 0 | \mathbf{l}_z | n \rangle \langle n | r^{-3} \mathbf{l}_z | 0 \rangle}{\Delta E_{n0}}$$

The other diagonal components can be derived by analogy, assuming the external

field is applied first along $\hat{\mathbf{x}}$ and then along $\hat{\mathbf{y}}$. Averaging, the resulting isotropic shielding is

$$\sigma^p = - \left(\frac{e^2 \mu_0}{12\pi m_e^2} \right) \sum_{n \neq 0} \frac{\langle 0 | \mathbf{l} | n \rangle \langle n | r^{-3} \mathbf{l} | 0 \rangle}{\Delta E_{n0}}$$

□

Many-electron chemical shielding The equations derived above hold true for one electron only, but can be simply generalized to the case in which there are N electrons which are spanned by the index $k = 1 \rightarrow N$. According to Ramsey's theory, when computing the chemical shielding for a specific magnetic nucleus, it proves convenient to assume that the other nuclei in the molecule have zero magnetic moment. As a matter of fact, the generic ij -component of the chemical shielding vector for a system with N electrons is [51, 50]

$$\sigma_{ij} = \overbrace{\left(\frac{e^2 \mu_0}{8\pi m_e^2} \right) \left\langle 0 \left| \sum_{k=1}^N \frac{\mathbf{r}_k \cdot \mathbf{r}_k \Delta_{ij} - r_{ki} r_{kj}}{r_k^3} \right| 0 \right\rangle}^{\sigma_{ij}^d} - \underbrace{\left(\frac{e^2 \mu_0}{4\pi m_e^2} \right) \sum_{n \neq 0} \frac{1}{\Delta E_{n0}} \left\langle 0 \left| \sum_{k=1}^N \mathbf{l}_{ki} \right| n \right\rangle \left\langle n \left| \sum_{k=1}^N \frac{\mathbf{l}_{kj}}{r_k^3} \right| 0 \right\rangle}_{\sigma_{ij}^p} \quad (5.2.49)$$

Proof. While a complete demonstration is found in [42], here just some useful hints are reported since the strategy is extremely similar to the one pursued for the previous derivations.

As far as the diamagnetic contribution is concerned, it is trivial to realize that the expression

$$\frac{\mathbf{r}_k \cdot \mathbf{r}_k \delta_{ij} - r_{ki} r_{kj}}{r_k^3}$$

is just a generalization of $(\mathbf{r} \times (-y\hat{\mathbf{x}} + x\hat{\mathbf{y}}))/r^3$ for a field which can be applied along $\hat{\mathbf{x}}$, or $\hat{\mathbf{y}}$ or $\hat{\mathbf{z}}$. In the latter case, it reduces to

$$\frac{\mathbf{r}_k \cdot \mathbf{r}_k \delta_{ij} - r_{ki} r_{kj}}{r_k^3} = \frac{x^2 + y^2 + z^2 - z^2}{r^3} = \frac{x^2 + y^2}{r^3}$$

For what concerns the paramagnetic contribution, the expression is obtained following the procedure proposed in the proof of Equation 5.2.48, formally replacing the orbital angular momentum operator with the sum of the operators of all electrons

$$\mathbf{l} \longrightarrow \sum_{k=1}^N \mathbf{l}_k$$

□

It has to be pointed out that only the sum of the paramagnetic and diamagnetic contributions has a physical meaning, while the numerical values individually associated with the two components are just a consequence of the gauge choice. A different gauge will result in different paramagnetic and diamagnetic shieldings, but their sum will remain unchanged. Actually, this is true only for exact solutions. However, one hardly ever deals with exact solutions and so a number of complications arise for the best choice of the gauge in practical computations.

Moreover, while the computation of σ^d , having contributions from the ground state wavefunction only, is relatively simple and can be achieved with satisfactory accuracy, the computation of σ^p , requiring the knowledge of excited wavefunctions, is significantly more involving. As a matter of fact, Ramsey's formulation, being simple and rational, is useful to understand the physical behaviour but it is suitable only for small molecules. Indeed, nowadays quantum chemistry computation software does not exploit these relations [50, 55]. In conclusion, the practical accurate evaluation of chemical shielding is rooted in the computational chemistry realm and it is still today a challenging task.

Some considerations on the contributions to shielding The **diamagnetic contribution** depends on the ability of the external field to force a circulating current in the electron ground state. These moving charges induce a field which opposes, at the nucleus of interest, the external field, thus resulting in an actual shielding of the latter. It is interesting to note that closed-shell free atoms, having a null electron orbital angular momentum (as already remarked in example 3.2.1), do not have any paramagnetic contribution. It is also the only contribution arising from inner shells (for instance s orbitals) of atoms in molecules, if they, as it is the usual case, maintain a spherical symmetry [53]. A rule of thumb which helps in quantifying this contribution follows from the fact that σ^d depends on the electron density of the atom of interest. Consequently, an increase in the electronegativity of a neighbouring atom leads to a withdraw of the electron cloud around the

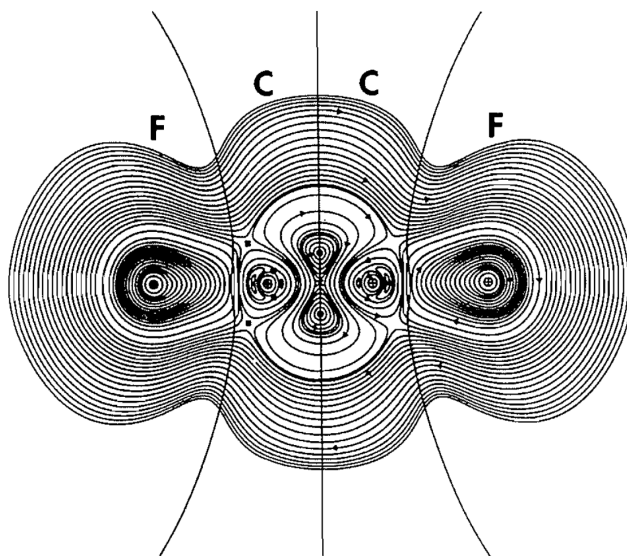


Figure 5.7: The current density in C_2F_2 . The external field is perpendicular to and directed out of the paper. From [56].

nucleus of interest and, so, to a reduction in shielding.

On the other hand, the **paramagnetic contribution** turns out to be zero in closed shell free atoms and around linear molecules axes, as the alkynes. A paramagnetic component arises when there are low-lying excited states, as it is clear from Equation 5.2.48, where the dependence on the inverse of the energy gap between ground and excited states is explicit, and the external field can “mix” the excited states into the ground state.

There is an important caveat which has to be remarked. In many NMR textbooks it is stated that for atoms different from H, the paramagnetic contribution is dominant. This statement is quite misleading since it should not be interpreted in reference to the *absolute magnitude* of the two components of the shielding vector, but in reference to the *extent to which these quantities vary*. It is clear that if σ^P is almost zero and σ^d is small, then σ is not expected to show large variations. This is, for instance, the case of hydrogen, which has $\sigma^d \sim 18$ ppm and a theoretically null paramagnetic contribution. On the other hand, for the majority of magnetic nuclei, the paramagnetic *variation* turns out to be larger than the diamagnetic one and it is broadly comparable with the overall variation of σ (and so of δ). A direct consequence is that atoms like carbon, fluorine and so on presents chemical shift ranges much wider than that of hydrogen for instance. The physical reason is that σ^d , even being a sum over all electrons (and so orbitals), is mainly affected by closer orbitals, which are not significantly “affected” changing from one chemical compound to the another. On the contrary, σ^P is wildly affected.

Atom	σ^d	σ^p	σ
F(0)	467.276	3.443	470.719
F(1)	467.276	3.443	470.719
C(2)	406.825	-259.879	146.946
C(3)	406.825	-259.879	146.946

Table 5.1: Chemical shielding for C_2F_2 . The number in parenthesis are used to identify the atoms inside the molecule, even if in this case the molecule is symmetric.

Example 5.2.5. As clear from Equation 5.2.49, the chemical shielding is mainly influenced by “near electrons”, because of its inverse dependence on the distance, and, as a consequence, by “near currents”. A graphical representation is often useful to get a feel for the subject. Figure 5.7 reports the current density distribution which arises in C_2F_2 , when the external field is perpendicular to and directed out of the paper. The arrows denote the sense of circulation. There is a large external region where the current flows clockwise, giving rise to a magnetic field which opposes, or *shields*, the applied one. Nevertheless, in the basins of the two carbon atoms, there are small regions where the current circulates anticlockwise, giving rise to a field which reinforces the external one. However, it has to be highlighted that the different currents can contribute to the local magnetic field at a particular nucleus with a shielding or deshielding effect, according to the position of the nucleus. For instance, the anticlockwise current which flows around the fluorine nuclei generates a magnetic field which opposes the external one at these nuclei, but it also has a deshielding effect on carbon nuclei.

The chemical shieldings reported in Table 5.1 are computed exploiting ORCA, at DSD-PBEP86 theory level with pcSseg-2 basis set, as suggested in [57], assuming water solvent and removing the frozen-core approximation ⁶. The results are in good agreement with the previous discussion, showing a modest paramagnetic shielding for F atoms and a more important one for C atoms. One should note that the paramagnetic shieldings for fluorine atoms are positive: this may seem wrong at first sight. Nevertheless, this is a simple consequence of the gauge choice carried out by ORCA: the reader is reminded that even if useful, the subdivision in paramagnetic and diamagnetic contributions is just arbitrary and only their sum has a sure physical meaning. Indeed, for different choices of the basis set and the numerical method, the paramagnetic and diamagnetic contributions change, but their sum is reasonably constant, for a similar level of accuracy. \triangle

⁶No RIJCOSX approximation is used since, being the molecule small, the CPU time is already reasonable. The results obtained adopting pcSseg-3 basis set are extremely similar.

5.2.3 A practical approach to chemical shielding

For the sake of completeness, it is worth mentioning the so-called empirical approach, which is sometimes adopted to simplify the analysis of the different contributions to the resulting shielding. It is customary to express the latter as

$$\sigma = \sigma(\text{local}) + \sigma(\text{neighbour}) + \sigma(\text{solvent}) \quad (5.2.50)$$

where $\sigma(\text{local})$ is the well-known sum of the paramagnetic and diamagnetic shieldings limited to the electrons of the atoms which include the magnetic nucleus. The local contribution has to be corrected with $\sigma(\text{neighbour})$, which arises from the interactions with the other atoms of the molecule. Finally, the liquid state NMR is usually performed on substances diluted in a solvent⁷, which, in turn, may affect the resulting shielding.

As far as the second contribution is concerned, if atoms are analysed on an individual basis, every nucleus is reasonably influenced by the circulating current induced in the *neighbouring* atoms. Consider an A-X group in a molecule: the currents induced in X by the external field give rise to a magnetic moment which can be expressed [53] as

$$\mathbf{m}_{\text{ind}}^x = \chi \mathbf{B}_0 \quad (5.2.51)$$

where χ is the magnetic susceptibility of X. The resulting magnetic field perceived by nucleus A can be computed similarly as done in the proof of Equation 5.1.1. The resulting isotropic chemical shielding is given by the McConnell equation [54]

$$\sigma(\text{neighbour}) = (\chi_{\parallel} - \chi_{\perp}) \frac{1 - 3 \cos^2(\theta)}{3r^3} \quad (5.2.52)$$

where θ is the angle between the direction of the induced moment $\mathbf{m}_{\text{ind}}^x$ and the A-X axis; r is the distance between the two nuclei and $(\chi_{\parallel} - \chi_{\perp})$ is the difference between the parallel and the perpendicular susceptibilities with respect to the symmetry axis of X [54]. Because of rapid tumbling in liquid solution, if X is magnetically isotropic, then $\chi_{\parallel} = \chi_{\perp}$ and $\sigma(\text{neighbour}) = 0$.

An interesting case occurs in **aromatic compounds**: the benzene ring, which, from the point of view of an atom bonded to it, can be regarded as single entity (as if it were the X atom of the previous discussion), has a strong magnetic susceptibility anisotropy.

⁷For instance, when optimizing the geometry of a molecule or when computing the NMR parameters with software like ORCA, it is always recommended to add a proper solvent, in order to obtain reliable results.

At first-order, it may be assumed that the π -electrons of the ring are free to circle around. When an external field is applied, an overall ring current arises, which is the origin of a magnetic field. The latter opposes the applied field at the centre of the nucleus (blue lines in Figure 5.8). Hence, hydrogen atoms which lie in the same plane of the ring are strongly deshielded. On the contrary, those which lie above or below, for instance as substituent groups, are shielded.

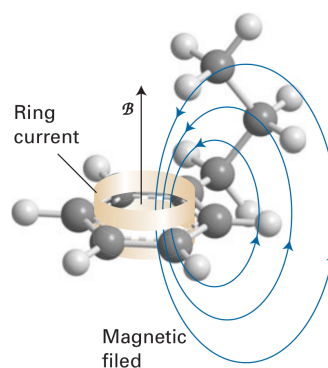


Figure 5.8: From [53].

Finally, as mentioned above, the presence of solvent molecules can vary the resulting field at one of the magnetic nuclei of interest. This effect can be a consequence of the field produced by strongly anisotropic solvent molecules (as aromatic compounds), or of some solute-solvent interactions (as hydrogen-bonds).

5.3 Indirect spin-spin coupling

Several experimental liquid state NMR spectra show the splitting of resonance lines, reported in Figure 5.9 for the ethanol, known as **fine structure**. The practical evidence reveals that the latter is independent of temperature and applied field, thus it cannot be a simple consequence of chemical shielding. Moreover, both the multiplicity of the line splitting and the relative intensities of a nucleus (for instance the H in CH₂ group) show a dependence on the z-component of the spin of the other species (as the H in CH₃ group). Finally, the frequency separations of adjacent lines $\Delta\omega^j$ in different species are identical. These properties led the first researchers to understand that this coupling must be related to the nuclear magnetic moments. However, it cannot be an effect of direct spin-spin coupling since it does not vanish in rapid tumbling molecules. Consequently, it must depend only on the relative orientation of the nuclear magnetic moments. Since the angle between two vectors is measured by their scalar product, the energy of the coupling must be

$$E_J \propto \mathbf{m}_1 \cdot \mathbf{m}_2 \quad (5.3.1)$$

The constant of proportionality is actually a 3×3 tensor known as the **J-coupling tensor** or **indirect coupling tensor** and defined as

$$\mathbf{J} = \begin{pmatrix} J_{xx} & J_{xy} & J_{xz} \\ J_{yx} & J_{yy} & J_{yz} \\ J_{zx} & J_{zy} & J_{zz} \end{pmatrix} \quad (5.3.2)$$

Since the latter is always measured in hertz, the corresponding Hamiltonian is

$$\mathcal{H}_J = \frac{2\pi}{\hbar} \mathbf{I}_1 \cdot \mathbf{J} \mathbf{I}_2 \quad (5.3.3)$$

In order to relate the theoretical computations of the J-coupling tensor to NMR experiments, it proves useful to define the so called **isotropic J-coupling** as the averaged trace of the coupling tensor

$$J = \frac{1}{3} \text{tr}(\mathbf{J}) = \frac{1}{3} (J_{xx} + J_{yy} + J_{zz}) \quad (5.3.4)$$

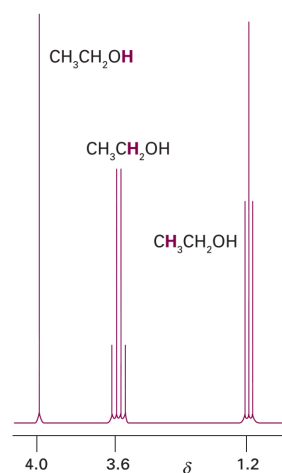


Figure 5.9: From [53].

and the Hamiltonian becomes

$$\mathcal{H}_J = \frac{2\pi J}{\hbar} \mathbf{I}_1 \cdot \mathbf{I}_2 = Q \mathbf{I}_1 \cdot \mathbf{I}_2 \quad (5.3.5)$$

It is clear that some configurations of the spin will increase the energy of the system, while others will decrease it, according to the sign of the J constant. To earn an intuitive understanding of the phenomenon, it is convenient to focus on the *weak coupling* case: consider two nuclei, A and X, whose relative coupling is much smaller than the difference between the respective resonance frequencies. In this case, as it will be clear in the following, the Hamiltonian can be approximated as

$$\mathcal{H}_J \sim \frac{2\pi J}{\hbar} \mathbf{I}_{zA} \cdot \mathbf{I}_{zX} \quad (5.3.6)$$

The energy eigenstates for a spin- $\frac{1}{2}$ system are

$$E_J = hJ m_I^A m_I^X = \pm \frac{hJ}{4} \quad (5.3.7)$$

It has to be pointed out that J-constant can be either

- Positive, if the **antiparallel** orientation of the two spins leads to a reduction of the system energy.
- Negative, if the **parallel** orientation of the two spins leads to a reduction of the system energy.

In Figure 5.10, an AX system is presented. In the absence of J-coupling, the four energy levels arise as a consequence of the Zeeman effect and depend on the orientation of the nuclear spins with respect to the externally applied field. Since it is a fundamental theoretical result that the allowed transitions have $\Delta m_I = 1$, when a transition of nucleus A takes place, nucleus X remains unchanged. The two possible transitions for the former are $|00\rangle \rightarrow |10\rangle$ and $|01\rangle \rightarrow |11\rangle$ and they require exactly the same amount of energy, that is, they are degenerate. Therefore, the A resonance consists of a single line, centred at the (chemically shifted) Larmor frequency and similarly for X. Conversely, when an indirect positive coupling is included, the antiparallel states $|01\rangle$ and $|10\rangle$ are lowered in energy of $-hJ/4$, while the parallel states $|00\rangle$ $|11\rangle$ show a $+hJ/4$ higher energy. It follows that, focusing again on the transitions of A, the $|00\rangle \rightarrow |10\rangle$ transition is lower in energy ($-hJ/2$) with respect to the $|01\rangle \rightarrow |11\rangle$ ($+hJ/2$). Hence, the A resonance

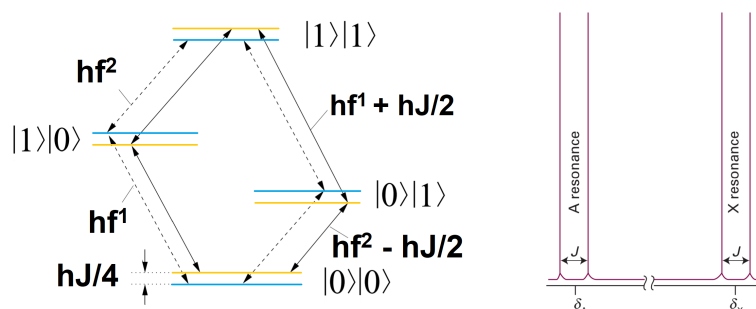


Figure 5.10: On the left, the energy levels for two uncoupled spins are reported in light blue, while those for two J-coupled spins are reported in orange. The Larmor frequencies of the two spins are f^1 and f^2 . On the right, the AX spectrum is shown [53].

consists of two lines, separated by J and centred on the chemically shifted Larmor frequency of A. The X resonance, also, consists of two lines, separated by J and centred on the chemically shifted Larmor frequency of X.

There are several interesting remarks which help in understanding first-order (i.e. weak coupling) spectra. First, *magnetically equivalent nuclei resonate like a single nucleus*. Two or more nuclei are said to be magnetically equivalent if they have the same resonant frequency and a single characteristic J-interaction with the nuclei of other groups. Magnetically equivalent nuclei are usually also chemically equivalent, but chemically equivalent nuclei are not necessarily magnetically equivalent. The point is that magnetically equivalent nuclei *can* couple together. However, the *relative* orientations of the nuclear spins cannot be changed, since it is not possible to address a single nucleus in magnetically equivalent groups. As a consequence, the J-coupling is undetectable (and cannot be “used” for quantum computation purposes).

Second, for spin- $\frac{1}{2}$ nuclei, the *multiplicity* of the line splitting is $n + 1$, where n is the number of nuclei in the neighbouring group. Different groups must be considered separately.

Third, the *relative intensities* of the resonant lines can be read directly from the Pascal triangle [53].

Example 5.3.1. Focus, for instance, on an AX₃ system. Considering the possible spin configurations of the X group reported in Table 5.2, it is clear that the A resonant lines must be 4, as expected since $n + 1 = 3 + 1 = 4$. Moreover, there are three combinations whose total spin is $-\frac{3}{2}$ or $+\frac{3}{2}$, while there is only one combination whose total spin is $-\frac{1}{2}$ or $+\frac{1}{2}$. Consequently, the relative intensities of A spectral lines must be 1:3:3:1, as expected from the Pascal triangle. Finally,

the X spectrum consists of two lines, because the the three magnetically equivalent X nuclei behave like a single nucleus.

Configuration	Total Spin	Combinations
$ 000\rangle$	$-\frac{1}{2}$	1
$ 001\rangle$ $ 010\rangle$ $ 100\rangle$	$-\frac{3}{2}$	3
$ 011\rangle$ $ 101\rangle$ $ 110\rangle$	$+\frac{3}{2}$	3
$ 111\rangle$	$+\frac{1}{2}$	1

Table 5.2: The allowed spin configurations of a X_3 magnetically equivalent nuclear group.



5.3.1 The origin of the J-coupling

It should be clear that the J-coupling phenomenon cannot be due to a direct magnetic interaction between nuclear spins since the latter averages to zero in rapid tumbling molecules. Indeed, it is an *indirect* coupling phenomenon mediated by the electrons: a nucleus somehow interacts with its electrons, these interact with the electrons of another nucleus, which, in turn, interact with their nucleus. The interaction orientation dependence is changed by the participation of electrons and an isotropic part of the coupling tensor which survives motional averaging in isotropic liquids is generated. The key point is to understand how the nucleus couples with the electrons via the so-called **hyperfine interactions**. The nuclear magnetic field can induce a magnetic field [58] in the electrons according to two main classes of phenomena:

- Electron spin polarization which occurs thanks to
 - Spin-dipole mechanism (SD).
 - Fermi contact mechanism (FC).
 - SD-FC cross term.
- Orbital ring current induction which occurs thanks to
 - Paramagnetic spin-orbital mechanism (PSO).
 - Diamagnetic spin-orbital mechanism (DSO).

Spin polarization The simple point-dipole approximation with which the nuclear magnetic field has been treated up to now is not satisfactory to describe the hyperfine interactions. Indeed, the electrons which have a finite probability of being located at the contact surface of the nucleus, that is the s-orbital electrons, can perceive the approximately uniform internal field of the nucleus (Figure 5.11). This gives rise to an electron spin polarization which is accounted for by the FC mechanism. Conversely, p, d, f-electrons see only the external field of the nucleus, which can be safely treated with the point dipole approximation. The consequent spin polarization is at the origin of the SD term. The main difference between FC and SD mechanism is that the former is described by an isotropic operator, while the latter by an anisotropic operator which must be isotropically averaged. Finally, the FC-SD term occurs when the FC mechanism on one nucleus is perceived via the SD mechanism by the second nucleus. This cross term usually

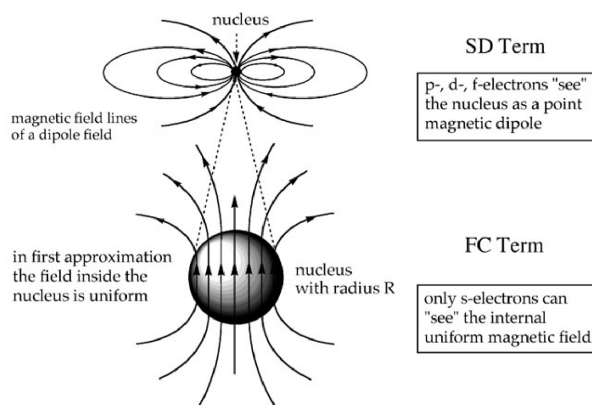


Figure 5.11: The nuclear field. From [59].

averages to zero in the computation of the isotropic J constant, but gives non-null contributions to the \mathbf{J} tensor [58].

Spin-orbit As the externally applied magnetic field causes electronic currents which modify the magnetic field perceived by the nucleus (chemical shielding), also the magnetic moment of the nucleus can induce electronic currents. According to the gauge choice, the induced current can be split into paramagnetic and diamagnetic contributions, giving rise, respectively, to the PSO and DSO terms.

Spin information transport As previously suggested, the magnetic field of the perturbing nucleus can induce either electronic currents or spin polarization in the electron system. Then, these local effects are transferred to other parts of the molecule, via chemical bonds. Finally, the responding nucleus perceives an extra magnetic field.

SD, PSO and DSO terms usually yield small contributions which are negligible for an intuitive understanding of the spin-spin coupling. Consequently, in this section, the focus is on the FC term, although some hints are given also on the SD term.

5.3.1.1 The spin-dipole mechanism

The SD mechanism is a simple direct dipolar interaction between the magnetic moment of the nucleus and of the electron, assuming that both behave as point magnetic dipoles and that they are far away from each other (s, d, f orbitals). An actual treatment of the spin-spin SD coupling requires the definition of an operator for each nucleus and a description of the interaction. Nevertheless, it is quite simple to understand why this contribution is very small without long calculations. The SD hyperfine Hamiltonian is obtained immediately from Equation 5.1.1, formally replacing the nuclear spin operator with the electron spin operator

$$\mathcal{H}_{SD} = \frac{\mu_0 g_e \gamma_e \gamma_n}{4\pi r^3} \left(\mathbf{s} \cdot \mathbf{I} - \frac{3(\mathbf{s} \cdot \mathbf{r})(\mathbf{r} \cdot \mathbf{I})}{r^2} \right) \quad (5.3.8)$$

where \mathbf{r} is the (not normalized) electron-nucleus position vector. Here too, the secular Hamiltonian in the presence of an external field applied along $\hat{\mathbf{z}}$ can be expressed as

$$\mathcal{H}_{SD} \sim \frac{\mu_0 g_e \gamma_e \gamma_n}{4\pi r^3} (1 - 3 \cos^2(\theta)) \mathbf{s}_z \cdot \mathbf{I}_z \quad (5.3.9)$$

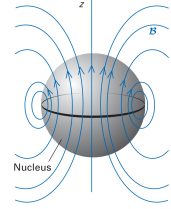
As known from the above discussion, the first-order correction to the energy is the average value of the Hamiltonian for the ground-state wavefunction. It is clear that for a spherically symmetric s-orbital

$$\left\langle \frac{1 - 3 \cos^2(\theta)}{r^3} \right\rangle = 0 \quad (5.3.10)$$

On the other hand, in non-s-orbitals, the expectation value is non zero. However, even if the SD interaction is non-zero for a specific relative orientation of the nuclear field and the electron orbital, when the molecule is allowed to freely tumble, then the average mean interaction is zero [34]. Hence, the spin-dipolar mechanism can be neglected in liquid-state NMR. A rigorous analysis of the small SD contribution to spin-spin coupling falls outside the scope of this research and can be found in [59].

5.3.1.2 The Fermi contact mechanism

The point magnetic dipole approximation is valid for all non-s-orbitals, since the probability to find a $l \neq 0$ electron *at* the nucleus is always zero. However, an **s-electron can be found at the nucleus**, which, consequently, cannot be regarded as dimensionless point. In this case, the nuclear magnetic moment can be thought to be originated from the circulation of a current in a loop whose radius is that of the nucleus itself. Close or inside the loop, the field is significantly different from that of a point dipole. The electron, then, perceives a non-zero average field. The Hamiltonian which describes the interaction, known as the Fermi *contact* Hamiltonian, is reported without providing a proof, which can be found in [34, 60]. Yet, some guesses can be advanced based on the physical background. One can expect that the Hamiltonian will depend on the relative orientation of the electron spin and the nuclear spin and, thus, be proportional to their scalar product. Moreover, it shall include a “contact term”.



$$\mathcal{H}_{FC} = -\frac{2\mu_0 g_e \gamma_e \gamma_n \delta(\mathbf{r}_n)}{3} \mathbf{s} \cdot \mathbf{I} \quad (5.3.11)$$

where $\Delta(\mathbf{r}_n)$ is the Dirac delta distribution and it represents the aforementioned contact term. As a matter of fact, the procedure requires the integration of the Dirac distribution which samples the electron wavefunction at the nucleus ($r_n = 0$):

$$E^{(1)} = -\frac{2\mu_0 g_e \gamma_e \gamma_n |\psi_0^e(0)|^2}{3} \langle 0 | \mathbf{s} \cdot \mathbf{I} | 0 \rangle \quad (5.3.12)$$

where ψ_0^e is the unperturbed total electron ground state wavefunction, $|\psi_0^e(0)|^2$ is the probability to find the electron *at* the nucleus and $|0\rangle$ is the *total* unperturbed ground state (see the proof for clarification).

Proof. In order to compute the first-order correction to the energy, the theory outlined in section §5.2.2.1 can be exploited. However, differently from the derivation of chemical shielding, the complete Hamiltonian of the system must take into account the electron Hamiltonian \mathcal{H}_e , the nuclear Hamiltonian \mathcal{H}_n and the interaction hyperfine Hamiltonian \mathcal{H}_{en} [42], which is here assumed to be limited to the FC term:

$$\mathcal{H} = \mathcal{H}_e + \mathcal{H}_n + \mathcal{H}_{en}$$

Since the hyperfine structure of the energy levels, arising from the **nuclear spins**, is here under investigation, *nuclear spin variables must be included* in the wavefunction and in the basis functions. In particular, assuming a weak interaction, the complete unperturbed wavefunction can be written as the product of the electron and the nuclear wavefunctions

$$\psi = \psi^e \psi^n$$

This wavefunction would be the exact one if \mathcal{H}_{en} were zero. The computation of the first-order correction to the energy requires to average the first-order perturbation Hamiltonian on the total ground state

$$E^{(1)} = \langle \psi_0^e \psi_0^n | \mathcal{H}_{FC} | \psi_0^n \psi_0^e \rangle$$

where the subscript zero refers to the ground state. The latter can be rewritten, according to [61, 34], making explicit the integration of the delta distribution

$$E^{(1)} = -\frac{2\mu_0 g_e \gamma_e \gamma_n}{3} \left(\int \psi_0^{e*} \delta(\mathbf{r}_n) \psi_0^e d\tau \right) \langle \psi_0^e \psi_0^n | \mathbf{s} \cdot \mathbf{I} | \psi_0^n \psi_0^e \rangle \quad (5.3.13)$$

Finally, denoting with $|0\rangle$ the *total* unperturbed ground state, Equation 5.3.12 is trivially obtained. \square

Note that in the final expression for the first-order correction to the energy, the ground state vector $|0\rangle$ acts only on the spin state. In this respect, it proves useful to introduce⁸ an *effective* \mathcal{H}^s Hamiltonian which contains only (electron and nuclear) spin operators: the **spin Hamiltonian**. The latter describes a kind of *model* spin system, whose behaviour obeys to the eigenvalue equation

$$\mathcal{H}^s \zeta = E \zeta \quad (5.3.14)$$

where ζ is the spin wavefunction. The spin Hamiltonian can be regarded as a *simplification of the actual system Hamiltonian*, from which all the complexities associated with electronic motion have been dropped, which is convenient to justify the experimental results, as seen for the NMR case.

In particular, the same first-order energy of Equation 5.3.12 is obtained if the following term is added to the spin Hamiltonian

$$\mathcal{H}_{FC}^s = -\frac{2\mu_0 g_e \gamma_e \gamma_n |\psi_0(0)|^2}{3} \mathbf{s} \cdot \mathbf{I} \quad (5.3.15)$$

⁸Actually, the spin Hamiltonian has already been adopted in the previous chapters. Indeed, while discussing NMR, the focus has always been on a Hamiltonian limited to the spin.

In fact, assuming now that $|0\rangle$ is the spin-only ground state, the first-order correction to the energy is simply

$$E^{(1)} = \langle 0 | \mathcal{H}_{FC}^s | 0 \rangle = -\frac{2\mu_0 g_e \gamma_e \gamma_n |\psi_0(0)|^2}{3} \langle 0 | \mathbf{s} \cdot \mathbf{I} | 0 \rangle \quad (5.3.16)$$

If the external field is very strong so that only the z-component is relevant, the previous expression can be rewritten as

$$E^{(1)} \sim +\frac{2\mu_0 g_e \mu_B \mu_N |\psi_0(0)|^2}{3} m_s m_I \quad (5.3.17)$$

The energy, then, is **minimized** if the nuclear spin and the electron spin are **antiparallel**.

5.3.1.3 The computation of the \mathbf{J} constant

As previously highlighted, there are several indirect mechanisms which can contribute to the nuclear coupling. In this section, the focus is on the Fermi contact mechanism for an AX system, bonded by a couple of electrons. This simplified case allows the understanding of the physical phenomenon at an intuitive level, adopting the so-called Dirac vector model. First, there is a hyperfine interaction

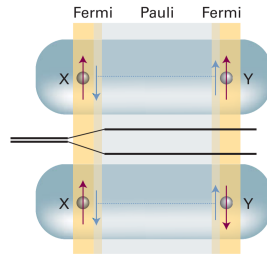


Figure 5.12: The electron mediated indirect coupling between two neighbouring nuclei, considering exclusively the Fermi contact contribution. From [53].

according to the Fermi contact mechanisms between the first nucleus and the corresponding electron. The antiparallel arrangement of the two spins is energetically favoured. Then, because of the Pauli exclusion principle, the two bonding electron spins are forced to have opposite orientations (actually, the spin information transport occurs via exchange interactions [59]). Finally, the second nuclear spin has an energy advantage to be antiparallel to the electron spin. Consequently, the antiparallel orientation of the nuclear spins lies lower in energy, as shown in Figure 5.12 and the FC mechanism contribution to the total \mathbf{J} -coupling is usually positive. Note that, as previously suggested, the indirect spin-spin coupling causes an energy difference between the *relative orientations* of the nuclear spins. The pq -component of the \mathbf{J} tensor due to the FC term only can be written as

$$J_{pq} = -\frac{8}{9}\mu_0^2 g_e^2 \gamma_e^2 \gamma_A \gamma_B \sum_{n \neq 0} \frac{1}{\Delta E_{n0}} \left\langle 0 \left| \sum_{i=1}^N \mathbf{s}_{pi} \delta(\mathbf{r}_{pi}^A) \right| n \right\rangle \left\langle n \left| \sum_{i=1}^N \mathbf{s}_{qi} \delta(\mathbf{r}_{qi}^X) \right| 0 \right\rangle \quad (5.3.18)$$

and the isotropic constant is

$$J = \frac{1}{3} \text{tr}(\mathbf{J}) \quad (5.3.19)$$

where $|n\rangle$ denotes an unperturbed (i.e. without considering nuclear spin) electron state, \mathbf{s}_{pi} is the p -component of the i -th electron spin operator and \mathbf{r}_{qi}^X is the q -component of the vector from nucleus X to electron i .

Proof. Defining

$$\mathbf{A} = \sum_i \mathbf{s}_i \delta(\mathbf{r}_i^A) \quad \mathbf{X} = \sum_i \mathbf{s}_i \delta(\mathbf{r}_i^X)$$

and considering Equation 5.3.11, the contact interaction Hamiltonian for the two nuclei is

$$\mathcal{H}^{(1)} = -\frac{2}{3}\mu_0 g_e \gamma_e [\gamma_A \mathbf{I}_A \cdot \mathbf{A} + \gamma_X \mathbf{I}_X \cdot \mathbf{X}] \triangleq -C [\gamma_A \mathbf{I}_A \cdot \mathbf{A} + \gamma_X \mathbf{I}_X \cdot \mathbf{X}]$$

The first-order correction to the energy is zero since in *singlet-state molecules*, that is, in molecules where all electrons are coupled and, so, the overall spin is null, the expectation value of the spin operator is zero. Conversely, the second-order correction is, in general, non zero and can be evaluated from Equation 5.2.23, taking into consideration $\mathcal{H}^{(1)}$ only. Once more, one has to use both the electron and the nuclear wavefunctions. In particular, let $|\psi_0^e\rangle$ be the many electrons unperturbed ground state with energy E_0^e and $|\psi_m^e\rangle$ a corresponding excited state with energy E_m^e , while the unperturbed nuclear ground state is denoted as $|\psi_0^n\rangle$ and similarly the excited states. Thus according to [42, 61]

$$E_0^{(2)} = \sum_{k,m \neq 0} \frac{\langle \psi_m^e \psi_k^n | \mathcal{H}^{(1)} | \psi_0^e \psi_0^n \rangle \langle \psi_0^e \psi_0^n | \mathcal{H}^{(1)} | \psi_m^e \psi_k^n \rangle}{(E_0^e - E_m^e) + (E_0^n - E_k^n)}$$

Since

$$(E_0^e - E_m^e) \gg (E_0^n - E_k^n)$$

then

$$E_0^{(2)} \sim \sum_{k,m \neq 0} \frac{\langle \psi_m^e \psi_k^n | \mathcal{H}^{(1)} | \psi_0^e \psi_0^n \rangle \langle \psi_0^e \psi_0^n | \mathcal{H}^{(1)} | \psi_m^e \psi_k^n \rangle}{E_0^e - E_m^e}$$

Replacing the first-order Hamiltonian

$$E_0^{(2)} = C^2 \sum_{k,m \neq 0} \frac{1}{E_0^e - E_m^e} \langle \psi_m^e \psi_k^n | \gamma_A \mathbf{I}_A \cdot \mathbf{A} + \gamma_X \mathbf{I}_X \cdot \mathbf{X} | \psi_0^e \psi_0^n \rangle \cdot \langle \psi_0^e \psi_0^n | \gamma_A \mathbf{I}_A \cdot \mathbf{A} + \gamma_X \mathbf{I}_X \cdot \mathbf{X} | \psi_m^e \psi_k^n \rangle$$

The numerator N can be rewritten as

$$N = [\langle \psi_m^e \psi_k^n | \gamma_A \mathbf{I}_A \cdot \mathbf{A} | \psi_0^e \psi_0^n \rangle + \langle \psi_m^e \psi_k^n | \gamma_X \mathbf{I}_X \cdot \mathbf{X} | \psi_0^e \psi_0^n \rangle] \cdot [\langle \psi_0^e \psi_0^n | \gamma_A \mathbf{I}_A \cdot \mathbf{A} | \psi_m^e \psi_k^n \rangle + \langle \psi_0^e \psi_0^n | \gamma_X \mathbf{I}_X \cdot \mathbf{X} | \psi_m^e \psi_k^n \rangle]$$

According to [42], the terms which are quadratic in \mathbf{I}_A or \mathbf{I}_X represent the energy changes if one or the other nuclei were the only one, while the terms bilinear in \mathbf{I}_A and \mathbf{I}_X represent the energy changes due to the interaction between the two nuclei. Since the aim is to determine the interaction energy, the quadratic terms are dropped and the numerator becomes

$$N = \langle \psi_m^e \psi_k^n | \gamma_A \mathbf{I}_A \cdot \mathbf{A} | \psi_0^e \psi_0^n \rangle \langle \psi_0^e \psi_0^n | \gamma_X \mathbf{I}_X \cdot \mathbf{X} | \psi_m^e \psi_k^n \rangle + \langle \psi_0^e \psi_0^n | \gamma_A \mathbf{I}_A \cdot \mathbf{A} | \psi_m^e \psi_k^n \rangle \langle \psi_m^e \psi_k^n | \gamma_X \mathbf{I}_X \cdot \mathbf{X} | \psi_0^e \psi_0^n \rangle$$

Since \mathbf{I}_A and \mathbf{A} are Hermitian operators and do commute, their inner product is still Hermitian and similarly for \mathbf{I}_X and \mathbf{X} . Hence, the second term in the previous equation is simply the complex conjugate of the first one. If the wavefunctions are real, then

$$N = 2 \langle \psi_0^e \psi_0^n | \gamma_A \mathbf{I}_A \cdot \mathbf{A} | \psi_m^e \psi_k^n \rangle \langle \psi_m^e \psi_k^n | \gamma_X \mathbf{I}_X \cdot \mathbf{X} | \psi_0^e \psi_0^n \rangle$$

Developing the inner product, the matrix elements separate into a product of electronic and nuclear factors [42, 61]

$$N = 2\gamma_A\gamma_X \sum_{p,q} \langle \psi_0^e | \mathbf{A}_p | \psi_m^e \rangle \langle \psi_m^e | \mathbf{X}_q | \psi_0^e \rangle \langle \psi_0^n | \mathbf{I}_{Ap} | \psi_k^n \rangle \langle \psi_k^n | \mathbf{I}_{Xq} | \psi_0^n \rangle$$

where p and q denote the Cartesian coordinates. Next, the second-order correction to the energy is written as

$$\begin{aligned} E_0^{(2)} &= 2C^2\gamma_A\gamma_X \sum_{p,q} \sum_{m \neq 0} \frac{\langle \psi_0^e | \mathbf{A}_p | \psi_m^e \rangle \langle \psi_m^e | \mathbf{X}_q | \psi_0^e \rangle}{E_0^e - E_m^e} \sum_k \langle \psi_0^n | \mathbf{I}_{Ap} | \psi_k^n \rangle \langle \psi_k^n | \mathbf{I}_{Xq} | \psi_0^n \rangle \\ &= 2C^2\gamma_A\gamma_X \sum_{p,q} \sum_{m \neq 0} \frac{\langle \psi_0^e | \mathbf{A}_p | \psi_m^e \rangle \langle \psi_m^e | \mathbf{X}_q | \psi_0^e \rangle}{E_0^e - E_m^e} \langle \psi_0^n | \mathbf{I}_{Ap} \mathbf{I}_{Xq} | \psi_0^n \rangle \end{aligned}$$

where the second line follows from the hypothesis that the set of nuclear spin states is complete [61]. It is trivial to realize that the same energy is obtained as

a first-order correction of an extra term in the spin effective Hamiltonian

$$\mathcal{H}^s = -\frac{8}{9}\mu_0^2 g_e^2 \gamma_e^2 \gamma_A \gamma_X \sum_{p,q} \mathbf{I}_{A_p} \mathbf{I}_{X_q} \left[\sum_{m \neq 0} \frac{\langle \psi_0^e | \mathbf{A}_p | \psi_m^e \rangle \langle \psi_m^e | \mathbf{X}_q | \psi_0^e \rangle}{E_m^e - E_0^e} \right]$$

The interesting point is that the term inside the square bracket is actually a constant. In other words, the J-coupling tensor when only the FC term is considered must be a constant. Indeed, it can be shown [62] that the spin vectors embedded in \mathbf{A} and \mathbf{X} operators must have the same Cartesian component. In order to simplify the notation, the electron ground state can be identified with $|0\rangle$ with energy E_0 and similarly for the excited states. According to [42], the previous equation becomes

$$\mathcal{H}^s = -\frac{8}{9}\mu_0^2 g_e^2 \gamma_e^2 \gamma_A \gamma_X \sum_{n \neq 0} \mathbf{I}_A \cdot \frac{\langle 0 | \mathbf{A} | n \rangle \langle n | \mathbf{X} | 0 \rangle}{E_n - E_0} \cdot \mathbf{I}_X$$

Replacing the expressions of \mathbf{A} and \mathbf{X} and keeping in mind the above mentioned property of their Cartesian components, the xx , yy and zz -components of the J-coupling tensor can be computed. Moreover, the latter turns out to be isotropic ($J_{xx} = J_{yy} = J_{zz}$) [58, 62]. As a consequence, the isotropic constant is [34, 59]

$$J = -\frac{8}{27}\mu_0^2 g_e^2 \gamma_e^2 \gamma_A \gamma_X \sum_{n \neq 0} \frac{1}{\delta E_{n0}} \left\langle 0 \left| \sum_{i=1}^N \mathbf{s}_i \delta(\mathbf{r}_i^A) \right| n \right\rangle \left\langle n \left| \sum_{i=1}^N \mathbf{s}_i \Delta(\mathbf{r}_i^X) \right| 0 \right\rangle$$

□

5.3.1.4 Hints on the molecular orbital interpretation of FC J-coupling

In molecular orbital theory, the electrons do not belong to a specific atom or bond but they spread throughout the whole molecule. If \mathcal{H} is the electronic Hamiltonian of the molecule, the molecular orbitals (MO) Ψ could in principle be found as the solutions of the Schrödinger equation

$$\mathcal{H}\Psi = E\Psi \quad (5.3.20)$$

However, an analytic solution can be found only for very simple cases. Hence an approximation must be introduced. A widely adopted one prescribes to write a molecular orbital as a linear combination of atomic orbitals (LCAO-MO)

$$\Psi = \sum_i c_i \phi_i \quad (5.3.21)$$

where the atomic orbitals (AO) ϕ_i constitute a basis set for the calculation of MOs. For instance, if an electron can be found in the AO ϕ_A of nucleus A and ϕ_B of B, then the corresponding MO is a superposition of the two:

$$\Psi_{\pm} = N(\phi_A \pm \phi_B) \quad (5.3.22)$$

where N is a normalization constant. If the + sign is chosen in the superposition, then

$$\Psi_+ = N(\phi_A + \phi_B) \quad (5.3.23)$$

is a **bonding** orbital, since the probability density of the electron is

$$|\Psi_+|^2 = N^2(\phi_A^2 + \phi_B^2 + 2\phi_A\phi_B) \quad (5.3.24)$$

where the $+2\phi_A\phi_B$ overlap density increases the probability of finding the electron in the internuclear region. In other words, the AOs overlap with constructive interference.

Conversely,

$$\Psi_- = N(\phi_A - \phi_B) \quad (5.3.25)$$

is an **antibonding** orbital, since the probability density of the electron is

$$|\Psi_-|^2 = N^2(\phi_A^2 + \phi_B^2 - 2\phi_A\phi_B) \quad (5.3.26)$$

where the $-2\phi_A\phi_B$ overlap density decreases the probability of finding the electron

in the internuclear region. In other words, the AOs overlap with destructive interference. It turns out the antibonding orbitals lay higher in energy than bonding orbitals.

In general, from N atomic orbitals, N molecular orbitals are obtained, which are schematically arranged according to their energy. In particular, the highest occupied molecular orbital is known as HOMO, while the lowest unoccupied molecular orbital is named LUMO. They are the **frontier orbitals**.

Finally, a molecular orbital that has cylindrical symmetry and zero orbital angular momentum around the internuclear axis is a σ orbital, while MOs which have one unit of orbital angular momentum around the internuclear axis are named π orbitals. At an intuitive level, σ -MOs are similar to s-AOs, while π -MOs to p-AOs.

It turns out [58] that instead of using a sum over excited state wavefunction to represent the perturbation of the ground state, as in Equation 5.3.27, one can write a mixing of unoccupied and occupied MOs

$$J_{pq} = \frac{8}{9} \operatorname{Re} \left\{ \sum_n^{\text{occ}} \sum_m^{\text{un}} \frac{\mu_0^2 g_e^2 \gamma_e^2 \gamma_A \gamma_B}{E_n - E_m} \left\langle \Psi_n \left| \sum_{i=1}^N \mathbf{s}_{pi} \Delta(\mathbf{r}_{pi}^A) \right| \Psi_m \right\rangle \left\langle \Psi_m \left| \sum_{i=1}^N \mathbf{s}_{qi} \Delta(\mathbf{r}_{qi}^X) \right| \Psi_n \right\rangle \right\} \quad (5.3.27)$$

where Ψ_n are the occupied orbitals with energy E_n , Ψ_m the unoccupied orbitals with energy E_m . Similarly to the excited states in the sum over states equation, the mixing of unoccupied orbitals in the occupied orbitals is a tool to describe the deformations spin polarizations and orbital currents cause to the occupied orbitals.

A term like

$$\left\langle \Psi_n \left| \sum_{i=1}^N \mathbf{s}_{pi} \Delta(\mathbf{r}_{pi}^A) \right| \Psi_m \right\rangle \quad (5.3.28)$$

samples the value of the product between occupied and unoccupied orbitals at the A nucleus. At this point, it is clear that, since an LCAO-MO is written as a combination of AOs and since only s-AOs have a non zero probability density at the nucleus, only MOs with a remarkable **s character on both nuclei** can contribute to the FC coupling. Moreover, the intensity of the coupling is inversely proportional to the energy gap between the couple of occupied-unoccupied MOs.

Hence, a large coupling is expected if both low-lying unoccupied σ MOs and high-lying occupied σ MOs are available.

The J constant contribution arising from each occupied MO can be simply expressed as

$$J_n = \sum_m^{un} J_{mn} \quad (5.3.29)$$

so that the overall J-coupling constant is

$$J = \sum_n^{occ} J_n \quad (5.3.30)$$

Instead of using canonical MOs, it proves useful to give a pictorial insight the adoption of **localized molecular orbitals** (LMOs), which can be shown to be fully equivalent to canonical MOs and which can be constructed from the latter by linear operations. LMOs are the theoretical representation of bonds and core orbitals and are closer to the standard chemical intuition. Moreover, differently from canonical MOs, for LMOs the total J constant is

$$J = \sum_{ab} J_{ab} = \sum_a J_a \quad (5.3.31)$$

where a and b refer to a pair of LMOs and $J_a = \sum_b J_{ab}$. This means that the summation only involves occupied orbitals since the contributions from unoccupied orbitals are already taken into consideration by each term [58].

Example 5.3.2. Consider the ethyne molecule C_2H_2 . The canonical MOs are computed resorting on ORCA at BP86 level of theory with def2-TZVPP basis set, according to [58]. Then, the LMOs reported in Figure 5.13 are constructed from the canonical MOs adopting the Intrinsic Atomic Orbitals and Intrinsic Bond Orbitals (IAOIBO) method which does not allow any $\sigma - \pi$ mixing, to get a simple pictorial representation very close to the chemical intuition. The obtained LMOs are visualized thanks to Avogadro [63].

It is known from fundamental chemical theory that the carbon presents an sp-hybridization in C_2H_2 molecule. Thus, each carbon atom is expected to use an sp-orbital to bond to the hydrogen atom and the other sp-orbital and the two non-hybrid p-orbitals to bond to the other carbon atom. This expectation is met by the chosen MO decomposition: HOMO–6 and HOMO–5 are the core 1s orbitals; HOMO–4 is the σ -MO originated by the superposition of the two sp-AOs; HOMO–3 and HOMO–1 are the π -MOs originated by the superposition

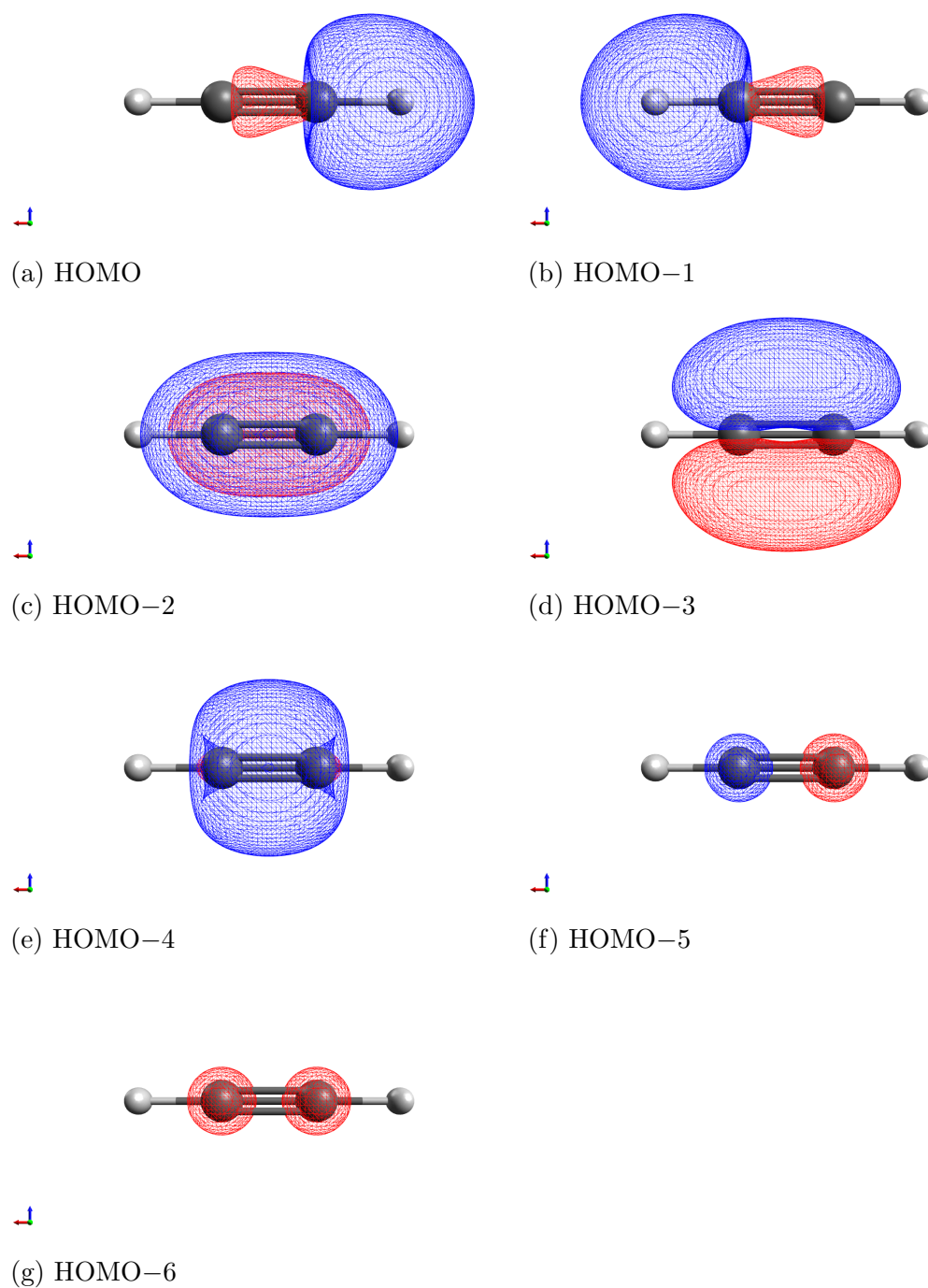


Figure 5.13: The occupied LMOs of C_2H_2 plotted with $\pm 0.060 \sqrt{\frac{e}{a_0^3}}$ isosurface.

of the four p-AOs; finally, HOMO-6 and HOMO-5 are the σ -MOs originated by the superposition of a carbon sp-AO and a hydrogen s-orbital.

As expected from the previous discussion and as reported in [58], the main contribution to J-coupling arises from the σ HOMO-4 orbital, since it has a large

s-character on both nuclei. On the other hand, HOMO–3 and HOMO–2, being π -orbitals and having zero s-character, do not contribute to the FC mechanism. Another interesting result is that HOMO–1 and HOMO yield a negative contribution. A possible justification is that the carbon atoms have to share some of their electrons to the C–H bonds, which, consequently, cannot participate to the C–C coupling. Finally, also HOMO–6 and HOMO–5 give a small contribution, which cannot be intuitively explained, being a consequence of the fact that, since all LMOs are mutually orthogonal, each of them must participate in the J-coupling [58].

In conclusion, the analysis of J-coupling from ethyne to ethene and ethane shows a strongly decreasing trend. The physical justification has to be looked for in two concomitant phenomena. First, the C–C distances increase. Second, there is a reduction of the s-character in the σ orbital, due to a variation of the carbon hybridization from sp to sp^2 to sp^3 . \triangle

5.3.1.5 The transmission of coupling

The previous discussion focuses on the coupling mechanism only between neighbouring nuclei. However, the experimental evidence shows that the coupling can be transmitted through more than one bond and even through non-magnetic nuclei. If a detailed discussion would be quite involved, a simple intuition can be earned considering the case reported in Figure 5.14. Suppose that the Y nucleus

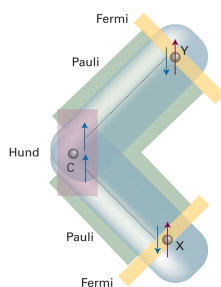


Figure 5.14: The transmission of the J-coupling. From [53].

has pointing-up spin $|\uparrow\rangle$. It polarizes its electron through a hyperfine interaction and, consequently, the latter is likely to be $|\downarrow\rangle$. Then, a $|\uparrow\rangle$ spin is likely to be found near the non-magnetic nucleus C. Because of Hund's rule (section §3.2.2.1), the most energetically favourable arrangement for the electron of the neighbouring bond is $|\uparrow\rangle$. It follows that the X nucleus minimizes the overall energy if it has a $|\uparrow\rangle$ spin. Note that, in this case, the J-coupling is negative.

Part III

Physical implementation of an NMR quantum computer

Chapter 6

The NMR quantum computer

The qubits can be encoded on several quantum systems. The main requirements are the possibility of characterizing them and manipulating them through an external perturbation, or, in other words, there shall exist a physical procedure to prepare the qubits and control them in order to perform the intended quantum calculation. Moreover, the physical representation must be unique and the relaxation and decoherence time constants shall be sufficiently long to allow the execution of quantum algorithms. Finally, techniques to initialize the system and measure the outcomes must be known. The nuclear magnetic system arises as a spontaneously suitable solution, able to satisfy the requirements. An isolated spin- $\frac{1}{2}$ in a static magnetic field is a natural implementation of a qubit. Thanks to the Zeeman effect, two well-defined energy eigenstates $|\uparrow\rangle$ and $|\downarrow\rangle$ arise, which can be associated with the quantum states $|0\rangle$ and $|1\rangle$, respectively. Diamagnetic molecules with magnetic nuclei can be exploited as quantum registers, as $^{13}\text{CHCl}_3$. The ^{13}C and ^1H interacting nuclear spins can be associated with two qubits. This chapter aims to outline how given such a system, described by a system Hamiltonian $\mathcal{H}_{\text{sys}} = \mathcal{H}_0 + \mathcal{H}_{\text{int}}$ and a control Hamiltonian \mathcal{H}_r , a desired unitary transformation U can be efficiently implemented. The task is to find the control parameters $\eta(t)$ in the total Hamiltonian $\mathcal{H} = \mathcal{H}_{\text{sys}} + \mathcal{H}_r$ such that the time development operator

$$U[\eta(t)] = \mathcal{T} \exp \left[-\frac{i}{\hbar} \int_0^\tau \mathcal{H}(\eta(t)) dt \right] = e^{-i \frac{\mathcal{H}(\eta(t_n))}{\hbar} \Delta t_n} \dots e^{-i \frac{\mathcal{H}(\eta(t_1))}{\hbar} \Delta t_1} \quad (6.0.1)$$

where \mathcal{T} is the time-ordered product and the control parameters are assumed to be piecewise constant.

6.1 The Hamiltonian for weakly coupled spins

Since every non trivial quantum algorithm requires at least two qubits, it is fundamental to describe the behaviour of molecules with **two coupled spins**. A typical NMR experiment is carried out on a macroscopic number ($\sim 10^{20}$) of liquid-state molecules in thermal equilibrium. Since each molecule is free to rotate with respect to the other molecules in the sample, the intramolecular interactions average to zero. As far as the intermolecular interactions are concerned, it is known from chapter 5 that short-range direct dipolar coupling averages to zero because of the translational motion of molecules. It follows that most liquid-state substances present only chemical shielding and J-coupling. Hence, the internal Hamiltonian is simply

$$\mathcal{H}_{\text{int}} = \frac{2\pi J}{\hbar} \sum_{k=x,y,z} \mathbf{I}_k \otimes \mathbf{I}_k \quad (6.1.1)$$

and the total Hamiltonian is

$$\mathcal{H} = \mathcal{H}_{\text{sys}} + \mathcal{H}_{r,1} + \mathcal{H}_{r,2} \quad (6.1.2)$$

where

$$\mathcal{H}_{\text{sys}} = -\omega_{0,1} \mathbf{I}_z \otimes \mathbb{I} - \omega_{0,2} \mathbb{I} \otimes \mathbf{I}_z + \frac{2\pi J}{\hbar} \sum_{k=x,y,z} \mathbf{I}_k \otimes \mathbf{I}_k \quad (6.1.3)$$

assuming that $\omega_{0,1}$ and $\omega_{0,2}$ are the **chemically shifted** Larmor frequencies. As far as the control Hamiltonian is concerned, assume that there are two oscillating RF fields along $-\hat{x}$ with amplitudes $2B_{r,1}$ and $2B_{r,2}$ and frequencies $\omega_{r,1}$ and $\omega_{r,2}$. The corresponding Hamiltonians are

$$\begin{aligned} \mathcal{H}_{r,1} &= +2 \cdot \omega_{*,1} \cos(\omega_{r,1}t - \phi_1) \left(\mathbf{I}_x \otimes \mathbb{I} + \frac{\gamma_2}{\gamma_1} \mathbb{I} \otimes \mathbf{I}_x \right) \\ \mathcal{H}_{r,2} &= +2 \cdot \omega_{*,2} \cos(\omega_{r,2}t - \phi_2) \left(\frac{\gamma_1}{\gamma_2} \mathbf{I}_x \otimes \mathbb{I} + \mathbb{I} \otimes \mathbf{I}_x \right) \end{aligned} \quad (6.1.4)$$

For the same reasons presented for the analysis of non interacting spins, it is convenient to describe the system using the concept of the rotating frame again. Actually, now it is mandatory to introduce two independent rotating frames, at frequencies ω_1 and ω_2 . By analogy with Equation 4.1.29, the operator which describes the transformation to the two rotating frames is

$$U_R = \exp\left(-i\frac{\omega_1\boldsymbol{\sigma}_z}{2}t\right) \otimes \exp\left(-i\frac{\omega_2\boldsymbol{\sigma}_z}{2}t\right) \quad (6.1.5)$$

and, as shown for Equation 4.1.31, the rotating frame Hamiltonian is

$$\tilde{\mathcal{H}} = \mathbf{U}_R \mathcal{H} \mathbf{U}_R^\dagger - i\hbar \mathbf{U}_R \frac{d\mathbf{U}_R^\dagger}{dt} = \mathbf{U}_R (\mathcal{H}_{\text{sys}} + \mathcal{H}_{r,1} + \mathcal{H}_{r,2}) \mathbf{U}_R^\dagger - i\hbar \mathbf{U}_R \frac{d\mathbf{U}_R^\dagger}{dt} \quad (6.1.6)$$

At this point it is necessary to differentiate the analysis between two types of molecules with multiple spins: heteronuclear molecules and homonuclear molecules. The former are easier to control, but the achievable number of qubits is limited by technical NMR limitations [45].

6.1.1 Heteronuclear molecules

In heteronuclear molecules, the difference in the Larmor frequencies $\Delta\omega_0 = \omega_{0,2} - \omega_{0,1}$ is large and allows to easily address individual spins. Without loss of generality, in the following it is always assumed that $\omega_{0,2} > \omega_{0,1}$. Assuming that the frequency of each rotating frame is equal to the corresponding RF field frequency $\omega_i = \omega_{r,i}$, it follows that

$$\mathbf{U}_R \mathcal{H}_{\text{sys}} \mathbf{U}_R^\dagger - i\hbar \mathbf{U}_R \frac{d\mathbf{U}_R^\dagger}{dt} \sim (\omega_{r,1} - \omega_{0,1}) \mathbf{I}_z \otimes \mathbb{I} + (\omega_{r,2} - \omega_{0,2}) \mathbb{I} \otimes \mathbf{I}_z + \frac{2\pi J}{\hbar} \mathbf{I}_z \otimes \mathbf{I}_z \quad (6.1.7)$$

Proof. The first step is the computation of the derivative of the \mathbf{U}_R operator:

$$\begin{aligned} \frac{d\mathbf{U}_R^\dagger}{dt} &= \frac{d}{dt} \left[\exp\left(i\frac{\omega_1 \sigma_z}{2} t\right) \otimes \exp\left(i\frac{\omega_2 \sigma_z}{2} t\right) \right] \\ &= i\frac{\omega_1 \sigma_z}{2} \exp\left(i\frac{\omega_1 \sigma_z}{2} t\right) \otimes \exp\left(i\frac{\omega_2 \sigma_z}{2} t\right) + \exp\left(i\frac{\omega_2 \sigma_z}{2} t\right) \otimes i\frac{\omega_1 \sigma_z}{2} \exp\left(i\frac{\omega_2 \sigma_z}{2} t\right) \end{aligned}$$

then

$$\begin{aligned} -i\hbar \mathbf{U}_R \frac{d\mathbf{U}_R^\dagger}{dt} &= \omega_1 \mathbf{I}_Z e^{-i\frac{\omega_1 \sigma_z}{2} t} e^{+i\frac{\omega_1 \sigma_z}{2} t} \otimes e^{-i\frac{\omega_2 \sigma_z}{2} t} e^{+i\frac{\omega_2 \sigma_z}{2} t} + \\ &\quad \omega_2 e^{-i\frac{\omega_1 \sigma_z}{2} t} e^{+i\frac{\omega_1 \sigma_z}{2} t} \otimes \mathbf{I}_Z e^{-i\frac{\omega_2 \sigma_z}{2} t} e^{+i\frac{\omega_2 \sigma_z}{2} t} = \omega_1 \mathbf{I}_Z \otimes \mathbb{I} + \omega_2 \mathbb{I} \otimes \mathbf{I}_Z \end{aligned}$$

since \mathbf{I}_z obviously commutes with itself. Next

$$\begin{aligned} \mathbf{U}_R \mathcal{H}_{\text{sys}} \mathbf{U}_R^\dagger &= -\omega_{0,1} \mathbf{I}_z \otimes \mathbb{I} - \omega_{0,2} \mathbb{I} \otimes \mathbf{I}_z + \frac{2\pi J}{\hbar} \mathbf{I}_z \otimes \mathbf{I}_z \\ &\quad e^{-i\frac{\omega_1 \sigma_z}{2} t} \otimes e^{-i\frac{\omega_2 \sigma_z}{2} t} \left(\frac{2\pi J}{\hbar} \sum_{k=x,y} \mathbf{I}_k \otimes \mathbf{I}_k \right) e^{+i\frac{\omega_1 \sigma_z}{2} t} \otimes e^{+i\frac{\omega_2 \sigma_z}{2} t} \end{aligned}$$

The last term can be rewritten exploiting the useful properties presented in the

proof of Equation 4.1.33:

$$\begin{aligned}
 & e^{-i\frac{\omega_1\sigma_z}{2}t}\mathbf{I}_xe^{+i\frac{\omega_1\sigma_z}{2}t} \otimes e^{-i\frac{\omega_2\sigma_z}{2}t}\mathbf{I}_xe^{+i\frac{\omega_2\sigma_z}{2}t} + e^{-i\frac{\omega_1\sigma_z}{2}t}\mathbf{I}_ye^{+i\frac{\omega_1\sigma_z}{2}t} \otimes e^{-i\frac{\omega_2\sigma_z}{2}t}\mathbf{I}_ye^{+i\frac{\omega_2\sigma_z}{2}t} \\
 &= (\cos(\omega_1t)\mathbf{I}_x + \sin(\omega_1t)\mathbf{I}_y) \otimes (\cos(\omega_2t)\mathbf{I}_x + \sin(\omega_2t)\mathbf{I}_y) + \\
 &\quad (\cos(\omega_1t)\mathbf{I}_y - \sin(\omega_1t)\mathbf{I}_x) \otimes (\cos(\omega_2t)\mathbf{I}_y - \sin(\omega_2t)\mathbf{I}_x) \\
 &= \cos(\Delta\omega t)\mathbf{I}_x \otimes \mathbf{I}_x + \sin(\Delta\omega t)\mathbf{I}_x \otimes \mathbf{I}_y - \sin(\Delta\omega t)\mathbf{I}_y \otimes \mathbf{I}_x + \cos(\Delta\omega t)\mathbf{I}_y \otimes \mathbf{I}_y
 \end{aligned}$$

from which

$$\frac{2\pi J}{\hbar} \sum_{k=x,y} \mathbf{I}_k \otimes \mathbf{I}_k = \pi J \hbar \begin{pmatrix} 0 & 0 & 0 & 0 \\ 0 & 0 & e^{i\Delta\omega t} & 0 \\ 0 & e^{-i\Delta\omega t} & 0 & 0 \\ 0 & 0 & 0 & 0 \end{pmatrix}$$

Assuming that $\omega_i = \omega_{r,i}$, in heteronuclear molecules the difference in RF frequencies is very large. Hence, in the **weak coupling limit** [64], that is for $|\Delta\omega_r| \gg |2\pi J|$, it is always possible to choose a time scale τ such that

$$|\Delta\omega_r|\tau \gg 2\pi \gg |2\pi J|\tau$$

where the last inequality must be satisfied for the effect of the J-coupling to be negligible in one-qubit operations. Thus, the exponentials in the previous matrix oscillate rapidly and are averaged to vanish. Equation 6.1.7 follows immediately. At an intuitive level, the disappearance of the \mathbf{I}_x and \mathbf{I}_y operators from the rotating frame Hamiltonian can be explained as follows. When no RF field is applied to the system, the two spins precess at the respective Larmor frequencies about the \hat{z} axis. Since the difference in Larmor frequencies is $\Delta\omega_0 \sim \Delta\omega_r$, the \hat{x} and \hat{y} axes in the rotating frames precess with relative frequency $\Delta\omega_0$. As a consequence, for $|\Delta\omega_0\tau| \gg 2\pi$, the $\mathbf{I}_x \otimes \mathbf{I}_x$ and $\mathbf{I}_y \otimes \mathbf{I}_y$ contributions are averaged to vanish.

□

Turning, now, to the RF fields, the corresponding resonance Hamiltonians in the rotating frames are

$$\begin{aligned}
 \mathbf{U}_R \mathcal{H}_{r,1} \mathbf{U}_R^\dagger &= \omega_{*,1} [\cos(\phi_1)\mathbf{I}_x \otimes \mathbb{I} + \sin(\phi_1)\mathbf{I}_y \otimes \mathbb{I}] \\
 \mathbf{U}_R \mathcal{H}_{r,2} \mathbf{U}_R^\dagger &= \omega_{*,2} [\cos(\phi_2)\mathbb{I} \otimes \mathbf{I}_x + \sin(\phi_2)\mathbb{I} \otimes \mathbf{I}_y]
 \end{aligned} \tag{6.1.8}$$

Proof. Considering the first RF field, in the doubly rotating field

$$\begin{aligned}
 \mathbf{U}_R \mathcal{H}_{r,1} \mathbf{U}_R^\dagger &= 2\omega_{*,1} \cos(\omega_{r,1}t - \phi_1) \left[e^{-i\frac{\omega_1\sigma_z t}{2}} \otimes e^{-i\frac{\omega_2\sigma_z t}{2}} (\mathbf{I}_x \otimes \mathbb{I}) e^{+i\frac{\omega_1\sigma_z t}{2}} \otimes e^{+i\frac{\omega_2\sigma_z t}{2}} + \right. \\
 &\quad \left. \frac{\gamma_2}{\gamma_1} e^{-i\frac{\omega_1\sigma_z t}{2}} \otimes e^{-i\frac{\omega_2\sigma_z t}{2}} (\mathbb{I} \otimes \mathbf{I}_x) e^{+i\frac{\omega_1\sigma_z t}{2}} \otimes e^{+i\frac{\omega_2\sigma_z t}{2}} \right] \\
 &= 2\omega_{*,1} \cos(\omega_{r,1}t - \phi_1) \left[e^{-i\frac{\omega_1\sigma_z t}{2}} \mathbf{I}_x e^{+i\frac{\omega_1\sigma_z t}{2}} \otimes \mathbb{I} + \right. \\
 &\quad \left. \frac{\gamma_2}{\gamma_1} \mathbb{I} \otimes e^{-i\frac{\omega_2\sigma_z t}{2}} \mathbf{I}_x e^{+i\frac{\omega_2\sigma_z t}{2}} \right] \\
 &= 2\omega_{*,1} (A + B)
 \end{aligned}$$

Writing the cosine as the sum of two complex exponentials, the A term becomes

$$\begin{aligned}
 A &= \frac{1}{2} [e^{i(\omega_{r,1}t - \phi_1)} + e^{-i(\omega_{r,1}t - \phi_1)}] [\cos(\omega_1 t) \mathbf{I}_x + \sin(\omega_1 t) \mathbf{I}_y] \otimes \mathbb{I} \\
 &= \frac{1}{2} [e^{i(\omega_{r,1}t - \phi_1)} + e^{-i(\omega_{r,1}t - \phi_1)}] \begin{pmatrix} 0 & e^{-i\omega_1 t} \\ e^{+i\omega_1 t} & 0 \end{pmatrix} \otimes \mathbb{I} \\
 &= \frac{1}{2} \left[\begin{pmatrix} 0 & e^{-i\phi_1} \\ e^{i(2\omega_{r,1}t - \phi_1)} & 0 \end{pmatrix} + \begin{pmatrix} 0 & e^{-i(2\omega_{r,1}t - \phi_1)} \\ e^{i\phi_1} & 0 \end{pmatrix} \right] \otimes \mathbb{I}
 \end{aligned}$$

where $\omega_1 = \omega_{r,1}$ is assumed. As known from the aforementioned rotating wave approximation, the terms oscillating at $2\omega_{r,1}$ average to zero. Then

$$A \sim \frac{1}{2} \begin{pmatrix} 0 & e^{-i\phi_1} \\ e^{+i\phi_1} & 0 \end{pmatrix} \otimes \mathbb{I}$$

Defining $\Delta\omega_r = \omega_{r,2} - \omega_{r,1}$ and $\Omega_r = \omega_{r,1} + \omega_{r,2}$, the B term is easily rewritten as

$$\begin{aligned}
 B &= \frac{\gamma_2}{2\gamma_1} [e^{i(\omega_{r,1}t - \phi_1)} + e^{-i(\omega_{r,1}t - \phi_1)}] \mathbb{I} \otimes \begin{pmatrix} 0 & e^{-i\omega_2 t} \\ e^{+i\omega_2 t} & 0 \end{pmatrix} \\
 &= \frac{\gamma_2}{2\gamma_1} \mathbb{I} \otimes \begin{pmatrix} 0 & e^{-i(\Delta\omega_r t + \phi_1)} + e^{-i(\Omega_r t - \phi)} \\ e^{+i(\Delta\omega_r t + \phi_1)} + e^{+i(\Omega_r t - \phi)} & 0 \end{pmatrix}
 \end{aligned}$$

Since for heteronuclear molecules $|\Delta\omega_r| \gg \omega_1$, for a time scale τ such that $|\Delta\omega_r \tau| \gg 2\pi$ and $\Omega_r \tau \gg 2\pi$, the B matrix vanishes. It follows that

$$\mathbf{U}_R \mathcal{H}_{r,1} \mathbf{U}_R^\dagger = \omega_{*,1} [\cos(\phi_1) \mathbf{I}_x \otimes \mathbb{I} + \sin(\phi_1) \mathbf{I}_y \otimes \mathbb{I}]$$

The derivation of $\mathbf{U}_R \mathcal{H}_{r,2} \mathbf{U}_R^\dagger$ proceeds in the same way. \square

It is of fundamental importance to highlight that an RF field at frequency $\omega_{r,1}$ influences only spin i , leaving the other unaffected. The reason is that the typical pulse width for heteronuclear molecules is $\tau \sim 10 \mu\text{s} \implies 100 \text{ kHz}$, while the difference in resonant frequencies $\Delta\omega_0$ is much larger. Consequently, the pulses at $\omega_{r,1}$ *do not have the Fourier components* which resonate with the other spin.

In conclusion, the Hamiltonian for a heteronuclear weakly coupled two-qubit molecule in the rotating frames is

$$\begin{aligned} \tilde{\mathcal{H}} = & \omega_{*,1} [\cos(\phi_1) \mathbf{I}_x \otimes \mathbb{I} + \sin(\phi_1) \mathbf{I}_y \otimes \mathbb{I}] + \omega_{*,2} [\cos(\phi_2) \mathbb{I} \otimes \mathbf{I}_x + \\ & \sin(\phi_2) \mathbb{I} \otimes \mathbf{I}_y] + (\omega_{r,1} - \omega_{0,1}) \mathbf{I}_z \otimes \mathbb{I} + (\omega_{r,2} - \omega_{0,2}) \mathbb{I} \otimes \mathbf{I}_z + \frac{2\pi J}{\hbar} \mathbf{I}_z \otimes \mathbf{I}_z \end{aligned} \quad (6.1.9)$$

Under the assumption that $|\Delta\omega_r \tau| \gg 2\pi \gg |2\pi J \tau|$. The extension to an n-qubit system is straightforward. Assuming, for the sake of simplicity, that $\omega_{r,i} = \omega_{0,1}$, the previous equation becomes

$$\tilde{\mathcal{H}} = \sum_{i=1}^n \omega_{*,i} [\cos(\phi_i) \mathbf{I}_{x,i} + \sin(\phi_i) \mathbf{I}_{y,i}] + \sum_{i < k}^n \frac{2\pi J_{i,k}}{\hbar} \mathbf{I}_{z,i} \mathbf{I}_{z,k} \quad (6.1.10)$$

6.1.2 Homonuclear molecules

The homonuclear case is more involved, since $|\Delta\omega_0| \ll \omega_{0,i}$. However, in the weak coupling limit $|\Delta\omega_0| \gg 2\pi J$, it is still possible to approximate

$$\mathbf{U}_R \mathcal{H}_{\text{sys}} \mathbf{U}_R^\dagger - i\hbar \mathbf{U}_R \frac{d\mathbf{U}_R^\dagger}{dt} \sim \frac{2\pi J}{\hbar} \mathbf{I}_z \otimes \mathbf{I}_z \quad (6.1.11)$$

assuming $\omega_{r,i} = \omega_{0,i}$ for simplicity. On the other hand, the rotating-frame RF contributions to the Hamiltonian, after the application of the rotating frame approximation, that is the dropping of terms oscillating at $\sim 2\omega_0$, are

$$\begin{aligned}
 U_R \mathcal{H}_{r,1} U_R^\dagger &= \omega_{*,1} [\cos(\phi_1) \mathbf{I}_x \otimes \mathbb{I} + \sin(\phi_1) \mathbf{I}_y \otimes \mathbb{I}] + \omega_{*,1} [\cos(\Delta\omega_0 t + \phi_1) (\mathbb{I} \otimes \mathbf{I}_x) + \\
 &\hspace{15em} \sin(\Delta\omega_0 t + \phi_1) (\mathbb{I} \otimes \mathbf{I}_y)] \\
 U_R \mathcal{H}_{r,2} U_R^\dagger &= \omega_{*,2} [\cos(\phi_2) \mathbb{I} \otimes \mathbf{I}_x + \sin(\phi_2) \mathbb{I} \otimes \mathbf{I}_y] + \omega_{*,2} [\cos(-\Delta\omega_0 t + \phi_2) (\mathbf{I}_x \otimes \mathbb{I}) + \\
 &\hspace{15em} \sin(-\Delta\omega_0 t + \phi_2) (\mathbf{I}_y \otimes \mathbb{I})]
 \end{aligned}
 \tag{6.1.12}$$

where the approximation $\omega_{0,1} \sim \omega_{0,2}$, reasonable for homonuclear systems, is adopted. The proof follows the same procedure as for the heteronuclear case. The second bracket of each Hamiltonian, which differentiates this result from the one obtained for heteronuclear molecules and which makes the Hamiltonian time dependent, can be neglected *only if the pulse width τ is sufficiently long* such that $|\Delta\omega_0\tau| \gg 2\pi$ or if $\omega_{*,i} \ll |\Delta\omega_0|$. A pulse which satisfies this requirement is known as **soft pulse**.

In conclusion, Equation 6.1.10 can be used also for homonuclear molecules if the hard pulses, that is, the short and strong pulses used for heteronuclear molecules, are replaced by soft pulses and the weak coupling approximation is satisfied. A typical pulse width for selective addressing is 10 μs for heteronuclear molecules and 1 ms for homonuclear molecules. On the other hand, a hard pulse with $\tau \sim 10 \mu\text{s}$ can be applied to homonuclear systems to address *all spins simultaneously*.

6.2 NMR quantum gates

It is known that one-qubit quantum gates and the CNOT gate constitute a universal set of quantum gates. In this section it is explained how to employ the previously introduced Hamiltonians to implement quantum gates. The key idea, derived from section §4.1.1.2, is to apply to the molecular system a static field \mathbf{B}_0 and a resonant radio frequency field \mathbf{B}_r . The latter is applied for a time τ , the so-called **pulse width** and with an amplitude ω_* , the so-called **pulse amplitude**. Figure 4.6 is reported here for the sake of clearness.

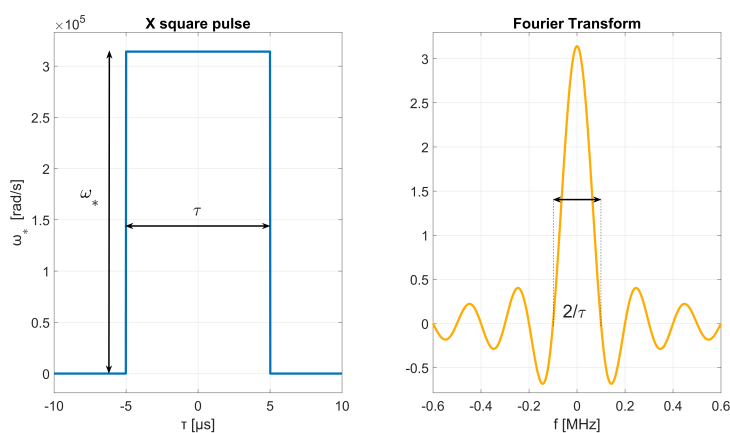


Figure 6.1: A π -pulse (or X-pulse) assuming $\tau = 10 \mu\text{s}$ on a ^{13}C nucleus spin and its Fourier transform.

6.2.1 One-qubit gates in many-qubit molecules

Single-qubit quantum gates can be implemented starting from the Hamiltonian of Equation 6.1.10, if the following conditions are satisfied

- Weak coupling regime $|\Delta\omega_0| \gg 2\pi J$.
- Resonant condition $\omega_{r,i} = \omega_{0,i}$.
- Difference in the Larmor frequencies such that selective addressing is achievable, that is $|\Delta\omega_0\tau| \gg 2\pi$ or $|\Delta\omega_0| \gg \omega_{*,i}$.
- Pulse width short enough to ignore at first order the indirect spin-spin coupling during the pulses $\tau \ll |1/J|$ or $\omega_{*,i} \gg |2\pi J|$.
- Time duration τ such that $|\Delta\omega_0\tau| \gg 2\pi \gg |2\pi J\tau|$.

Under these hypotheses, if only the RF field resonant with qubit 1 is switched on for a time τ , then the time evolution operator associated with the Hamiltonian of Equation 6.1.10 is

$$\mathbf{U}(\tau) = \exp\left(-\frac{i}{\hbar} \int_0^\tau \tilde{\mathcal{H}} dt\right) = \exp\left(-i\frac{\theta}{2} [\cos(\phi_1)\boldsymbol{\sigma}_x + \sin(\phi_1)\boldsymbol{\sigma}_y]\right) \otimes \mathbb{I} \quad (6.2.1)$$

where

$$\theta = \omega_{*,1}\tau \quad (6.2.2)$$

where $\mathbb{I} = \mathbb{I}_2 \otimes \mathbb{I}_3 \otimes \dots \otimes \mathbb{I}_n$. This operator describes a rotation of an angle θ about the axis $\begin{pmatrix} \cos(\phi) & \sin(\phi) & 0 \end{pmatrix}$. In the following of this section, the tensor product $\otimes \mathbb{I}$ is dropped for convenience of notation. There are two properties of the corresponding Hamiltonian which have to be pointed out. First, it is clearly traceless and the following theorem holds true for traceless Hamiltonians.

Theorem 6.2.1. *A traceless Hamiltonian \mathcal{H} can generate only elements of $\mathbb{SU}(2^n)$.*

Proof. Let λ_k be the eigenvalues of \mathcal{H} and \mathbf{V} be a unitary matrix which diagonalizes \mathcal{H} and, hence, the corresponding time evolution operator \mathbf{U} . Then

$$\det(\mathbf{U}) = \det(\mathbf{V}\mathbf{U}\mathbf{V}^\dagger) = \det(\text{diag}(e^{-i\lambda_k t})) = \prod_k e^{-i\lambda_k t} = e^{-i \text{tr}(\mathcal{H})t} = 1$$

□

However, this is by no means a limitation. Every unitary gate \mathbf{G} can be mapped to a special unitary gate $e^{-i\alpha}\mathbf{G} \in \mathbb{SU}(2^n)$, multiplying by a phase factor $e^{-i\alpha}$. The reader is reminded that every quantum state is defined up to a phase factor.

Second, it lacks the \mathbf{I}_z generators. Nevertheless, this is not an issue, since a rotation about $\hat{\mathbf{z}}$ can be implemented in several ways. A first possibility is to note that

$$\mathbf{R}_z(\alpha) = \mathbf{R}_x\left(\frac{\pi}{2}\right) \mathbf{R}_y(\alpha) \left(-\frac{\pi}{2}\right) \quad (6.2.3)$$

so that a rotation about \hat{z} is decomposed in rotations about \hat{x} and \hat{y} . A second and more efficient approach is to adopt the so-called **virtual-z** method [65]. Instead of rotating the spin of an angle α about the \hat{z} axis, one can rotate the frame of an angle $-\alpha$ about \hat{z} , which, in practice, corresponds to add a phase shift to the RF field for all subsequent pulses. In order to understand the approach, consider that after a generic \mathbf{G} gate, one wants to perform an α -rotation about \hat{z} , followed by a θ -rotation about \mathbf{X} (cf. Table 6.1):

$$\mathbf{R}_x(\theta)\mathbf{R}_z(\alpha)\mathbf{G} \quad (6.2.4)$$

Instead of introducing the z-rotation, a phase offset $-\alpha$ is added to the following pulse

$$\exp\left(-\frac{\theta}{2}[\cos(-\alpha)\sigma_x + \sin(-\alpha)\sigma_y]\right)\mathbf{G} \quad (6.2.5)$$

which can be decomposed as usual as

$$e^{\frac{i\phi}{2}\sigma_z}e^{-\frac{i\theta}{2}\sigma_x}e^{-\frac{i\phi}{2}\sigma_z}\mathbf{G} = \mathbf{R}_z(-\alpha)\mathbf{R}_x(\theta)\mathbf{R}_z(\alpha)\mathbf{G} \quad (6.2.6)$$

The additional $\mathbf{R}_z(-\alpha)$ gate, due to the fact that the analysis is carried out in the qubit reference frame, keeps track of the fact that the phase offset $-\alpha$ must be carried through for all subsequent gates. For instance, if the previous group of gates is followed by a θ -rotation about \hat{y} , then

$$\begin{aligned} & \exp\left(-\frac{\theta}{2}\left[\cos\left(\frac{\pi}{2}-\alpha\right)\sigma_x + \sin\left(\frac{\pi}{2}-\alpha\right)\sigma_y\right]\right)\mathbf{R}_z(-\alpha)\mathbf{R}_x(\theta)\mathbf{R}_z(\alpha)\mathbf{G} \\ &= \mathbf{R}_z(-\alpha)\mathbf{R}_y(\theta)\mathbf{R}_z(\alpha)\mathbf{R}_z(-\alpha)\mathbf{R}_x(\theta)\mathbf{R}_z(\alpha)\mathbf{G} \\ &= \mathbf{R}_z(-\alpha)\mathbf{R}_y(\theta)\mathbf{R}_x(\theta)\mathbf{R}_z(\alpha)\mathbf{G} \end{aligned} \quad (6.2.7)$$

This approach allows the implementation of perfect z-rotations, whose duration is zero. For further details the reader is referred to [65]. Finally, if some z-rotations can be shifted to the end of the quantum algorithm execution, then they can be ignored if the measurement is carried out in the Zeeman eigenbasis since a quantum state is defined up to a phase factor.

As a consequence of this discussion, all fundamental SU one-qubit quantum gates can be implemented resorting only to \mathbf{I}_x and \mathbf{I}_y generators, which are contained in the Hamiltonian. The control parameters θ and ϕ required for the execution of the quantum gates are reported in Table 6.1.

There is still a frequently used gate which is missing: the Hadamard gate. The

Rotation	QASM	Matrix	ϕ	θ
$\mathbf{R}_x(\pi/2)$		$\frac{1}{\sqrt{2}} \begin{pmatrix} 1 & -i \\ -i & 1 \end{pmatrix}$	0	$\frac{\pi}{2}$
$\mathbf{R}_x(\pi)$	$-i\mathbf{X}$	$\begin{pmatrix} 0 & -i \\ -i & 0 \end{pmatrix}$	0	π
$\mathbf{R}_x(-\pi/2)$		$\frac{1}{\sqrt{2}} \begin{pmatrix} 1 & i \\ i & 1 \end{pmatrix}$	π	$\frac{\pi}{2}$
$\mathbf{R}_y(\pi/2)$		$\frac{1}{\sqrt{2}} \begin{pmatrix} 1 & -1 \\ 1 & 1 \end{pmatrix}$	$\frac{\pi}{2}$	$\frac{\pi}{2}$
$\mathbf{R}_y(\pi)$	$-i\mathbf{Y}$	$\begin{pmatrix} 0 & -1 \\ 1 & 0 \end{pmatrix}$	$\frac{\pi}{2}$	π
$\mathbf{R}_y(-\pi/2)$		$\frac{1}{\sqrt{2}} \begin{pmatrix} 1 & 1 \\ -1 & 1 \end{pmatrix}$	$-\frac{\pi}{2}$	$\frac{\pi}{2}$

Table 6.1: The control parameters for one-qubit quantum gates.

SU gate equivalent to the Hadamard gate can be obtained multiplying \mathbf{H} by i or by $-i$. Since, as stated in section §2.1.6.3, every SU gate can always be rewritten as the product of three rotation gates, one shall enforce

$$\mathbf{R}_z(\alpha)\mathbf{R}_y(\beta)\mathbf{R}_z(\gamma) = -i\mathbf{H} \quad (6.2.8)$$

It turns out that $\alpha = \pi$, $\beta = -\pi/2$ and $\gamma = 0$. Another convenient way to write a generic SU is [5, 44]

$$\mathbf{R}_x(\alpha)\mathbf{R}_y(\beta)\mathbf{R}_x(\gamma) \quad (6.2.9)$$

where $\alpha = \pi$, $\beta = \pi/2$ and $\gamma = 0$ allow the implementation of the Hadamard gate. Therefore, the Hadamard gate can be decomposed as

$$\mathbf{H} \sim -i\mathbf{H} = \mathbf{R}_z(\pi)\mathbf{R}_y\left(-\frac{\pi}{2}\right) = \mathbf{R}_x(\pi)\mathbf{R}_y\left(\frac{\pi}{2}\right) \quad (6.2.10)$$

6.2.2 Two-qubit gates in two-qubit molecules

6.2.2.1 The CNOT gate

As well known from the previous discussion, every quantum algorithm can be implemented with one-qubit gates and CNOT gates only. Since $\det(\mathbf{CX}) = -1$, the CNOT gate must be multiplied by $e^{\pm i\pi/4}$ to obtain an element of $\mathbb{SU}(4)$. The CNOT gate *cannot be decomposed into a tensor product of one-qubit quantum gates*, hence the J-coupling mechanism must be properly employed. When no RF field is applied to the molecule and assuming, for the sake of simplicity, that there are only two qubits, Equation 6.1.10 becomes

$$\tilde{\mathcal{H}} = \frac{2\pi J_{1,2}}{\hbar} \mathbf{I}_z \otimes \mathbf{I}_z \quad (6.2.11)$$

and the associated time evolution operator is

$$\mathbf{U}(t) = \exp\left(-i\frac{\pi J_{1,2}}{2} \boldsymbol{\sigma}_z \otimes \boldsymbol{\sigma}_z t\right) = \begin{pmatrix} e^{-i\frac{\pi J}{2}t} & 0 & 0 & 0 \\ 0 & e^{+i\frac{\pi J}{2}t} & 0 & 0 \\ 0 & 0 & e^{+i\frac{\pi J}{2}t} & 0 \\ 0 & 0 & 0 & e^{-i\frac{\pi J}{2}t} \end{pmatrix} \quad (6.2.12)$$

In order to understand the complex evolution of J-coupled spins and see how this can be engineered to obtain the CNOT gate, it proves reasonable to focus on a simple case. Suppose that $J > 0$ and that one of the two qubits is in a Zeeman eigenstate. From the energy level diagram reported in Figure 5.10, it is clear that if qubit 2 is in the $|0\rangle$ eigenstate, then the energy required for the transition

$$|00\rangle \longleftrightarrow |10\rangle \quad (6.2.13)$$

is *reduced* by the J-coupling. Similarly, if qubit 1 is in the $|0\rangle$ eigenstate, then the energy required for the transition

$$|00\rangle \longleftrightarrow |01\rangle \quad (6.2.14)$$

is *reduced* by the J-coupling. Therefore, it follows immediately that the precession frequency of spin a is shifted by $-\frac{J_{a,b}}{2}$ if spin b is in $|0\rangle$. Conversely, if qubit 2 is in the $|1\rangle$ eigenstate, then the energy required for the transition

$$|01\rangle \longleftrightarrow |11\rangle \quad (6.2.15)$$

is *increased* by the J-coupling. Similarly, if qubit 1 is in the $|1\rangle$ eigenstate, then the energy required for the transition

$$|10\rangle \longleftrightarrow |11\rangle \quad (6.2.16)$$

is *increased* by the J-coupling. Hence

- The precession frequency of spin a is shifted by $-\frac{J_{a,b}}{2}$ if spin b is in $|0\rangle$. This means that in a frame rotating at frequency $\omega_{0,a}$, the spin a precesses **anticlockwise** with a frequency $\frac{J_{a,b}}{2}$.
- The precession frequency of spin a is shifted by $+\frac{J_{a,b}}{2}$ if spin b is in $|1\rangle$. This means that in a frame rotating at frequency $\omega_{0,a}$, the spin a precesses **clockwise** with a frequency $\frac{J_{a,b}}{2}$.

Thus, it is possible to exploit the J-coupling to make one spin rotate according to the state of the *other* spin. In other words, the J-coupling enables the implementation of *controlled rotations*.

The CNOT gate flips the second qubit (the **target qubit**) if and only if the first qubit (the **control qubit**) is in state $|1\rangle$. Otherwise, the target qubit is unaffected. Suppose, for the time being, that one wants to realize an NMR CNOT gate when both the control and the target qubits are in an eigenstate of the Hamiltonian, referring to Figure 6.2 and Figure 6.3.

The control qubit is in state $|0\rangle$ Assume that both qubits are in state $|0\rangle$ at the beginning (Figure 6.2a). Then, a selective $\mathbf{R}_y(\pi/2)$ rotation is applied to the target qubit, which ends up along the $+\hat{x}$ axis (Figure 6.2b). Next, the system is left free to evolve without any RF field applied for a time $\tau = \frac{1}{2J}$. The corresponding time evolution operator is

$$U_J\left(\frac{1}{2J}\right) = \exp\left(-i\frac{\pi}{4}\sigma_z \otimes \sigma_z\right) = \begin{pmatrix} e^{-i\frac{\pi}{4}} & 0 & 0 & 0 \\ 0 & e^{+i\frac{\pi}{4}} & 0 & 0 \\ 0 & 0 & e^{+i\frac{\pi}{4}} & 0 \\ 0 & 0 & 0 & e^{-i\frac{\pi}{4}} \end{pmatrix} \quad (6.2.17)$$

Accordingly, the target qubit is rotated of an angle $\pi/2$ about the \hat{z} axis (Figure 6.2c) and arrives to the $+\hat{y}$ axis. Finally, a selective $\mathbf{R}_x(\pi/2)$ rotation is applied to the target qubit, which comes back to the $|0\rangle$ state (Figure 6.2d). If the target qubit initial state is $|1\rangle$, the corresponding evolution can be derived by analogy.

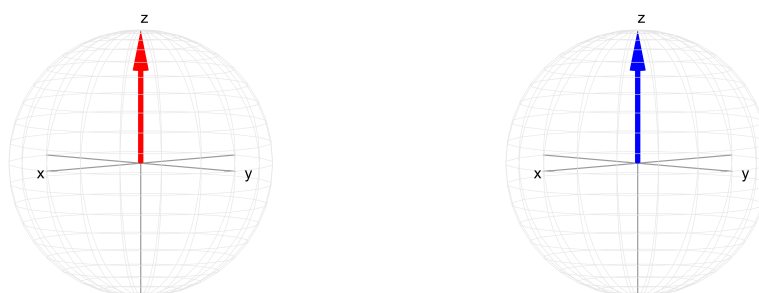
The control qubit is in state $|1\rangle$ Assume that initially the target qubit is in state $|0\rangle$, while the control qubit is in state $|1\rangle$ (Figure 6.3a). Then, a selective $\mathbf{R}_y(\pi/2)$ rotation is applied to the target qubit, which ends up along the $+\hat{x}$ axis (Figure 6.3b). Next, the system is left free to evolve without any RF field applied for a time $\tau = \frac{1}{2J}$. Accordingly, the target qubit is rotated of an angle $-\pi/2$ about the \hat{z} axis (Figure 6.3c) and arrives to the $-\hat{y}$ axis. Finally, a selective $\mathbf{R}_x(\pi/2)$ rotation is applied to the target qubit, which ends up in the $|1\rangle$ state (Figure 6.3d). If the target qubit initial state is $|1\rangle$, the corresponding evolution can be derived by analogy.

Therefore, if the control qubit is qubit-1 and the target qubit is qubit-2, the core of the CNOT gate must be

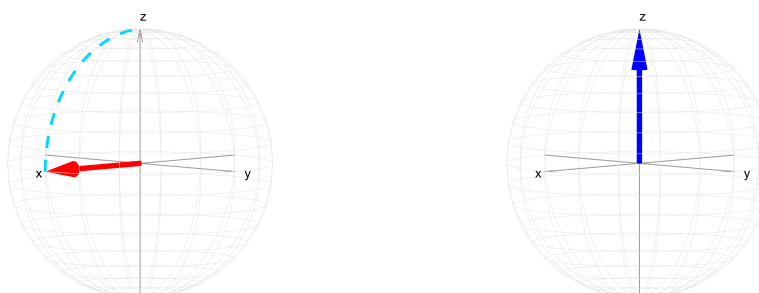
$$\left[\mathbb{I} \otimes \mathbf{R}_x \left(\frac{\pi}{2} \right) \right] \mathbf{U}_J \left(\frac{1}{2J} \right) \left[\mathbb{I} \otimes \mathbf{R}_y \left(\frac{\pi}{2} \right) \right] = \frac{1}{\sqrt{(2)}} \begin{pmatrix} 1-i & 0 & 0 & 0 \\ 0 & 1+i & 0 & 0 \\ 0 & 0 & 0 & -1-i \\ 0 & 0 & 1-i & 0 \end{pmatrix} \quad (6.2.18)$$

However, this cannot be an actual CNOT gate since the matrix elements have different reciprocal phases. On the other hand, it is mandatory that all elements have the same phase for the sequence to work also on a *superposition of eigenstates* (the reader is reminded of the concept of clean computation, discussed in section §2.2.2.3). It turns out [33, 5, 45, 17] that a proper CNOT gate is obtained adding a couple of rotations about the \hat{z} axis:

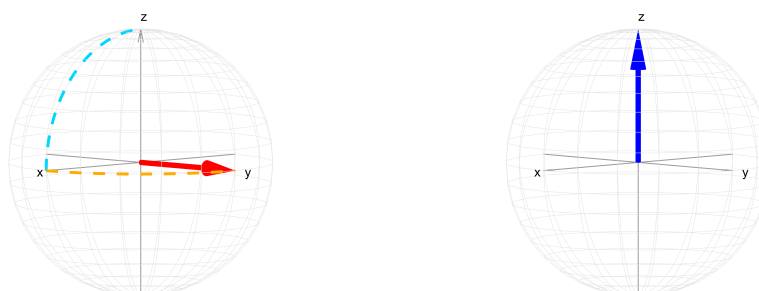
$$\begin{aligned} \mathbf{C}\mathbf{X} \sim e^{-i\pi/4} \mathbf{C}\mathbf{X} &= \left[\mathbf{R}_z \left(\frac{\pi}{2} \right) \otimes \mathbb{I} \right] \left[\mathbb{I} \otimes \mathbf{R}_z \left(-\frac{\pi}{2} \right) \right] \\ &\quad \left[\mathbb{I} \otimes \mathbf{R}_x \left(\frac{\pi}{2} \right) \right] \mathbf{U}_J \left(\frac{1}{2J} \right) \left[\mathbb{I} \otimes \mathbf{R}_y \left(\frac{\pi}{2} \right) \right] \quad (6.2.19) \end{aligned}$$



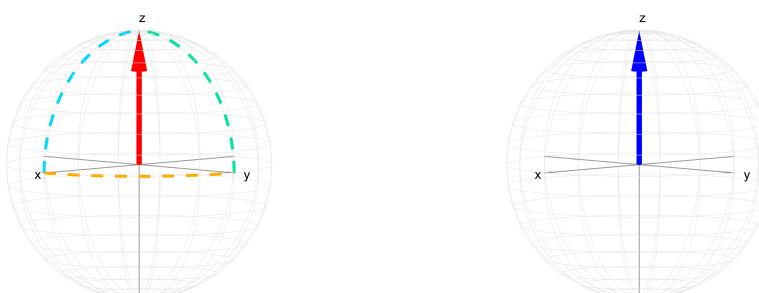
(a) At the beginning the target qubit is in state $|0\rangle$, and also the control qubit is in state $|0\rangle$.



(b) A $\pi/2$ pulse about \hat{y} is applied to the target qubit, after which it lies on the $+\hat{x}$ axis.

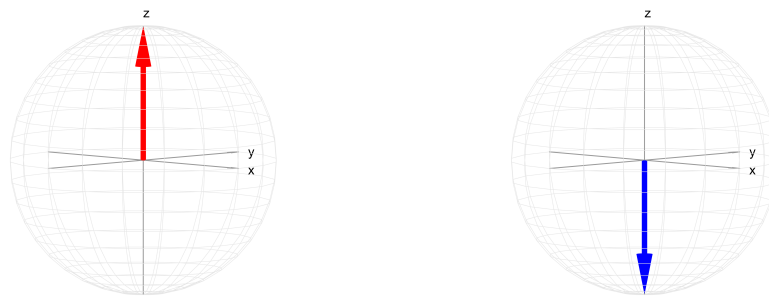


(c) The system evolves for a time $t = \frac{1}{2J}$, after which the target qubit lies on the $+\hat{y}$ axis.

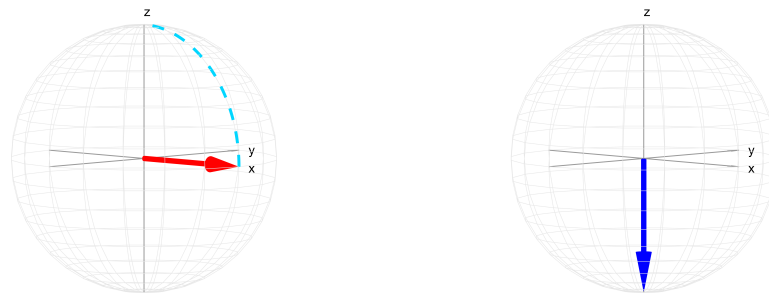


(d) A $\pi/2$ pulse about \hat{x} is applied to the target qubit, which comes back to the $|0\rangle$ state.

Figure 6.2: The CNOT gate when the control qubit (blue) is in state $|0\rangle$ and the target qubit (red) is in state $|0\rangle$.



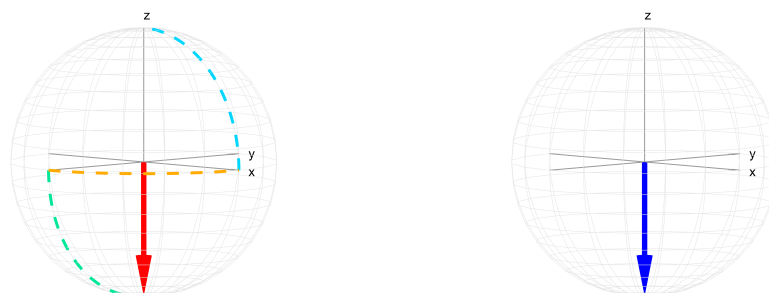
(a) At the beginning the target qubit is in state $|0\rangle$, while the control qubit is in state $|1\rangle$.



(b) A $\pi/2$ pulse about \hat{y} is applied to the target qubit, after which it lies on the $+\hat{x}$ axis.



(c) The system evolves for a time $t = \frac{1}{2J}$, after which the target qubit lies on the $-\hat{y}$ axis.



(d) A $\pi/2$ pulse about \hat{x} is applied to the target qubit, which ends up in the $|1\rangle$ state.

Figure 6.3: The CNOT gate when the control qubit (blue) is in state $|1\rangle$ and the target qubit (red) is in state $|0\rangle$.

Negative J-coupling What does it happen if the J-coupling is negative? It does not have any physical meaning to say that the system is subjected to a free evolution for a time $t = \frac{1}{2J} < 0$. There are several possible workarounds to face this issue, but the simplest one is probably to slightly change the receipt for the CNOT gate. If $J < 0$ and the system evolves for a time $t = \frac{1}{|2J|}$, then the target qubit rotates *in the opposite direction* with respect to the previous case: clockwise if the control qubit is in $|0\rangle$ and anticlockwise if the control qubit is in $|1\rangle$. However, the same overall behaviour is obtained if the target qubit is subjected to a selective $\mathbf{R}_x(-\pi/2)$ rotation, instead of a $\mathbf{R}_x(+\pi/2)$ rotation. Hence

$$\begin{aligned} \mathbf{CX} \sim e^{-\text{sgn}(J)i\pi/4}\mathbf{CX} &= \left[\mathbf{R}_z\left(\text{sgn}(J)\frac{\pi}{2}\right) \otimes \mathbb{I} \right] \left[\mathbb{I} \otimes \mathbf{R}_z\left(-\text{sgn}(J)\frac{\pi}{2}\right) \right] \\ &\quad \left[\mathbb{I} \otimes \mathbf{R}_x\left(\text{sgn}(J)\frac{\pi}{2}\right) \right] \mathbf{U}_J\left(\left|\frac{1}{2J}\right|\right) \left[\mathbb{I} \otimes \mathbf{R}_y\left(+\frac{\pi}{2}\right) \right] \end{aligned} \quad (6.2.20)$$

On the time duration It is worth highlighting that the time required to perform a CNOT gate is significantly longer than that required to perform a one-qubit quantum gate. As a matter of fact, if the latter is in the order of $\sim 10\ \mu\text{s}$, at least for a heteronuclear system, for the former one has to consider that typical J-coupling values are in the order of dozens or hundreds of hertz. It follows that

$$\tau_J = 5\ \text{ms to } 50\ \text{ms} \quad (6.2.21)$$

6.2.2.2 The controlled Z gate

Even if a controlled-Z gate can be decomposed in terms of CNOT and Hadamard gates (cf. section §2.1.6.3), it is also true that a controlled-Z rotation can be naturally executed by an NMR quantum computer thanks to the J-coupling. Indeed, it is known from the discussion on the CNOT gate that, if the control qubit is a Zeeman eigenstate, the target qubit, in a time τ , executes a rotation about \hat{z} of an angle

- $\theta = \pi J\tau$ if the control qubit is in state $|0\rangle$.
- $\theta = -\pi J\tau$ if the control qubit is in state $|1\rangle$.

If $J > 0$, then the rotation about the \hat{z} axis must be nullified when the control qubit is in state $|0\rangle$. Intuitively, this can be done if a rotation $\mathbf{R}_z(-\pi/2)$ is first applied to the target qubit. Next, the system evolves freely for a time $t = \frac{1}{2J}$, so that the target qubit comes back to the initial position. On the other hand, when the control qubit is in state $|1\rangle$, the overall rotation executed by the target qubit is $\mathbf{R}_z(-\pi) = \mathbf{R}_z(+\pi)$ as expected.

If $J < 0$, the same behaviour is obtained if the upstream rotation $\mathbf{R}_z(-\pi/2)$ is replaced by $\mathbf{R}_z(+\pi/2)$. It follows that the core of the controlled-Z gate must be

$$U_J \left(\left| \frac{1}{2J} \right| \right) \left[\mathbb{I} \otimes \mathbf{R}_z \left(-\text{sgn}(J) \frac{\pi}{2} \right) \right] \quad (6.2.22)$$

The actual controlled-Z gate turns out [66, 44] to be

$$\mathbf{CZ} \sim e^{\text{sgn}(J)i\pi/4} \mathbf{CX} = U_J \left(\left| \frac{1}{2J} \right| \right) \left[\mathbb{I} \otimes \mathbf{R}_z \left(-\text{sgn}(J) \frac{\pi}{2} \right) \right] \left[\mathbf{R}_z \left(-\text{sgn}(J) \frac{\pi}{2} \right) \otimes \mathbb{I} \right] \quad (6.2.23)$$

6.2.3 Two-qubit gates in many-qubit molecules: the refocusing

Consider, now, a molecule with several coupled qubits. Obviously, it is not possible to turn off inter-qubit couplings when they are not needed. As far as one-qubit quantum gates are concerned, the operations are usually faster than $\sim 1/J$ and so the effect of J-coupling can be safely neglected¹. On the other hand, two-qubit operations involve the J-coupling. In order to execute the expected algorithm, it is mandatory to remove the *other unwanted J-couplings*. This **interaction on demand** is achieved thanks to a technique known as **refocusing**.

In order to understand the procedure, suppose that there are three spins such that spin-1 is coupled to spin-2 and spin-2 is coupled to spin-3. The rotating frame Hamiltonian when no RF field is applied is

$$\mathcal{H} = \frac{2\pi J_{1,2}}{\hbar} \mathbf{I}_z \otimes \mathbf{I}_z \otimes \mathbb{I} + \frac{2\pi J_{2,3}}{\hbar} \mathbb{I} \otimes \mathbf{I}_z \otimes \mathbf{I}_z \quad (6.2.24)$$

Assume that the desired gate is

$$\mathbf{U}_G = \exp\left(-i\frac{\alpha}{4}\sigma_z \otimes \sigma_z \otimes \mathbb{I}\right) \quad (6.2.25)$$

Fixing $\tau = \frac{\alpha}{2\pi J_{1,2}}$, the NMR time evolution operator is

$$\mathbf{U}_J\left(\frac{\alpha}{2\pi J_{1,2}}\right) = \exp\left(-i\frac{\alpha}{4}\sigma_z \otimes \sigma_z \otimes \mathbb{I}\right) \exp\left(-i\frac{\alpha}{4}\frac{J_{2,3}}{J_{1,2}}\mathbb{I} \otimes \sigma_z \otimes \sigma_z\right) \quad (6.2.26)$$

since $\sigma_z \otimes \sigma_z \otimes \mathbb{I}$ and $\mathbb{I} \otimes \sigma_z \otimes \sigma_z$ commute. How is it possible to get rid of the second unwanted exponential? The aim, in practice, is to nullify the coupling between the second and the third qubit. Consider Figure 6.4, where, for simplicity, only qubit-2 (in red) and qubit-3 (in blue) are represented, focusing exclusively on their reciprocal interaction. Suppose that at time $t = 0$, qubit-2 lies along $+\hat{x}$ axis and qubit-3 is in $|0\rangle$ state. (Figure 6.4a). The system evolves freely for a time $t = \tau/2$, after which qubit-2 lies along $+\hat{y}$ (Figure 6.4b). Then, a rotation $\mathbf{R}_x(\pi)$ is applied to qubit-3, which ends up in $|1\rangle$ state (Figure 6.4c). During the following time interval $t = \tau/2$, qubit-2 precesses in the *opposite* direction and comes back to its initial position. It shall be clear that this happens independently of the precession angle: during the first rime interval spin-2 precesses of an angle

¹This is almost always the case for heteronuclear molecules. For homonuclear molecules controlled via soft pulses, it may happen that the effect of J-coupling is not negligible in one-qubit operations.

$\theta = \pi J\tau/2$, then during the second interval it precesses of an angle $\theta = -\pi J\tau/2$, so that the total precession angle is $\theta = 0$ (Figure 6.4d). Finally, rotation $\mathbf{R}_x(\pi)$ is applied to qubit-3, which comes back to $|0\rangle$ state (Figure 6.4e). Therefore, this procedure removes the coupling between qubit-2 and qubit-3. In the following *proof*, a formal justification is provided to show that this approach is successful irrespectively of the initial state of both qubits.

Proof. The mathematical foundation of the refocusing technique is the following equivalence

$$\mathbf{R}_x(-\pi)\mathbf{I}_z\mathbf{R}_z(+\pi) = -\mathbf{I}_z$$

from which it follows that in general

$$[\mathbf{R}_x(\pi) \otimes \mathbb{I}] \mathbf{U}_J \left(\frac{\tau}{2} \right) [\mathbf{R}_x(\pi) \otimes \mathbb{I}] = \mathbf{U}_J \left(-\frac{\tau}{2} \right) = [\mathbb{I} \otimes \mathbf{R}_x(\pi)] + \mathbf{U}_J \left(\frac{\tau}{2} \right) [\mathbb{I} \otimes \mathbf{R}_x(\pi)]$$

which means the application of the π -pulses it is equivalent with reversing the direction of time. Hence

$$[\mathbf{R}_x(\pi) \otimes \mathbb{I}] \mathbf{U}_J \left(\frac{\tau}{2} \right) [\mathbf{R}_x(\pi) \otimes \mathbb{I}] \mathbf{U}_J \left(\frac{\tau}{2} \right) = \mathbb{I}$$

Considering in more details the three-qubit case previously presented, the complete time evolution operator is

$$\mathbf{U} = [\mathbb{I} \otimes \mathbb{I} \otimes \mathbf{R}_x(\pi)] \mathbf{U}_J \left(\frac{\tau}{2} \right) [\mathbb{I} \otimes \mathbb{I} \otimes \mathbf{R}_x(\pi)] \mathbf{U}_J \left(\frac{\tau}{2} \right)$$

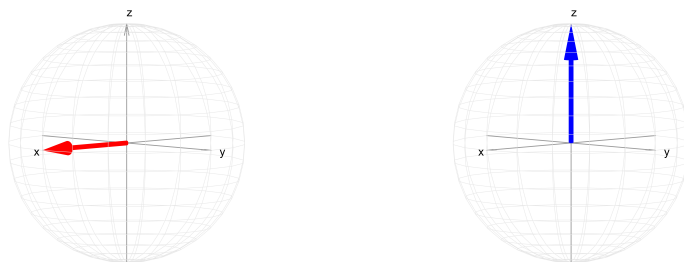
Applying the well known properties of tensor products and the previously reported equivalence, it is possible to rewrite

$$\begin{aligned} & [\mathbb{I} \otimes \mathbb{I} \otimes \mathbf{R}_x(\pi)] \exp \left[-i \frac{\pi\tau}{4} (J_{1,2}\sigma_z \otimes \sigma_z \otimes \mathbb{I} + J_{2,3}\mathbb{I} \otimes \sigma_z \otimes \sigma_z) \right] [\mathbb{I} \otimes \mathbb{I} \otimes \mathbf{R}_x(\pi)] \\ &= \exp \left[-i \frac{\pi\tau}{4} (J_{1,2}\sigma_z \otimes \sigma_z \otimes \mathbb{I} - J_{2,3}\mathbb{I} \otimes \sigma_z \otimes \sigma_z) \right] \end{aligned}$$

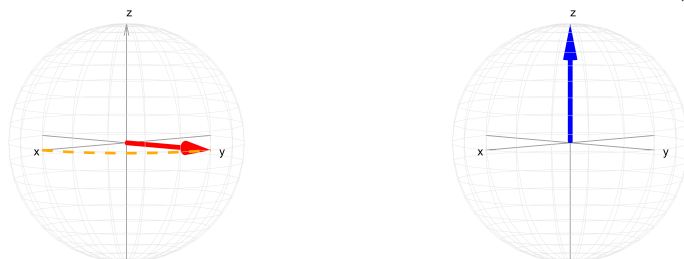
And so

$$\begin{aligned} \mathbf{U} &= \exp \left[-i \frac{\pi\tau}{4} (J_{1,2}\sigma_z \otimes \sigma_z \otimes \mathbb{I} - J_{2,3}\mathbb{I} \otimes \sigma_z \otimes \sigma_z) \right] \\ &\quad \exp \left[-i \frac{\pi\tau}{4} (J_{1,2}\sigma_z \otimes \sigma_z \otimes \mathbb{I} + J_{2,3}\mathbb{I} \otimes \sigma_z \otimes \sigma_z) \right] \\ &= \exp \left[-i \frac{\pi\tau J_{1,2}}{2} \sigma_z \otimes \sigma_z \otimes \mathbb{I} \right] \end{aligned}$$

□



(a) Initial configuration: qubit-2 lies along the $+\hat{x}$ while qubit-3 is in $|0\rangle$ state.



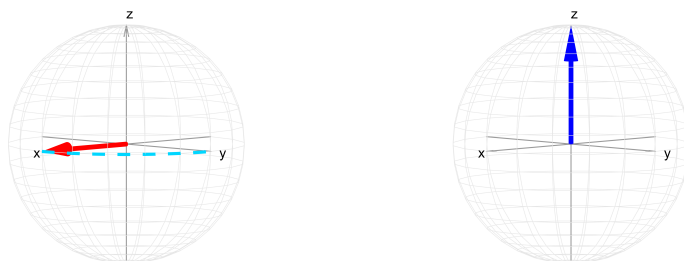
(b) The system evolves freely for a time $t = \tau/2$ and qubit-2 precesses of an angle $\theta = \pi J\tau/2$.



(c) A rotation $\mathbf{R}_x(\pi)$ is applied to qubit-3 which ends up in the $|1\rangle$ state.



(d) The system evolves freely for a time $t = \tau/2$ and qubit-2 precesses of an angle $\theta = -\pi J\tau/2$.



(e) A rotation $\mathbf{R}_x(-\pi)$ is applied to qubit-3 which ends up in the $|0\rangle$ state.

Figure 6.4: The refocusing technique.

The underlying idea is that a coupling between qubits i and k acts forward when time flows in the normal direction and in reverse when time flows in the reverse direction. Let associate $+1$ to an interval in which time flows in the normal direction and -1 to an interval in which time flows in the reversed direction. Then, the refocusing scheme for the previous case is the one reported in Table 6.2. Whenever a coupling acts forward and in reverse for the same amount of time,

Qubit	$\tau/2$	$\tau/2$
1	+1	+1
2	+1	+1
3	+1	-1

Table 6.2: Refocusing scheme eliminating the coupling between qubit-2 and qubit-3.

it has no net effect. Hence, the rows corresponding to qubits among which the J-coupling **must be nullified are orthogonal**. There are several systematic methods to design a refocusing scheme. One of the most widely adopted is based on **Hadamard matrices**. A Hadamard matrix of order n is a $n \times n$ matrix with ± 1 entries such that

$$\mathbf{H}(n)\mathbf{H}(n)^\dagger = n\mathbb{I} \quad (6.2.27)$$

For instance

$$H(4) = \begin{pmatrix} +1 & +1 & +1 & +1 \\ +1 & -1 & +1 & -1 \\ +1 & +1 & -1 & -1 \\ +1 & -1 & -1 & +1 \end{pmatrix} \quad (6.2.28)$$

represents a possible refocusing scheme to remove *all* couplings between four qubits. If one wants to preserve a coupling between spin i and spin k , it is sufficient to replace the k -th row by the i -th row in $\mathbf{H}(n)$. For instance, to preserve the coupling between qubit-2 and qubit-4 in a four-qubit system, the following refocusing scheme can be adopted

$$H(4) = \begin{pmatrix} +1 & +1 & +1 & +1 \\ +1 & -1 & +1 & -1 \\ +1 & +1 & -1 & -1 \\ +1 & -1 & +1 & -1 \end{pmatrix} \quad (6.2.29)$$

The Hadamard matrix approach to refocusing provides a refocusing scheme for n qubits in only n time intervals if $\mathbf{H}(n)$ exists. If $\mathbf{H}(n)$ does not exist, it is

sufficient to take the first n rows of $\mathbf{H}(m)$, where m is the smallest integer that satisfies $m > n$ with known $\mathbf{H}(m)$.

In conclusion, it has to be highlighted that the proposed scheme may require simultaneous rotations of multiple qubits. If the available NMR instrumentation is not able to perform simultaneous rotations, other refocusing schemes can be adopted, even if they are significantly less compact, causing a significant increase of the number of required time intervals.

6.3 Hints on experimental issues

6.3.1 Pseudopure states

Conventional NMR experiments deal with a large ensemble of spins, as explained in section §4.2. Therefore, the state of the system is described by a density operator. At thermal equilibrium, the density operator is a statistical mixture (cf. section §4.2.1) obviously inadequate for quantum information processing, which requires a **fiducial initial state**. For a two-qubit molecule, the thermal density matrix can be shown to be

$$\rho_0 = \frac{e^{-\frac{\mathcal{H}}{k_B T}}}{\text{tr}\left(e^{-\frac{\mathcal{H}}{k_B T}}\right)} \sim \left(\frac{\mathbb{I}}{2}\right)^{\otimes 2} + \frac{\hbar}{8k_B T} \begin{pmatrix} \omega_{0,1} + \omega_{0,2} & 0 & 0 & 0 \\ 0 & \omega_{0,1} - \omega_{0,2} & 0 & 0 \\ 0 & 0 & -\omega_{0,1} + \omega_{0,2} & 0 \\ 0 & 0 & 0 & -\omega_{0,1} - \omega_{0,2} \end{pmatrix} = \left(\frac{\mathbb{I}}{2}\right)^{\otimes 2} + \Delta\rho_0 \quad (6.3.1)$$

following the same procedure of the proof of Equation 4.2.9. The first term represents a uniformly mixed ensemble of all possible states, while the second term is a very tiny deviation from the uniformly mixed ensemble. The density matrix expression is trivially generalised to n qubits. The aim is to prepare a so-called **pseudopure state** out of the thermal equilibrium state. Suppose that it is possible to transform the density matrix such that

$$\left(\frac{\mathbb{I}}{2}\right)^{\otimes n} + \Delta\rho_0 \longrightarrow \left(\frac{\mathbb{I}}{2}\right)^{\otimes n} + \alpha \begin{pmatrix} 1 & 0 & \dots & 0 \\ 0 & 0 & \dots & 0 \\ \vdots & \ddots & \dots & 0 \\ 0 & 0 & \dots & 0 \end{pmatrix} \quad (6.3.2)$$

Since it can be shown that the signal used to measure NMR spectra arises only from the traceless deviation matrix [5, 17], it follows that the obtained matrix, that is, the pseudopure state, effectively yields a signal from the pure state $\rho = |00\rangle\langle 00|$, but the amplitude is multiplied by α which turns out [5] to be of the order of

$$\alpha \sim \frac{\hbar\omega_0}{2^n k_B T} \quad (6.3.3)$$

where n is the number of qubits. It follows that the signal from a particular initial state reduces exponentially as a function of the number of qubits. This is one of the main issues against the scalability of liquid-state NMR quantum computers.

There are several techniques to produce pseudopure states, as temporal averaging, spatial averaging and state labelling [17], which have in common the fact that non-unitary operations must be exploited.

6.3.2 Quantum state tomography

In conclusion, once a fiducial pseudopure state has been obtained and the designed pulses have been applied to the system to implement the required quantum algorithm, it is necessary to characterize the output state. Since NMR always deals with ensembles and not with single spins, the measurement procedure is not a projective measurement, as it is for other candidates of quantum computers, but an **ensemble measurement** [5]. Moreover, in many cases, one wants a full characterization of the system state, rather than a simple readout. The full reconstruction of the density matrix, known as **quantum state tomography**, requires to perform a series of measurements and to combine the results to obtain the density matrix elements. First of all, it has to be pointed out that the rotating frame density operator $\tilde{\rho}$ evolves in time during the measurement ($t > 0$) because of the J-coupling

$$\rho(t) = U_J(t) \tilde{\rho} U_J^\dagger(t) \quad (6.3.4)$$

The first step is to transform $\tilde{\rho}$ back to the laboratory frame, where the measurement is actually carried out:

$$\rho = U_R^\dagger \tilde{\rho} U_R \quad (6.3.5)$$

where U_R is the unitary operator which describes the transformation from the laboratory frame to the multiple rotating frame. The aim is to measure the terms of ρ and compute those of $\tilde{\rho}$. The corresponding magnetization vector, while precessing, decays as explained in section §4.3. The signal corresponding to the x-component of the magnetization vector is recorded and Fourier transformed. Tilting the density matrix with appropriate rotations and repeating several measurements of the x-component of the magnetization vector, it is possible to determine experimentally all terms of the density operator [5].

Chapter 7

Quantum_MOLE: an NMR quantum computer model

The relations ruling nuclear magnetic resonance phenomena, derived from first physical principles in the previous chapters, are exploited to design a flexible, fully parametric, NMR quantum computer model, able to run quantum algorithms and to measure the performances achievable with different kinds of molecules. The output data, supported by highly intuitive charts, can be useful to find an optimal operating point as a compromise between molecule physical properties and the quantities which can be controlled by nowadays NMR instrumentation. The input technological parameters, as chemical shielding and J-coupling, can be determined resorting on computational chemistry software, as ORCA, or obtained from experimental data.

As known from the previous discussion, an actual real-world NMR quantum computing experiment consists of three main steps: preparation of pseudopure states, execution of the quantum algorithm and measurement of the outcome. The proposed model focuses on the second step, for a molecule with a theoretically arbitrary number of nuclear spins.



Figure 7.1: NMR quantum computing experiment.

This chapter describes the structure of the model, the main approximations and their justification and explains how to get the most out of it.

7.1 The structure of the model

An NMR quantum computer model shall be able to simulate the execution of one-qubit quantum gates and two-qubit CNOT and CZ quantum gates on the nuclear spins of a chosen diamagnetic molecule and evaluate the corresponding performances. A reasonable set of performance figures of merit consists in

- Execution time.
- Fidelity.
- Measurement probabilities.

Moreover, it has to take into account some non-idealities, *when they are relevant*. For instance

- Off-resonance unwanted evolution.
- J-coupling unwanted evolution during one-qubit gate execution.
- Relaxation and decoherence phenomena.

As usual, the accuracy with which the computation is carried out has to be traded off with the CPU time, which can easily reach inconvenient values. This is the realm of several approximations which can be introduced to speed up the computation. Quantum computing MOlecular Emulator (Quantum_MOLE) can be run at several levels of approximation and it is extremely flexible. In particular there three main possibilities offered by the simulator

- Approximate computation when the conditions enumerated at the beginning of section §6.2.1 hold true and Equation 6.1.10 is a satisfactory approximation of the actual Hamiltonian.
- An exact computation which proceeds with a direct integration of Equation 6.1.6 (CPU intensive).
- An exact computation supported by an automatic refocusing routine, particularly suitable for some homonuclear molecules.

A high-level flow chart of the proposed software model is reported in Figure 7.2.

7.1.1 The input parameters

The designed emulator needs physical and logical input parameters to carry out the required simulation.

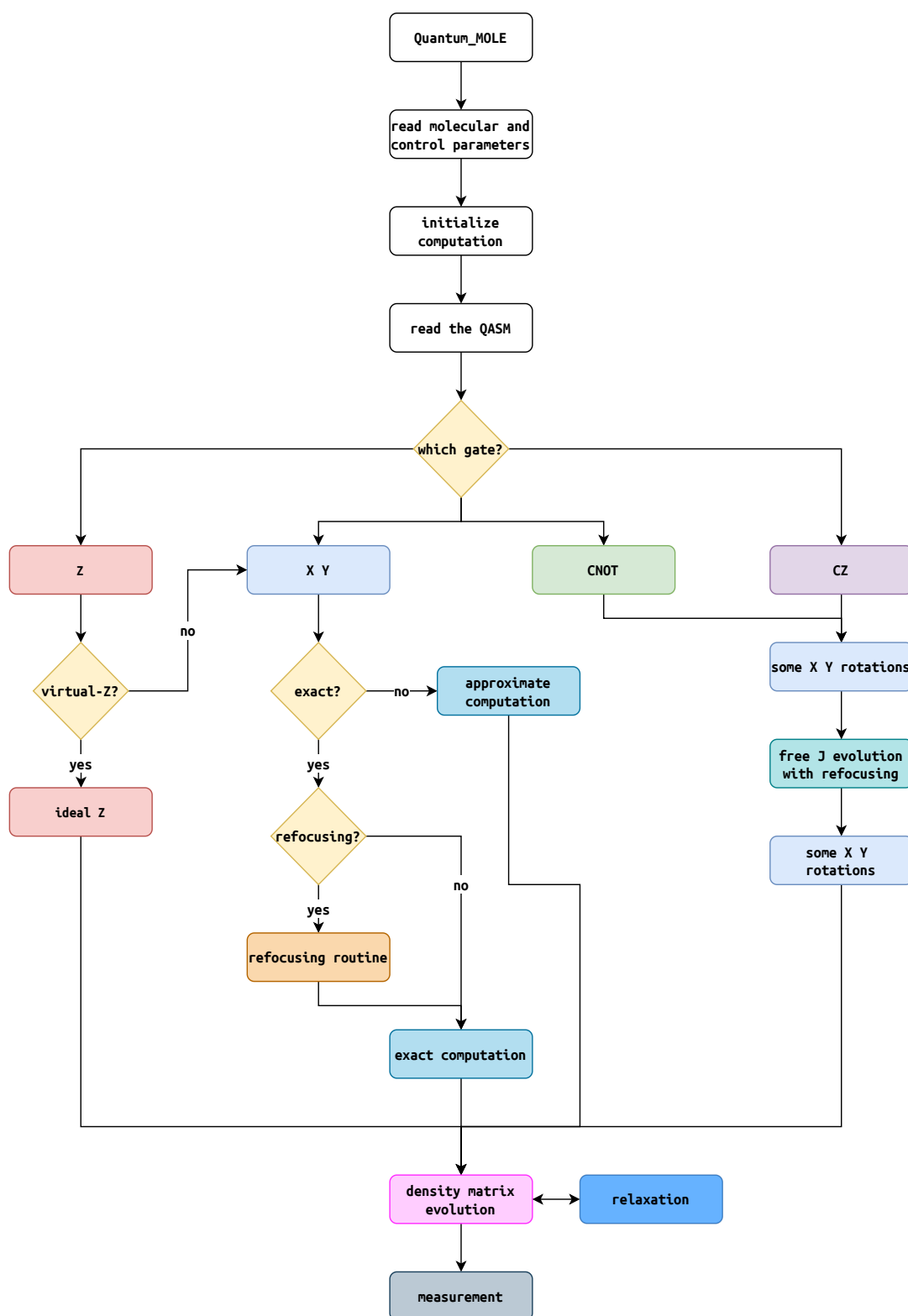


Figure 7.2: Flow chart of the model.

7.1.1.1 The input physical parameters

An NMR molecule can be characterized in terms of several physical parameters, which have been thoroughly discussed in the previous chapters. These have to be provided in input to the model:

- Number of magnetic nuclei in the molecule.
- Gyromagnetic ratio γ_n per each magnetic nucleus.
- Isotropic chemical shift constant δ per each magnetic nucleus.
- Relaxation constants T_1 and T_2 per each magnetic nucleus.
- Indirect spin-spin coupling constant J for each couple of magnetic nuclei.

Once the molecule is well defined, one has to select proper values for the control parameters:

- The magnitude of the static field B_0 which is applied along the \hat{z} axis.
- The amplitude B_r of the radio-frequency field.
- The time duration τ of each pulse.

In particular, as clear from Equation 6.2.2, the amplitude of the RF field and the time duration are strictly interdependent, since the product of τ and ω_* must be equal to the desired rotation angle. The model accepts in input either B_r or τ and computes the other according to θ . In particular, a specific value of B_r or τ can be declared for each magnetic nucleus.

The software runs several checks on the reciprocal consistency of the provided input data.

7.1.1.2 The QASM description of the algorithm

The model can read the quantum algorithm description from a `.qasm` file, written according to IBM QASM syntax, which is presented in section §2.3. For instance, one can use **IBM Q experience** [1] graphical editor, download the corresponding `.qasm` file and then run `Quantum.MOLE` to simulate the execution on an NMR quantum processor. The complete set of single-qubit quantum gates and the CNOT and the CZ gates are fully supported. A dedicated routine reads the input file and prompts different scripts according to the identified gate, computing, when needed, the required rotation angle and phase, according to section §6.2. At the

same time, a corresponding “ideal gate”, based on the Pauli matrices and the ideal rotations presented in section §2.1.6 is built up so that, at the end of the execution, the software can compare the ideal and the actual outcomes, computing the corresponding **fidelity**.

7.1.2 The approximate computation

The approximate execution can be selected when the system is described by the rotating frame Hamiltonian of Equation 6.1.10, that is for all heteronuclear molecules and for some homonuclear ones. Even if already explained, it is worth repeating the limits of validity of this expression:

- Weak coupling regime $|\Delta\omega_0| \gg |2\pi J|$, so that for a time scale $|\Delta\omega_0\tau| \gg 2\pi \gg |2\pi J\tau|$ the $\mathbf{I}_x \otimes \mathbf{I}_x$ and $\mathbf{I}_y \otimes \mathbf{I}_y$ contributions are averaged to vanish (Equation 6.1.7).
- Difference in the Larmor frequencies such that selective addressing is achievable, that is $|\Delta\omega_0\tau| \gg 2\pi$ or $|\Delta\omega_0| \gg \omega_{*,i}$ (Equation 6.1.8). This means that soft pulses must be adopted for homonuclear molecules.
- Pulse width short enough to ignore at first order the indirect spin-spin coupling during the pulses $\tau \ll |1/J|$ or $\omega_{*,i} \gg |2\pi J|$, so that the unwanted J-evolution does not affect the execution of the desired quantum gate.
- Time duration τ such that $\left| \frac{2\pi}{\Delta\omega_0} \right| \ll \tau \ll \left| \frac{1}{J} \right|$ [67].

In the following, the procedure adopted to efficiently implement the supported gates is detailed.

7.1.2.1 The qubit representation and the initial state

As argued in section §4.2, liquid-state NMR is most suitably described by density operators, rather than state vectors. Quantum_MOLE adopts a full density matrix formalism to represent the quantum state of the system. The initial pseudopure state is approximated with an ideal state

$$\rho = \begin{pmatrix} 1 & 0 & \cdots & 0 \\ 0 & 0 & \cdots & 0 \\ \vdots & \ddots & & \\ 0 & 0 & \cdots & 0 \end{pmatrix} \quad (7.1.1)$$

7.1.2.2 Rotation about \hat{x} or \hat{y}

As known from section §6.2, all quantum gates can, in the end, be reduced to rotations about \hat{x} and \hat{y} axes. Hence, the implementation of these rotations is the computational core of the simulator. In particular, the rotating frame contributions due to J-coupling and the difference between the alternating field frequency (i.e. the frequency of the rotating frame) and the corresponding Larmor frequency of the spin (Equation 6.1.7), which are respectively denoted by H_0 and H_J for the sake of simplicity, can be precomputed at the beginning and used every time a \hat{x} or \hat{y} -rotation is required.

```

1 H_J = zeros(2^Nspin); % initialization
2 H_0 = H_J; % initialization
3
4 for a = 1 : Nspin
5     for b = 1 : a-1
6         if J_coupling(a,b) ~= 0
7             P_za = kron(eye(2^(a-1)), kron(Z/2, eye(2^(Nspin-a))));
8             P_zb = kron(eye(2^(b-1)), kron(Z/2, eye(2^(Nspin-b))));
9             H_J = H_J + 2*pi*J_coupling(a,b)*P_za*P_zb;
10            end
11        end
12        H_0 = H_0 + (omega_rf(a) - omega_0(a)) * kron(eye(2^(a-1)), kron(Z/2,
    ↪ eye(2^(Nspin-a))));
13    end
14    % P_za and P_zb are temporary variables used to build up the required
    ↪ operators I_za and I_zb for each spin couple a-b.
15    % J_coupling is a matrix which stores the J-coupling constants for all couples
    ↪ of spins.

```

Then either the pulse duration τ (τ)

```

1 tau(length(tau) + 1) = rotation_angle/omega_ast(target_qubit);

```

or the radio frequency field amplitude B_r (Br)

```

1 omega_ast = rotation_angle/tau(target_qubit);
2 Br(length(Br) + 1) = omega_ast/gamma(target_qubit);

```

is computed, according to the user choice. The variable `target_qubit` denotes the qubit on which the quantum gate is expected to be applied. The final step is

the computation of the RF contribution to the rotating frame Hamiltonian H_{rf} and the overall time evolution operator U

```
1 P_x = kron(eye(2^(target_qubit-1)), kron(X/2, eye(2^(Nspin-target_qubit))));
2 P_y = kron(eye(2^(target_qubit-1)), kron(Y/2, eye(2^(Nspin-target_qubit))));
3
4 H_rf = omega_ast(target_qubit)*( cos(phase)*P_x + sin(phase)*P_y );
5
6 H_tot = H_rf+ H_J + H_0; % total rotating frame Hamiltonian
7 U = expm(-1i*H_tot*tau(end)); % time evolution operator
```

This piece of code reports the case in which Br is an input parameter and τ is computed consequently. The opposite case is easily derived by analogy. The reader should note that the unwanted J-coupling evolution during single-qubit pulses is taken into consideration by the time evolution operator U , thus making the model more realistic with respect to Equation 6.2.1.

7.1.2.3 Rotation about z

An arbitrary rotation about the \hat{z} axis can be implemented by means of some x-y-rotations (Equation 6.2.3) or resorting to the Virtual-Z method. As far as the first approach is concerned, the routine which implements the z-rotation shall simply call the x-y-rotation routine three times with an appropriate choice of the corresponding rotation angle and phase.

```
1 rotation_angle_z = rotation_angle; % angle by which the qubit shall be rotated
  ↪ about the z-axis.
2
3 % Rx(-pi/2)
4 rotation_angle = pi/2;
5 phase = pi;
6 nmr_x_y_rotation
7
8 % Ry(rotation_angle)
9 rotation_angle = rotation_angle_z;
10 phase = pi/2;
11 nmr_x_y_rotation
12
13 % Rx(pi/2)
14 rotation_angle = pi/2;
15 phase = 0;
16 nmr_x_y_rotation
```

On the other hand, the Virtual-Z method allows to implement a perfect rotation about \hat{z} , with a null time duration. This approach can be modelled using an ideal z-rotation matrix R_z (as Equation 2.1.52), instead of the NMR Hamiltonian, to build the time evolution operator up:

```
1 U = kron(eye(2^(target_qubit-1)), kron(Rz(rotation_angle),  
  ↪ eye(2^(Nspin-target_qubit))));
```

7.1.2.4 The Hadamard gate

The simulator automatically selects the most efficient approach to implement the Hadamard gate. In particular, if the Virtual-Z method is available, then the Hadamard gate is implemented as a rotation $R_y(-\pi/2)$ followed by a rotation $R_z(\pi)$:

```
1 % Ry(-pi/2)  
2 rotation_angle = pi/2;  
3 phase = -pi/2;  
4 nmr_x_y_rotation  
5  
6 % Rz(pi)  
7 rotation_angle = pi;  
8 nmr_z_rotation
```

If the Virtual-Z method is not available, then the Hadamard gate is implemented as a rotation $R_y(\pi/2)$ followed by a rotation $R_x(\pi)$:

```
1 % Ry(pi/2)  
2 rotation_angle = pi/2;  
3 phase = pi/2;  
4 nmr_x_y_rotation  
5  
6 % Rx(pi)  
7 rotation_angle = pi;  
8 phase = 0;  
9 nmr_x_y_rotation
```

7.1.2.5 Free J-evolution with refocusing

As well known from the previous discussion on NMR quantum computation, the implementation of two-qubit quantum gates requires the evolution under J-coupling between a couple of qubits, while the interactions with the other qubits must be switched off applying the refocusing techniques (cf. section §6.2.3). In order not to overly complicate the model and cause a useless increase of the CPU time required to run the simulation, the refocusing technique is emulated by simply assuming that the unwanted interactions are turned off. In other words, when a quantum gate requires the implementation of the operator U_J between a `control_qubit` and a `target_qubit`, Quantum_MOLE assumes that proper refocusing techniques are implemented during the actual experiment and simply drops the operators for the other qubits:

```

1 P_z_a = kron(eye(2^(control_qubit-1)), kron(Z/2, eye(2^(Nspin-control_qubit))));
2 P_z_b = kron(eye(2^(target_qubit-1)), kron(Z/2, eye(2^(Nspin-target_qubit))));
3 % note that only the operators corresponding to the target and control qubit
  ↪ are taken into consideration.
4
5 H_J_tmp = 2*pi*J_coupling(control_qubit,target_qubit)*P_z_a*P_z_b;
6
7 U = expm(-1i*H_J_tmp*tau_J(end));

```

where `tau_J` is the time duration of the free J-evolution.

7.1.2.6 The CNOT gate

As explained in section §6.2.2.1, the CNOT gate is implemented as a cascade of rotations about \hat{z} , \hat{y} and \hat{z} axes, the rotation angle of each depending on the sign of the J-coupling, and a free J-coupling evolution for a time $\tau = |1/2J|$. The CNOT routine prompts the execution of the previously introduced routines with a proper choice of the rotation angle and the phase.

```

1 sgn_J = sign(J_coupling(control_qubit, target_qubit));
2
3 % Ry(pi/2) target qubit
4 rotation_angle = pi/2;
5 phase = pi/2;
6 nmr_x_y_rotation
7

```

```
8 % Free evolution for tau = 1/2J
9 tau_J(length(tau_J)+1) = abs(1/(2*J_coupling(control_qubit, target_qubit)));
10 nmr_free_j_evolution
11
12 % Rx(sgn(J)pi/2) target qubit
13 rotation_angle = pi/2*sgn_J;
14 phase = 0;
15 nmr_x_y_rotation
16
17
18 % Rz(-sgn(J)pi/2) target qubit
19 rotation_angle = -pi/2*sgn_J;
20 nmr_z_rotation
21
22 % Rz(sgn(J)pi/2) control qubit
23 target_qubit = control_qubit; %CNOT control qubit is the target of this
   ↪ rotation
24 rotation_angle = pi/2*sgn_J;
25 nmr_z_rotation
```

Note that the CNOT gate can be executed between an arbitrary couple of qubits, granted that a non-zero J-coupling does exist between them.

7.1.2.7 The controlled-Z gate

As shown in section §6.2.2.2, the controlled-Z gate is implemented as a cascade of rotations about \hat{z} axis, the rotation angle of each depending on the sign of the J-coupling, and a free J-coupling evolution for a time $\tau = |1/2J|$. The controlled-Z routine prompts the execution of the previously introduced routines with a proper choice of the rotation angle and the phase.

```
1 sgn_J = sign(J_coupling(control_qubit, target_qubit));
2 target_qubit_CZ = target_qubit; % target of CZ gate
3
4 % Rz(-sgn(J)pi/2) target qubit
5 target_qubit = target_qubit_CZ;
6 rotation_angle = -pi/2*sgn_J;
7 nmr_z_rotation
8
9 % Rz(-sgn(J)pi/2) control qubit
10 target_qubit = control_qubit; %CZ control qubit is the target of this rotation
11 rotation_angle = -pi/2*sgn_J;
```

```

12 nmr_z_rotation
13
14 % Free evolution for tau = 1/2J
15 target_qubit = target_qubit_CZ;
16 tau_J(length(tau_J) +1) = abs(1/(2*J_coupling(control_qubit, target_qubit)));
17 nmr_free_j_evolution

```

Note that also the controlled-Z gate can be executed between an arbitrary couple of qubits, granted that a non-zero J-coupling does exist between them.

7.1.2.8 The time evolution of the density operator

The time evolution of the density operator is known to be

$$\rho(t) = U \rho U^\dagger \quad (7.1.2)$$

However, during the update of the density operator, that is, during the execution of the quantum gate, decoherence and relaxation phenomena take place, affecting the resulting matrix. In section §4.3, a phenomenological model for one-qubit density matrices is proposed, according to which both the coherences and the populations are subjected to an exponential decay. In particular, in the rotating frame after a time interval $0 \rightarrow \tau$, the density matrix becomes

$$\rho(t)_{0 \rightarrow \tau} = \begin{pmatrix} (\rho_\alpha(0) - \rho_\alpha^{\text{eq}}) e^{-\frac{\tau}{T_1}} + \rho_\alpha^{\text{eq}} & [\tilde{\rho}_+(0) e^{-i\xi t}] e^{-\frac{\tau}{T_2}} \\ [\tilde{\rho}_-(0) e^{i\xi t}] e^{-\frac{\tau}{T_2}} & (\rho_\beta(0) - \rho_\beta^{\text{eq}}) e^{-\frac{\tau}{T_1}} + \rho_\beta^{\text{eq}} \end{pmatrix} \quad (7.1.3)$$

Assuming the resonance condition, the previous expression becomes

$$\rho(t)_{0 \rightarrow \tau} = \begin{pmatrix} (\rho_\alpha(0) - \rho_\alpha^{\text{eq}}) e^{-\frac{\tau}{T_1}} + \rho_\alpha^{\text{eq}} & \tilde{\rho}_+(0) e^{-\frac{\tau}{T_2}} \\ \tilde{\rho}_-(0) e^{-\frac{\tau}{T_2}} & (\rho_\beta(0) - \rho_\beta^{\text{eq}}) e^{-\frac{\tau}{T_1}} + \rho_\beta^{\text{eq}} \end{pmatrix} \quad (7.1.4)$$

The generalization of this phenomenological model to a density operator which describes a multi-spin partially coupled system is by no means a trivial task [33] since each coherence and each population is expected to decay with a particular time constant. Moreover, if it is relatively simple to find in the currently available scientific literature the experimental values of single-nucleus time constants T_1 and T_2 (which cannot be computed with ORCA), it is very hard to find data on the decay time constants for coupled systems. At the time of writing, Quantum_MOLE handles the issue adopting a simplified worst-case approach. In particular, every coherence is assumed to decay with a time constant equal to the minimum T_2

(T2_min) and every population is assumed to decay with a time constant equal to the minimum T_1 (T1_min).

```
1 for a = 1 : 2^Nspin
2   for b = 1 : 2^Nspin
3     if a == b
4       rho(a,b) = rho(a,b)*exp(-tau_relax/T1_min) +
        ↪ rho_eq(a,b)*(1-exp(-tau_relax/T1_min)); % population
5     else
6       rho(a,b) = rho(a,b)*exp(-tau_relax/T2_min); % coherence
7     end
8   end
9 end
10 % tau_relax is the time duration (expressed as input parameter or computed) of
    ↪ the pulse or of the the free J-evolution
```

The evaluation of decoherence and relaxation phenomena is arbitrarily carried out per each quantum gate before the actual update of the density operator with the time evolution operator.

```
1 decoherence %evaluation of the decoherence and relaxation
2 rho = U*rho*U'; % update of the density matrix
```

7.1.2.9 The handling of output data

In the end, the outcome of the actual execution is stored in a $N \times N$ density matrix, where N is the number of qubits. Quantum_MOLE provides several supporting charts and data which help in understanding the obtained result. First, the **estimated time** to run the algorithm on the chosen molecule is computed as the sum of the time durations required by the single quantum gates. Second, as known from section §4.2, the populations represent the *probability* of finding a member of the ensemble in one of the basis states, when performing a measurement. Consequently, the diagonal elements of the density matrix are used to plot a **histogram** of the probability of each eigenstate. The latter is compared with the corresponding histogram resulting from the ideal computation. Third, the methodology introduced in section §1.2.4.3 is exploited to compute the density operators describing single qubits. In other words, each qubit is considered ad subsystem which is derived from the composite system tracing out the other

subsystems. From the obtained density matrices, meaningful exclusively for non-entangled qubits, the generalized Bloch vector can be derived, according to section §2.1.5.2. This allows to plot a Bloch vector in a **Bloch ball** for each qubit and is a formidable tool to visually understand the outcome of a quantum algorithm. Furthermore, the same procedure is carried out for the density matrix resulting from the ideal computation, so that the user can compare the physical world and the ideal world results with a glimpse. Finally, the **fidelity** of the actual result against the ideal one, is computed for each qubit and for the complete system density matrix, according to section §1.2.4.6. Thanks to an accurate design of the software utilities, the output graphic interface is automatically adapted to the number of qubits, preserving the readability and rational arranging.

7.1.3 The exact computation

The exact computation is designed to be adopted in two different scenarios:

- One or more conditions reported at the beginning of section §7.1.2 are not satisfied. In this case, the approximate model is not expected to provide reliable results and shall not be used.
- The conditions reported at the beginning of section §7.1.2 are satisfied and the user wants to optimize the RF pulses to maximize the fidelity of some specific gate sequences or minimize the execution time.

In both cases, the exact computation module provides reliable and useful results, but the CPU time increases considerably. In the following, the differences with respect to the approximate computation are detailed.

7.1.3.1 Rotation about x or y

The exact computation module proceeds with direct numerical integration of the rotating frame Hamiltonian to compute the time evolution operator. The operation is CPU intensive, in particular if there are several qubits and the Hamiltonian is a large complex matrix.

The first step is the evaluation of the complete laboratory frame¹ J-coupling Hamiltonian H_J . In this case, also the I_x and I_y operators are retained, differently with respect to the approximate execution.

¹Please, note that the symbol H_J is here used to denote the laboratory frame Hamiltonian

```

1 for a = 1 : Nspin
2   for b = 1 : a-1
3     if J_coupling(a,b) ~= 0
4       P_xa = kron(eye(2^(a-1)), kron(X/2, eye(2^(Nspin-a))));
5       P_xb = kron(eye(2^(b-1)), kron(X/2, eye(2^(Nspin-b))));
6       P_ya = kron(eye(2^(a-1)), kron(Y/2, eye(2^(Nspin-a))));
7       P_yb = kron(eye(2^(b-1)), kron(Y/2, eye(2^(Nspin-b))));
8       P_za = kron(eye(2^(a-1)), kron(Z/2, eye(2^(Nspin-a))));
9       P_zb = kron(eye(2^(b-1)), kron(Z/2, eye(2^(Nspin-b))));
10
11
12     H_J = H_J + 2*pi*J_coupling(a,b)*(P_xa*P_xb + P_ya*P_yb + P_za*P_zb);
13   end
14 end
15 H_0 = H_0 + (omega_rf(a) - omega_0(a)) * kron(eye(2^(a-1)), kron(Z/2,
    ↪ eye(2^(Nspin-a))));
16 end

```

Note that the *rotating frame* H_0 contribution is also computed in parallel for efficiency optimization. Once either the time duration or the RF field amplitude has been computed, as in the approximate case, the complete laboratory frame Hamiltonian, except for the aforementioned H_0 contribution, is

```

1 P_x = zeros(2^Nspin);
2 for k = 1 : Nspin
3   P_x = P_x + gamma(k)/gamma(target_qubit) * kron(eye(2^(k-1)), kron(X/2,
    ↪ eye(2^(Nspin-k))));
4 end
5
6 H_lab_frame = @(t) 2*omega_ast(target_qubit)*cos(omega_rf(target_qubit)*t -
    ↪ phase)*P_x + H_J;

```

The operator which introduces the transformation from the laboratory frame to the multi-rotating frame is given by

```

1 U_rot = @(t) f_rotating_frame(Nspin, omega_rf, Z, t);

```

where

```

1 function a = f_rotating_frame(Nspin, omega_rf, Z, t)
2 a = 1;

```

```

3 for k = 1 : Nspin
4     a = kron(a, expm(-1i*omega_rf(k)*Z/2*t));
5 end
6 end

```

according to a generalization of Equation 6.1.5. The complete rotating frame Hamiltonian is simply

```

1 H_rot_frame = @(t) U_rot(t)*H_lab_frame(t)*U_rot(t)' + H_0;

```

as in Equation 6.1.6. Eventually, the time evolution operator is computed via direct integration of the rotating frame Hamiltonian in the time interval $0 \rightarrow \tau$:

```

1 U = expm(-1i*integral(H_rot_frame,1e-10,tau(end),'ArrayValued',true));

```

7.1.3.2 Free J-evolution with refocusing

The only difference with respect to section §7.1.2.5 is that Quantum_MOLE takes into account not only the I_z operators for `control_qubit` and `target_qubit`, but also I_x and I_y operators. Hence, the laboratory frame Hamiltonian, except for the H_0 contribution becomes

```

1 P_xa = kron(eye(2^(control_qubit-1)), kron(X/2, eye(2^(Nspin-control_qubit))));
2 P_xb = kron(eye(2^(target_qubit-1)), kron(X/2, eye(2^(Nspin-target_qubit))));
3 P_ya = kron(eye(2^(control_qubit-1)), kron(Y/2, eye(2^(Nspin-control_qubit))));
4 P_yb = kron(eye(2^(target_qubit-1)), kron(Y/2, eye(2^(Nspin-target_qubit))));
5 P_za = kron(eye(2^(control_qubit-1)), kron(Z/2, eye(2^(Nspin-control_qubit))));
6 P_zb = kron(eye(2^(target_qubit-1)), kron(Z/2, eye(2^(Nspin-target_qubit))));
7
8 H_lab_frame = 2*pi*J_coupling(control_qubit,target_qubit)*(P_xa*P_xb +
↪ P_ya*P_yb + P_za*P_zb);

```

The time evolution operator becomes

```

1 U_rot = @(t) f_rotating_frame(Nspin, omega_rf, Z, t);
2 H_J_tmp = @(t) U_rot(t)*H_lab_frame*U_rot(t)' + H_0;
3
4 U = expm(-1i*integral(H_J_tmp,1e-10,tau_J(end),'ArrayValued',true));

```

7.1.4 The exact computation with automatic refocusing

Heteronuclear molecules are characterized by a large difference in Larmor frequencies. Therefore, an approximate execution is expected to provide reliable results, which can be optimized running some parametric exact computations to find, for instance, the values of τ or B_r which maximize the fidelity for some gates. However, the use of heteronuclear molecules for NMR quantum computation is limited by the physical availability of magnetic nuclei, since each spin has to be encoded on a different kind of nucleus. Therefore, homonuclear molecules are often adopted in actual NMR quantum computing experiments. For some homonuclear molecules with a difference in Larmor frequencies which is anyway significantly larger than the J-coupling constants, as cytosine, rectangular soft pulses can be found which guarantee satisfactory fidelities on simple quantum algorithms. On the other hand, other homonuclear molecules with large couplings and small frequency shifts, as crotonic acid, do not allow a simple determination of optimized soft rectangular pulses. In these cases, there are two viable approaches. The first one is the adoption of numerically optimised pulses (also non-rectangular pulses), as provided by the gradient ascent pulse engineering optimizations (GRAPE). This approach is not currently supported by Quantum_MOLE. The second one is the exploitation of hard pulses to implement a kind of auto-refocusing. According to [68], a generic rotation about \hat{x} or \hat{y} can be implemented as

$$\mathbf{R}(\theta) = \mathbf{R}_z(\phi) \mathbf{R}_y\left(\frac{\pi}{2}\right) \mathbf{R}_z(\theta) \mathbf{R}_y\left(-\frac{\pi}{2}\right) \mathbf{R}_z(\phi) \quad (7.1.5)$$

where

$$\phi = \begin{cases} 0 & \longrightarrow \mathbf{R}_x(\theta) \\ \frac{\pi}{2} & \longrightarrow \mathbf{R}_y(\theta) \end{cases} \quad (7.1.6)$$

The rotations about \hat{y} in blue are **hard** pulses, that is, pulses for which τ is short enough to ensure that the Fourier spectrum has the components which resonate with *all* homonuclear spins. Otherwise stated, a single hard pulse prompts all homonuclear spins to perform the rotation about \hat{y} . The reader is referred to the aforementioned reference for a detailed treatment of this equation. The rotations about \hat{z} can be made J-coupling independent by adopting the refocusing techniques presented in section §6.2.3 or by resorting to the Virtual-Z method, which, as well known, allows the implementation of zero-lag ideal gates. Quantum_MOLE assumes that Virtual-Z method is implemented when the exact computation with

the auto-refocusing module is run. At the code level, the implementation of this procedure is obtained replacing the previously introduced routine for the rotations about \hat{x} and \hat{y} with an ad hoc routine.

7.1.4.1 Rotation about x and y

The following piece of code implements Equation 7.1.5.

```
1 rotation_angle_autorefocusing = rotation_angle;
2 phase_autorefocusing = phase;
3
4 %% Rotation about Z of -gamma
5 rotation_angle = -phase_autorefocusing; % axis angle is 0 for a rotation about
   ↪ X and pi/2 for a rotation about Y
6 nmr_z_rotation
7
8 %% Strong pulse about -Y of pi/2
9 rotation_angle = pi/2;
10 phase = -pi/2;
11 nmr_x_y_rotation
12
13 %% Rotation of an angle rotation_angle about Z
14 rotation_angle = rotation_angle_autorefocusing;
15 nmr_z_rotation
16
17 %% Strong pulse about Y of pi/2
18 rotation_angle = pi/2;
19 phase = pi/2;
20 nmr_x_y_rotation
21
22 %% Rotation about Z of gamma
23 rotation_angle = phase_autorefocusing; % axis angle is 0 for a rotation about
   ↪ X and pi/2 for a rotation about Y
24 nmr_z_rotation
```

It is clear the the execution is meaningful only if proper values of τ or B_r for hard pulses are provided in input.

7.2 User manual

This section is devoted to a short user manual for the optimal use of `Quantum_MOLE`.

Input molecular parameters The user is expected to provide the following physical parameters:

- The number of qubits `Nspin`.
- The gyromagnetic ratio per each qubit, ordered² from qubit 1 to qubit `Nspin` in the `gamma` vector.
- The longitudinal relaxation constant per each qubit, ordered from qubit 1 to qubit `Nspin` in the `T1` vector.
- The transverse relaxation constant per each qubit, ordered from qubit 1 to qubit `Nspin` in the `T2` vector.
- The isotropic chemical shift constant per each qubit, ordered from qubit 1 to qubit `Nspin` in the `delta` vector.
- The J-coupling constant between each couple of qubits as `J_coupling_tm_j`
 $p(a,b) = J$.

Input control parameters The user is expected to provide the following control parameters:

- The value of the magnitude of the static field `B_0`.
- The value of the magnitude of the RF field per each qubit, ordered from qubit 0 to qubit `Nspin` in the `Br` vector.
- The pulse time duration per each qubit, ordered from qubit 0 to qubit `Nspin` in the `tau` vector.

Choose the kind of execution The user shall also specify:

- The name of the input `.qasm` file `file_name`.
- The flag `virtual_z` enables the Virtual-Z method, if set to 1.

²The spins are ordered from 1 to `Nspin`, according to `Matlab` convention. Conversely, qubits are ordered from 0 to `Nspin - 1`, according to `QASM` convention.

- The flag `exact_computation` enables the exact computation module, if set to 1.
- The flag `autorefocusing` enables the auto-refocusing method, if set to 1. It requires the Virtual-Z method to be enabled.
- The flag `save_workspace` enables the automatic saving of the workspace, if set to 1.

7.3 Hints on the use of ORCA

ORCA [3, 2] is a free computational chemistry software, able to compute molecular and atomic properties. As far as NMR is concerned, it can evaluate chemical shielding and J-coupling tensors. While the computation of the former is quite reliable, to get accurate J-couplings is demanding, even with deep knowledge in quantum computational chemistry. This is an issue well known to the NMR scientific community. In the following, it is explained how to start ORCA and compute NMR parameters.

The first step is to find an unoptimized geometry of the molecule, for instance in [69]. Then, open the .mol file with Avogadro [63], go to **Extensions -> ORCA -> Generate Orca Input -> Geometry optimization** and save. The obtained .inp file has to be properly modified to run the required computation. Consider the following input file for a chloroform molecule:

```
1 !B3LYP D3BJ def2-TZVPP def2/JK tightopt tightscf CPCM(water)
2
3 * xyz 0 1
4 C1      0.93343      1.59184      0.61140
5 C1     -1.50886      0.29931      1.50276
6 C1      0.94758     -1.23285      1.28287
7 C      -0.00990      0.08528      0.57081
8 H      -0.26062     -0.16585     -0.48031
9 *
10
11 %pal nprocs 10 end
12
13 %eprnmr
14 Nuclei = all C {ssall, shift, ist=13}
15 Nuclei = all H {ssall, shift, ist=1}
16 end
```

It asks ORCA to compute the chemical shielding tensor and the J-coupling tensor for carbon and hydrogen atoms. The structure of the input file is explained in the following, for any further doubt the reader is referred to ORCA user manual.

- B3LYP D3BJ is the functional adopted by ORCA for the computation. In particular, B3LYP is a hybrid functional which selects a density functional theory (DFT) method. In other words, it is the modelling method used by ORCA to investigate the molecular properties. D3BJ is a correction term added to include dispersion forces.

- `def2-TZVPP` is a doubly polarized triple-zeta basis set. A basis set is the set of orbitals used to build molecular orbitals.
- `def2/JK` is an auxiliary basis set.
- `CPCM(water)` is the solvent.
- `* xyz 0 1` denotes the beginning of the molecular coordinates. `0` is the charge and `1` is the spin multiplicity.
- `pal nprocs 10` is used to specify the number of available parallel processors on which the simulation can be run.
- `eprnmr` is used to start the computation of NMR parameters. `all C` means all carbon atoms, `ssall` that all contributions to J-coupling tensors are evaluated and `shift` that the chemical shielding tensor is computed. Please, note that to obtain the chemical shift constant which can be used in `Quantum_MOLE` it is mandatory to compute the chemical shielding tensor of the reference compound, and use Equation 5.2.9.

Another possibility is to use the functional and the basis set suggested in [57]. Since the results obtained with `ORCA` are still not fully satisfactory, the `Quantum_MOLE` simulations are carried out resorting to experimental data.

Chapter 8

Simulations and characterizations

This final chapter pulls the strings of the whole research. The knowledge acquired in the previous chapters is put to the test in some simulations. The quantum circuit design know-how is acquired in chapter 2 while chapters 3, 4 and 5 address the natural phenomena ruling nuclear magnetic resonance. Finally, chapters 6 and 7 lay the foundation for the understanding of the techniques adopted for the implementation and the simulation of nuclear magnetic resonance quantum computers. After all, a rigorous physical and logical treatment is mandatory for a deep understanding and for appropriate modelling.

This chapter presents some simulations on three different molecules: chloroform, cytosine and crotonic acid. The first is heteronuclear, while the other two are homonuclear. Chloroform and cytosine are two-qubit molecules, while crotonic acid is a four qubit molecule. For each molecule, the RF pulse width is optimized maximizing the fidelity when a $\mathbf{R}_x\left(\frac{\pi}{2}\right)$ rotation is sequentially applied to all qubits. The choice of this kind of benchmark is motivated by the fact the rotation of $\pi/2$ about \hat{x} axis is a fundamental rotation and by the fact that once a qubit is along the $-\hat{y}$ axis, it is sensitive to the unwanted J-coupling evolution which, as well known, mainly causes an unwanted rotation about \hat{z} . On the basis of the obtained results, the most suitable execution module of `Quantum_MOLE` is selected to run the two-qubit Grover's search algorithm as a benchmark. The static field is always assumed to have magnitude $B_0 = 11.74\text{ T}$, which is a typical choice.

8.1 Chloroform

The chloroform CHCl_3 is a two-qubit molecule: the qubit-0 is encoded on the nuclear spin of ^1H and the qubit-1 is encoded on the nuclear spin of ^{13}C . The

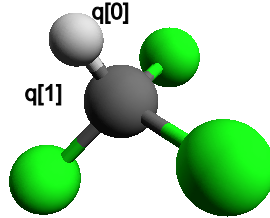


Figure 8.1: CHCl_3 molecule.

nuclear gyromagnetic ratios are [70]

$$\begin{aligned}\gamma_n(^1\text{H}) &= 267.522 \times 10^6 \text{ rad s}^{-1} \text{ T}^{-1} \\ \gamma_n(^{13}\text{C}) &= 67.283 \times 10^6 \text{ rad s}^{-1} \text{ T}^{-1}\end{aligned}\tag{8.1.1}$$

The isotropic chemical shift constants are [71, 72]

$$\begin{aligned}\delta(^1\text{H}) &= 7.26 \times 10^{-6} \\ \delta(^{13}\text{C}) &= 77.22 \times 10^{-6}\end{aligned}\tag{8.1.2}$$

The relaxation constants are [73]

$$\begin{aligned}T_1(^1\text{H}) &= 10.9 \text{ s} \\ T_1(^{13}\text{C}) &= 18.8 \text{ s} \\ T_2(^1\text{H}) &= 3.3 \text{ s} \\ T_2(^{13}\text{C}) &= 0.35 \text{ s}\end{aligned}\tag{8.1.3}$$

The J-coupling constant is [73]

$$J(0,1) = 215.09 \text{ Hz}\tag{8.1.4}$$

8.1.1 Fidelity optimization

As already highlighted, the chosen benchmark for the optimization of the fidelity versus the pulse width τ is a series of $\mathbf{R}_x(\pi/2)$ pulses, one per each qubit. The behaviour of the fidelity when τ ranges from $0.1 \mu\text{s}$ to $250 \mu\text{s}$ is reported in Figure 8.2. The chart is obtained resorting to the exact computation module of `Quantum_MOLE`,

executing fifty runs with different values of τ . The results are then interpolated with Matlab fitting toolbox, selecting the 'smoothingspline' option. As ex-

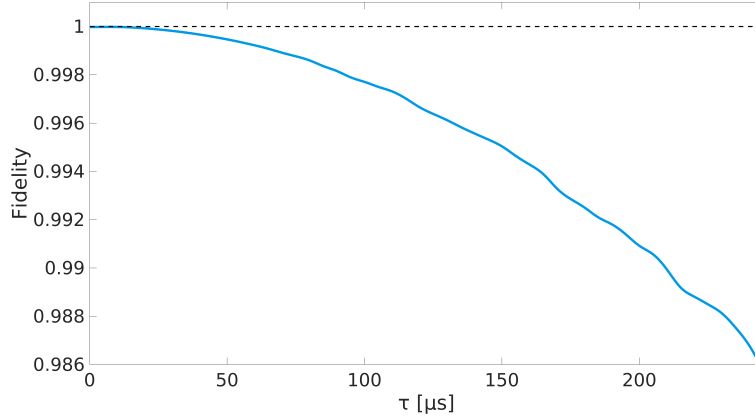


Figure 8.2: Fidelity versus τ in CHCl_3 molecule when a $\mathbf{R}_x\left(\frac{\pi}{2}\right)$ pulse is applied to each qubit.

pected there is a large range of values for which the fidelity is almost unitary. The reason is that chloroform is a heteronuclear molecule and so the condition

$$\frac{2\pi}{\Delta\omega_0} \ll \tau \ll \frac{1}{J} \longleftrightarrow 2.67 \text{ ns} \ll \tau \ll 4.65 \text{ ms} \quad (8.1.5)$$

is easily satisfied. In particular, the best results are obtained for $\tau < 10 \mu\text{s}$, that is with hard pulses. A reasonable compromise among fidelity, time duration and amplitude of the RF pulses can be

$$\tau = 5 \mu\text{s} \quad (8.1.6)$$

Since the conditions reported at the beginning of section §7.1.2 are satisfied, the approximate computation module can be safely adopted to run two-qubit quantum algorithms on this molecule.

8.1.2 The Grover's search benchmark

The Grover's search quantum algorithm is used as a benchmark to test the molecule performances. The pulse duration is set to $\tau = 5 \mu\text{s}$ for clarity. This means that a π -pulse about \hat{x} requires a $B_r(\pi_x)$ amplitude

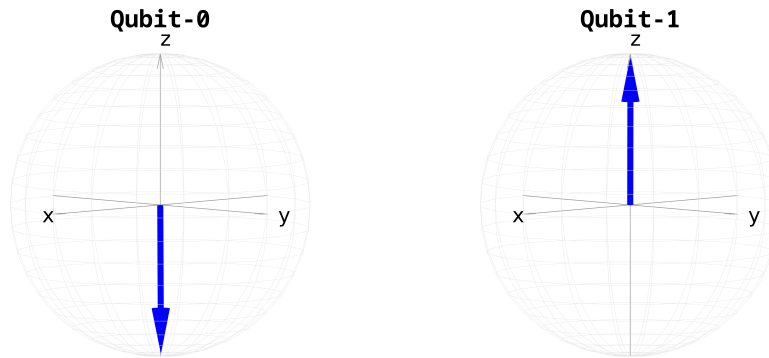
$$B_r(\pi_x) = \begin{cases} {}^1\text{H} & \longrightarrow 2.3 \text{ mT} \\ {}^{13}\text{C} & \longrightarrow 9.3 \text{ mT} \end{cases} \quad (8.1.7)$$

which are reasonable values for hard pulses. However, if the available hardware is not able to generate all the required different B_r amplitudes, one can fix B_r and let τ vary. For instance, setting $B_r \sim 4$ mT, similar results would be obtained. The simulated quantum circuit is the two-qubit version derived from first principles in section §2.2.2.3 and simulated also with IBM Quantum Experience (cf. section §2.3.3). It has to be highlighted that, since NMR quantum computers offer a natural support for control-Z gates, there is no need to replace the latter with Hadamard and CNOT gates.

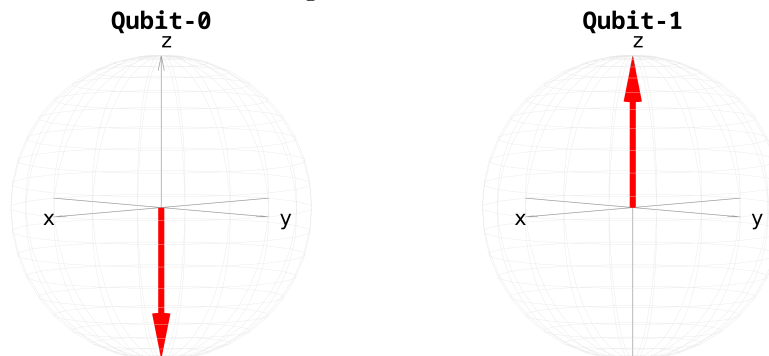
The main simulation results are summarized in Table 8.1. As expected, the

Quantity	Without VZ method	With VZ method
Execution time	4.82 ms	4.70 ms
Fidelity qubit 0	0.9930	0.9933
Fidelity qubit 1	0.9930	0.9933
Total fidelity	0.9896	0.9900
CPU time	286 ms	220 ms

Table 8.1: Approximate execution of Grover 10 quantum algorithm on chloroform.

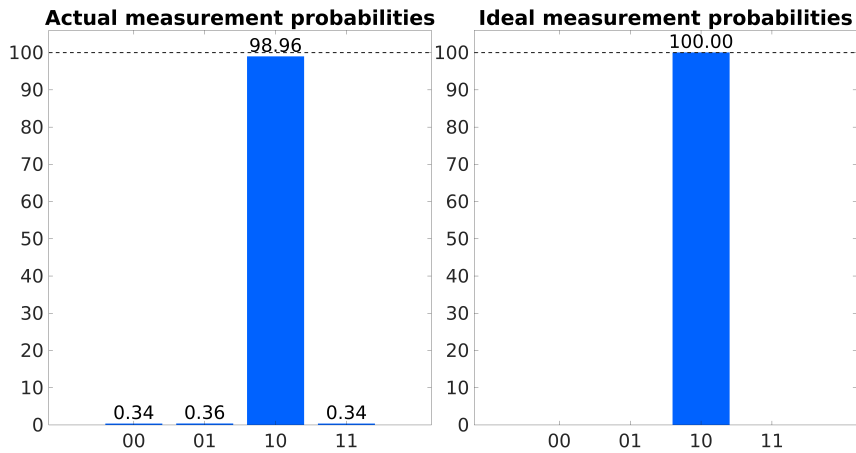


(a) Actual execution of Grover 10 algorithm on chloroform.

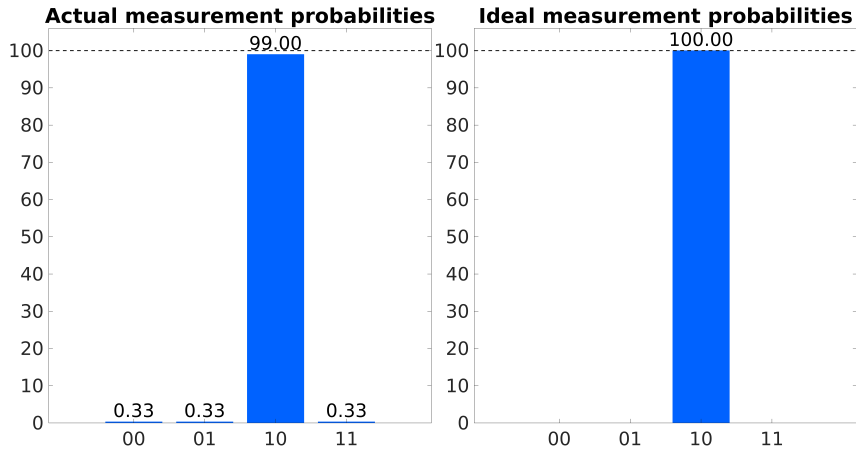


(b) Ideal execution of Grover 10 algorithm on chloroform.

Figure 8.3: The Grover 10 quantum algorithm on chloroform.



(a) Probability histogram for Grover 10 algorithm on chloroform without the Virtual-Z method.



(b) Probability histogram for Grover 10 algorithm on chloroform with the Virtual-Z method.

Figure 8.4: The Grover 10 quantum algorithm probability histogram.

approximate computation module is efficient, allowing for fast simulation of the quantum algorithm. Moreover, the fidelity is extremely high, providing an almost exact result. Obviously, the application of the Virtual-Z method improves both the fidelity and the execution time. The simulation outcomes are also reported in graphical format, for the convenience of the reader. In Figure 8.3, the individual qubit Bloch balls for ideal and actual computations are compared, assuming that no Virtual-Z method is applied. Finally, Figure 8.4 presents the probability histograms for actual and ideal computations.

8.1.3 Exact computation

Even if definitely not necessary in actual simulations for chloroform, the exact computation module of `Quantum.MOLE` is adopted to run the same two-qubit Grover algorithm, in order to prove the reliability of the approximate module for heteronuclear molecules. The main results¹ are summarized in Table 8.2, and the corresponding histogram is reported in Figure 8.5. The similarity with Table 8.2

Quantity	Without VZ method
Execution time	4.82 ms
Fidelity qubit 0	0.9929
Fidelity qubit 1	0.9929
Total fidelity	0.9895
CPU time	1.13×10^3 s

Table 8.2: Exact run of Grover 10 quantum algorithm on chloroform.

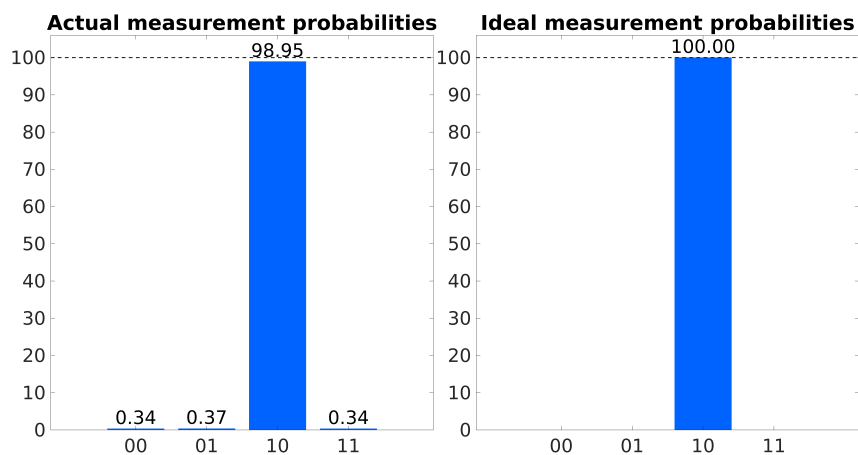


Figure 8.5: Probability histogram for Grover 10 algorithm on chloroform: exact computation without Virtual-Z method.

and Figure 8.4 proves the reliability of the approximate routine.

¹The CPU time is evaluated running the simulator on a nine-year-old i7-2630QM Intel processor.

8.2 Cytosine

Cytosine is a two-qubit homonuclear molecule: both qubits are encoded on ^1H nuclei, as reported in Figure 8.6. The nuclear gyromagnetic ratios are for both

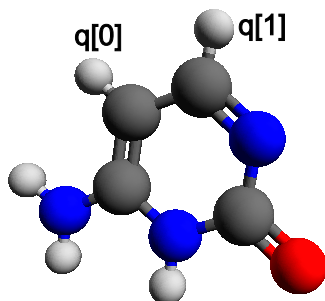


Figure 8.6: Cytosine molecule.

qubits [70]

$$\gamma_n(^1\text{H}) = 267.522 \times 10^6 \text{ rad s}^{-1} \text{ T}^{-1} \quad (8.2.1)$$

The isotropic chemical shift constants are [71]

$$\begin{aligned} \delta(\text{q}[0]) &= 7.50 \times 10^{-6} \\ \delta(\text{q}[1]) &= 5.97 \times 10^{-6} \end{aligned} \quad (8.2.2)$$

The relaxation constants are [67]

$$\begin{aligned} T_1(\text{q}[0]) &= 7.0 \text{ s} \\ T_1(\text{q}[1]) &= 7.0 \text{ s} \\ T_2(\text{q}[0]) &= 1.0 \text{ s} \\ T_2(\text{q}[1]) &= 1.0 \text{ s} \end{aligned} \quad (8.2.3)$$

The J-coupling constant is [67]

$$J(0,1) = 7.10 \text{ Hz} \quad (8.2.4)$$

8.2.1 Fidelity optimization

The usual set of quantum gates is adopted as a benchmark for the fidelity optimization. The behaviour of the latter when τ ranges from 1 ms to 10 ms is reported in Figure 8.7. The chart is obtained resorting to the exact computation module of

Quantum_MOLE, executing forty runs with different values of τ . The results are then interpolated with Matlab fitting toolbox, selecting the 'smoothingspline' option. There are some striking differences with respect to the chloroform fidelity

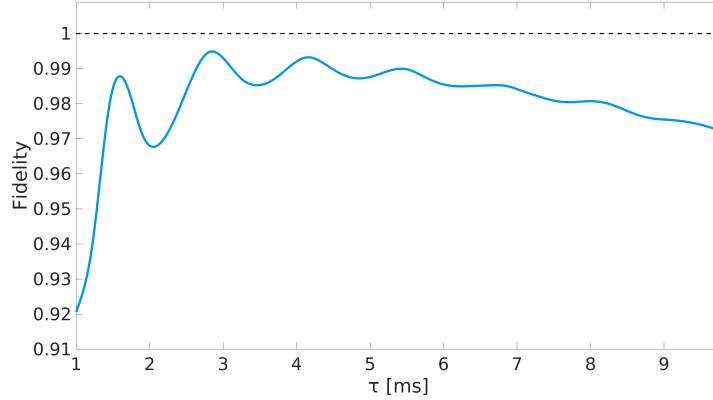


Figure 8.7: Fidelity versus τ in cytosine molecule when a $\mathbf{R}_x\left(\frac{\pi}{2}\right)$ pulse is applied to each qubit.

plot reported in Figure 8.2. The most evident is the range in which τ varies, which is in the order of ms, instead of μs . This is a clear signature of soft pulses, which must be employed for selective addressing of homonuclear molecules. Second, the fidelity plot shows a remarkable ringing with local maxima when τ is an integer multiple of $2\pi/\Delta\omega_0 \sim 1.31$ ms. The physical reason is readily understood considering the B matrix in the derivation of Equation 6.1.8, which is reported here for the two-qubit case for convenience

$$B = \frac{\gamma_2}{2\gamma_1} \mathbb{I} \otimes \begin{pmatrix} 0 & e^{-i(\Delta\omega_r t + \phi_1)} + e^{-i(\Omega t - \phi)} \\ e^{+i(\Delta\omega_r t + \phi_1)} + e^{+i(\Omega t - \phi)} & 0 \end{pmatrix} \quad (8.2.5)$$

where $\Delta\omega_r = \omega_{r,2} - \omega_{r,1} \sim \omega_{0,2} - \omega_{0,1}$ and $\Omega_r = \omega_{r,1} + \omega_{r,2} \sim \omega_{0,1} + \omega_{0,2}$. Clearly, this matrix represents the unwanted effects that a field intended to act on qubit-1 has on qubit-2. For every practical value of τ , it turns out that the terms oscillating at Ω_r can be safely neglected. Conversely, $\Delta\omega_r$ can be very small in homonuclear molecules. Hence, the terms oscillating at $\Delta\omega_r$ may not be negligible. It follows that if $\tau = 2\pi/\Delta\omega_0$, the B matrix reduces to an identity matrix and the unwanted effects are removed.

A reasonable choice for the RF pulse width can be

$$\tau = 5.229 \text{ ms} \quad (8.2.6)$$

as suggested in [67]. Since the conditions reported at the beginning of section

§7.1.2 are not satisfied, the exact computation module shall be used to obtain reliable results, even if it is CPU intensive.

8.2.2 The Grover’s search benchmark

The Grover’s search quantum algorithm is again used as a benchmark to test the molecule performances. The pulse duration is set to $\tau = 5.229$ ms for clarity. This means that a π -pulse about $\hat{\mathbf{x}}$ requires a $B_r(\pi_x)$ amplitude

$$B_r(\pi_x) = 2.25 \mu\text{T} \quad (8.2.7)$$

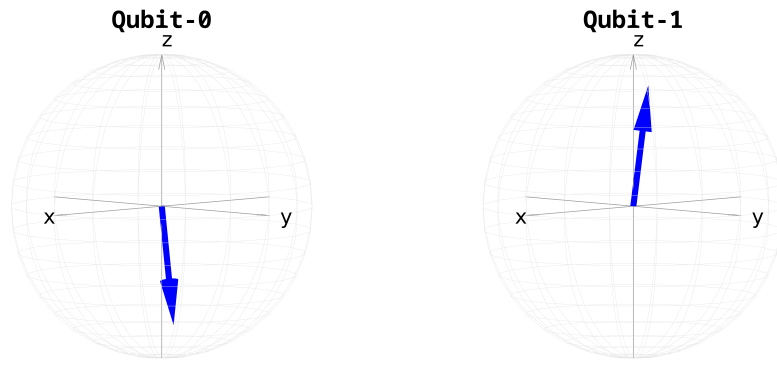
which is a reasonable value for soft pulses. As in the previous case, `Quantum_MOLE` takes advantage of the NMR native control-Z support.

The main simulation results are summarized in Table 8.3.

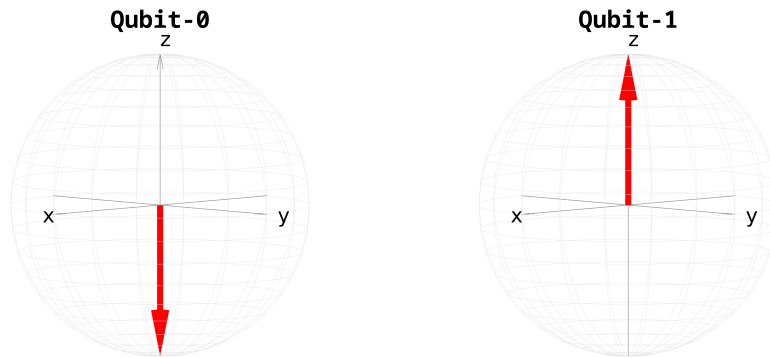
Quantity	Without VZ method	With VZ method
Execution time	318.63 ms	193.14 ms
Fidelity qubit 0	0.6875	0.8962
Fidelity qubit 1	0.6871	0.8948
Total fidelity	0.6175	0.8494
CPU time	1.265×10^3 s	284 s

Table 8.3: Exact run of Grover 10 quantum algorithm on cytosine.

As expected, the exact computation module is CPU intensive and the time required to run a simulation is significantly larger. Although the accurate optimization of the rectangular RF pulses, the fidelity is poorer, even with the Virtual-Z method, with respect to chloroform, thus reflecting the difficulty in achieving an almost unitary fidelity on homonuclear molecules, with simple rectangular pulses. In order to obtain higher fidelities, properly numerically optimized pulses or refocusing techniques shall be adopted. However, the desired outcome, when Virtual-Z is enabled, is still characterized by a probability notably higher than those of the other eigenstates. The simulation outcomes are also reported in graphical format, for the convenience of the reader. In Figure 8.8, the individual qubit Bloch balls for ideal and actual computations are compared, assuming that the Virtual-Z method is applied. Finally, Figure 8.9 presents the probability histograms for actual and ideal computations.



(a) Actual execution of Grover 10 algorithm on cytosine.



(b) Ideal execution of Grover 10 algorithm on cytosine.

Figure 8.8: The Grover 10 quantum algorithm on cytosine.

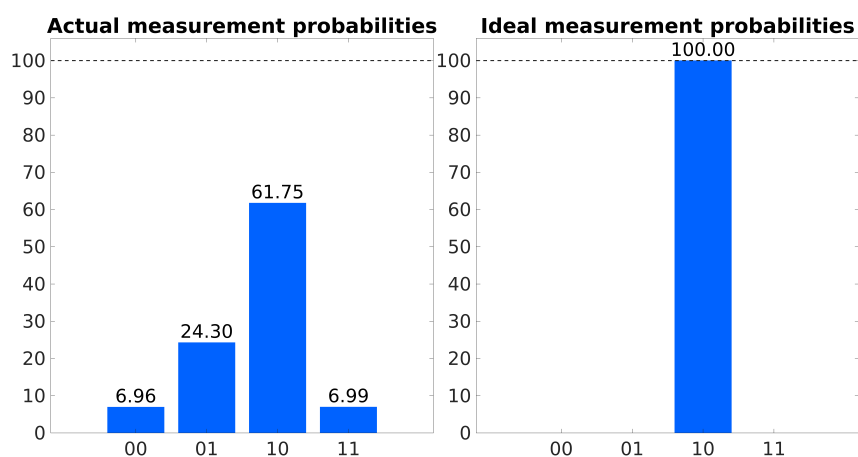
8.2.2.1 Automatic refocusing

A possibility to further improve the fidelity is to adopt the auto-refocusing technique introduced in section §7.1.4. The pulse width is fixed to $\tau = 10 \mu\text{s}$, which is a typical value for hard pulses. The main simulation results are summarized in Table 8.4 and in Figure 8.10. As expected, the fidelity is significantly higher.

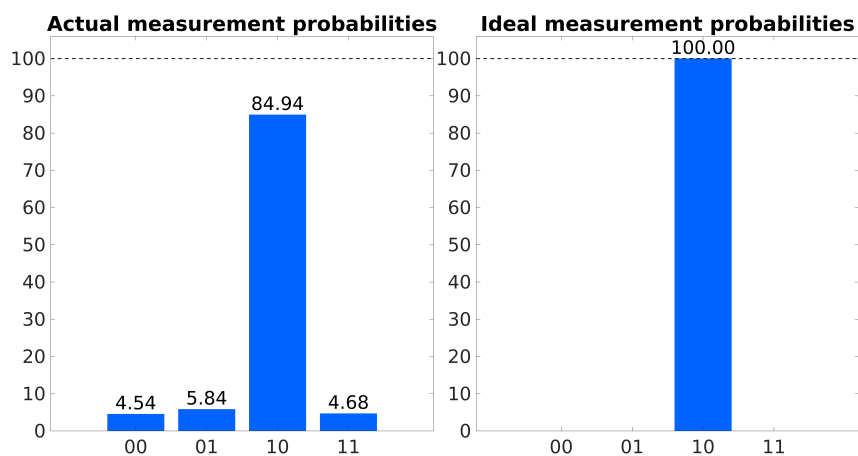
Quantity	With VZ method
Execution time	141.04 ms
Fidelity qubit 0	0.9342
Fidelity qubit 1	0.9342
Total fidelity	0.9013
CPU time	582 s

Table 8.4: Exact run of Grover 10 quantum algorithm on cytosine acid, with automatic refocusing.

Anyway, it is not almost unitary and the reason is that the J-coupling is extremely weak, thus the CNOT or CZ gates need a long time to be executed. The resulting long execution time makes decoherence and relaxation effects not negligible.



(a) Probability histogram for Grover 10 algorithm on cytosine without the Virtual-Z method.



(b) Probability histogram for Grover 10 algorithm on cytosine with the Virtual-Z method.

Figure 8.9: The Grover 10 quantum algorithm probability histogram for cytosine.

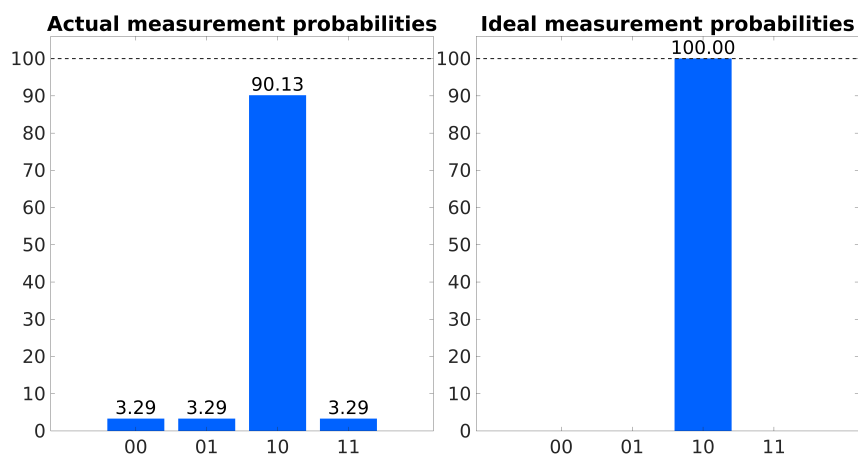


Figure 8.10: Probability histogram for Grover 10 algorithm on cytosine with the Virtual-Z method and automatic refocusing.

8.3 Crotonic acid

Crotonic acid is a four-qubit homonuclear molecule: the four qubits are encoded on ^{13}C nuclei, as reported in Figure 8.11. The nuclear gyromagnetic ratios are for

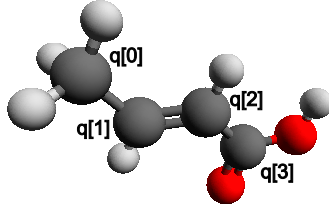


Figure 8.11: Crotonic acid molecule.

all qubits [70]

$$\gamma_n(^{13}\text{C}) = 67.283 \times 10^6 \text{ rad s}^{-1} \text{ T}^{-1} \quad (8.3.1)$$

The isotropic chemical shift constants are [71, 74]

$$\begin{aligned} \delta(\text{q}[0]) &= 18.08 \times 10^{-6} \\ \delta(\text{q}[1]) &= 147.55 \times 10^{-6} \\ \delta(\text{q}[2]) &= 122.38 \times 10^{-6} \\ \delta(\text{q}[3]) &= 172.35 \times 10^{-6} \end{aligned} \quad (8.3.2)$$

The relaxation constants² are [74, 75]

$$\begin{aligned} T_1(\text{q}[0]) &= 5.1 \text{ s} \\ T_1(\text{q}[1]) &= 5.3 \text{ s} \\ T_1(\text{q}[2]) &= 5.6 \text{ s} \\ T_1(\text{q}[3]) &= 10.2 \text{ s} \\ T_2(\text{q}[0]) &= 0.84 \text{ s} \\ T_2(\text{q}[1]) &= 0.92 \text{ s} \\ T_2(\text{q}[2]) &= 0.66 \text{ s} \\ T_2(\text{q}[3]) &= 0.79 \text{ s} \end{aligned} \quad (8.3.3)$$

²After a long a detailed research in the currently available scientific literature, only [75] seems to report T_1 time constants for crotonic acid. The other papers only report T_2 which is, obviously, the one which sets an upper limit to the total duration of the quantum algorithm.

The J-coupling constants are [74]

$$\begin{aligned}
 J(0,1) &= 41.64 \text{ Hz} \\
 J(0,2) &= 1.46 \text{ Hz} \\
 J(0,3) &= 7.04 \text{ Hz} \\
 J(1,2) &= 69.72 \text{ Hz} \\
 J(1,3) &= 1.18 \text{ Hz} \\
 J(2,3) &= 72.36 \text{ Hz}
 \end{aligned}
 \tag{8.3.4}$$

8.3.1 Fidelity optimization

The usual set of quantum gates is adopted as a benchmark for the fidelity optimization. The behaviour of the latter when τ ranges from 1 ms to 2 ms is reported in Figure 8.12. The chart is obtained resorting to the exact computation module of `Quantum_MOLE`, executing forty runs with different values of τ . The results are then interpolated with Matlab fitting toolbox, selecting the `'smoothingspline'` option. There are some interesting characteristics of crotonic acid which can be

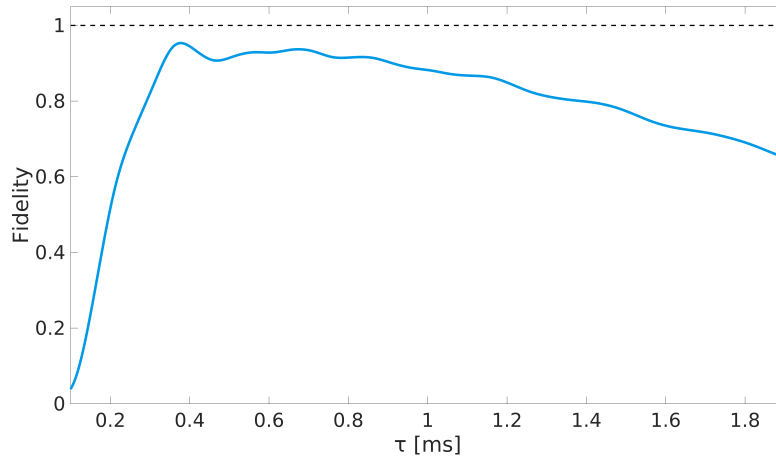


Figure 8.12: Fidelity versus τ in crotonic acid molecule when a $R_x\left(\frac{\pi}{2}\right)$ pulse is applied to each qubit.

understood from this plot. The range of pulse width values for which the fidelity is not poor is limited and significantly smaller with respect to cytosine. Moreover, even in this range, the fidelity does not reach high, almost unitary, values. In order to see the physical motivation behind this behaviour, consider the magnitudes of the molecular parameters. The largest J-coupling is

$$J_{\max} = 72.36 \text{ Hz} \tag{8.3.5}$$

while the minimum difference in chemically shifted Larmor frequencies is

$$\frac{\Delta\omega_{0,\min}}{2\pi} = 3.16 \text{ kHz} \quad (8.3.6)$$

so that the pulse width has to be

$$\frac{2\pi}{\Delta\omega_{0,\min}} \sim 321 \text{ } \mu\text{s} \ll \tau \ll \frac{1}{J} \sim 14 \text{ ms} \quad (8.3.7)$$

However, even for $\tau = 1.2 \text{ ms}$, the fidelity is already greatly reduced. The reason is that several J-couplings actually act on each qubit, causing unwanted evolutions. Therefore, it is a reasonable choice to use the exact computation with auto-refocusing module of `Quantum.MOLE`. Finally, the fidelity plot ringing is less evident than for cytosine, since there is a $\Delta\omega_0$ for each couple of spins. Anyway, it can be argued that local maxima occur in the neighbourhood of integer multiples of $\frac{2\pi}{\Delta\omega_{0,\min}}$.

8.3.2 The Grover’s search benchmark

The Grover’s search quantum algorithm is again used as a benchmark to test the molecule performances. The quantum algorithm is run on qubit-0 and qubit-1. The pulse duration is set to $\tau = 10 \text{ } \mu\text{s}$ to implement hard pulses. This means that a π -pulse about \hat{x} requires a $B_r(\pi_x)$ amplitude

$$B_r(\pi_x) = 1.17 \text{ mT} \quad (8.3.8)$$

which is a reasonable value for hard pulses. As in the previous cases, `Quantum.MOLE` takes advantage of the NMR native control-Z support. The auto-refocusing module is adopted, with Virtual-Z method enabled. As a matter of fact, the simulation with exact computation without auto-refocusing results in a very poor fidelity, even fixing $\tau = 700 \text{ } \mu\text{s}$.

The main simulation results are summarized in Table 8.5. As expected, also the exact computation module with auto-refocusing is CPU intensive and the time required to run a simulation is significantly longer than the approximate computation. However, the resulting fidelity of the outcome is remarkable: the probability to measure the expected eigenstate is higher than 97%, thanks to the auto-refocusing routine which practically removes the unwanted evolutions due to the J-coupling patterns. The key point to highlight is that an optimization of the

Quantity	With autofocusing	Without autofocusing
Execution time	24.21 ms	31.01 ms
Fidelity qubit 0	0.9819	0.9017
Fidelity qubit 1	0.9820	0.9287
Fidelity qubit 2	0.9998	0.8470
Fidelity qubit 3	0.9999	0.8849
Total fidelity	0.9728	0.6415
CPU time	1.61×10^3 s	9.34×10^3 s

Table 8.5: Exact run of Grover 10 quantum algorithm on crotonic acid, with and without auto-refocusing. In both cases, Virtual-Z method is enabled.

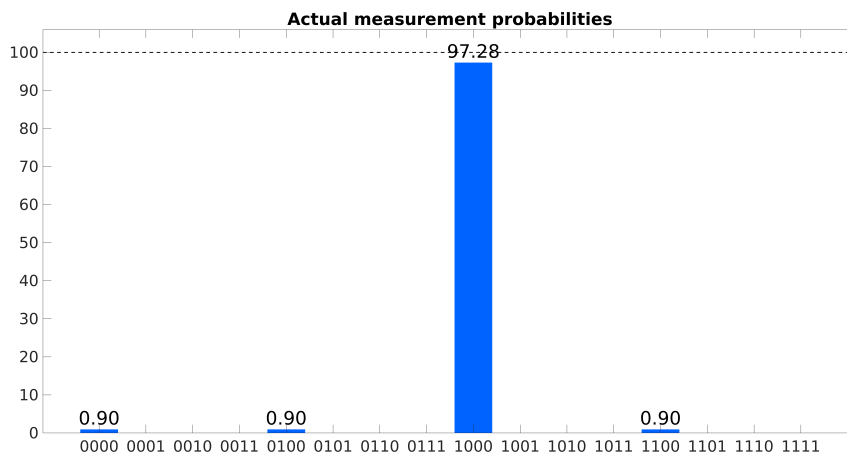
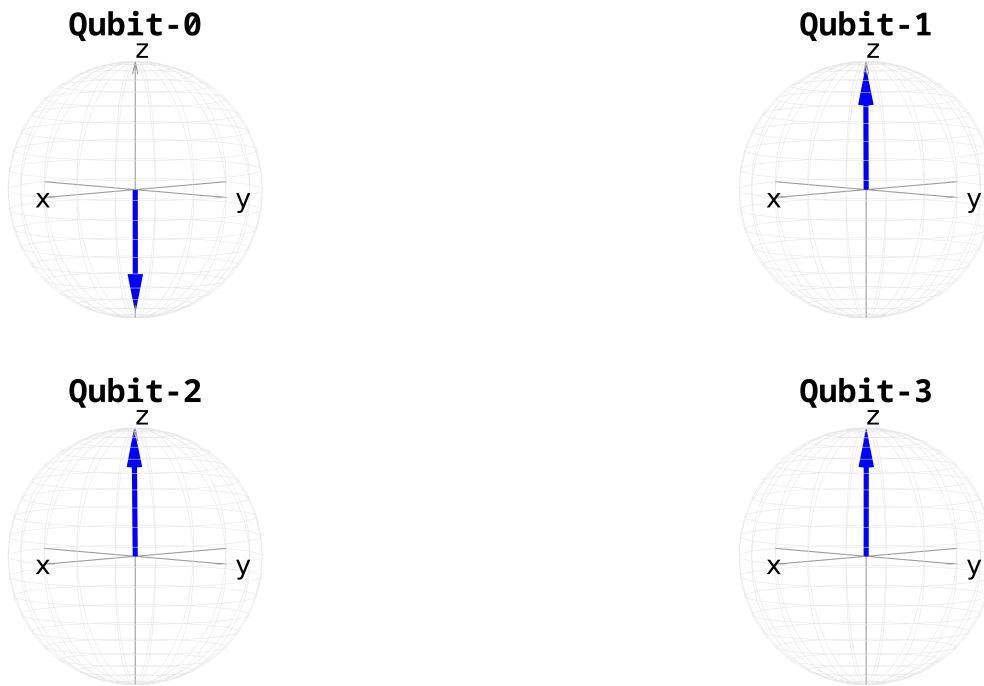
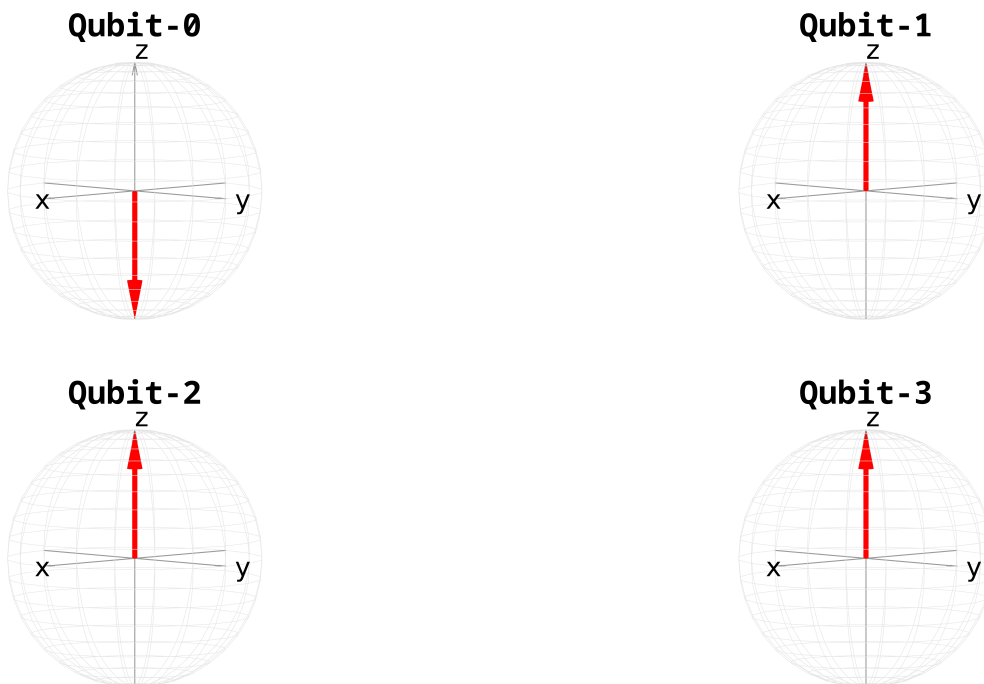


Figure 8.13: Probability histogram for Grover 10 algorithm on crotonic acid with the Virtual-Z method and auto-refocusing.

control RF pulses, as the maximization of the fidelity with soft pulses when possible (cf. cytosine) or the auto-refocusing technique (as in this case), is mandatory to obtain reliable results in homonuclear molecules. Finally, it has to be highlighted that the fidelity achievable with crotonic acid is higher than those achievable with cytosine. The motivation has to be looked for in the higher J-coupling constants, which allows for faster execution of CNOT and CZ gates. As a consequence, the time required to run a quantum algorithm is shorter and decoherence and relaxation effects are less effective. The simulation outcomes are also reported in graphical format, for the convenience of the reader. Figure 8.13 presents the probability histograms for actual computation. Finally, in Figure 8.14, the individual qubit Bloch balls for ideal and actual computations are compared.



(a) Actual execution of Grover 10 algorithm on crotonic acid.



(b) Ideal execution of Grover 10 algorithm on crotonic acid.

Figure 8.14: The Grover 10 quantum algorithm on crotonic acid with automatic refocusing.

8.4 Future improvements

A research work, whatever field it addresses, is never actually completed and one will always find something else to discover, understand or improve. There are no real limits to the search for knowledge. Every new concept brings with itself an endless series of *why* questions, the answers to which are just starting points to begin further investigations. Were not for the finite time which poses an insurmountable limit, one will probably never get some closure.

This research is not different. There is still plenty of things to improve and to further understand, even if the proposed model is already a good starting point to connect the physical and chemical backgrounds of molecules, thoroughly addressed to in this paper, to the quantum computation science, a role which, for classical computation science, has historically been prerogative of electronic engineering.

At a simulation level, it would be interesting to acquire a deeper understanding of **pseudopure state** preparation and include it in `Quantum_MOLE`, to better simulate the real-world behaviour of thermal mixtures. Also, a deeper physical knowledge of relaxation and **decoherence** phenomena is mandatory to improve the corresponding simulation module which, at the time of writing, provides only approximate results. As stated several times, many NMR experiments adopt **non rectangular pulses**, the behaviour of which must be included in future releases of `Quantum_MOLE`. Moreover, approaches to **speed up** the execution of the exact computation module for homonuclear molecules shall be investigated, for instance finding more computationally efficient ways of writing the same equations or trying to exploit parallel computation. Also, the final measurement of the outcome shall be improved, including the **quantum state tomography** procedure.

As far as the theory is concerned, a deepening of chemical understanding, in particular the molecular orbital theory, will help both the awareness of hardware behaviour and the interface with computational chemistry software, as `ORCA` and `Spinach` [76].

Finally, it would also be interesting to explore different technologies, as trapped ions, solid-state NMR, molecular magnets, superconductors and others and, hopefully, include the simulation of their behaviour in `Quantum_MOLE`.

Conclusions

Quantum computation is a thoroughly new way of thinking to electronics. The research is focusing on the design and the ideation of quantum algorithms able to outperform the classical counterpart in some fields. For instance, quantum computation is regarded to be naturally suitable to simulate complex quantum systems, as large molecules. Indeed, quantum chemistry is expected to be one of the most promising application areas. Chemistry means also medicine and quantum computers will enable the modelling of complex molecules, paving the way for the discovery of innovative drugs and more efficient treatments. Other application fields where quantum computation may improve human lives are quantum cryptography, thanks to an efficient integer factorization using Shor's algorithm; quantum search in large databases, which can be solved by Grover's search algorithm; quantum annealing for optimization problems and many others.

However, the future of quantum computing depends not only on the further development of quantum computer science but also (and mainly) on the improvement of hardware solutions capable of running quantum algorithms, which is the focus of this thesis.

A rigorous physical and mathematical treatment is mandatory for a deep understanding and for appropriate modelling of quantum technologies. The leading idea while writing has been to make things as simple as possible, assuming the reader has no familiarity with fine mathematical and physical jargon. In this respect, chapter 1, devoted to the essential preliminaries, lays the foundation for the understanding of the thesis. Chapter 2 is a gentle introduction to quantum computation which gradually gets to address the design of quantum algorithm, highlighting the main differences with respect to the classical counterpart and suggesting the requirements a physical quantum computer shall satisfy. Chapters 3, 4 and 5 deal with the physical background of a possible hardware implementation of quantum computers: the encoding of qubits on magnetic nuclear spins in diamagnetic molecules. The techniques routinely adopted to manipulate nuclear spins, namely the application of radio-frequency magnetic fields, are detailed. The analysis begins with a general introduction to magnetism, followed by a discussion of an idealized case: the behaviour of an isolated non-interacting spin. These hypotheses are removed in the following and interacting spin ensembles are treated with a full density matrix formalism, introducing several non-ideal effects,

as relaxation and decoherence phenomena. A particular emphasis is given on the chemical and physical origins of chemical shielding and J-coupling tensors.

The last two chapters, starting from the strong foundations built in the previous chapters, propose a model for the simulation of quantum algorithm execution on a nuclear magnetic resonance quantum computer: `Quantum_MOLE`. The latter can be run at different levels of approximation, trading off CPU time and accuracy. `Quantum_MOLE` is able to predict the outcome of a quantum algorithm, taking into consideration several non-idealities, as decoherence, relaxation, unwanted coupled evolution due to J-coupling during one-qubit operations and the effect of off-resonance pulses on not-addressed qubits in homonuclear molecules. `Quantum_MOLE` is provided with embedded support for Virtual-Z method and refocusing techniques.

Chapter 8 presents the results obtained for the execution of Grover's search quantum algorithm and the characterization of fidelity on three representative molecules. The first, chloroform, is a two-qubit heteronuclear molecule, for which non-ideal effects as unwanted J-evolution and off-resonance effects are negligible, thanks to a large difference in resonance frequencies. The second, cytosine, is a two-qubit homonuclear molecule with a weak J-coupling. Hence, the run time for two-qubit gates is long and the effects of decoherence and relaxation phenomena become evident. The third, crotonic acid, is a four-qubit homonuclear molecule for which the ratio between the difference in resonance frequencies and J-coupling is small, making it hard to optimize the soft-pulses. A specific automatic refocusing approach is introduced, to improve the control and increase the outcome fidelity.

The obtained results are encouraging. Liquid-state NMR qubits can implement a universal set of elementary quantum gates. Moreover, they have long relaxation times which enable the execution of simple quantum algorithms with negligible errors. More complex algorithms, anyway, would require the introduction of Quantum Error Correction (QEC) techniques. Another interesting advantage of NMR is that the techniques to initialize the system, control the evolution and measure the outcome are known and the required hardware is similar to the one which has been routinely adopted for decades for magnetic resonance imaging and nuclear magnetic resonance chemical spectroscopy. Moreover, the experiments are carried out at room temperature, while other hardware solutions require extremely low temperatures. On the other hand, scalability is a limiting issue in liquid-state NMR, because of the exponential loss of sensitivity of the NMR signal upon increasing the number of qubits. Some proposals have appeared in literature to try to overcome this limitation, as the handling of solid-state NMR.

Nowadays, several hardware solutions for the implementation of quantum computers are currently under investigation. It is still not known which will be the definitive technology or even if there will be a single established one or if the peculiar characteristics of several different hardware solutions will be carefully exploited to optimize different classes of algorithms. In any case, the way for empowering the research of tomorrow in many fields is already paved and the consequent social impact will be unprecedented.

Bibliography

- [1] IBM. Ibm q experience, 2019. [Online at <https://quantum-computing.ibm.com/>].
- [2] Frank Neese. Software update: the orca program system, version 4.0. *Wiley Interdisciplinary Reviews: Computational Molecular Science*, 07 2017.
- [3] Frank Neese. The orca program system. *Wiley Interdisciplinary Reviews: Computational Molecular Science*, 2, 2012.
- [4] B. Zwiebach. Dirac's bra and ket notation. Technical report, Massachusetts Institute of Technology, October 2013.
- [5] Mikio Nakahara and Tetsuo Ohmi. *Quantum Computing From Linear Algebra to Physical Realizations*. CRC Press, 1 edition, 2008.
- [6] Leon van Dommelen. *Quantum Mechanics for Engineers*. Web book, August 2018.
- [7] R. L. Jaffe. Supplementary notes on dirac notation, quantum states, etc, 1996.
- [8] V. Dorobantu. The postulates of quantum mechanics.
- [9] Zach Weinersmith. The talk, 2016. [Online at <http://smbc-comics.com/comic/the-talk-3>; accessed 09-August-2019].
- [10] Wikibooks. Materials in electronics/wave-particle duality/the two-slit experiment, 2009. [Online at https://en.wikibooks.org/wiki/Materials_in_Electronics/Wave-Particle_Duality/The_Two-Slit_Experiment; accessed 29-July-2019].
- [11] EECS Berkely. Measurement in quantum mechanics.
- [12] David J. Griffiths. *Introduction to Quantum Mechanics*. Pearson, 2 edition, 2014.
- [13] Frank Rioux. Elements of dirac notation, 2019. Saint John's University.
- [14] Roger Balian. *From Microphysics to Macrophysics: Methods and Applications of Statistical Physics*. Springer, New York, 1st edition, 2007.
- [15] Richard Jozsa. Fidelity for mixed quantum states. *Journal of Modern Optics*, 41:2315–2323, 12 1994.
- [16] Giovanni Amedeo Cirillo. A quantum computation model for molecular nanomagnets. Master thesis, Politecnico di Torino, April 2018.
- [17] Ivan S. Oliveira, Tito J. Bonagamba, Roberto S. Sarthour, Jair C.C. Freitas, and Eduardo R. deAzevedo. *NMR Quantum Information Processing*.

- Elsevier, 1 edition, 2007.
- [18] Noson S. Yanofsky and Mirco A. Mannucci. *Quantum computing for computer scientists*. Cambridge university press, 1 edition, 2008.
- [19] Colin P. Williams. *Explorations in Quantum Computing*. Springer, 2 edition, 2011.
- [20] IBM Q Experience. Introduction to quantum circuits, 2019. [Online at <https://quantum-computing.ibm.com/support/guides/introduction-to-quantum-circuits?page=5cae6f7735dafb4c01214bbe>; accessed 16-August-2019].
- [21] Adriano Barenco, Charles H. Bennett, Richard Cleve, David P. DiVincenzo, Norman Margolus, Peter Shor, Tycho Sleator, John A. Smolin, and Harald Weinfurter. Elementary gates for quantum computation. *Physical Review*, 52(5):3457–3467, November 1995.
- [22] Juan Carlos Garcia-Escartin and Pedro Chamorro-Posada. Equivalent quantum circuits, October 2011. Arxiv repository: arXiv:1110.2998 [quant-ph].
- [23] Mike van der Lans. Quantum algorithms and their implementation on quantum computer simulators. Bachelor of science in applied physics and applied mathematics, TU Delft, June 2017.
- [24] Jonathan Hui. Quantum computing : The strength and the weakness of qubits in quantum computing, November 2018. [Online at https://medium.com/@jonathan_hui/qc-the-strength-and-the-weakness-of-qubits-in-quantum-computing-dc54c442fcb3; accessed 19-August-2019].
- [25] Andy Matuschak and Michael A. Nielsen. How does the quantum search algorithm work?, April 2019. [Online at <https://quantum.country/search>; accessed 19-August-2019].
- [26] C. Lavor, L. R. U. Manssur, and R. Portugal. Grover’s algorithm: Quantum database search, 2003. Arxiv repository: arXiv:quant-ph/0301079.
- [27] Andrew W. Cross, Lev S. Bishop, John A. Smolin, and Jay M. Gambetta. Open quantum assembly language, 2017. Arxiv repository: arXiv:1707.03429.
- [28] Stohr Joachim and Hans Christoph. Siegmann. *Magnetism: from fundamentals to nanoscale dynamics*. Springer, 1 edition, 2006.
- [29] P. Mazzoldi, M. Nigro, and C. Voci. *Elementi di fisica: elettromagnetismo e onde*. EdiSES, Napoli, 2008.
- [30] David J. Griffiths. *Introduction to Electrodynamics*. Pearson Education, 4th edition, 2012.
- [31] Timothy H. Boyer. The force on a magnetic dipole. *American Journal of*

- Physics*, 56(8):688–692, August 1988.
- [32] Cheng Yu-Chung Norman and Haacke E. Mark. Magnetic moment of a spin, its equation of motion, and precession. *Current Protocols in Magnetic Resonance Imaging*, 14(1):B1.1.1–B1.1.10, 2007.
- [33] Malcolm Levitt. *Spin dynamics : basics of nuclear magnetic resonance*. John Wiley & Sons, Ltd, Chichester, England Hoboken, NJ, 2008.
- [34] Peter Atkins. *Molecular Quantum Mechanics*. Oxford University Press, New York, 2005.
- [35] Wikipedia contributors. Stern and gerlach experiment Wikipedia, the free encyclopedia, 2019. [Online at https://en.wikipedia.org/w/index.php?title=Stern%E2%80%93Gerlach_experiment&oldid=904918332 accessed 5-September-2019].
- [36] J. M. D. Coey. *Magnetism and Magnetic Materials*. Cambridge University Press, 2010.
- [37] David Griffiths. *Introduction to electrodynamics*. Pearson, Boston, 4th edition, 2013.
- [38] S. V. Vonsovsky. *Magnetism of elementary particles*. MIR publishers, Moscow, 1973.
- [39] Vladimir Chizhik. *Magnetic resonance and its applications*. Springer, Cham, 2014.
- [40] Wikipedia contributors. Elementary particle, Wikipedia, the free encyclopedia, 2019. [Online at https://en.wikipedia.org/w/index.php?title=Elementary_particle&oldid=914841942 accessed 10-September-2019].
- [41] MRI Questions contributors. Predicting nuclear spin, 2019. [Online at <http://mriquestions.com/predict-nuclear-spin-i.html> accessed 12-September-2019].
- [42] C.P. Slichter. *Principles of Magnetic Resonance*. Springer, Urbana, Illinois, 3rd edition, 1989.
- [43] S. Focardi, I. Massa, A. Uguzzoni, and M. Villa. *Fisica Generale : Meccanica e Termodinamica*. Casa Editrice Ambrosiana, Milan, 2nd edition, 2014.
- [44] Lieven M. K. Vandersypen and Isaac L. Chuang. Nmr techniques for quantum control and computation. 2004. Arxiv repository: arXiv:0404064 [quant-ph].
- [45] Mikio Nakahara, Shigeru Kanemitsu, Martti Salomaa, and Shin Takagi. *Physical realizations of quantum computing : are the DiVincenzo criteria fulfilled in 2004?* World Scientific, Singapore Hackensack, N.J, 1 edition, 2006.
- [46] John Cavanagh, Wayne J. Fairbrother, Arthur G. Palmer, Mark Rance, and

- Nicholas J. Skelton. *Protein NMR Spectroscopy : Principles and Practice*. Elsevier Science, 2nd edition, 2010.
- [47] Danila Barskiy. Dipole-dipole interactions in nmr: explained, May 2018. [Online at <https://danilabarskiy.com/2018/05/15/dipole-dipole-interactions-in-nmr-explained/>; accessed 24-November-2019].
- [48] Lukas Zidek. Physical principles of nmr, December 2015.
- [49] Frank A. L. Anet and Daniel J. O’Leary. The shielding tensor. part i: Understanding its symmetry properties. *Concepts in Magnetic Resonance Part A*, 3, 1991.
- [50] Cory M. Widdifield and Robert W. Schurko. Understanding chemical shielding tensors using group theory, mo analysis, and modern density-functional theory. *Concepts in Magnetic Resonance Part A*, 34A, 2009.
- [51] Norman F. Ramsey. Magnetic shielding of nuclei in molecules. *Physical Review (Series I)*, 78, 6 1950.
- [52] Norman F. Ramsey. Chemical effects in nuclear magnetic resonance and in diamagnetic susceptibility. *Physical Review (Series I)*, 86, 4 1952.
- [53] Peter Atkins and Julio de Paula. *Physical Chemistry*. W H Freeman and Co, 9 edition, 2009.
- [54] Harald Günther. *NMR Spectroscopy: Basic Principles, Concepts and Applications in Chemistry*. Wiley-VCH, 3 edition, 2013.
- [55] Julio C. Facelli. Calculations of chemical shieldings: Theory and applications. *Concepts in Magnetic Resonance Part A*, 20A, 2004.
- [56] T.A. Keith and R.F.W. Bader. Properties of atoms in molecules: Nuclear magnetic shielding. *Canadian Journal of Chemistry*, 74:185–200, 02 2011.
- [57] Georgi L. Stoychev, Alexander A. Auer, and Frank Neese. Efficient and accurate prediction of nuclear magnetic resonance shielding tensors with double-hybrid density functional theory. *Journal of Chemical Theory and Computation*, 14(9):4756–4771, 2018.
- [58] Jochen Autschbach and Boris Le Guennic. Analyzing and interpreting nmr spin spin coupling constants using molecular orbital calculations. *Journal of Chemical Education*, 84(1):156, 2007.
- [59] Jurgen Cremer, Dieter; Grafenstein. Calculation and analysis of nmr spin spin coupling constants. *Physical Chemistry Chemical Physics*, 9, 2007.
- [60] Manfred Bucher. The electron inside the nucleus: an almost classical derivation of the isotropic hyperfine interaction. *European Journal of Physics*, 21(1):19–22, jan 2000.

- [61] R. McWeeny. *Methods of molecular quantum mechanics*. Theoretical chemistry. Academic Press, 2nd ed edition, 1992.
- [62] Juha Vaara; Jukka Jokisaari; Roderick E. Wasylshen; David L. Bryce. Spin spin coupling tensors as determined by experiment and computational chemistry. *Progress in Nuclear Magnetic Resonance Spectroscopy*, 41, 2002.
- [63] Avogadro: an open-source molecular builder and visualization tool. version 1.20. [Online at <http://avogadro.cc/>].
- [64] Robabeh Rahimi Mikio Nakahara, Yukihiro Ota. *Molecular realizations of quantum computing 2007*. Kinki University series on quantum computing 2. World Scientific, 2009.
- [65] David C. McKay, Christopher J. Wood, Sarah Sheldon, Jerry M. Chow, and Jay M. Gambetta. Efficient z-gates for quantum computing. 2016.
- [66] Ivan Djordjevic (Auth.). *Quantum Information Processing and Quantum Error Correction. An Engineering Approach*. Academic Press, 2012.
- [67] Yasushi Kondo, Mikio Nakahara, Kazuya Hata, and Shogo Tanimura. Hamiltonian of homonucleus molecules for nmr quantum computing, 2005.
- [68] Noah Linden; Barjat Herve; Rodrigo J. Carbajo; Ray Freeman. Pulse sequences for nmr quantum computers: how to manipulate nuclear spins while freezing the motion of coupled neighbours. *Chemical Physics Letters*, 305, 1999.
- [69] Royal Society of Chemistry. Chempider. [Online at <https://www.chemspider.com/Default.aspx>; accessed 15-March-2020].
- [70] Wikipedia contributors. Gyromagnetic ratio — Wikipedia, the free encyclopedia, 2020. [Online at https://en.wikipedia.org/w/index.php?title=Gyromagnetic_ratio&oldid=940096649; accessed 12-March-2020].
- [71] National Institute of Advanced Industrial Science and Technology. Spectral database for organic compounds, 2020. [Online at <https://sdfs.db.aist.go.jp>; accessed 12-March-2020].
- [72] Yao; Hao Liang; Zhang Fei-Hao; Long Gui-Lu Feng, Guan-Ru; Lu. Experimental simulation of quantum tunneling in small systems. *Scientific Reports*, 3, 12 2013.
- [73] Tao Xin, Julen S. Pedernales, Lucas Lamata, Enrique Solano, and Gui-Lu Long. Measurement of linear response functions in nuclear magnetic resonance. 2016. Arxiv repository: arXiv:1606.00686 [quant-ph].
- [74] Jingwei Wen, Xiangyu Kong, Shijie Wei, Bixue Wang, Tao Xin, and Guilu Long. Experimental realization of quantum algorithms for linear system inspired by adiabatic quantum computing. 2018. Arxiv repository:

- arXiv:1806.03295 [quant-ph].
- [75] Youning; Han Muxin; Lu Sirui; Zhou-Jie; Ruan Dong; Long Guilu; Wan Yidun; Lu Dawei; Zeng Bei; Laflamme Raymond Li, Keren; Li. Quantum spacetime on a quantum simulator. *Communications Physics*, 2, 12 2019.
- [76] H.J. Hogben; M. Krzystyniak; G.T.P. Charnock; P.J. Hore; Ilya Kuprov. Spinach a software library for simulation of spin dynamics in large spin systems. *Journal of Magnetic Resonance*, 208, 2011.